BADMINTON PRESS
16 THE FALCROFT
SYSTON
LEICESTER LE7 8LD
ENGLAND
TEL: 0533 602917

PLASMA AND CORONA DISCHARGE PRETREATMENT OF POLYETHERETHERKETONE FOR ADHESIVE BONDING

by

Gaozhi Xiao, M Eng

A doctoral thesis submitted in partial fulfilment

of the requirements for the award of the degree of

Doctor of Philosophy

of Loughborough University of Technology

March 1995

Supervisors: Dr L. Mascia

Dr J. Comyn

Institute of Polymer Technology and Materials Engineering

PLASMA AND CORONA DISCHARGE PRETREATMENT OF POLYETHERETHERKETONE FOR ADHESIVE BONDING

SYNOPSIS

To enhance the bondability of polyetheretherketone (PEEK), surface treatment techniques of plasma and corona discharge have been evaluated. The results have shown that these two methods are effective and practical. The treated materials not only reach their highest possible joint strength, but also show very promising joint durability. In addition, the various environments, e. g. atmosphere, heat, water, and solvent, have little effects on the enhanced bondability of the treated materials.

By using Contact Angle Measurement, Scanning Electron Microscopy (SEM), X-ray Photoelectron Spectroscopy (XPS) and Time of Flight Secondary Ion Mass Spectrometry (TOF-SIMS) to characterise the PEEK surfaces before and after treatment, it was established that the lack of active chemical groups, which if present can form strong interatomic and intermolecular forces across the adhesive/PEEK interface, is the main cause for the poor bondability of the untreated PEEK. Both plasma and corona discharge treatment introduce such active functional groups, for instance, hydroxyl, carboxylic acid, amine and etc., onto the surface of PEEK film and so greatly enhance the intrinsic adhesion at the interface between treated PEEK surfaces and epoxy adhesive, as confirmed by the TOF-SIMS interfacial analysis.

It is deduced that low molecular weight molecules (LMWM) are formed on treated surfaces, which contain high concentration of oxygen and/or nitrogen, and can be removed by solvent washing. The removal of LMWM will drastically reduce the wettability of the treated surfaces, but does not impair the enhanced bondability.

It has been found that both plasma and corona discharge treated surfaces are in a thermodynamically unstable state. When exposed to the atmosphere, the treated surfaces tend to lose their improved wettability and decrease their surface polarity. Increasing temperature can not only accelerate these processes but also change the surface chemical structures of the treated materials back to that of the untreated films to some extent, as revealed by the TOF-SIMS analysis. Water immersion, on the contrary, tend to reverse the above processes.

ACKNOWLEDGEMENTS

I would like to thank my supervisors, Dr. L. Mascia and Dr. J. Comyn, for their guidance, support and encouragement during this project.

My thanks also go to Dr. B. M Parker of DRA Farnborough for many helpful discussions. Grateful acknowledgement is made to the Ministry of Defence for financial assistance which enabled this work to be undertaken.

A special thanks to my family who encouraged me to continue my studies, especially my wife Jinmei and baby daughter Helen for being patient and quiet (respectively!) whilst I put the manuscript together.

My thanks are extended to Dr. E. Sheng for his help on the XPS derivatisation experiment. Without his help this part of work could not be undertaken.

Finally, I wish to express my gratitude to the staff and technicians in IPTME who helped me at various times.

Dedicated to

my wife Jinmei

and my daughter Helen

CONTENTS

ABBREVIATIONS

DMSO Dimethylsulfoxide
DSC Differential scanning calorimetry
ED Ethanediol
ENHPK Epoxy resin coated ammonia plasma treated PEEK after 24 hours acetone immersion
EOPK Epoxy resin coated oxygen plasma treated PEEK after 24 hours acetone immersion
EUPK Epoxy resin coated untreated PEEK after 24 hours acetone immersion
FTIR Fourier transform infrared spectroscopy
HMWM High molecular weight molecules
IPA 2-propanol
LMWM Low molecular weight molecules
MDI Methylene diiodide
MIR Multiple internal reflectance
OM Optical microscopy
PEEK Polyetheretherketone
SEM Scanning electron microscopy
SIMS Secondary ion mass spectrometry
SRIRS Surface reflectance infrared spectroscopy
SSIMS Static secondary ion mass spectrometry
STEM Scanning transmission electron microscopy
TOF-SIMS Time of flight secondary Ion Mass Spectrometry
WBL Weak boundary layer
XPS X-ray photoelectron spectroscopy

CHAPTER 1 INTRODUCTION

Poly(ether ether ketone), PEEK, is a linear aromatic polymer with a repeat unit of three benzene rings separated by two ether bonds and one carbonyl bond (as shown in Fig. 1.1).

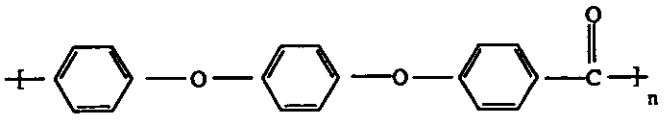

Fig. 1.1 Chemical structure of PEEK

It is a semi-crystallisable polymer with glass transition temperature (T_g) of 143°C and melting point (T_m) of 334°C, hence according to the thermal history it can be amorphous or semi-crystalline. Due to its exceptionally high performances (see Table 1.1), particularly with respect to thermal oxidative stability, chemical resistance, mechanical and electrical properties[2,3], PEEK and its composites are being widely exploited in many fields[3-5], especially in the aerospace industry as structural materials.

Table 1.1 Key properties of PEEK[1]

Mechanical	Tough; ductile; abrasion resistant; excellent fatigue characteristics; load-bearing at high temperature
Thermal	High melting point; high continuous service temperature
Flammability	Low flammability; good fire and smoke resistant properties
Chemical	Essentially inert to organics; high degree of acid and alkali resistance
Hard radiation	No significant degradation below 1100 Mrad
Processing	Easily processed on conventional equipment

The majority of structural applications, however, require joints to be made for the assembling of various structure members. Generally speaking, joining of plastics and composites can be broadly divided into mechanical fastening, adhesive bonding and

welding. Among these joining methods, adhesive bonding has many advantages (as shown in Table 1.2) and is, therefore, widely used, particularly in the aerospace industry, where sometimes other joint methods cannot be used. Perhaps the best example, of particular importance in the aircraft industry, is the bonding of thin composite or metal skins to honeycomb cores, to provide lightweight, rigid structures and suitable aerodynamic surface.

Table 1.2 Advantages of structural adhesive bonding

---

* Minimises stress concentration and exhibits outstanding fatigue resistance
* Provides significant weight savings
* Can join any shape of similar or dissimilar materials
* Provides integrity of materials and smooth surfaces
* Seals joint, insulates heat, electricity and moisture
* The only practical joining method for certain applications
* Can reduce manufacturing costs

The strength of a bonded joint is determined by the strength of its weakest component, which is generally designed to be adhesive or adherend. A successful adhesive bonded joint depends mainly upon the following factors:

(a) Appropriate design of the joint,
(b) Selection of a suitable adhesive,
(c) Adequate pretreatment of the adherend surface,
(d) Controlled fabrication of the joint.

Among these factors, surface pretreatment before adhesive bonding is critical to bond reliability and integrity, as adhesives must function by surface attachment only. Surface usually refers to that portion of the adherend with which the adhesive interacts. Proper surface pretreatment ensures that joint failure occurs within the adhesive or adherend, not at the adhesive-adherend interface. This type of fracture is known as "cohesive". When fracture occurs at the adhesive/adherend interface, failure is said to be "adhesive". Joint failure modes can be described in terms of the percentage of failure that is adhesive or the percentage that is cohesive. A specimen with 100% cohesive failure would be ideal in terms of surface pretreatment.

There are many surface pretreatment methods that have been developed, These methods can be divided into four categories:

(a) Surface cleansing;
(b) Mechanical treatment;
(c) Chemical Treatment;
(d) Physical Treatment.

Among them, surface cleansing is the simplest method, but for some polymers, this is not adequate. Mechanical treatment use sand or other particles to abrade or blast the adherend surface. This method is often used to treat metals or composites, but is not effective for most polymers. Chemical treatments are very effective for both metals and polymers, but these methods are toxic and pollute environment. Physical treatment methods, especially plasma treatment and corona discharge treatment, are usually very effective to polymers and do not cause pollution or discharge health hazards.

Kinloch and Taig[6] studied the bondability of PEEK composites(APC-2), and found that the intrinsic bond strength of untreated APC-2 is very low. These authors also found that the conventional surface pretreatment methods used for thermosetting composites, such as mechanical abrasion, solvent cleaning etc. are not adequate for PEEK composites[6,7]. Thus, in order to improve the bondability of PEEK and its composites, special surface pretreatments need to be employed.

This study focuses on the surface pretreatment of PEEK by means of plasma and corona discharge to improve its adhesive joint strength. A literature survey was carried out on the following aspects:

(a) the relations between surface properties and adhesion;
(b) surface characterisation methods and their applications in adhesion studies;
(c) evaluation of bondability; and
(d) recent developments for surface treatments of PEEK and its composites.

CHAPTER 2 SURFACE PROPERTIES AND ADHESION

Adhesive bonding is a surface phenomenon and, therefore, the bond strength is governed by surface properties. Both the initial bond strength and bond durability are critically dependent on the interactions between the adhesive ((and/or) primer) and the adherend surface. Thus, it is necessary to know the relations between surface properties and bondability.

2.1 Wettability and Adhesion

Wettability of an adherend is the ability of the adherend to be wetted by liquids. When an adherend is easily wetted by a liquid, it is said that the adherend has a good wettability and vice versa. Wettability is evaluated by liquid contact angles.

The adsorption theory of adhesion is the most widely applicable theory and proposes that, provided sufficiently intimate molecular contact is achieved at the interface, the materials will adhere because of the interatomic and intermolecular forces which are established between the atoms and molecules in the surfaces of the adhesive and substrate. The most common forces at interfaces are van der Waals forces. However, van der Waals forces diminish rapidly with distance, varying with the inverse of the sixth power of the distance between two neighbouring molecules and with the inverse cube of distance between two flat plate surfaces[8]. Appreciable attractions are obtained only when the distance of separation is at or near an equilibrium intermolecular distance of the order of 0.5 nm[9]. Besides van der Waals forces, chemical bond such as covalent bond can also only be formed when the intermolecular or interatomic distance is within 0.1~0.2 nm[10]. Thus, close proximity of molecules from the two surfaces is a fundamental requirement for forming a strong adhesive joint.

Moreover, the wettability of the adherend not only determines the extent of interfacial molecular contact, but also affects joint strength in two ways[11]. First, incomplete wetting will produce interfacial defects, thereby lowering the adhesive bond strength. Second, better wetting can increase the adhesive bond strength by increasing the work of adhesion, which is directly proportional to the fracture energy.

2.2 Chemical Composition and Adhesion

Interfaces can be classified into two types[12]: (a) sharp interfaces and (b) diffuse interfaces. A sharp interface is obtained when little or no interfacial diffusion occurs; a

Table 2.1 Bond types and typical bond energies[13-15]

Type	Bond Energy(KJ mol^{-1})
Primary Bonds	
Ionic	600-1100
Covalent	60-700
Metallic	110-350
Donor-acceptor Bonds	
Bronsted acid-base interactions	Up to 40
Lewis acid-base interactions	Up to 80
Secondary Bonds	
Hydrogen bonds involving fluorine	Up to 40
Hydrogen bonds excluding fluorine	10-25
Van der Waals bonds	
Permanent dipole-dipole interactions	4-20
Dipole-induced dipole interactions	Less than 2
Dispersion (London) forces	0.08-40

diffuse interface is obtained, on the other hand, when sufficient diffusion across the interface takes place. If interfacial attractions are very low, as in the case of dispersion forces (as shown in Table 2.1), interfacial molecular slippage can occur at a sharp interface during fracture, resulting in low energy absorption and low mechanical strength. But if interfacial attractions are very strong, as for example, with primary bonds (as shown in Table 2.1), molecular slippage at a sharp interface may be prevented and a high joint strength will result.

Thus, in order to form a strong adhesive joint, the adherend surface should provide some chemical groups which can form strong interfacial attraction with the adhesives.

2.3 Surface Topography and Adhesion

Roughening the surface of adherend may increase the adhesive joint strength by several ways:

(a) Providing mechanical anchoring sites.
The mechanical anchoring sites will provide obstacles to failure through interface slippage, and hence improve the bondability of the adherends.

(b) Promoting wetting
Roughness tends to lower the contact angle when the intrinsic angle is less than 90°, or increase it when the intrinsic angle is larger than 90°[16]. As the contact angles of adhesives on adherends are usually less than 90°, roughness will improve the wettability of the adherends.

(c) Increasing the surface area
Compared with a smooth surface, a rough surface has a larger contact area, which will result in a larger joint area, thereby increasing the adhesive joint strength.

(d) Increasing fracture energy dissipation
The measured adhesive joint strength basically includes two components: the intrinsic adhesion and the energy dissipated, normally plastically at the tip of the propagating crack and plastically or viscoelastically in the body of the joint. The energy dissipation component usually predominates in measurements of joint strengths. Several research workers[17-22] have suggested that an increase in roughness may even increase the energy dissipated viscoelastically and plastically during joint failure.

(e) Randomising the directions of the interfacial weakness
If the macroscopic surface roughness is random, it can be effective in preventing any small cracks, flaws, voids or other points of stress concentration from aligning and rapidly propagating along any line of interfacial weakness in the joint, as might be envisaged in the case of a smooth planar interface.

However, exaggerated roughness may damage the surface since deep cracks lead to the trapping of air, vapours, water and other contamination, and also provide stress concentrations for the substrate, thus decreasing joint strength.

2.4 Weak boundary layer and adhesion

If any weak layer exists on the adherend surface, obviously, the locus of joint failure is likely to be through this region and a relatively low joint strength will be observed. Weak boundary layers are usually formed by low molecular weight species on the

surface, e.g. plasticizers which have migrated to the surfaces of polymers; contamination; layers of protective oils or greases and so on.

2.5 Other surface properties and adhesion

Other properties of material surface such as surface crystallinity, crosslinking, mobility of surface chain segments, glass transition temperature and solubility parameters also have an effect on the bondability of the adherends, according to the diffusion theory proposed by Voyutskii[23]. This theory states that the intrinsic adhesion of polymers to themselves (autohesion), and to each other, is due to mutual diffusion of polymer molecules across the interface. The theory requires that the macromolecules, or chain segments of the polymers (adhesive and substrate) possess sufficient mobility and are mutually soluble. This latter requirement may be restated by the condition that they possess similar value of solubility parameter[24]. The solubility parameter, δ_S may be defined by:

$$\delta_s = \left(\frac{\Delta H_v - RT}{V}\right)^{\frac{1}{2}} \qquad (2.1)$$

Where ΔH_V is the molar heat of vaporisation, R is the gas constant, T is the absolute temperature (K) and V is the molar volume. Hence, the solubility parameter is an index of the miscibility of two components, e.g. if an amorphous polymer and a solvent have similar values then they will form a solution.

2.6 Summary

Only when the adherend possess the first, second and some of the other surface properties listed below, does it have a good bondability.

(a) No weak boundary layers on the surface;
(b) Good wettability;
(c) Some chemical groups on the surface which can form strong interfacial attraction with adhesives;
(d) A specific surface topography which can form mechanical interlocking with adhesives;
(e) Miscibility with adhesives.

CHAPTER 3 SURFACE CHARACTERISATION

The selection of surface treatment methods requires careful evaluation. The most important factor is the effectiveness of the method. As discussed in the above chapter, the bondability of an adherend mainly depends on its surface properties. Thus, in order to evaluate the effectiveness of surface treatments and to understand the mechanism of bondability improvement, it is necessary to characterise the adherend surfaces before and after the surface treatment.

A variety of surface analysis techniques have been developed for the last twenty years, but not all of them are suitable for polymer surface analysis. Here are discussed only the methods which are effective to analyse polymer surfaces. Surface characterisation methods can be generally divided into three categories: contact angle measurement, microscopy techniques, and spectroscopy techniques.

3.1 Contact Angle Measurement

Contact angle measurement is mainly employed to evaluate the wettability of adherends. The surface energy of a polymer can be estimated by contact angle measurement using interfacial tension theory. The main advantages of this technique lie on two aspects: (a) it is highly surface sensitive as it depends on forces which are effective only over a few atomic diameters (accounts for a layer less than 1 nm)[25]; (b) it is simple and inexpensive.

3.1.1 Young's contact angle

Consider a drop of pure liquid with surface energy γ_{LV} resting on a smooth, homogeneous, rigid, isotropic solid surface with surface energy γ_S. When the system reaches equilibrium, the angle θ in Fig. 3.1 is called Young's contact angle (also called equilibrium contact angle).

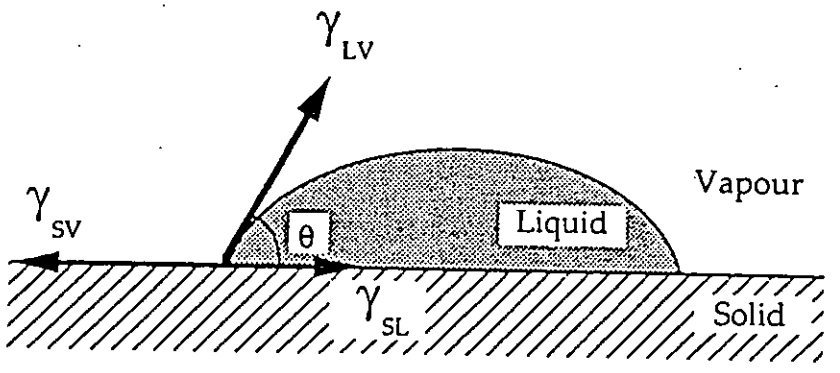

Fig. 3.1 Schematic illustration for Young's contact angle

The surface energy of the solid can be related to the Young' contact angle by the Young's equation (Eq. (3.1)).

$$\gamma_{LV}(1+\cos\theta)=\gamma_{SV}-\gamma_{LS}=\gamma_S-\gamma_{LS}-\pi_e \qquad (3.1)$$

where γ_{LV} is the surface energy of the liquid in equilibrium with its saturated vapour, θ is the Young's contact angle, γ_{LS} is the interfacial tension between the liquid and the solid, and γ_{SV} is the surface energy of the solid in equilibrium with the saturated vapour of the wetting liquid. The surface energy of the solid γ_S is

$$\gamma_S=\gamma_{SV}+\pi_e \qquad (3.2)$$

where π_e is the spreading pressure which represents the vapour pressure contribution to the spreading of the liquid on the solid. It has been suggested that π_e is negligible when $\theta>10°$[26-28]

3.1.2 Measurement techniques[29,30]

Choosing an appropriate contact angle measurement method is subjected to the nature of the sample and other practical factors (like convenience, etc.). For a flat surface, a variety of techniques are available for the measurement of equilibrium contact angle, including the sessile drop or the adhering gas bubble method, the Wilhelmy

gravitational method, the tilting plate method, and the reflection method. Among these, the sessile drop method is most widely used as it only requires a small amount of liquid and a small size of sample. Measurements can be carried out by directly observing the angle from the drop profile or drop dimensions, or by interference microscopy. By drawing a tangent to the profile at the point of three-phase contact after the drop profile has been enlarged either by image projection or photography, or by using a telescope fitted with a goniometer eyepiece. The accuracy of sessile drop method is commonly claimed to be about 2 degrees.

3.1.3 Contact angle hysteresis[31]

Many real surfaces are rough or heterogeneous. A liquid drop resting on such a surface may reside in a stable equilibrium (lowest energy), or in a metastable equilibrium (energy trough separated from neighbouring states by energy barriers). The equilibrium contact angle θ_e corresponds to the lowest energy state for the system. On an ideally smooth and compositionally homogeneous surface, the equilibrium contact angle is the Young's angle θ_Y, which is also the microscopic local contact angle on any rough or heterogeneous surface, hence it is also known as the 'intrinsic contact angle'.

Consider a liquid drop having a steady contact angle on a horizontal planar surface. If the surface is ideally smooth and homogeneous, the addition of a small volume of liquid from the drop will cause the drop front to advance, and the same contact angle will be obtained. Subtraction of a small volume of the liquid from the drop will cause the front to recede, and the same contact angle will again be formed. On the other hand, if the surface is rough or heterogeneous, addition of the liquid will make the drop grow taller without moving its periphery, and the contact angle will become larger. When enough liquid is added, the drop will suddenly advance in a jerk. The angle at the onset of this sudden advance is the maximum advancing contact angle θ_a. Removal of the liquid will make the drop become flatter without moving its periphery, and the contact angle will suddenly retract. The angle at the onset of this sudden retraction is the minimum receding contact angle θ_r. The phenomenon related to advancing and receding angles is known as hysteresis, and the difference $(\theta_a-\theta_r)$ is called the extent of hysteresis.

3.1.4 Estimation of surface free energy

Surface free energy has the same value with surface tension, but with different unit.

These two terms are frequently used interchangably in the literature. In this study, only the term of surface free energy was used.

A variety of methods[32-49] have been developed for the estimation of surface free energy using equilibrium contact angle results, e.g. Zisman and co-workers' approach[32-36], Good and Girifalco's approach[37,38], Fowkes' approach[26,39,40], Owens and Wendt's approach[41,42], Wu's approach[43-45], and other methods[46,47].

Here, we only discussed the geometric-mean method which is based on the Fowkes', the Owens and Wendt's and other researchers' methods and the harmonic-mean method which has been proposed by Wu.

3.1.4.1. Geometric-mean method

Fowkes[40] first proposed that the surface free energy of a pure phase, γ_a, could be represented by the sum of the contribution arising from different types of force components. He[50] identified at least seven components but Schultz *et al.*[51] have suggested that the surface free energy may be generally expressed by two terms, namely, a dispersion and a polar component, as shown in Eq. (3.3).

$$\gamma_a = \gamma_a^d + \gamma_a^p \qquad (3.3)$$

where γ_a^d is the dispersion force component and γ_a^p is the polar force component. This latter term incorporates all the non-dispersion force components. Fowkes[26,52] also proposed that the geometric mean of the dispersion force component is a reliable predication of the interaction energies at the interface caused by dispersion forces, hence the interfacial free energy between a saturated hydrocarbon liquid ($\gamma_{LV}^p = 0$, $\gamma_{LV} = \gamma_{LV}^d$) and a solid can be expressed as,

$$\gamma_{SL} = \gamma_S + \gamma_{LV} - 2(\gamma_S^d \gamma_{LV}^d)^{\frac{1}{2}} \qquad (3.4)$$

Owens and Wendt[41,42] and Kaelble and Uy[49] extended Fowkes' Equation (Eq. (3.4)) and introduced the following equation:

$$\gamma_{SL} = \gamma_S + \gamma_{LV} - 2(\gamma_S^d \gamma_{LV}^d)^{\frac{1}{2}} - 2(\gamma_S^p \gamma_{LV}^p)^{\frac{1}{2}} \qquad (3.5)$$

If one of the phases is nonpolar, Eq. (3.5) will be the same as Eq. (3.4).

Combining Eq. (3.5) with Young's equation (Eq. (3.1)) and neglecting the spreading pressure π_e gives

$$(1+\cos\theta)\gamma_{LV} = 2[(\gamma_{LV}^d \gamma_S^d)^{\frac{1}{2}} + (\gamma_{LV}^p \gamma_S^p)^{\frac{1}{2}}] \qquad (3.6)$$

Consequently, if the contact angles of two liquids on a solid surface are measured, simultaneous equations may be formed from Eq. (3.6) and solved to obtain values of $\gamma_S{}^d$ and $\gamma_S{}^p$. Or alternatively a straight line can be plotted with $X = (\frac{\gamma_{LV}^p}{\gamma_{LV}^d})^{\frac{1}{2}}$ and $Y = \frac{(1+\cos\theta)\gamma_{LV}}{2(\gamma_{LV}^d)^{\frac{1}{2}}}$, the slope here equals to $(\gamma_S^p)^{1/2}$, and the Y-axis intercept is $(\gamma_S^d)^{1/2}$. Hence, the total surface free energy of the solid surface γ_S, is then simply the sum of its components.

3.1.4.2. Harmonic-mean method

The harmonic mean method rather than the geometric mean method when calculating forces acting across the interface was proposed by Wu[43],

$$\gamma_{SL} = \gamma_S + \gamma_{LV} - 4(\frac{\gamma_S^d \gamma_{LV}^d}{\gamma_S^d + \gamma_{LV}^d} - \frac{\gamma_S^p \gamma_{LV}^p}{\gamma_S^p + \gamma_{LV}^p}) \qquad (3.7)$$

Eq. (3.7) was claimed to give more accurate results on the interfacial free energy between two polymers or between a polymer and an ordinary liquid[43,44]. Combining Eq. (3.7) with Young's equation (Eq. (3.1)) and neglecting the spreading pressure π_e, gives

$$(1+\cos\theta_1)\gamma_1 = 4(\frac{\gamma_S^d \gamma_1^d}{\gamma_S^d + \gamma_1^d} - \frac{\gamma_S^p \gamma_1^p}{\gamma_S^p + \gamma_1^p}) \qquad (3.8)$$

$$(1+\cos\theta_2)\gamma_2 = 4(\frac{\gamma_S^d \gamma_2^d}{\gamma_S^d + \gamma_2^d} - \frac{\gamma_S^p \gamma_2^p}{\gamma_S^p + \gamma_2^p}) \qquad (3.9)$$

Where $\gamma = \gamma^d + \gamma^p$ and the subscripts 1 and 2 refer to the testing liquids 1 and 2 respectively. If γ_j^p and γ_j^p of the testing liquids (j=1 and 2) are known, the dispersion and polar components of the solid surface energy (γ_S^d and γ_S^p) can be obtained from the contact angles θ_1 and θ_2 by solving the two simultaneous equations.

Water and diiodomethane are commonly used as the testing liquids in this method.

3.2 Microscopic Techniques

Complete analysis of an adhesion bond necessarily involves establishing the topography of the adherend surface, and the failure locus analysis. The microscopy methods are employed to fulfil this task. It includes OM (Optical Microscopy)[53], SEM (Surface Electron Microscopy)[54,55] and STEM (Scanning Transmission Electron Microscopy)[55]. Among them, SEM is most widely used. A comprehensively comparison for various microscopic techniques used in adhesion studies was made by Ledbury[56].

3.3 Spectroscopic Techniques

Spectroscopic methods are utilised to study the surface chemical compositions. Ideally, the surface sensitive techniques for surface chemical analysis[57] should provide elemental identification and a quantitative analysis of the first monolayer of the surface and identify the type of bonding present at the surface. In addition, the measurement process should not alter the surface; it should be capable of probing only a small surface area to resolve regions of inhomogeneity; it should have near-uniform high sensitivity for all elements; it should be suitable for any sample of interest; it should be amenable to rapid and simple measurement and analysis; and it should provide, or at least permit, a profile into the near-surface (<1 μm) region of the sample. However, no one technique satisfies all of these criteria. In some cases, it is not necessary that all criteria be met, then one analytical technique may be able to answer all the questions raised. In other cases, the surface will have to be examined by more than one method, thus leading to a more complete understanding of a problem.

The spectroscopic techniques mainly used for polymers include Surface Reflectance Infrared Spectroscopy (SRIRS), X-ray Photoelectron Spectroscopy (XPS), and Secondary Ion Mass Spectrometry (SIMS).

3.3.1 Surface Reflectance Infrared Spectroscopy (SRIRS)[55,58-61]

A number of reflection methods are used to study surface by infrared. Fig. 3.2 shows schematic diagrams of three types of reflection[55].

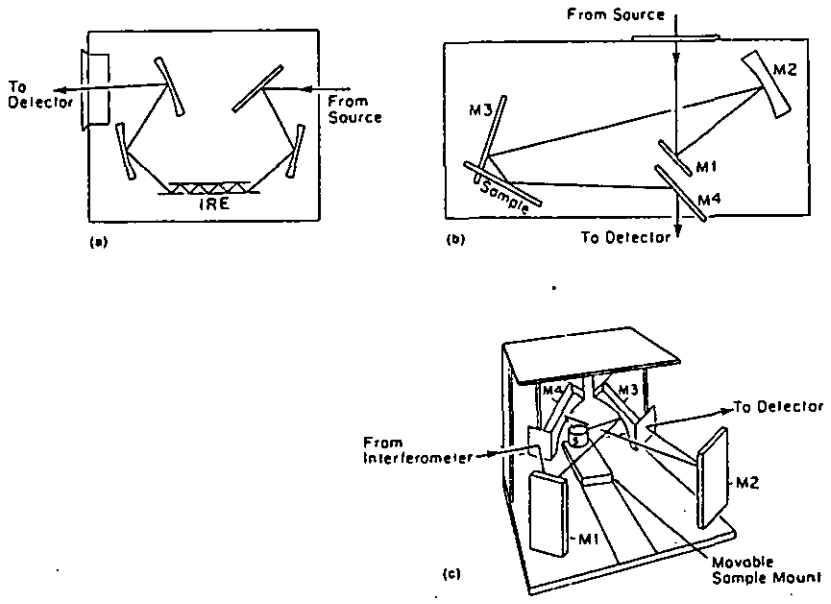

Fig. 3.2 IR reflectance attachments[55]: (a) MIR; (b) specular reflectance; (c) diffuse reflectance

An internal reflection technique commonly used is multiple internal reflectance or MIR, with a typical MIR cell shown in Fig. 3.2a. Samples such as polymer films, oils, or gels are put in intimate contact with a crystal of high refractive index such as

germanium or KRS-5 (bromide thallium iodide). When the angle of incidence of the light is higher than the critical angle for the crystal, internal reflection occurs through the crystal and the radiation is attenuated by absorption of radiation by the sample. in specular reflection, the sample itself is reflective (as shown in Fig. 3.2b). Either the substrate or a thin film in contact with the substrate can be studied making this an excellent technique for the study of interfaces. When the sample to be studied is not reflective, but rather scatters light, a diffuse reflectance attachment can be used, as shown in Fig. 3.2c, where the externally reflected light is scattered by the sample, collimated, and detected.

The advantage of SRIRS[55] is the ability to detect surface functional groups in contrast to the detection of surface elements by other surface analytical techniques. When infrared radiation impinges on a sample, groups of atoms (functional groups) absorb energy at characteristic frequencies, allowing for qualitative identification. Other information can be obtained from SRIRS include the molecular structure, orientation, chemical reaction, conformation, crystallinity and etc.

Therefore, reflectance infrared spectroscopy can yield chemical information about substrate surface composition and, important for the study of adhesion, interaction between adsorbed species and substrates.

However, SRIRS is not very surface sensitive compared with other surface analysis techniques. In MIR the sampling depth can be calculated by the following equation[58]

$$d_p = \frac{\lambda_0}{2\pi n_1 [\sin^2\theta - (n_2 / n_1)^2]^{\frac{1}{2}}} \qquad (3.10)$$

where d_p is defined at the distance below the surface at which the amplitude of the electric field is 1/e of its initial value, θ is the angle of incidence between the IR beam and the surface normal, n_1 and n_2 are the refractive indices of the reflecting element and sample respectively, and λ_0 is the wavelength of the radiation. Hence if we know the refractive indices for PEEK and the reflection element, the sampling depth of PEEK by MIR can be obtained from Eq. (3.10). Table 3.2 gives the sampling depth for PEEK at 1720 cm^{-1} with reflection elements germanium (Ge) and KRS-5.

Table 3.2 MIR conditions and sampling depth for PEEK at 1720 cm^{-1} with reflection elements germanium (Ge) and KRS-5.

Reflection element	n_2 / n_1^*	Angle of incidence	d_p / λ_0	d_p at 1720 cm^{-1} (μm)
GE	0.375	45	0.066	0.38
GE	0.375	60	0.051	0.30
KRS-5	0.625	45	0.200	1.16
KRS-5	0.625	60	0.111	0.65

* Ratio of refractive index of PEEK (for polymers in general $n_2 \approx 1.5$, hence the refractive index of PEEK was assumed as 1.5 here) to that of reflection element (Ge =4.0, KRS-5=2.4)[62]

3.3.2 X-Ray Photoelectron Spectroscopy (XPS)[57,63-65]

XPS or ESCA(electron spectroscopy for chemical analysis) is perhaps the most useful of the surface-sensitive technique for investigating problems associated with adhesive bonding, especially with polymer adherends, its sampling depth is about 3-5 nm [66].

In XPS a soft X-ray, usually Al Kα (1486.6eV) or Mg Kα (1253.6eV) irradiates the sample under ultra-high vacuum and causes photoelectrons to be ejected and detected. Elements are identified by their binding energies. The measured kinetic energy, E_k, of the ejected photoelectron is a function of the incident X-ray energy (hv), the binding energy of the photoelectron (E_b), and the work function Φ, as shown in Eq. (3.11)

$$E_k = h\nu - E_b + \Phi \qquad (3.11)$$

As the incident X-ray energy and the work function are constant for a given equipment, the binding energy of an electron, which is characteristic of the element to which the electron was bound, can be determined with high precision.

XPS has several advantages compared with other techniques. Firstly, it is not only capable of detecting relative changes in the surface composition as a function of different surface treatments, it can also provide a good absolute concentration for all elements except hydrogen. Additionally, the detection limits for all possible elements

generally vary less than an order of magnitude and average about 0.1-1 at%, with data acquisition times of several minutes[57]. (In principle the minimum detectable concentrations can be made as low as desired by increasing the data acquisition times; however, time constraints rarely permit significant improvements.)

Secondly, it provides information about the chemical state. This information is conveyed by shifts in binding energy of the photoelectron peaks, which occur as a result of the transfer of electrons from one atom to another during chemical bond formation. In many cases, the shifts are large enough so that the concentrations of the different chemical states can be easily determined separately. Tabulations exist of the chemical shifts for some element [63-65] to assist in the analysis.

Finally, the surface composition of nearly all vacuum-compatible samples can be measured by XPS with little, if any, chemical changes being caused for most classes of samples by the X-ray bombardment.

However, XPS measurement alone cannot achieve high reliability in qualitative or quantitative analysis as the chemically shifted peak can be obscured by peak overlap which is contributed by a variety of factors, including the small chemical shifts, energy resolution of the electron energy analyser and the line width of the photo source used. Hence measures capable of converting the functional groups into derivatives that are capable of more accurate XPS measurement have been tried[67-74]. It uses a chemical reagent which can react specifically with a particular kind of functional group. The derivative has a unique element, such as F, Br or Ag which can be easily detected and quantified by XPS, thereby indicating surface concentration of functional groups present on the surface. Chemical derivatisation reactions for some functional groups have been summarised by Briggs[67]. There are two kinds of derivatisation, one is solvent reaction[68,69], the other is vapour-phase reaction[70-74]. The latter is more commonly used, as the solvent derivatisation has some inherent problems. For example, the solvent used may increase the polymer chain mobility on the surface and result in the reorientation of some functional groups into the bulk; it could also dissolve low molecular weight materials on the surface into solution, especially for modified surfaces.

XPS can be applied to several aspects of adhesion studies, such as evaluating surfaces prior to bonding, which will yield whether the adherend has the functionalities which can assist bonding or if there are any contaminants on the adherend surface; and the failure analysis, which will decide the locus of failure in the system and also lead to

information about the reactions occurred in the interface.

3.3.3 Static Secondary Ion Mass Spectrometry (SSIMS)

SIMS is the mass spectrometry of ionised particles which are emitted when a surface, usually a solid, though sometimes a liquid, is bombarded by energetic primary particles. The primary particles may be electrons, ions, neutrals, or photons. The emitted (so called 'secondary') particles will be the secondary ions which are detected and analysed by a mass spectrometer. It is this process which provides a mass spectrum of a surface and enables a detailed chemical analysis of a surface or solid to be performed. In a development of SIMS those particles initially emitted as neutrals may be post-ionised and contributed to the analysis[75]

SIMS is usually operated in either dynamic or static mode. In the dynamic mode, a high flux of primary ions is directed at the material surface to obtain a very high yield of secondary ions. The surface is eroded (sputtered) very rapidly and it is possible to monitor changes of elemental composition with depth and thus a depth profile may be generated[76]. However, it is clear that analytical conditions using highly destructive primary beam densities are not suitable for surface analysis. In the static mode (SSIMS), which was introduced by Benninghoven [77], the current density of primary beam is maintained at a very low level so that secondary ions are emitted from area not previously damaged and the surface monolayer lifetime is many hours (well in excess of the time required for analysis). SSIMS also uses high sensitivity pulse counting devices which permit high analytical sensitivity.

Essentially static SIMS provides a mass spectrum of the surface. The mix of elemental and cluster ions in the spectrum can generate a rich store of information regarding the chemistry of the surface layer. It offers extreme surface sensitivity coupled with the ability to elucidate not only the elemental composition but also the chemical structure of surfaces.

Since 1980s, SSIMS has emerged as a complimentary technique to XPS for the surface analysis of polymers, and has been shown to provide valuable insight into the surface structure of conventional and surface-modified polymers[78-91]. The work done by Briggs and co-workers has proved that SSIMS can be used in the following three areas:

(a) high spatial resolution analysis of polymer surfaces[80]

(b) Identification of a broad range of polymers[78]
(c) imaging and microanalysis of the heterogeneous polymer surface using focused/scannable ion beams[79,87,88]

SSIMS can supplement XPS in many aspects, namely,

Firstly, from many direct comparisons of XPS and SIMS data from the same surface it is quite clear that SIMS is more surface sensitive than XPS (under routine conditions)[89]. It has been established[90] that the sampling depth of SIMS is generally about 1 nm, i.e. about two monolayers. This is routinely equivalent to that of very low take-off angle XPS.

Secondary, quantitative analysis of surface molecules is possible with XPS only when the molecule provides some spectroscopic feature that distinguishes it from the underlying substrate, e.g. a unique core level peak. However, most polymer molecules only contain the same principal elements as the common polymers (H, C, O, N), This is causing problems for XPS analysis. SSIMS has advantage over XPS in this area, it recognises molecules through their characteristic fragmentation patterns.

Thirdly, the ability to monitor XPS chemical shifts in electron binding energy due to changes in the chemical state of surface atoms has been particularly valuable. However, in many cases these shifts are very small and the resulting chemical state information can be rather imprecise. SSIMS can probe molecular structure more precisely because the mass spectrum is discrete and not superimposed on a continuum.

Finally, SSIMS can provide much better spatial resolution than XPS.

The applications of SSIMS in the field of adhesion are similar to those of XPS, i.e. contaminant detection; surface treatment effects monitoring; failure analysis and adhesion mechanism studying and etc.

3.4 Summary

A number of surface analytical techniques, of which only a limited number have been discussed above, are readily adaptable to the study of different aspect of adhesion.

The physical structure of adherend and failure surfaces can be obtained with microscopy methods, like SEM. The chemical compositions of surfaces and the

presence of contaminants and/or residuals can be determined using XPS and SIMS. These results are often correlated to bond performance aiding in determining mechanisms of bond failure. Surface functional groups are identified by SRIRS or XPS derivatisation. Indeed, basic questions in adhesion science, such as the mechanism of adhesion, bond durability, and locus of failure, can be addressed experimentally today with increasing confidence due to the availability of these techniques.

CHAPTER 4 EVALUATION OF BONDABILITY

The bondability of an adherend can be evaluated by several methods, which may be divided into before-bonding assessment and mechanical tests.

4.1 Before-bonding Assessment[92]

Prebonding assessment are designed to check the surface chemical or physical properties, as chemical composition, surface roughness, wettability, and etc.. These tests will not yield values of joint strength.

4.1.1 Physical-chemical analysis

Physical-chemical analysis techniques are commonly used to detect the presence of any surface contamination or to ensure that the surface pretreatment has been correctly carried out, and hence that good adhesion to the adherend should result. Obviously, modern surface analytical methods such as XPS may readily undertake these tasks, but these techniques are not non-destructive with respect to the specimen needed and the size of a typical bonded component, and are difficult to apply on a production line. Moreover, as no widely accepted quantitative relation has been established between surface properties and adhesion, this method is just qualitative.

4.1.2 Water-break test

The water-break test is very easily to carry out, it is based on the principle that a well-prepared surface will hold a continuous film of water rather than isolated droplets. A continuous water film indicates an adequate surface preparation has been achieved, whereas a break in the film is thought that there are some contaminants on the surface. However, the danger exists that a continuous film of water may form if a layer of the cleaning solution remains on the surface, and care must be taken to ensure that the surface is thoroughly dried.

4.1.3 Contact angle test

This test is based on the same principle as the last one. It measures wettability by determining the contact angle between the prepared adherend surface and a drop of

reference liquid, often distilled water. Large contact angles indicate poor wettability and inadequate surface pretreatment, whereas very small angles show the opposite.

4.2 Mechanical Tests

Mechanical tests are destructive, but can give quantitative results of the bondability of the adherends. In industry, they are also the only accepted methods for evaluating the bondability of adherends. The mechanical tests give two kinds of information about the bondability of adherends, their joint strength and failure locus. The first is the quantitative assessment of the bondability of adherends, while the latter can be used to evaluate whether the surface pretreatment is adequate or not. This section will briefly discuss the test methods and failure analysis.

4.2.1 Test methods

Many test methods have been developed in government laboratory, industry, and by university investigators. The American Society for Testing Materials (ASTM), has been particularly active in this respect. Finalised ASTM test methods are published in the ASTM standards. These tests can be rather generally classified in three groups, i.e., tension, shear, and peel (as shown in Fig. 4.1)

4.2.1.1. Tensile tests

Tensile tests are very simple tests (as depicted in Fig. 4.1). The tensile strength of the joint is determined by the maximum tensile load at fracture divided by the contact area of the bond. Common tensile tests can be found in ASTM standards, such as the "pi tensile test" described by ASTM D897, bar and rod tensile test described by ASTM D2094-69.

In all tensile tests, it is critical to properly align the specimens in the testing machine. Any misalignment will cause inconsistent load distribution and increase in data scatter. Another related problem is variation in adhesive thickness which causes nonuniform stresses in the adhesive and large scatter in the strength obtained.

It should be noted that it is difficult to compare tensile strength obtained from the different test techniques. Each method has unique stress distribution which alter the values of tensile strength. These variations in properties are also exhibited in the other testing modes.

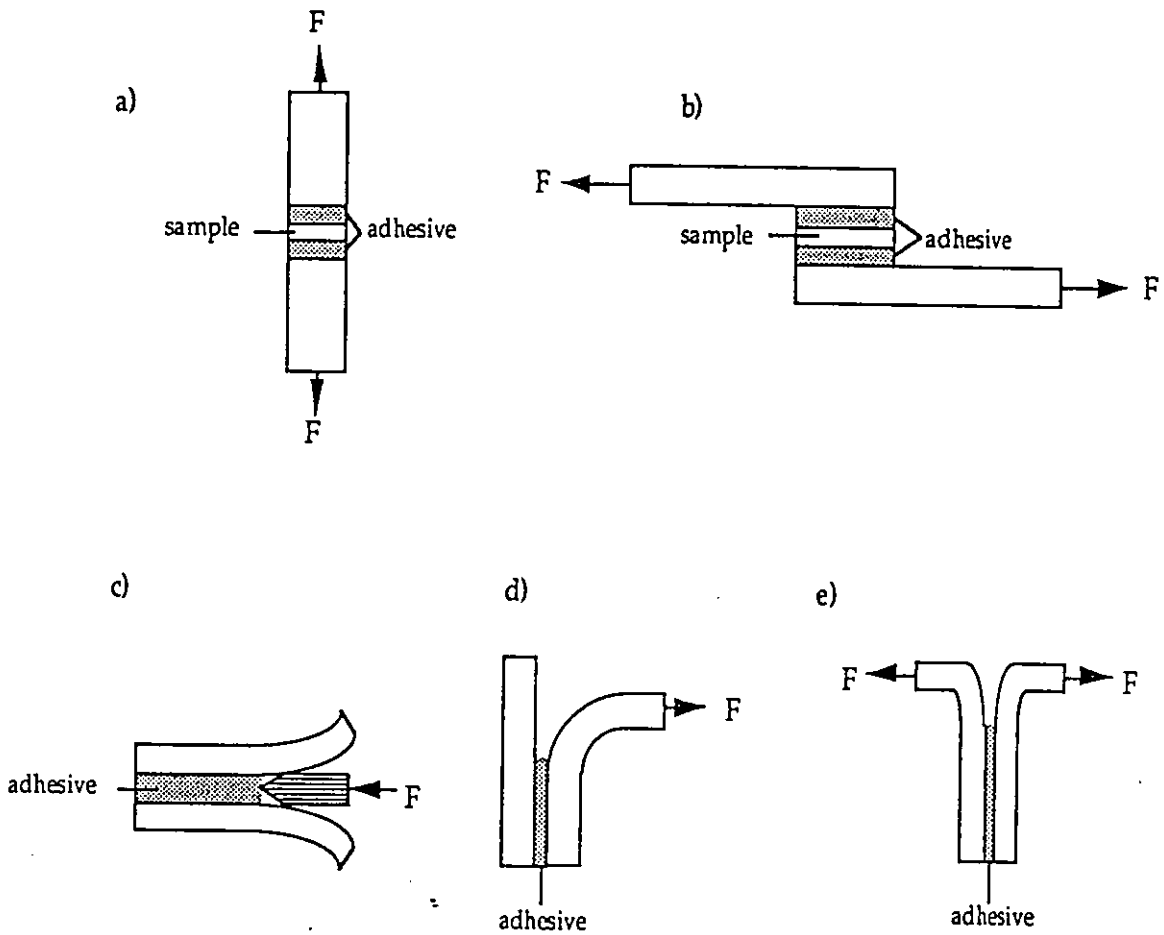

Fig. 4.1 Commonly used adhesion test methods[93] a)tensile, b)single lap shear, c)wedge, d)90°peel, e)T-peel. (The bondline thickness is much exaggerated)

4.2.1.2. Shear tests

Shear tests are very common because sample are simple to fabricate and closely duplicate the geometry and service condition. When applied loads act in the plane of the adhesive layer, the adhesive joint is considered to be in a state of shear. The shear strength is given as the load at fracture divided by the bonding area. In a shear test two things should be noted, one is that the stress distribution is not uniform, hence the maximum stress at the bondline may differ dramatically from the average; the other is that usually the stress is not pure shear and the actual state of stress depends on such factors as adhesive thickness, adherend stiffness, etc..

(a) Lap Shear tests

Lap shear tests involve two adherends which are overlapped by a certain length, while the adhesive forms the layer between the overlap area. Various lap shear tests have been described in ASTM standards, such as the single lap shear test described by ASTM D1002-72; the lap shear sandwich joint for testing plastic film (ASTM D3164-73, as depicted in Fig. 4.1); and the double-lap shear test (ASTM D3528-76).

The single lap-joint is the simplest and most common joint used today for several reasons [94]:

i. it is easy to fabricate;
ii. many designs used in industry rely on this overlap geometry as their foundation; and
iii. it is a common test piece used to determine the performance of adhesives

However, the stresses induced in a single lap-joint loaded in tension are quite nonuniform and complicated. Differential straining of the adherends in the overlap region produces shear stresses, whereas eccentric bending of the adherends (as shown in Fig. 4.2) produces tearing (peel) stresses. These two stresses are highest at or near the overlap ends.

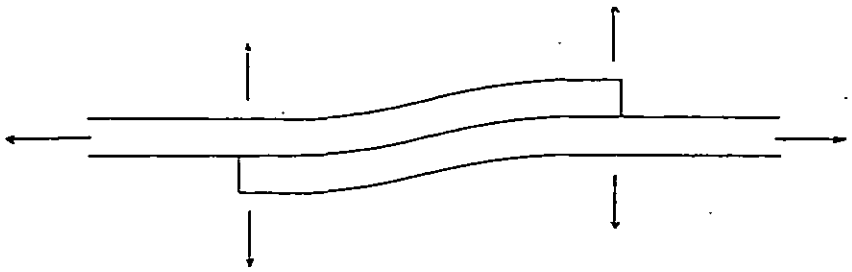

Fig. 4.2 Bending of the overlap region of a loaded single lap joint [95]

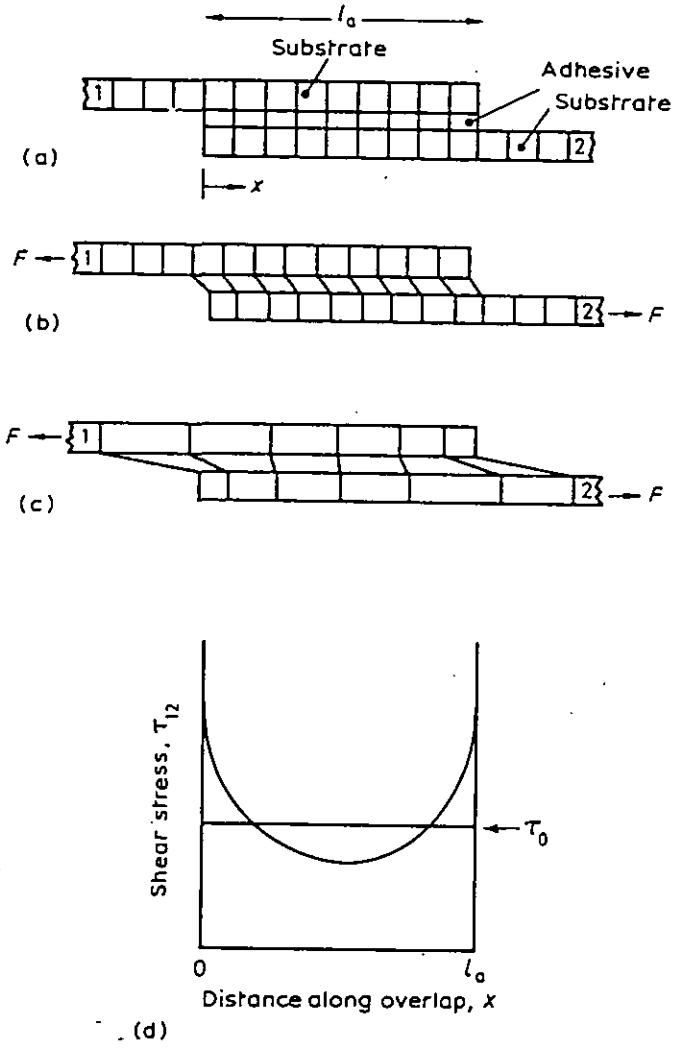

Fig. 4.3 Schematic representation of single lap-joint[95a]. (a) Unloaded; (b) loaded in tension, inextensible substrate; (c) loaded in tension, elastic substrates; and (d) distribution of elastic shear stress in the adhesive layer.

resembling a single-lap bond.

(c) Torsional shear test

A torsional shear test is described by ASTM E229-70. This test can provide very uniform stress distribution and the bond system is in an almost pure shear condition.

For every shear test, as in tensile tests, sample alignment, adhesive thickness etc. have to be well controlled.

4.2.1.3. Peel tests

In general, peel tests involve the controlled stripping of a flexible adherend that is adhesive bonded to either a flexible or rigid adherend. The peel forces are determined by the average load needed to maintain the peeling of the adherend after initiation. Average peeling forces are obtained from plots of the peeling load versus the peeling distance. The peel strength is quoted as force per unit width.

There are several kinds of peel tests, one of the simplest is the T-peel test (as depicted in Fig. 4.1, described by ASTM D1876-72). In this test, part of two flexible adherends are bonded together, while the unbonded ends are bent at 90° to the adhesive layer.

ASTM D903-49 describes a 180° peel test, in this test, a flexible adherend is peeled at an angle of 180° from either a flexible or rigid adherend.

ASTM D1781-76 and ASTM D3167-76 describe a climbing drum peel test and a floating roller peel test respectively, both of them are used to determine the adhesive performance of bonding metal or composite skins to honeycomb structures.

In peel tests, peeling angle and adhesive thickness should be controlled and hold constant as they affect the peel strength significantly. It should be also noted that the stress distribution is not simple and can depend on a number of the testing parameters, including geometry.

Fig. 4.5 schematically shows the peeling of a flexible adherend from a rigid adherend, to which it is bonded using a flexible adhesive [97]. The specimen is placed on the abscissa with its origin O at the point of detachment where the normal tensile stress in the adhesive is the greatest. In the region AO (curved region), the peeling strip is

the rigid adherend. If there are no unbroken ligaments, the normal stress should drop to zero at a distance infinitesimally to the right of the origin O. However, because of the unbroken ligaments, large tensile stresses persist in the region AO. In the region to the right of A (straight region), the peeling strip becomes straight and coincides with the direction of applied peel force P. The angle between the applied peel force and the rigid adherend is the peel angle θ. In the region OD (strained region), the cleavage stress is a highly damped harmonic function consisting of alternating zones of tension and compression. In the region to the left of D (unstrained region), the original adhesive bond is not disturbed.

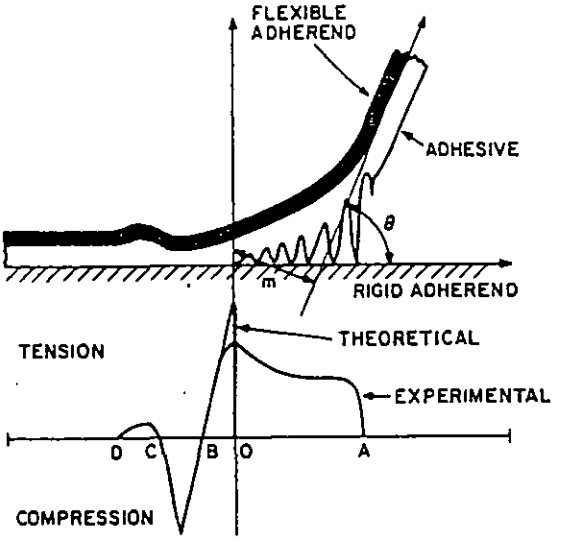

Fig. 4.5 Schematics of peel profile and normal stresses in adhesive layer [97]

Kaelble (98-99) gives the theoretical cleavage stress σ at a distance -x from the point of rupture O (x=0) as

$$\sigma = \sigma_0(\cos\beta x + K\cos\beta x)\exp(\beta x) \qquad (4.1)$$

where

$$\beta = (\frac{E_a b}{4EIt_a}) \qquad (4.2)$$

$$K = \frac{\beta m}{\beta m + \sin\theta} \qquad (4.3)$$

σ_0 is the boundary cleavage stress at x=0, E_a the elastic modulus of the adhesive, E the elastic modulus of the flexible adherend, t_a the adhesive layer thickness, b the bond width, I the moment of inertia of the peeling strip cross section, m the moment arm of the peel force, and θ the peeling angle.

Hence according to Equation 4.1, the reduction of stress concentration and consequent improvement in joint strength can be achieved by [95]

i. increasing adhesive flexibility i.e. reducing E_a
ii. increasing the modulus of the tape E
iii. increasing thickness of the tape
iv. increasing glue line thickness

4.2.2 Failure analysis

Failure analysis is a critically important aspect of evaluating the bondability of adherends. Identification of the locus of failure can provide useful information, such as effectiveness of surface treatment; cause of the failure; mechanisms of crack initiation and propagation and identification of the weakest point in adhesive joint.

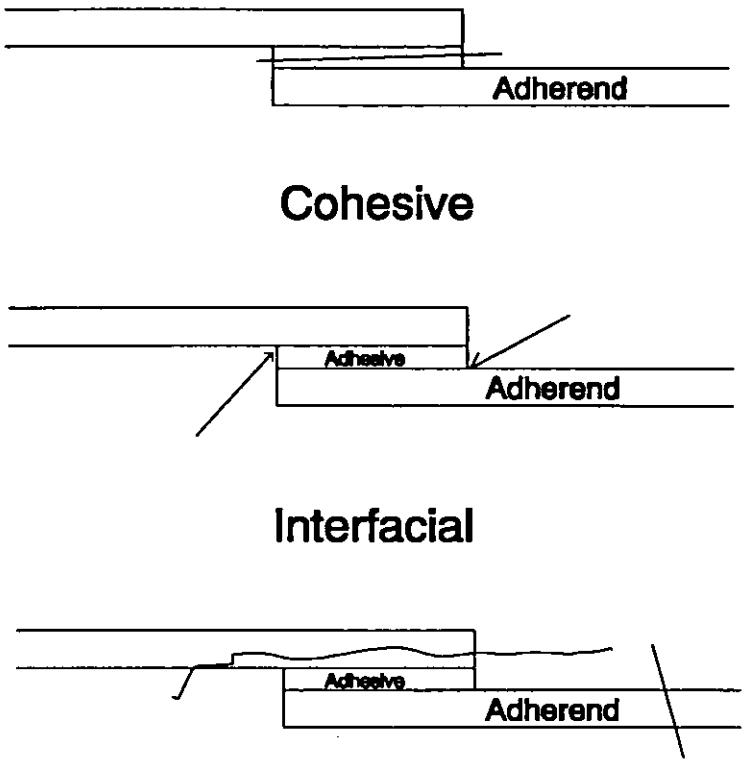

Fig. 4.6 Failure Modes of Adhesive Joints[95]

Bond failure occurs in one, or a combination of the following three modes [95] (as shown in Fig. 4.6): cohesive; interfacial (adhesive); or material. Cohesive and material failure are identified as fracture occurs within the adhesive system and in the adherends respectively. These kinds of failure indicate that the adherend has a very good bondability and the ultimate performance has been reached for the joint of this adherend and a given adhesive. Improved performance can only be achieved by redesigning the joint or by replacing the weakest component i.e. the adhesive or the adherends. On the other hand, an interfacial failure is defined as a fracture occurring along the adhesive/adherend interface, which indicates that the bondability of the adherends is not optimum and that further bond performance can be obtained by strengthening the interface, in other words by selecting a suitable surface treatment for the adherend.

Failure analysis usually goes through two steps: the first step is a visual inspection. In a few cases, this examination is sufficient to identify the locus of failure, such as a

failure occurring through the middle of an adhesive. However, in most situations, this may not be possible as the eye is not usually able to detect a layer less than 100 nm thick on a sample[57]. For example, a failure may visually appear adhesive, but the real fracture may occur within one of the bond components close to the interface. The second step is examining the surface by surface analysis techniques, e.g. SEM and XPS.

Several aspects are worthy noting in failure analysis, firstly, it is preferred to examine both sides of the failure, otherwise, the identification of the failure locus can only be inferred and cannot usually be conclusively established. Secondly, post-failure contamination should be avoided, as it can irreparably alter the surface chemistry. Thirdly, post-failure damage of the surface should be also avoided, or it is impossible to detect the actual locus of failure. Fourthly, it is important to realise, that SEM specimens are routinely coated with a conductive film. This film may mask the fine structures of the surface morphology that could help to determine the locus of failure.

CHAPTER 5 SURFACE PRETREATMENT OF PEEK AND ITS COMPOSITES

Proper adherend surface pretreatment is critical for a good adhesive bond. The purpose of any particular surface pretreatment may be manifold, but the main aims are usually to produce one or more of the surface properties discussed in chapter 2.

As the bondability of untreated PEEK and its composites is very poor, a variety of surface pretreatment methods have been employed to improve their bondability. In this chapter, a briefly review is given from the relevant articles recently published.

5.1 Solvent Cleansing

Solvent cleansing is the simplest surface pretreatment method, its main purpose is to remove any contamination on the surface. This treatment is carried out either with vapour, or by wiping the surface with solvent-dipped clean cloths, or most effectively in liquid and vapour degreasing baths, possibly using an ultrasonic agitator.

Though solvent cleansing is quite effective for some materials, such as epoxy based composites, it seems to have no effect on PEEK and its composites[6,7,100-103]. Kinloch and Taig[6] found that if continuous carbon fibres reinforced PEEK is bonded with a structural epoxy adhesive, the solvent-wiping treatment is clearly inadequate. The resulting joints are weak and the locus of joint failure occurs at the interface between adhesive and the PEEK composite. These results indicated that in order to enhance the bondability of PEEK or its composites, their surface physical and chemical properties should be modified.

5.2 Mechanical Abrasion and Blasting

5.2.1 Introduction

The main purposes of mechanical abrasion and blasting are to roughen the surface of the adherend and remove any weak boundary layers.

The methods available include wire brushes, sand and emery papers, abrasive pads and grit- or shot-blasting. The techniques of grit- or shot- blasting give the most reproducible results and, are preferred for industrial processes. The equipment basically consists of an air pressure-fed grit-blasting machine in which the abrasive is stored in a pressure vessel, and is introduced through a small feed orifice into the blast line. The abrasive is typically angular chilled iron abrasive of size G04 to British Standard 254 or angular alumina abrasive of 180/220 mesh. It is ultimately propelled through a nozzle of convergent/divergent cross-section onto the work surface [104].

5.2.2 Abrasion

Though abrasion is effective for some materials, such as thermosetting composites, it results in low-strength bonds with failure in the PEEK or its composites/adhesive interface[7,100,103].

Hamdan and Evans[100] obtained very low joint strength (as shown in Table 5.1) by abrading PEEK strips with 600 grade silicon carbide paper and then degreasing the surface.

Table 5.1 Effects of abrasion on the lap shear joint strength of PEEK and its composites/adhesive joints (ref. 100)

Adherend	Adherend thickness	Shear strength (MPa)	Failure locus
Unreinforced	3 mm	2.3	I
20 Vol% glass reinforced	3 mm	2.8	I
20 Vol% glass reinforced	9 mm	3.6	I

I: Interface

The data in Table 5.1 (taken from ref. 100) show that abrasion treatment is ineffective in producing a high joint strength. The abraded surface revealed by SEM did not show pronounced roughness or re-entrant contours, and the fracture surface is at, or very close to, the interface.

5.2.3 Blasting

Compared with abrasion, blasting pretreatment is much more effective to improve the bondability of PEEK and its composites[100-103].

Silverman and Griese[102] employed Al_2O_3 grit to blast AS-4/PEEK lap shear coupons until the blasted surface had a uniform surface appearance. Samples were then scrubbed clean in deionized water and dried. Using FM 300 film adhesive, the lap shear strength reached 20.9 MPa, and failure occurred in the adhesive. In this study, the increase of surface area available for bonding with the adhesive was believed to be the main mechanism of bondability improvement.

YOON and McGraph found[103] that grit blasting increased the bond strength of APC-2/AS-4 PEEK/Graphite composite, using PI-30% polydimethylsioxide (PDMS) adhesive, by about 300% compared to that obtained with wash only. By utilising SEM and XPS to characterise the treated surface, they showed that:

(a) The surface of washed samples were relatively smooth and flat, except for the small portions of fibres exposed. Grit blasting, however, removed the top layer of the matrix and left bare fractured fibre pieces.

(b) Washed samples exhibited three peaks at binding energy values of 285, 286.7, 288 and 291.6 eV which may correspond to C-C, C-O, C=O bonds and satellite peak from aromatic rings of PEEK[102,105], while grit blasted sample showed an additional peak at 289.5 eV, which probably corresponds to the O-C=O groups. From these results they concluded that the bond strength increase could be attributed in part to O-C=O bonds but was mainly due to cleaning and surface roughness effects.

However, Davies *et al.* [106] obtained different results. They employed 150μm sand particles to blast the PEEK/carbon fibre composite surface. This treatment alone resulted in low strength bonds(less than 8 MPa, lap shear strength) with failure at the composite-adhesive interface.

Thus, the results of mechanical abrasion and blasting suggest that simple roughening the surface is not adequate for improving the bondability of PEEK and its composite and modification of the surface chemical compositions is needed.

5.3 Chemical Treatment

5.3.1 Introduction

Chemical treatment can cause physical and chemical changes on the surfaces. When a polymer is soaked in a strongly oxidative chemical liquid and treated under suitable conditions, polar groups are introduced on the polymer surface and the surface characteristics are improved. Various types of chemicals, such as chromic/sulphuric acid[7,102,106], tetra-etch solution (mixed naphthalene and tetrahydrofuran with metallic sodium)[7], potassium permanganate-sulphuric acid mixtures[101] (1% solution of potassium permanganate in a 5:2:2 solution of sulphuric acid, orthophosphoric acid and distilled water), sulphuric/dichromate mixture[100] (300g/l sulphuric acid (SG=1.84) and 75g/l dichromate), nitric/sulphuric acid mixtures[100] (one part by volume nitric acid (SG=1.42) and 3 parts by volume sulphuric acid (SG=1.84) diluted to 10% with distilled water, a solution of 1g 2,4-dinitrophenylhydrazine with 3 ml of methanol and 2 ml of sulphuric acid[100] have been employed to modify the surface of PEEK and its composites. Among them, the most effective and common chemicals are chromic/sulphuric acid and sulphuric/dichromate.

5.3.2 Adhesion studies

Davies *et al.* [106] reported results using chromic/sulphuric acid solution at room temperature to treat carbon fibre reinforced PEEK composites. As short treatment of a 5s acid etching shifted the failure locus from the interface to the adhesive. A 7.5 min or longer treatment resulted in lap shear strengths that were as high as it is possible to be obtained with the given specimen geometry.

Employing chromic/sulphuric acid, Wu *et al.* [7] obtained similar results. The lap shear test results for Graphite/PEEK laminates after acid treatment, was over 28 MPa using FM 300 adhesive film.

To understand better the effect of chromic/sulphuric acid etching on the composite surface, AS-4/APC-2 laminated were etched at different temperatures for various times. The lap shear test results are presented in Table 5.2[7], which show that the bond strength increased with exposure time, but only to a point. It was observed that at room temperature a 15 min etching of AS-4/APC-2 composite gave a proper surface for good adhesive bond strength.

The chromic/sulphuric acid treated surfaces were also bonded with other film adhesives. The results are summarised in Table 5.3[7]. The chromic/sulphuric acid etched surface provided stronger bond strengths with both epoxy and bismaleimide film adhesives. It seems that the chromic/sulphuric acid etching is a very good method to prepare PEEK composite surfaces for adhesive bonding.

Table 5.2 The effect of chromic/sulphuric acid etching conditions on the adhesive bonding (from ref. 7)

Chromic/sulphuric acid etching		Lap shear strength (MPa)	
Temperature(°F)	Time (min)	FM-300	EA-9673
120	20	26.3	----
Room Temperature	60	24.5	----
	30	----	21.3
	15	----	22.8
	10	----	18.8
	5	----	17.8
Untreated		13.6	8.9

Table 5.3 Adhesive bonding of AS-4/APC-2 laminates (from ref. 7)

Adhesives	Lap Shear (MPa)
FM-300	30.3
FM-137	21.4
FM-250	23.5
FM-73	22.7
EA-9673	21.3
R-319A	18.9
Torlon Tape (a)	17.7
PEEK film (a)	25.4

(a): Lap shear coupons were bonded with an ultrasonic welder

In order to study the mechanism of bondability improvement, Evans *et al.* [107] employed XPS, SEM and contact angle measurement to characterise the surfaces of PEEK before and after chromate etching.

The XPS survey spectrum for the chromate etched unreinforced polymer was very similar to that of the polished sample, but clearly showed an increased oxygen content (130%) on the surface compared with the stoichiometric value. O_{1s} spectra indicated that the carbonyl oxygen peaks at 532 eV has increased as a result of oxidation and accounts for most of the oxygen present. The form of the oxygen peak was quite different from that for the untreated polymers. The C_{1s} spectrum was modified after etching, showing an increase in the size of peaks at higher binding energies, which corresponds to carbon-oxygen bonds, and the appearance of a new peak at 289 eV.

Surface energy data shown in Table 5.4 indicate that the polar component of the surface energy was significantly increased by the chromate etching, confirming the XPS results.

Table 5.4 Effects of chromate etching on the wettability of PEEK (after ref. 107)

Treatment condition	Contact angle (degree)				Surface energy (mJm^{-2})		
	water	GC	FMD	TTPH	γ_S^d	γ_S^p	γ_S
Chromate-etched (30min, 65°C)	58	50	32	18	30	18	48
Polished and degreased	79	65	64	24	31	5	36

GC: glycerol
FMD: formamide
TTPH: tritolyphosphate

The surface topography was also affected by the etching treatment[7,107]. In view of the limited effect of abrasion on adhesive joint strength, this roughening effect was considered to have little effect on adhesion enhancement.

5.4 Plasma Treatment

5.4.1 Introduction

Plasma is an excited gas which consists of atoms, molecules, ions, free radicals, free electrons and metastable species[108]. The use of plasma to treat polymers has been known for more than 20 years. Plasma employed for surface treatment is usually a low temperature plasma, generated under reduced pressure.

In plasma treatment of materials, all significant reactions are thought to be based on free radical chemistry[108]. The low temperature plasma is efficient in creating a high density of free radicals, both in the gas phase and on the surface of organic materials, even the most stable polymers. These surface free radicals are created by direct attack of gas-phase free-radicals, ions, or by photodecomposition of the surface by vacuum-ultraviolet light generated in the primary plasma. The surface free-radicals then are able to react either with each other or with species in the plasma environment.

The major effects of a plasma pretreatment may include the following: (a) surface cleaning; (b) ablation and degradation, a form of dry micro-etching; (c) crosslinking; (d) surface activation; (e) polymerisation and grafting; (f) ion implantation.

These effects may occur concurrently and, depending on processing conditions and reaction chamber design, one or more of these effects may predominate. In all cases, these processes affect only the top surface layers and do not change the appearance or bulk properties of the material[109,110].

Many different gases and plasma operating parameters are used in the surface treatment of different polymers. It has been found that, for best results (in terms of bondability), different polymers may require a different plasma treatment. In some cases it has been noted that a plasma which gives excellent bonding on one polymer may give very poor bonding on another polymer.

5.4.2 Adhesion studies and surface characterisation

Surface characterisation of plasma treated PEEK and its composites has been carried out by many researchers[7,97,100,102,103,106,107,111-113], However, bondability studies have been made mainly on composites with PEEK as a matrix..

Plasma treatments has been found to enhance the bondability of PEEK composites significantly[7,100,102,103,106,111], no matter which gas is employed, as shown in Table 5.5.

Table 5.5 The effect of various plasma on the lap shear strength of APC-2/AS-4 composite Joints

Treatment Condition	Adhesive	Adherend	Lap shear strength(MPa)
O_2, 5 min[103]	PI-30%PDMS	APC-2/AS-4	32.6
NH_3, 5 min[103]	PI-30%PDMS	APC-2/AS-4	33.3
O_2, 15 min, 0.3 Torr[7]	EM-300	APC-2/AS-4	28.2
CF_4+O_2, 5 min[102]	FM-300	CARBON/PEEK	42.2

Table 5.6 Tensile strength of plasma-treated Carbon/PEEK composite joint as a function of treatment gas, RF power and treatment time (after ref. 111)

Gas Type	Power (W)	Time (S)	Tensile strength (MPa)
----	----	----	0
Oxygen	20	30	9.1
Nitrogen	20	30	11.3
Argon	20	30	9.9
Oxygen	100	30	9.8
Nitrogen	100	30	11.0
Argon	100	30	9.0
Oxygen	50	60	9.7
Nitrogen	50	60	11.8
Argon	50	60	11.5
Oxygen	30	30	8.9
Nitrogen	30	30	8.8
Argon	30	30	11.8

Occhiello *et al.* [111] studied the effects of plasma processing parameters on the tensile strength of joints of Carbon/PEEK composite with conventional epoxy adhesive, and found that plasma treated samples reached high strengths and cohesive failure even with very short treatment times (<30S). Tensile strengths were relatively insensitive to the nature of the treatment gas and plasma parameters. (As shown in Table 5.6).

To analyse the mechanism of bondability enhancement, XPS, SEM and Contact angle measurement were used to characterise the plasma modified surfaces of PEEK composites.

SEM studies revealed that[103] the roughness of the composite (APC-2/AS-4) surface was slightly changed by an oxygen plasma treatment of 5 min, but no difference was observed for the sample treated by ammonia plasma for 5 min even though both treatments enhanced the bond strength greatly. The results indicated that the bondability improvement is due to other mechanisms.

XPS studies shown a different trend, after plasma treatment, the surface oxygen/carbon ratio increase considerably[7,103,106,111] (as shown in Table 5.7)

Table 5.7 XPS compositions (atom%) of untreated and plasma treated Carbon/PEEK samples (After ref. 111)

Sample	O	C	N
Molecular Structure	13.6	86.4	0
Untreated	13.9	86.1	0
Oxygen Plasma Treated	24.9	75.1	0
Air Plasma Treated	23.3	72.5	4.2
Nitrogen Plasma Treated	24.5	70.8	4.7
Argon Plasma Treated	20.3	76.7	3.0

Washed APC-2/AS-4 samples exhibited three peaks at binding energy of 285, 286.7, 288 and 291.6 eV which may correspond to C-C, C-O, C=O bonds, and satellite peak from the aromatic rings of PEEK[102,105]. Oxygen plasma treatment of 5 min enhanced the intensity of the peaks corresponding to C-O and C=O bonds, and generated a new peak at 289.5 eV corresponding possibly to O-C=O bond. However, NH_3 plasma treatment of 5 min showed only three peaks at 285, 288 eV corresponding possibly to C-C, C-N and C=O bonds, together with a very weak satellite peak[103]. The peak at 286.5 eV could be a mixture of C-O and C-N bonds[112]. The deconvolution exercise indicated that the bond strength increase after oxygen plasma treatment of 5 min could be attributed to O-C=O as well C=O bond, while the adhesive bond strength enhancement by NH_3 plasma for 5 min could be due to C=O bond and possibly to C-N bonds.

Another significant effect of plasma treatment is the improvement of wettability. By contact angle studies, Occhiello *et al.* [111] found that both advancing and receding angle of water for carbon/PEEK composites decreased greatly by various type plasma treatments. This is believed to be the results of the introduction of polar groups on the composite surface.

Thus, the increased joint strength of PEEK composites by plasma treatment is thought to be due to the introduction of polar groups and the increased wettability. However, the mechanism of plasma treatment has not been clearly elucidated, as the composition of the surface after plasma treatment is still not clear because of the limitation of surface analysis techniques employed, XPS peak fitting cannot, in fact, confirm the existence of specific chemical groups.

5.4.3 Effects of Ageing

Table 5.8 Effects of storage conditions on the tensile joint strength and contact angle of Carbon/PEEK composite (after ref. 111)

Treatment Condition	Ageing Time (day)	Contact Angle (degree)		Pull Strength (MPa)
		Advancing	Receding	
O_2, 50W, 30S	0, RT	23	7	8.9
	14, RT	32	8	9.3
	6h,120°C	35	10	9.3
Air, 50W, 30S	0, RT	24	8	8.8
	14, RT	34	10	9.2
	6h,120°C	34	9	9.2
N_2, 50W, 30S	0, RT	28	9	11.8
	14, RT	32	9	12.1
	6h,120°C	33	8	12.1
Ar, 50W, 30S	0, RT	27	10	9.9
	14, RT	35	9	12.9
	6h,120°C	36	11	12.9

For plasma treated Carbon/PEEK composites, it seems that exposure to air for more than 10 days or 120° for 6 hours does not make much difference to its surface

properties. Only the contact angle with water and the tensile joint strength increase slightly, as shown in Table 5.8, suggesting that the surface of plasma treated carbon/PEEK is very stable.

However, for unreinforced PEEK, though no adhesion properties versus ageing condition have been reported, some other surface properties have been found to be changed significantly with the ageing condition.

Brennan *et al.* [113] studied the ageing behaviour of oxygen plasma treated unreinforced PEEK, and showed that some hydrophobic recovery occurs upon ageing. They found that:

(a) Immediately after treatment most samples were almost completely wetted by water. After approximately 5 min the contact angle could be measured and was found to be in the region of 4° to 15°, tending to be lower for the less crystalline samples.

(b) Temperature has a remarkable effect on contact angle. The higher the ambient temperature, the more rapid is the attainment of the plateau contact angle.

(c) XPS studies show no significant increase in the amount of oxygen at take off angle of either 70° or 35°. However, the C_{1s} envelope does show an apparent increase in the proportion of oxygen functionalised carbon to hydrocarbon.

From the above results, the authors concluded that:

(a) The initial very rapid change in contact angle observed in the first few minutes after plasma modification is probably due to the reorientation of highly mobile fragments created by the treatment. The change in the surface over the next few days are due mainly to migration of fragments from the surface into the bulk.

(b) Increasing the crystallinity and orientation of the samples increase the degree of order and reduces the free volume in a significant proportion of the polymer matrix. This hinders the movement of the polymer chain and therefore slows the ageing processes which give rise to migration and reorientation. Conversely, raising the temperature of the PEEK increases the mobility of the polymer chains, that causing the ageing processes to occur at a faster rate.

Previous work on ageing effects has shown, therefore, that up to almost 15 days ageing does not affect the bondability and wettability of PEEK composites. However, studies for longer ageing period are necessary as several months ageing is sometimes experienced in the industry before a joint is made.

5.4.4 Effects of solvents

Pawson *et al.* [97] investigated the effects of rinsing the plasma treated PEEK surface with methanol. Employing XPS and TOF-SIMS these authors found that there are several points worth noting

(a) Low molecular weight molecules (LMWM) created on the polymer surface by the plasma is easily removed by rinsing the polymer surface with a non-solvent for the polymer. Removal of LMWM from the polymer surface considerably reduces the complexity of both the TOF-SIMS and XPS spectra. From the XPS spectra it is evident that the LMWM removed by rinsing contains a high proportion of phenols and of more highly oxidised carbon functionalities (e.g. carbonyls, carboxylates, carbonates).

(b) However, rinsing does not regenerate the TOF-SIMS and XPS spectra of clean PEEK. The XPS spectra reported show a small, but significant, concentration of phenolic alcohols and acid groups (or similar) remain in the rinsed polymer surface. In the ToF-SIMS spectra, the low intensities of ions diagnostic of PEEK indicate that the plasma treated and rinsed surface as structurally different to that of the original PEEK.

(c) In both the positive and negative ions ToF-SIMS spectra a series of new ions are revealed by rinsing the plasma treated surface. Free radicals created in the polymer surface by the plasma may combine to cross-link the polymer surface. Further, oxygen incorporation into the benzene rings does not result immediately in chain scission, and in the production of LMWM. Both processes will produce a surface that is stable to methanol rinsing. Methanol rinsing possibly has the effect of revealing surface structures masked by the presence of the LMWM.

Thus, methanol can change the surface composition of oxygen plasma treated PEEK, but the effects of methanol or other solvents on the bondability and wettability of plasma treated PEEK are still unknown.

5.5 Corona Discharge Treatment

5.5.1 Introduction

Corona is a term used to describe a gas discharge generated in air at atmospheric pressure. It is composed of ions, excited atoms and molecules, electrons, etc. A detailed descriptions of various corona discharge can be found in ref. 114. The effects of corona discharge treatment is similar to the plasma treatment. But the former has both an advantage and a disadvantage as it is generated in air, the advantage is that it is easily set up with low cost and also easily applied in the industry; the disadvantage is the composition of a corona discharge is not as easily controlled as in plasma treatment.

5.5.2 Adhesion studies

Corona discharge treatment was employed by Kinloch and co-workers[101,115-117] to improve the bondability of PEEK composites (APC-2). They studied the effects of corona discharge treatment on the fracture energy (G_C) of the adhesive joint, wettability and surface compositions of APC-2. Their results can be summarised as follows:

Table 5.9 Effects of corona discharge treatment on the adhesive bonding of APC-2 (from ref. 117)

Treatment level(i) ($J\ mm^{-2}$)	9303 Adhesive		FM73M adhesive	
	$G_C(kJ\ m^{-2})$	L of F (ii)	$G_C(kJ\ m^{-2})$	L of F
0.0	0.015	interf.(iii)	0.015	interf.
0.5	0.038	interf.	0.17	interf.
1.0	0.11	interf.	0.54	interf.
5.0	0.96	interf.	1.44	interf.+cohesive
10.0	1.74	interf.+cohesive		cohesive
20.0	3.79	cohesive	1.84	cohesive
30.0	3.85	cohesive	1.86	cohesive

(i) Treatment level is energy output of corona;
(ii) "L of F" is locus of failure;
(iii) "interf." is interfacial failure.

(a) The corona discharge treatment increased the adhesive fracture energy of APC-2 significantly. Increasing the corona power can increase the adhesive fracture energy, but only to a point, after that, the fracture energy remains the same as the corona power increased further, as shown in Table 5.9.

(b) The corona discharge treatment also increased the wettability of APC-2 greatly. The contact angle of double-distilled water on the APC-2 decreased from about 80° to about 3° as the energy level of the corona discharge treatment was increased from 0 to 20 J mm^{-2} and beyond.

(c) XPS studies suggested that the corona discharge treatment increase type and concentration of oxygen containing groups

(d) SEM studies found that the corona discharge treatment roughened the APC-2 surface and attacks exposed fibres.

(e) Failure locus analysis show that when the corona power is higher than a certain value (that is dependent on the adhesive used), failure occurred in the adhesive (as shown in Table 5.9)

Therefore, corona discharge treatment is an effective way to improve the bondability of PEEK composites. However, there are some areas that need further studies, such as the ageing effect, environmental effect, the interaction between corona and PEEK, etc..

CHAPTER 6 AIMS OF THE PROJECT

The purpose of this project was to enhance the bondability of PEEK by means of plasma and corona discharge treatments, particularly with respect to the following:

(a) Effects of plasma and corona discharge treatment on the bondability of PEEK

Although other surface properties have been widely investigated, there are no data on the bondability of plasma and corona discharge treated unreinforced PEEK. Moreover, PEEK is a crystallisable polymer, it is not known whether there is any relationship between crystallinity and bondability, and plasma or corona discharge treatments.

The aim was to employ T-peel test and lap shear test to evaluate the bondability of untreated and various plasma or corona discharge treated PEEK. A novel feature was to add other gases to corona in air. Studies of the relation between crystallinity and adhesive joint strength were to be included.

(b) Characterisation and modelling of the treated surfaces

Before analysing the mechanism of bondability enhancement, it is necessary to know the surface physical and chemical properties. More important, to model the treated surface structures. Though previous work has revealed that both plasma and corona discharge treatment can change the surface topography, wettability and surface chemical compositions, the chemical species and functional groups produced by the treatment are still not clear, particularly the low molecular weight molecules.

The intention was to employ contact angle measurement, SEM, XPS and XPS chemical derivatisation, TOF-SIMS and FTIR to characterise the treated surfaces and low molecular weight molecules produced by the treatment.

(c) Surface dynamics and adhesion

In this project, the changes of surface properties after ageing are referred to as surface dynamics. Studying the relation between the surface dynamics and adhesion has

practical significance, as in the industry, plasma or corona discharge treated PEEK products may experience transportation, storage or other forms of ageing before adhesive bonding. Thus from a practical aspect, it is necessary to know the effects of atmospheric exposure, hot environment and humid environment on the bondability of treated PEEK.

It has been found that about half a month atmospheric exposure does not affect the bondability and wettability of plasma treated carbon/PEEK composites[111], but a short time atmospheric exposure changes the wettability of plasma treated PEEK significantly[113], the results indicate that atmospheric exposure has a different effects on the plasma treated unreinforced and reinforced PEEK. Moreover, the longer period exposure effects are still unknown and the effects of atmospheric exposure or other environmental conditions on the bondability of PEEK have not been reported.

(d) Durability of plasma and corona treated PEEK/adhesive joints

There are no data on the durability of plasma or corona treated PEEK/adhesive joints. Since PEEK and its composites are being actively evaluated for high performance applications, it is essential that their performances in hostile environments are understood, it is necessary to know the effect of moisture, solvents, physical and thermal ageing. Some initial work will be done in this project to examine the hot/wet performance of plasma and corona treated PEEK/adhesive joints.

CHAPTER 7 EXPERIMENTAL

7.1 Materials

7.1.1 PEEK and adhesive

Amorphous PEEK film, STABAR K200 (250 μm thickness) purchased from ICI, was utilised as adherend. While 3M AF-163-2K structural epoxy adhesive film with a carrier, kindly supplied by 3M, was employed as adhesive.

7.1.2 Solvents and gases

HPLC grade (99.9+%) acetone and 2-propanol (IPA), brought from Aldrich Chemical Company Ltd, and distilled water were used as solvents.

Oxygen, argon, ammonia, sulfur dioxide brought from BOC (their purity is 99.5+%), and laboratory air were used as plasma and corona gas respectively.

7.2 Surface Pretreatment

Before plasma and corona discharge treatment, samples were cleaned by tissue wiping. The procedure is the following:

(a) wipe the sample surface with a tissue soaked with acetone
(b) wipe the sample surface with a clean tissue
(c) repeat (a) and (b) until the clean tissue can not pick up anything

7.2.1 Plasma treatment

The film adherends treated by plasma under different processing conditions. The plasma apparatus employed was a Plasma Technology `System 80' barrel type etcher (as illustrated in Fig. 7.1). The barrel diameter is approximately 300 mm and the electrode cage is large enough to hold specimens 150 mm long. The operating frequency on this equipment is 10^5 Hz and the power available is up to approximately 1000 watts. Using a rotary vacuum pump, a base pressure of approximately 260 mtorr can be attained in a few minutes. The treatment procedures are as follows:

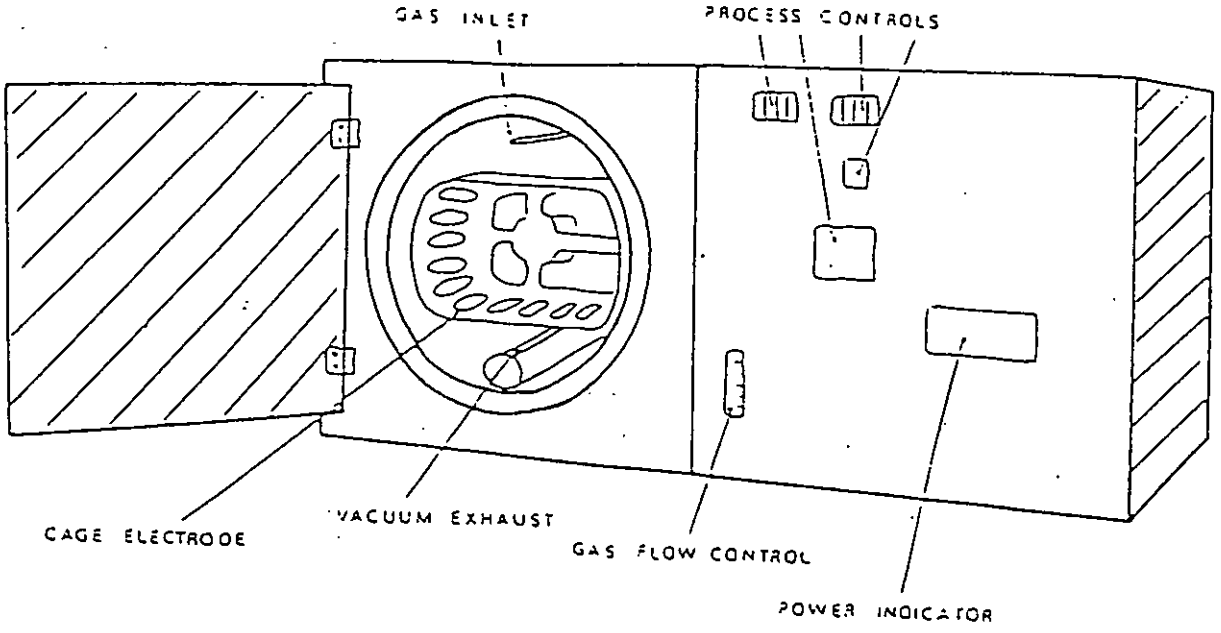

Fig. 7.1 Schematic diagram of the plasma apparatus. `System 80' Plasma Technology Ltd [117a].

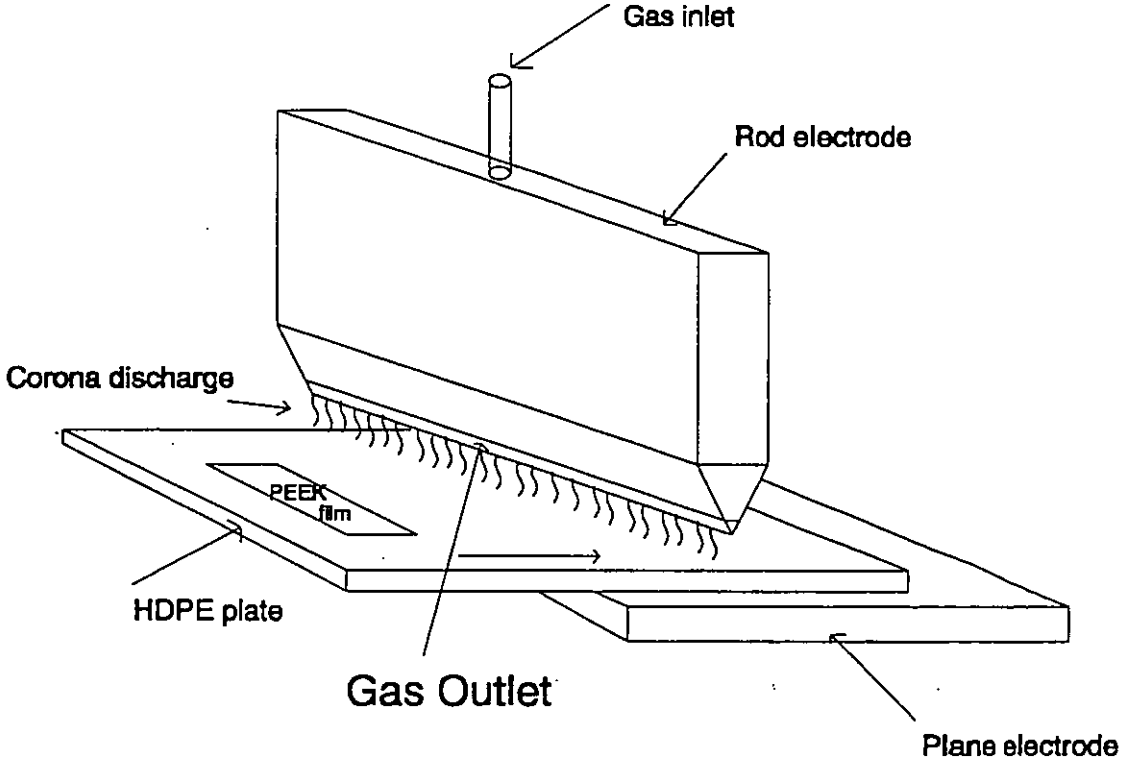

Fig. 7.2 Simplified schematic diagram of corona discharge treatment station

(a) pump chamber to the base pressure
(b) inject gas while pump is on
(c) switch off the gas inlet
(d) pump the chamber to the base pressure again
(e) repeat procedure (b) to (d) twice
(f) using gas inlet valve to adjust the chamber pressure to the required value
(g) switch on plasma and hold it for a required period
(h) switch off plasma
(i) let air into the chamber

7.2.2 Corona discharge treatment

The corona treatment station is schematically shown in Fig. 7.2. The generator employed is model HV 05-2, solid state (made by Tantec). The output power range from 0 to 350 watts, while the output frequency is from 20 KHz to 30 KHz depending on load. During treatment, the sample was placed on a HDPE supporting plate, which is installed between two electrodes (the upper one and the lower one) and its moment can be controlled by a gear box. The highest speed (HS) of the plate is 8.0 mm s^{-1}, and the lowest speed (LS) is 1 mm s^{-1}. The length of the electrode used is 100 mm. The gap between the electrode and the sample is fixed as 1.1 mm. Both sides of the sample were treated separately at the same condition. The treating gas was injecting to the upper electrode from the compressed gas cylinder by a plastic pipe and the flow rate is controlled as 10 l min^{-1}.

The energy output per unit area from the electrode on to the films may be determined from[101]

$$E = \frac{PN}{LV} \qquad (7.1)$$

Where E is the energy output per unit area (termed as treating level), P is the power of the generator, N is the number of the passes of the supporting plate, L is the length of the electrode and V is the velocity of the plate.

7.2.3 Solvent washing of the treated surfaces

Some plasma and corona discharge treated films were washed with either acetone, or IPA, or distilled water. The procedure was carried out by immersing the treated samples (five minutes after treatment) in the solvent for 30 seconds, and then hang-dry in an air circulated clean container. Tests were made at least one hour after the washing.

7.3 Joint Preparation and Testing

7.3.1 T-peel joints

A schematic diagram of a T-peel joint is shown in Fig. 7.3. The dimensions of the specimens were 125 mm long and 25 mm wide. The bonded area was 75 mm by 25 mm. Curing of the adhesive was carried out at 120°C for 1.5 hour (as recommended by the manufacturer) and then cooled down to room temperature naturally. During the curing process, the specimens were placed between steel plates and kept under a pressure of about 17 KPa by means of steel weights.

The joints were tested by loading the T-peel test pieces in a Lloyd 1000 tensile tester at room temperature and at a crosshead speed of 254 mm/min. The peel strength was obtained by the average load divided by the width of the bonded part. At least three replicates for each type of joints were tested and the average value and its standard deviation were reported.

7.3.2 Lap shear joints

Lap shear joints were prepared as sandwich appearance according to ASTM D3164-73, as shown in Fig. 7.4. PEEK film was put between the adhesive and the steel adherend. The bonding area was 25 mm by 12 mm, and the size of the adherend was 110 mm×25 mm×3 mm.

Curing of the adhesive was carried out in three stages (as recommended by the supplier), i.e. (a). increasing the temperature to 120°C; (b). keeping the temperature at 120°C for 1.5 hour; (c). lowering the temperature to ambient naturally. During all three stages, each specimen was kept under pressure by means of two strong clips.

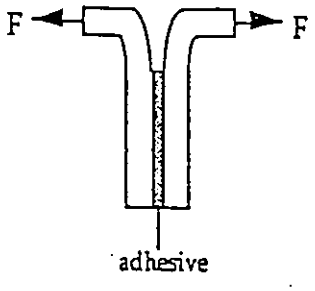

Fig. 7.3 Schematic diagram of a T-peel joint

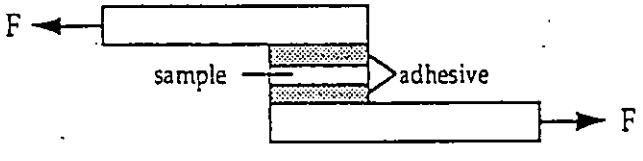

Fig. 7.4 Schematic diagram of the lap shear joint

Testing was conducted by applying a tensile load using a Lloyd 1000 tensile tester at room temperature. In the test, the crosshead speed is programmed as 1.3 mm/min. The shear strength is obtained by dividing the maximum load by the bonded area. At least four samples were tested for each type of joints, and the results reported are their averages and the standard deviations.

7.3.3 Failure Analysis

Failure analysis for both peel test and shear test samples were carried out by examining the fracture surfaces visually and by Scanning electron Microscopy (SEM).

7.4 Surface Characterisation

7.4.1 Scanning electron microscope (SEM) analysis

A scanning electron microscope (Cambridge Instruments Microscope) was employed in this work to examine some surfaces of the PEEK films prior to bonding and some fracture surfaces of the joints. Before analysis, the specimens were sputter coated with gold to improve the conductivity of the surfaces and to reduce charging.

7.4.2 Contact angle measurement

Contact angles were measured using a Kruss G40 contact angle measuring system (as shown in Fig. 7.5) with the liquid drops in an enclosed chamber at room temperature (between 20°C and 25°C). The liquids used for the measurements were triply distilled water and high purity (99.9+%) ethanediol (ED), dimethylsulfoxide (DMSO) and methylene diiodide (MDI). ED and DMSO were obtained from Romil Chemical Ltd, Shepshed, UK. MDI was obtained from the Aldrich Chemical Company. The total surface free energy of each liquid at room temperature was determined by the ring-pull method using a torsion balance[118]. The results are shown in Table 7.1. They agree very well with the literature values. Table 7.1 also includes literature values for the dispersion and polar components of surface free energy, denoted by γ_L^d and γ_L^p respectively. These values were used in the calculations which followed.

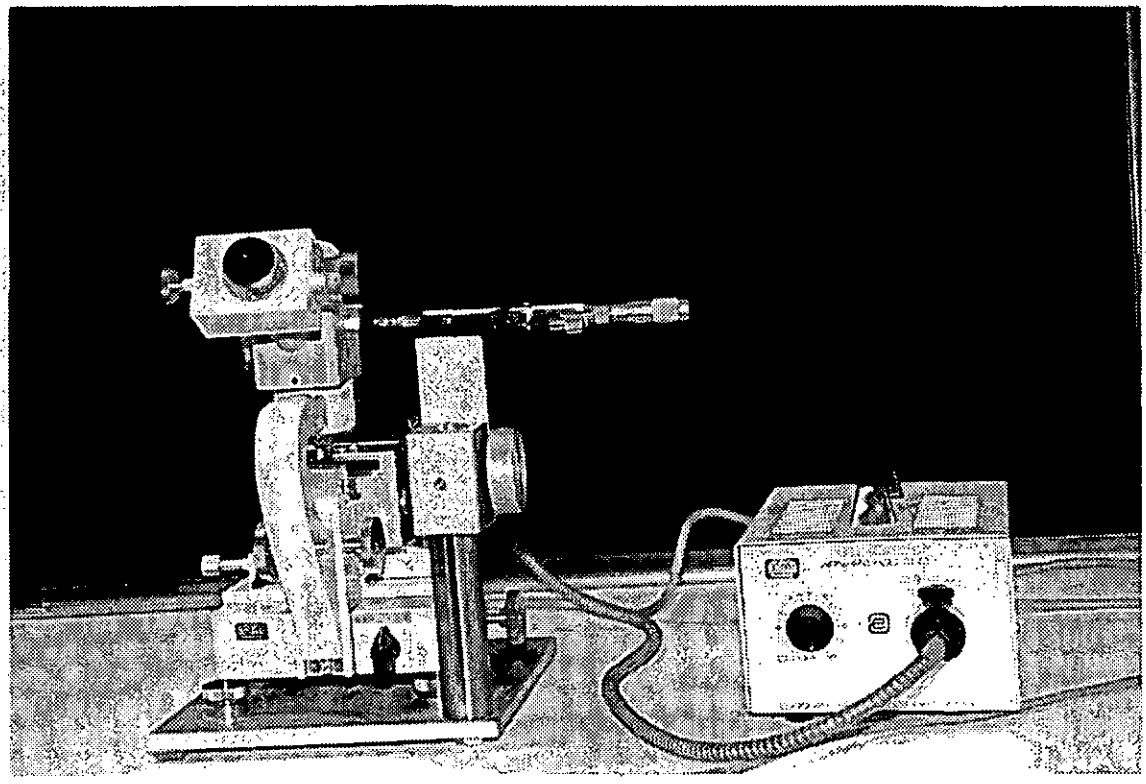

Fig. 7.5 Contact angle measurement system

Table 7.1 Literature data on test liquids together with measured values of total surface free energy

Liquid	Surface free energy (mJm^{-2})				ref
	γ_L^d	γ_L^p	γ_L		
			Literature	This study	
Water	21.8	51.0	72.8	71.9	26
ED	29.3	19.0	48.3	47.5	119
DMSO	34.9	8.7	43.6	43.5	120
MDI	49.5	1.3	50.8	50.3	41

The syringes which were used to place small drops of the liquids on the film surfaces were each dedicated to handle only one of the liquids. Each syringe was washed using their respective liquids before being finally filled. The volumes of the drops were about 3 µl. The sessile contact angles[30] were measured from each side of the drops for all mentioned liquids. Readings were taken 30 s after delivery of the drop. Contact angles obtained in this way were designated as "equilibrium" contact angles and used to estimate the surface free energy and polarity. They are thought to be similar to those obtained in Zisman's laboratory, whose measuring procedure was described in ref. 29. The advancing (θ_a) and receding contact angles (θ_r) of water were obtained by increasing or decreasing the drop volume until moving the three phase boundary over the surface. During the advancing and receding contact angle measurement, the capillary pipette of the syringe was kept immersed in the drop as described in ref. 121. The contact angle hysteresis[45] is defined as $H=\theta_a-\theta_r$, where H is the extent of the hysteresis. For every measurement, more than five drops are used and the results were averaged. The standard deviation of contact angles was found to be within 2°.

7.4.3 Estimation of surface free energy and surface polarity

The results of the contact angle measurements were analysed in accordance with the geometric-mean method in order to obtain estimates of the surface free energy and the polarity of the surfaces.

Surface free energy (γ_S) is the summary of a dispersion component (γ_S^d); and polar component (γ_S^p) which arise from two kinds of intermolecular forces, as shown in Eq. 7.2[41,49, 51].

$$\gamma_s = \gamma_s^d + \gamma_s^p \qquad [7.2]$$

The equilibrium contact angles for the testing liquids can be related to the solid surface free energy by Young's equation (Eq. 7.3)

$$\gamma_{LV}\cos\theta = \gamma_S - \gamma_{LS} - \pi_e \qquad [7.3]$$

Where γ_{LV} is the surface free energy of the liquid in equilibrium with its saturated vapour, θ is the equilibrium contact angle, γ_{LS} is the interfacial tension between the solid and the liquid, π_e is the spreading pressure which has been found to be negligible for liquids which have a non-zero contact angle on polymer surfaces[122].

The interfacial tension between the solid and the testing liquid can be obtained by the geometric-mean method (Eq. 7.4)[41,42]

$$\gamma_{LS} = \gamma_S + \gamma_{LV} - 2(\gamma_s^d\gamma_{LV}^d)^{\frac{1}{2}} - 2(\gamma_s^p\gamma_{LV}^p)^{\frac{1}{2}} \qquad [7.4]$$

where γ_{LV}^d and γ_{LV}^p are dispersion component and polar component of the surface free energy of the testing liquid respectively.

Combining Eq. 7.3 with Eq. 7.4 and neglecting the spreading pressure π_e gives

$$(1+\cos\theta)\gamma_{LV} = 2[(\gamma_{LV}^d\gamma_s^d)^{\frac{1}{2}} + (\gamma_{LV}^p\gamma_s^p)^{\frac{1}{2}}] \qquad [7.5]$$

By arranging Equation (7.5), we obtain

$$\frac{(1+\cos\theta)\gamma_{LV}}{2(\gamma_{LV}^d)^{\frac{1}{2}}} = (\gamma_s^d)^{\frac{1}{2}} + \left(\frac{\gamma_{LV}^p}{\gamma_{LV}^d}\right)^{\frac{1}{2}}(\gamma_s^p) \qquad [7.6]$$

This can be plotted as a straight line with

$$X = \left(\frac{\gamma_{LV}^{p}}{\gamma_{LV}^{d}}\right)^{\frac{1}{2}} \qquad [7.7]$$

$$Y = \frac{(1+\cos\theta)\gamma_{LV}}{2(\gamma_{LV}^{d})^{\frac{1}{2}}} \qquad [7.8]$$

The slope equals to $(\gamma_S^p)^{1/2}$, while the Y-axis intercept is $(\gamma_S^d)^{1/2}$. The results will be reported with their standard deviations which are calculated according to the method used by Comyn *et al.* [118]

Then the polarity of polymer surfaces X^p, as defined in ref. 123, can be obtained from Eq. 7.9

$$X^p = \gamma_s^p / \gamma_s \qquad [7.9]$$

7.4.4 X-Ray photoelectron spectroscopy (XPS) analysis

7.4.4.1 XPS analysis

The survey spectra, C_{1s} and O_{1s} Spectra were obtained using a VG E Scalab MKII at Loughborough Consultants Ltd, while the high resolution analysis of C_{1s} and O_{1s} peaks were conducted with a Surface Sciences M-Probe at CSMA Ltd. The primary beam in both cases was AlKα X-rays.

7.4.4.2 Vapour-phase derivatisation [124]

A vacuum frame was designed and built for vapour-phase derivatisation. It is schematically illustrated in Fig. 7.6. A vacuum of ~10^{-4} torr in the frame was obtained by the use of a rotary pump, a diffusion pump and two liquid nitrogen traps. There were three sub-frames under the main frame. Each sub-frame was exclusively used for one derivatisation reaction only. To avoid cross contamination, different derivatisation reactions were carried out at a time interval of at least one day. A derivatising reagent was kept in a flask on one side of a sub-frame. Air in the flask was pumped out through the main frame by opening the valve above the flask after the flask had been immersed in liquid nitrogen bath for ~5 min. After 10 min, the valve was then closed and the reagent allowed to melt by removing the liquid nitrogen bath. This pumping process was repeated several times in order to expel the impurities in the flask.

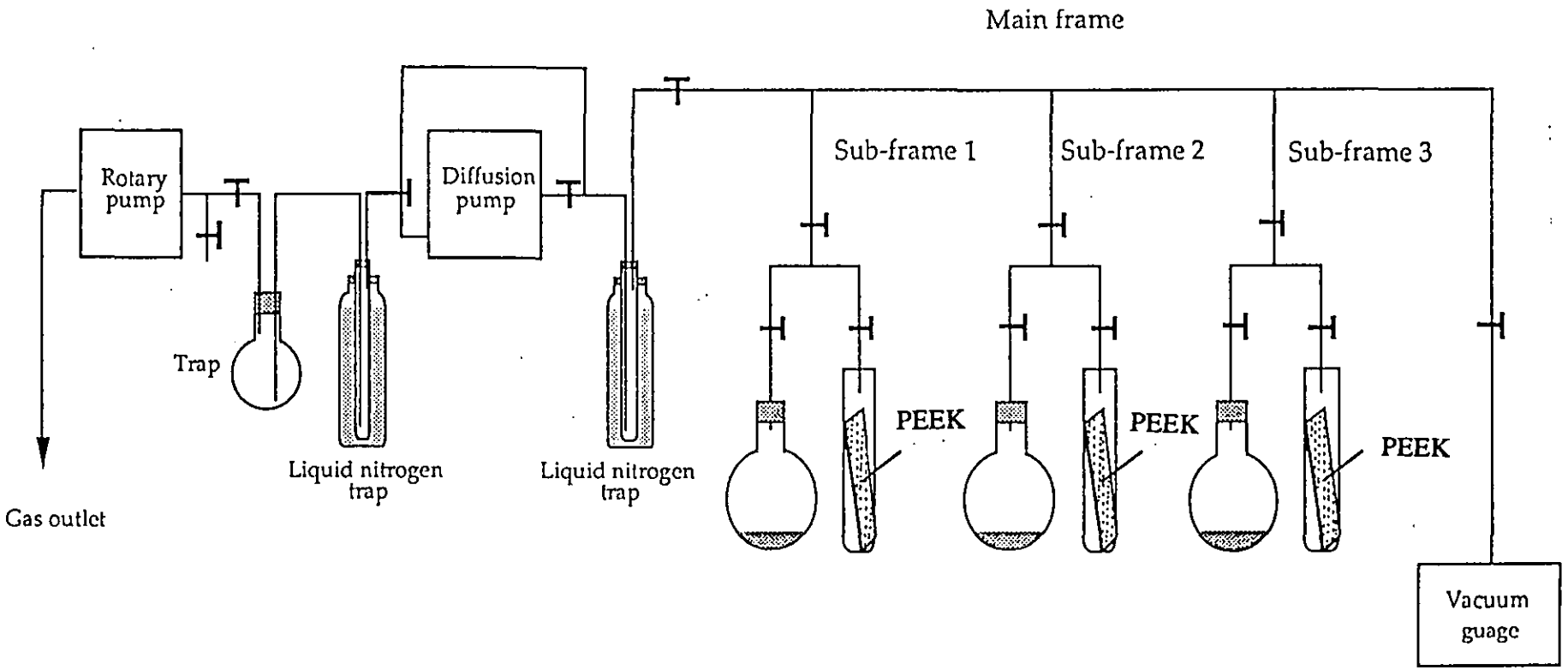

Fig. 7.6 Schematic illustration of vapour-phase derivatisation process vacuum frame

A tube containing specimens was put on the other side of the sub-frame and pumped down to a vacuum of ~10^{-4} torr by opening the valve above the tube. The reaction was started by closing the valve above the sub-frame and opening the valve above the flask. The flask was kept at ~20°C (room temperature ~25°C) using a water bath during the reaction to avoid the condensation of the reagent on the specimens. After the reaction, a jar containing liquid nitrogen was used to freeze the reagent, followed by pumping the sub-frame for ~10 min. The reagent was then sealed and the specimen was pumped for ~24 hours. XPS analysis of the specimen was performed on the same day.

7.4.4 Time of Flight Secondary Ion Mass Spectrometry (TOF-SIMS)

SIMS analysis was performed on a TOF-SIMS fitted with a pulsed gallium ion source in CSMA. Both positive and negative ion spectra were recorded.

Samples analysed by TOF-SIMS are listed in Table 7.2

Table 7.2 Samples examined by TOF-SIMS

---

1. Untreated PEEK
2. Oxygen plasma treated PEEK[a]
3. Oxygen plasma treated PEEK, rinsed in acetone
4. Oxygen plasma treated PEEK, heat treated at 150°C for 1 hour
5. Ammonia plasma treated PEEK[a]
6. Ammonia plasma treated PEEK, rinsed in acetone
7. Ammonia plasma treated PEEK, heat treated at 150°C for 1 hour
8. MY750[b] epoxide resin coated untreated PEEK after 24 hours acetone immersion (EUPK)[c]
9. MY750 epoxide resin coated oxygen plasma treated PEEK after 24 hours acetone immersion (EOPK)[c]
10. MY750 epoxide resin coated ammonia plasma treated PEEK after 24 hours acetone immersion (ENHPK)[c]

(a) Plasma treatment condition: 1 min, 500 w, 0.3 torr

(b) MY750 is a standard epoxy based on the glycidation of bisphenol-A with epichlorohydrin

(c) Sample preparation for EUPK, EOPK and ENHPK are given in section 12.3.2

7.5 Other Analysis Techniques

7.5.1 Fourier transform infrared (FTIR) analysis

A Galaxy Series 3000 FTIR Spectrometer, made by Mattson Instruments was employed to analyse the composition of the solvents rinsed by plasma treated PEEK film. The samples were prepared by immersing the plasma treated PEEK film (100 mm × 90 mm) in 2 ml acetone immediately after the treatment, and keeping immersed for one week.

7.5.2 Differential scanning calorimetry (DSC) analysis

A Thermal Analyst 2000 type DSC from Du Pont Instruments was used to study the melting behaviour of various condition annealed PEEK films. The scan rate was 10 °K min^{-1}, while the scan range was from room temperature to 400°C.

CHAPTER 8 ADHESION STUDIES

8.1 Effects of Processing Parameters

8.1.1 Plasma treatment

8.1.1.1 T-peel tests

Ideally, the peel force should be constant at a constant peel rate. In practice the peel force fluctuates, either randomly or in a slip-stick fashion [124a]. In the present experiments, although the peel force appears to fluctuate at random with respect to the variability in the height of the load spikes, the amplitude of the fluctuations appears to be quite constant over the entire bonded area, as shown in Fig. 8.1. The T-peel strength was expressed as force per unit width of the joint.

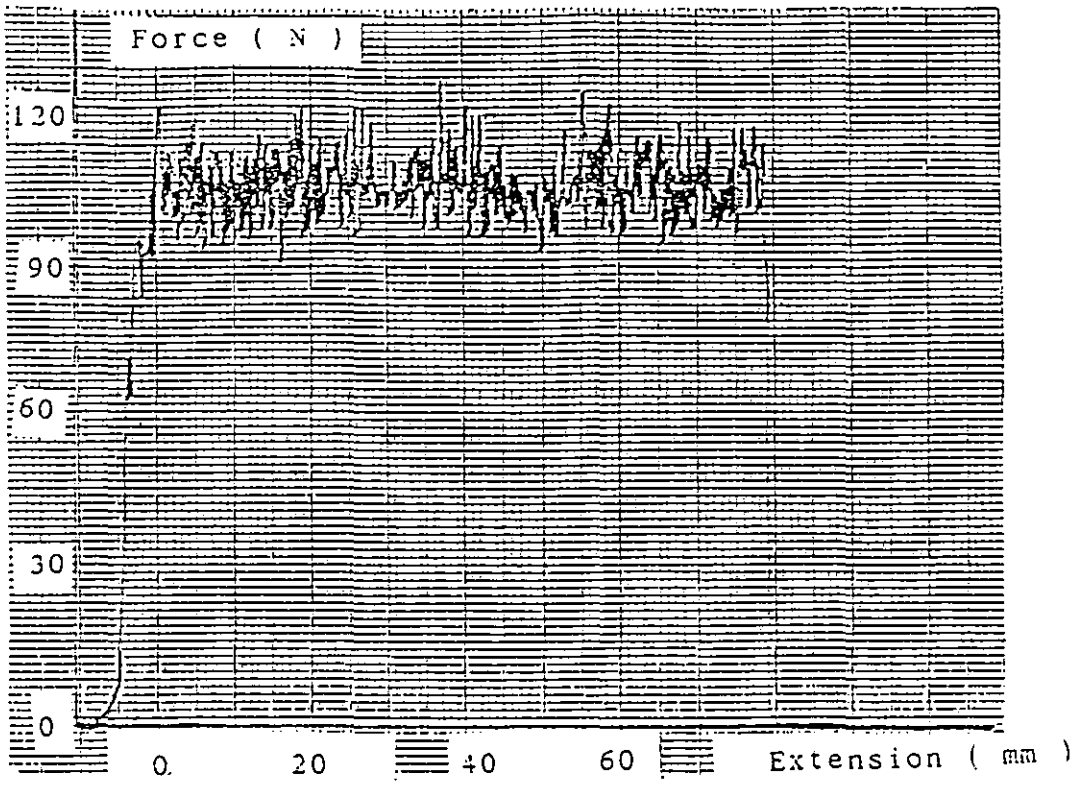

Fig. 8.1 Typical peel force with continuous failure for T-peel of plasma treated PEEK film joints (Treatment condition: oxygen plasma, 1 min, 300 w, 0.3 torr)

Table 8.1 shows the peel test results for PEEK treated with different oxygen plasma processing parameters, i.e. treatment time, power and chamber pressure. Where the following codes are used to indicate locus of failure judged by the naked eyes.

I: Interfacial between the adhesive and PEEK film
C: Cohesive failure in the adhesive
M: Material failure of PEEK

Table 8.1 Effects of oxygen plasma processing parameters on the T-peel joint strength of PEEK

Parameters	T-peel strength (N mm^{-1})	Locus of failure
Untreated	0	I
300 w, 0.3 torr, 0.5 min	0.84±0.04	I+C
1 min	4.23±0.34	C
2 min	4.18±0.09	C+M
6 min	3.90±0.02	C
10 min	3.80±0.35	C+M
30 min	4.07±0.06	C
1 min, 0.3 torr, 300 w	4.23±0.34	C
400 w	4.29±0.03	C+M
500 w	4.64±0.02	C+M
600 w	4.84±0.11	C+M
10 min, 0.3 torr, 300 w	3.80±0.35	C+M
400 w	3.88±0.06	C
600 w	3.72±0.29	C+M
600 w, 1 min, 0.3 torr	4.84±0.11	C+M
0.4 torr	4.13±0.10	C
0.5 torr	4.42±0.16	C+M
600 w, 10 min, 0.3 torr	3.72±0.29	C
0.4 torr	3.77±0.35	C

As it can be seen, oxygen plasma treatment can significantly increase the T-peel joint strength of PEEK. One minute and longer treatment resulted in peel strength values which are as high as it is possible to obtain with the T-peel tests. Changing the processing parameters do not have a large effect on the T-peel joint strength of PEEK, though it seems that there is an optimum treatment condition for the material.

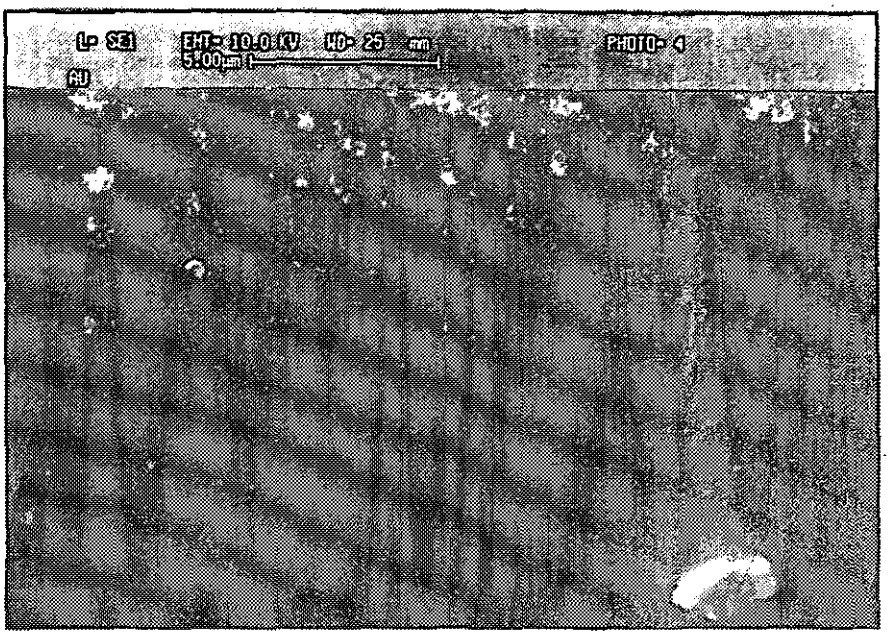

(a) 'adhesive' side

(b) 'PEEK' side

Fig. 8.2 Scanning electron micrographs of the peel fracture surfaces for untreated PEEK/adhesive joint

To study further the failure locus of PEEK/adhesive joints, the fractured specimens were examined by SEM. Micrographs of both the adhesive and PEEK substrate from opposite sides of the fracture plane, are shown in Fig. 8.2a and 8.2b respectively for untreated material. Both sides are very smooth while the PEEK side resembles strongly that of an unbonded control specimen (shown in Fig. 8.3). In other words, there is no sign of any substrate transfer to the adhesive or any adhesive transfer to the substrate, either from the visual or electron microscopy observations. Hence, there can be no disagreement as to the interfacial failure for untreated PEEK joints.

For oxygen plasma treated PEEK/adhesive joints, only one side of the fracture plane was analysed by SEM as visual observations showed that the opposite sides of the fractured plane were exactly the same. SEM studies have found that the failure of these joints occurred at the adhesive through plastic deformation (as shown in Fig. 8.4), suggesting the existence of a strong interfacial bond between plasma treated PEEK and epoxy adhesive.

The treatment effects of different gas plasma are shown in Table 8.2, As it can be seen that argon gives joints which are some what weaker than when oxygen is the plasma gas, while ammonia and air improve peel strength of PEEK to the same extent as oxygen is employed.

Table 8.2 Effects of plasma treatment gas on the T-peel joint strength

Treatment Condition	Peel Strength (N/mm)	Locus of Failure
O_2, 1 min, 500 w, 0.3 torr	4.64±0.02	C+M
1 min, 600 w, 0.4 torr	4.13±0.10	C
Ar, 1 min, 500 w, 0.3 torr	3.36±0.32	C
5 min, 500 w, 0.3 torr	3.85±0.27	C+M
Air, 1 min, 500 w, 0.3 torr	4.19±0.07	C+M
1 min, 600 w, 0.4 torr	4.00±0.38	C
NH_3, 1 min, 500 w, 0.3 torr	4.05±0.11	C
1 min, 600 w, 0.4 torr	4.00±0.09	C

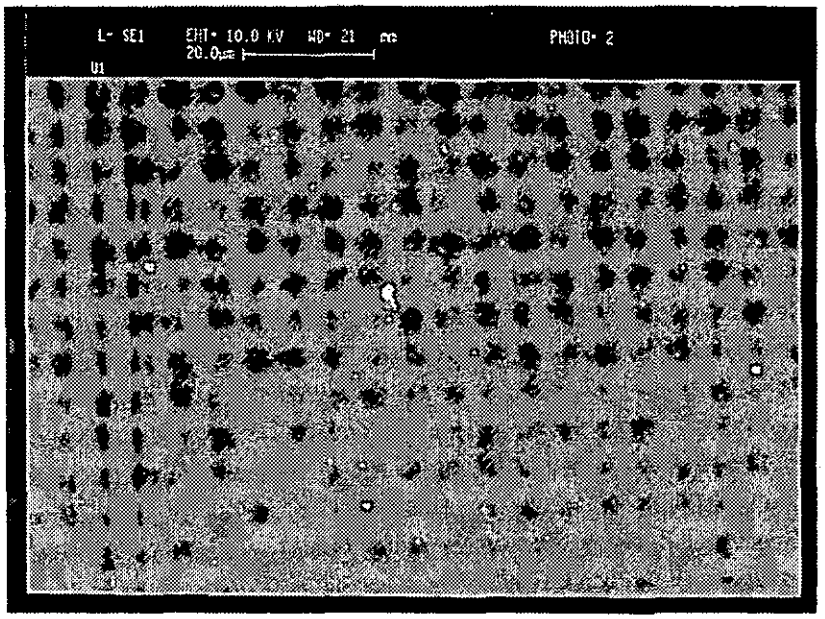

Fig. 8.3 Scanning electron micrograph of untreated PEEK surface

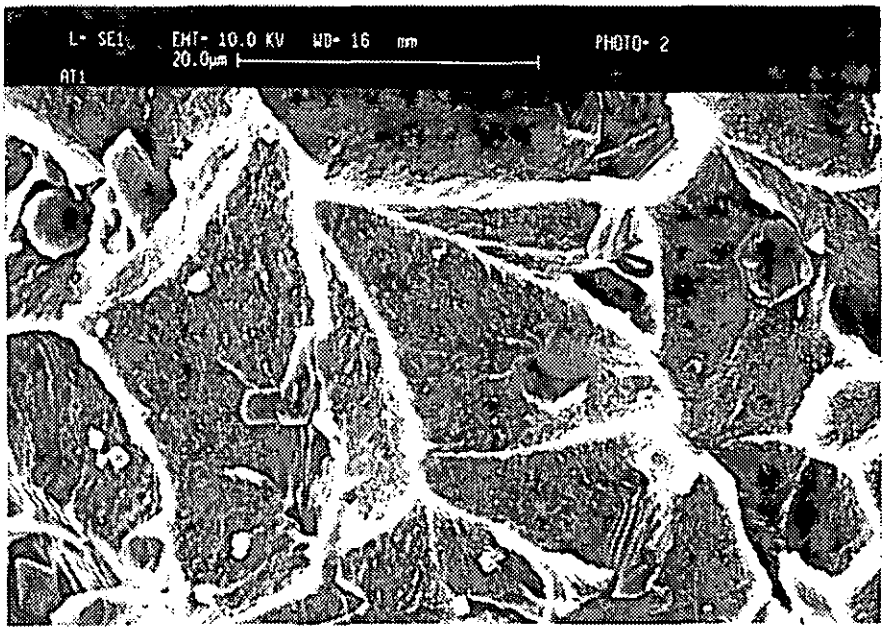

Fig. 8.4 Scanning electron micrograph of the T-peel fracture surface for oxygen plasma treated PEEK/adhesive joint (Treatment condition: 1 min, 500 w, 0.3 torr)

8.1.1.2 Lap shear tests

In addition to the peel tests discussed above, lap shear joint test was also employed to assess the plasma treatment effects. Fig. 8.5 shows a typical force/extension curve of the lap shear tests. The shear strength was obtained by dividing the maximum load by the bonded area. The results are shown in Table 8.3, also listed are the results of the untreated material.

Table 8.3 Effects of plasma treatment gas on the lap shear joint strength

Treatment Gas (a)	Shear strength (MPa)	Locus of failure
Untreated	16.9±1.3	I+C
Oxygen	34.0±1.4	C+M
Ammonia	32.2±2.1	C+M
Sulfur Dioxide	32.8±0.9	C+M
Air	29.1±1.8	C+M
Adhesive (b)	37.1±2.0	C

(a) Treatment condition: 1 min, 500 w, 0.3 torr

(b) Steel/Adhesive/Steel lap-joint

The results reveal that whilst untreated PEEK gives zero peel strength, it gives a moderate lap shear strength. In addition, the lap shear joint failure is the mixture of interfacial and cohesive instead of interfacial failure, which is the case of peel test. The scanning micrograph of the shear joints failure for untreated film is shown in Fig. 8.6

The results in Table 8.3 also show that plasma treatment can significantly increase the lap shear joint strength of PEEK, which is only slightly lower than the joint strength of steel/adhesive/steel single lap-joint. The difference here is believed to be due to that the thickness of overlapping area for adhesive only joint is smaller than that for the treated PEEK film sandwich samples. As it can be seen, oxygen, ammonia, sulfur dioxide and air give similar joint strength and joint failure locus, i.e. the plastic deformation of both adhesive and PEEK film.

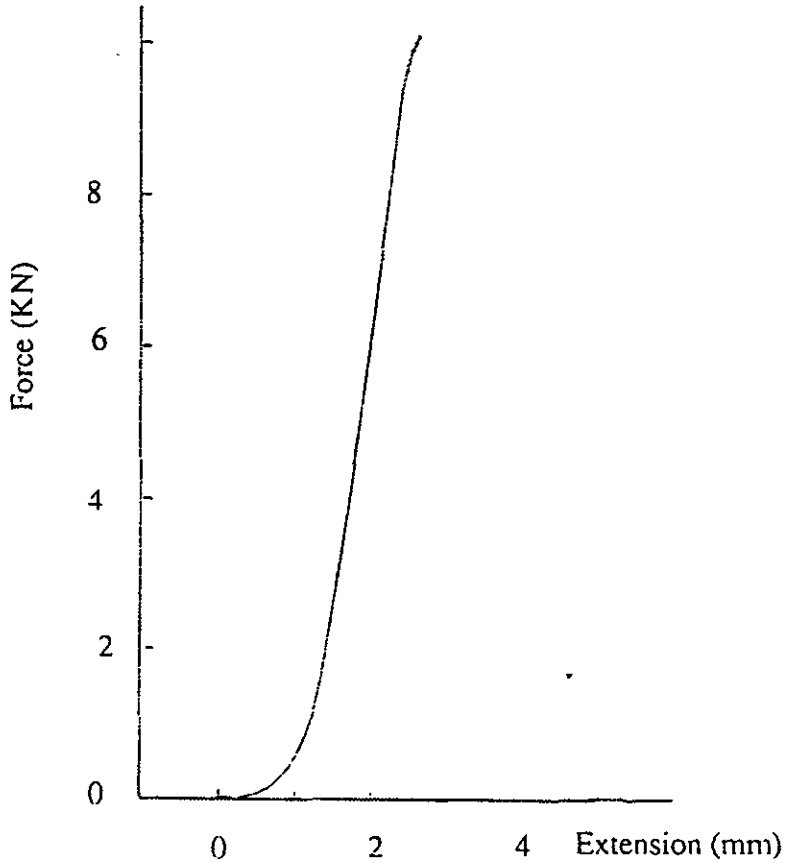

Fig. 8.5 Typical force/extension curve of the lap shear tests
(Treatment condition: 1 min, 500w, 0.3 torr)

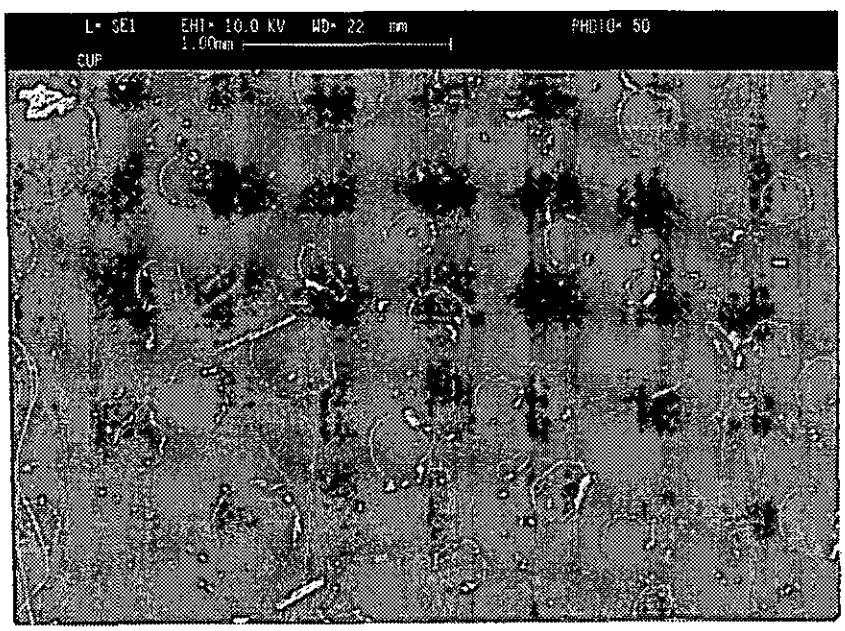

Fig. 8.6 Scanning electron micrograph of the shear fracture surface for untreated PEEK/adhesive joint

8.1.2 Corona discharge treatment

The processing parameters of corona discharge treatment in this work include treatment level and gas type. Table 8.4 gives the results of different air corona discharge treatment level on the lap shear joint strength of PEEK. The results show that as long as the treatment level pass the lowest value available in this work, the lap shear joint strength for PEEK films reaches its maximum value and the failure locus moves to adhesive and PEEK, i.e. both adhesive and PEEK film are plastically deformed (as shown in Fig. 8.7). Increasing the treatment level does not further change the joint strength and failure locus.

Table 8.4 Effects of air corona discharge treatment level on the lap shear joint strength of PEEK

Treatment level (J mm^{-2})	Shear strength (MPa)	Locus of failure
0	16.9±1.3	I+C
0.05	28.3±0.9	C+M
0.2	28.9±2.2	C+M
0.4	28.5±1.8	C+M
0.6	29.1±0.4	C+M
0.8	29.5±0.6	C+M
2.0	29.3±0.5	C+M

Table 8.5 shows the effects of different gas injecting into the corona discharge on the lap shear joint strength of PEEK films. The results show that all the gases employed in this work make very little difference on the treatment effect. Air, oxygen, argon, ammonia and sulfur dioxide corona discharge produce very similar joint strength and failure locus for PEEK.

Table 8.5 Effects of type of gas injected in the corona discharge on the lap shear joint strength of PEEK

Treatment level (J/mm^2)	Gas	Shear strength (MPa)	Locus of failure
0.05	Air	28.3±0.9	C+M
	Oxygen	29.9±0.5	C+M
	Argon	28.1±0.3	C+M
0.4	Air	28.5±1.8	C+M
	Oxygen	30.2±0.7	C+M
	Argon	28.8±0.8	C+M
	Ammonia	28.0±0.7	C+M
	Sulfur dioxide	32.0±1.2	C+M

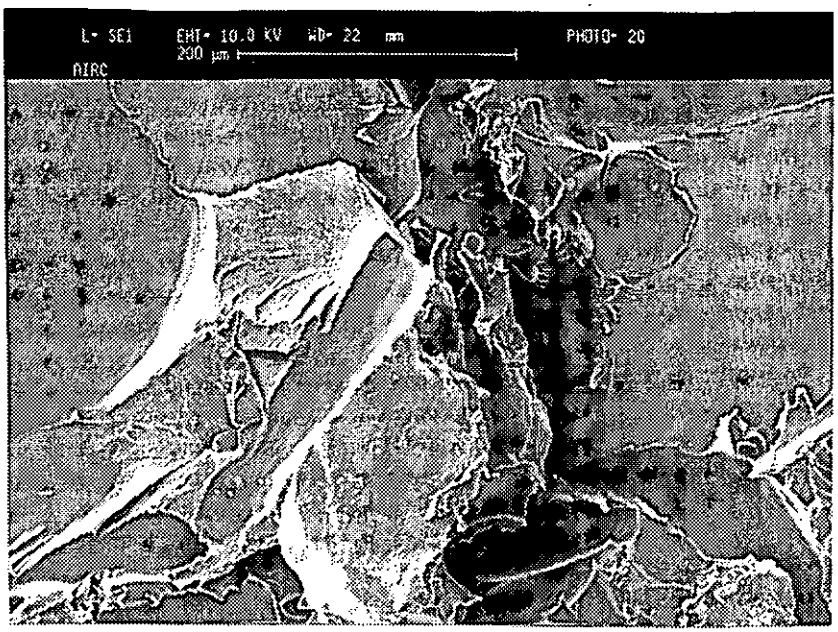

Fig. 8.7 Scanning electron micrograph of the shear fracture surface for air corona discharge treated PEEK/adhesive joint (Treatment level: 0.4 J/mm^2)

8.2 Crystallinity and Treatment Effects

To obtain different levels of crystallinity, the received film was annealed at 180°C for different time, and then cooled slowly to room temperature. The crystallinity of the annealed samples were calculated from the DSC thermograms (a typical DSC curve is shown in Fig. 8.8). Details of the calculation is shown in Appendix 1, whereas the results are given in Table 8.6. As it can be seen, a very short annealing time can produce a high degree of crystallinity and that prolonging annealing time does not produce further increase.

Table 8.6 Relation between annealing time and crystallinity*

Annealing Time (hour)	Melting peak area ($J\ g^{-1}$)	Crystallinity
0		0
0.5	40.28	31.0
1.0	41.21	31.7
2.0	42.23	32.5
4.0	44.46	34.2

*Calculation of crystallinity is shown in Appendix 1

The crystallised films were treated with oxygen plasma and air corona respectively. The bondability results are shown in Table 8.7. The relations between crystallinity and the lap shear joint strength of PEEK before and after treatment can be summarised as follows:

(a) Before treatment, crystallised films give similar joint strengths as their amorphous counterparts except for the sample with 34.2% crystallinity.

(b) Oxygen plasma treatment makes little difference to the joint strength between amorphous and crystallised samples.

(c) Air corona discharge treatment tends to produce slightly higher joint strength for crystallised samples.

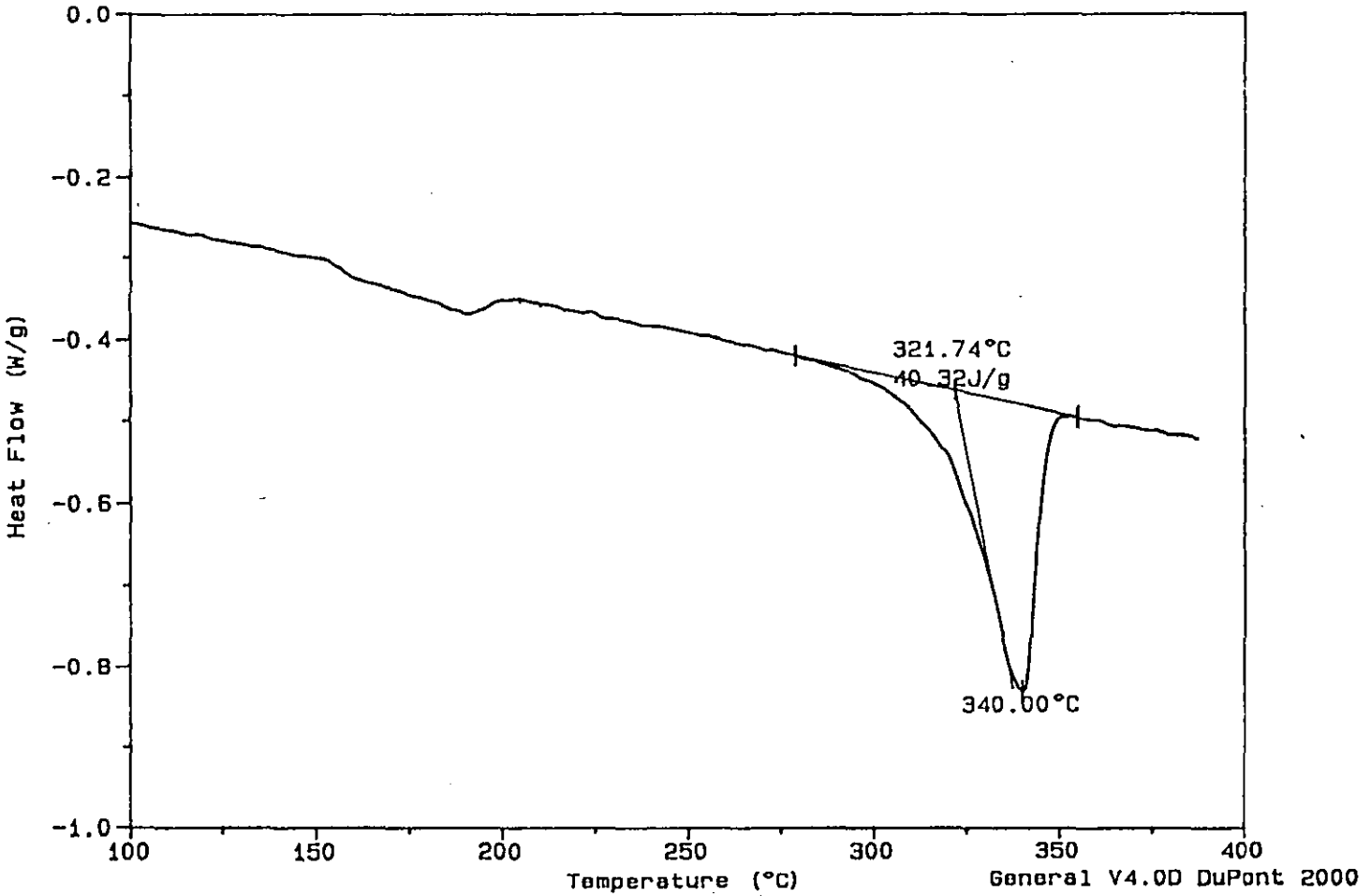

Fig. 8.8 Typical DSC thermogram for annealed PEEK films (Annealing condition: 180°C, 1 hour)

Table 8.7 Relations between crystallinity and the lap shear joint strength of PEEK

Crystallinity (Wt%)	Treatment method	Shear strength (MPa)	Locus of failure
0	Untreated	16.9±1.3	I+C
	Oxygen Plasma	34.0±1.4	C+M
	Air Corona	28.5±1.8	C+M
31.0	Untreated	15.5±3.5	I+C
	Oxygen Plasma	30.8±1.6	C+M
	Air Corona	31.6±0.6	C+M
31.7	Untreated	13.0±3.8	I+C
	Oxygen Plasma	31.3±0.7	C+M
	Air Corona	32.3±1.3	C+M
32.5	Untreated	12.6±3.1	I+C
	Oxygen Plasma	30.9±1.4	C+M
	Air Corona	30.8±0.4	C+M
34.2	Untreated	9.8±0.7	I+C
	Oxygen Plasma	32.1±0.3	C+M
	Air Corona	32.5±1.6	C+M

Oxygen plasma treatment condition: 1 min, 500 w, 0.3 torr
Air Corona Treatment level: 0.4 J/mm^2

8.3 Hot/wet Performance of Plasma and Corona Discharge Treated PEEK/Adhesive Joints

The initial studies were made on the durability (hot/wet performances) of the plasma and corona discharge treated PEEK/adhesive joints.

After curing, oxygen plasma and air corona treated PEEK/adhesive lap shear joints were put into the oven at temperature of 180°C for one hour, then the temperature was lowered naturally. The effect of this heat treatment is shown in Table 8.8.

Table 8.8 Hot performance of the joints for oxygen plasma and air corona discharge treated PEEK (180°C, 1 hour)

Sample	Heat treatment	Lap shear strength (MPa)	Locus of failure
Joints for oxygen plasma treated PEEK	Before	34.0±1.4	C+M
	After	29.4±0.7	C+M
Joints for air corona treated PEEK	Before	28.5±1.8	C+M
	After	28.3±1.3	C+M

Plasma treatment condition: 1 min, 500 w, 0.3 torr
Corona treatment level: 0.4 J/mm^2

As it can be seen, the joints for oxygen plasma treated materials seem more sensitive to heat treatment than the joints for air corona discharge treated films. After heat treatment, the joint strengths for oxygen plasma treated samples are slightly lowered, but those for corona treated materials remain unchanged.

The wet performance of the joints for oxygen plasma and ammonia plasma treated PEEK films was assessed by immersing the T-peel joints in distilled water for one month. The results are shown in Table 8.9. The data listed in Table 8.9 suggest that the effect of one month water immersion on the adhesive joints for both oxygen plasma and ammonia plasma treated PEEK can be neglected.

Table 8.9 Effect of one month water immersion on the T-peel joint strength of plasma treated PEEK films

Sample	Water immersion	Peel strength (N/mm)	Locus of failure
Joints for oxygen plasma treated films	Before	4.64±0.02	C+M
	After	4.48±0.02	C+M
Joints for ammonia plasma treated films	Before	4.05±0.11	C
	After	3.97±0.08	C

Plasma treatment condition: 1 min, 500 w, 0.3 torr

The wet performance of the joints for sulfur dioxide plasma treated films was also studied by immersing both T-peel joints and lap shear joints in distilled water for 1000 hours at the temperature of 70°C. The results are shown in Table 8.10. The peel results do not reveal that any change on the strength and the failure locus has been induced by the water immersion. However, the lap shear joint strengths were lowered after 1000 hours water immersion, the failure locus also move from the adhesive plus film to adhesive plus interface. Nevertheless, the interfacial failure here occurred between the steel and the adhesive while no any sign of failure occurred at the interface between the adhesive and PEEK films. Hence, both peel and shear test results indicate that the joints for sulfur dioxide plasma treated PEEK films can stand 1000 hours water immersion at the temperature of 70°C.

Table 8.10 Effect of 1000 hours water immersion on the joint strength of sulfur dioxide plasma treated films

Joint type	Water immersion	Strength	Failure locus
Lap shear	Before	32.8±0.9 MPa	C+M
	After	24.4±1.1 MPa	C+I*
T-peel	Before	3.98±0.06 N/mm	C
	After	3.99±0.05 N/mm	C

*Interface between steel and adhesive

CHAPTER 9 WETTABILITY STUDIES

9.1 Contact Angle Analysis

Table 9.1 and 9.2 listed the contact angles against plasma and corona discharge treated materials, also listed in these two tables are the data for untreated films

Table 9.1 shows the effect of plasma treatment on the contact angles against PEEK films. Oxygen plasma is particularly effective in reducing the contact angles. After oxygen plasma treatment, all the testing liquids give very small contact angles. Both ammonia and sulfur dioxide plasma reduce the contact angles for almost all the testing liquids, but not as significantly as oxygen plasma. From the water contact angle results, the effects of air and argon plasma are similar to oxygen plasma.

Table 9.1 Effect of plasma treatment on the contact angles against PEEK films

Treatment gas*	Contact angle (degree)			
	Water	ED	DMSO	DMI
Untreated	73	51	42	31
Oxygen	<5	<5	<5	11
Ammonia	37	28	20	36
Sulfur dioxide	43	27	29	24
Air	<5	--	--	22
Argon	10	--	--	28

* Treatment condition: 1 min, 500 w, 0.3 torr

Table 9.2 gives the contact angle results of corona discharge treated materials. As it can be seen, unlike plasma treatment, all corona discharge treatment produce similar contact angle results, i.e. the contact angles for all the testing liquids (excluding DMI) are reduced after treatment.

Therefore, from the contact angle results, it is clear that both plasma and corona discharge treatment improve the wettability of PEEK films.

Table 9.2 Effect of corona discharge treatment on the contact angles against PEEK films

Treatment gas*	Contact angle(degree)			
	Water	ED	DMSO	DMI
Untreated	73	51	42	31
Air	30	25	12	26
Ammonia	45	28	18	34
Sulfur dioxide	45	22	14	27
Oxygen	38	23	10	23
Argon	37	22	5	26

* Treatment level: 0.4 J mm^{-2}

9.2 Surface Free Energy and Polarity

The results of the contact angle measurements were analysed in accordance with the method discussed in Section 7.4.3 in order to obtain estimates of the polar and dispersion components of the surface free energies and the surface polarity. The estimation results are shown in Table 9.3 and 9.4 respectively.

Table 9.3 Effect of plasma treatment on the surface free energy and polarity of PEEK films*

Treatment condition	Surface energy (mJm^{-2})			Surface polarity
	γ_s^p	γ_s^d	γ_s	
Untreated	7.2±3.9	31.5±8.3	38.7	0.186
O_2, 1 min, 500 w, 0.3 torr	42.5±18.1	23.5±13.6	66.0	0.644
O_2, 1 min, 600 w, 0.4 torr	43.5±17.6	22.6±12.8	66.1	0.658
NH_3, 1 min, 500 w, 0.3 torr	32.4±11.6	22.7±9.8	55.1	0.587
NH_3, 1 min, 600 w, 0.4 torr	34.6±11.7	23.2±9.7	57.8	0.598
SO_2, 1 min, 500 w, 0.3 torr	26.3±11.2	26.0±11.3	52.3	0.503
SO_2, 1 min, 500 w, 0.3 torr	19.5±9.7	27.5±11.6	47.0	0.416

* When the contact angle approaches zero (<5°), the equilibrium spreading pressure π_e in Young's equation can be quite significant and can not be neglected. But since the value of π_e is difficult to obtain, the surface free energy values of some plasma and corona treated films reported in this thesis are only approximated values by omitting the spreading pressure.

Table 9.4 Effect of corona discharge treatment on the surface free energy and polarity of PEEK films

Gas	Treatment level ($J\ mm^{-2}$)	Surface energy(mJm^{-2}) γ_s^p	γ_s^d	γ_s	Surface polarity
Untreated		7.2±3.9	31.5±8.3	38.7	0.186
Air	0.05	28.6±12.1	26.5±11.7	55.1	0.519
	0.2	22.8±7.6	26.9±8.3	49.7	0.460
	0.4	34.5±14.3	24.0±12.0	58.5	0.590
	0.6	30.1±11.9	25.4±11.0	55.5	0.543
	0.8	33.0±13.4	26.4±12.1	59.4	0.555
	2.0	33.6±13.8	26.2±12.3	59.8	0.562
Ammonia	0.05	24.6±9.2	25.2±9.4	49.8	0.494
	0.4	25.9±8.7	25.7±8.7	51.6	0.502
Sulfur dioxide	0.4	24.6±8.3	28.0±9.0	52.6	0.467
Oxygen	0.05	21.0±6.6	28.2±7.7	49.2	0.428
	0.4	28.7±11.3	26.8±11.0	55.5	0.518
Argon	0.05	26.1±9.1	27.2±9.4	53.3	0.489
	0.4	29.8±11.1	26.2±10.5	56.0	0.532

Table 9.3 gives surface free energy and polarity of PEEK films before and after plasma treatment. As it can be seen, oxygen, ammonia and sulfur dioxide plasma significantly increase the polar component of surface free energy, while at same time lower the dispersion component. The total surface free energy increased after treatment. The surface polarity calculated from the surface free energy results also increased remarkably suggesting that the treated surfaces have much higher polarity than their untreated counterpart.

The data listed in Table 9.4 show that the effect of corona discharge treatment on the surface free energy is quite similar to that of plasma treatment, i.e. corona treatment increases the polar component of the surface free energy and lowers the dispersion component, but the total surface free energy is increased after treatment.

Therefore the surface free energy and polarity results indicate that both plasma and corona discharge treatment change the surface structure and increase the surface polarity.

9.3 Contact Angle Hysteresis

Table 9.5 and 9.6 show the effect of plasma and corona discharge treatment on the contact angle hysteresis of water respectively.

Table 9.5 Contact angle hysteresis of water before and after plasma treatment

Treatment Gas	Contact angle hysteresis (degree)		
	θ_a	θr	$\theta_a - \theta r$
Untreated	78	32	46
Oxygen	<5	<5	--
Ammonia	41	<5	>36
Sulfur dioxide	43	<5	>38
Air	<5	<5	--
Argon	10	10	0

Treatment condition: 1 min, 500 w, 0.3 torr

Table 9.6 Contact angle hysteresis of water before and after corona discharge treatment

Treatment Gas	Contact angle hysteresis (degree)		
	θ_a	θr	$\theta_a - \theta r$
Untreated	78	32	46
Air	30	<5	>25
Ammonia	45	<5	>42
Sulfur dioxide	46	<5	>41
Oxygen	39	<5	>34
Argon	37	<5	>32

Treatment level: 0.4 J mm^{-2}

Untreated PEEK has a large extent of contact angle hysteresis with the advancing contact angle having a value of 78 and the receding angle of 32, as shown in Table 9.5. Plasma treatment reduce the value of advancing and receding angle simultaneously with the receding angle reach the values of zero (<5) while the advancing angle to a different value depending on the gas used. Oxygen and air plasma also decrease the advancing angle to the value of zero (<5), but ammonia and sulfur dioxide plasma only

reduce that to ~40. However, all corona discharge treatment decrease the receding angle to the value near zero and the advancing angle to values between 30 and 46.

Contact angle hysteresis is thought to be mainly influenced by two aspects, one is the surface heterogeneity[125], the other is surface roughness[126,127]. Wu[128] suggested that any hysteresis on an optically smooth surface must arise from surface heterogeneity. SEM analysis has revealed that the materials used in this work are very smooth before and after treatment (These will discussed in next Chapter). Thus, it is believed that the changes of contact angle hysteresis are induced by the altering of the surface heterogeneity after plasma and corona discharge treatment.

In addition, the results obtained are the typical behaviour of heterogeneous surfaces composed by a higher energy and a lower energy part[125,129,130]. The advancing angles tend to reflect the lower energy part of the heterogeneous surface. Hence, plasma and corona discharge treatment increase the surface free energy of both higher and lower energy parts of the surface.

CHAPTER 10 SURFACE CHARACTERISATION

10.1 SEM Analysis

SEM analysis has revealed that both plasma and corona discharge treatment do not change the surface topography of PEEK films or, the effect is too small to be detected, as shown in Fig. 10.1-10.3.

Fig. 10.1-10.3 show the scanning electron micrographs of untreated, oxygen plasma treated and air corona treated films respectively. The untreated surface is very smooth (as shown in Fig. 10.1). After either plasma or corona discharge treatment, the surface remains unchanged (as shown in Fig. 10.2 and Fig. 10.3). Therefore, the SEM results imply that the bondability and wettability improvement after treatment is attributed to the modification of other surface properties.

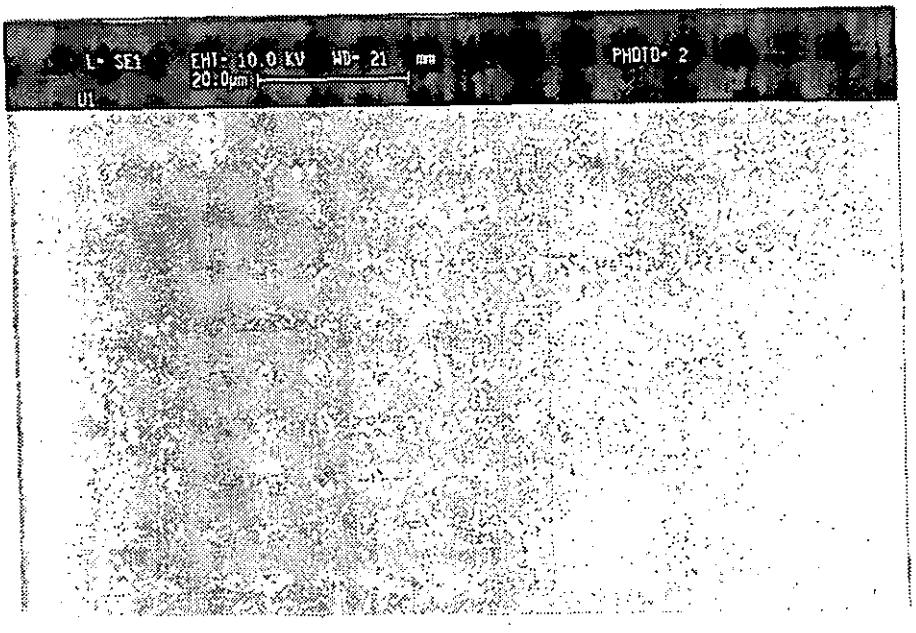

Fig. 10.1 Scanning electron micrograph of untreated film

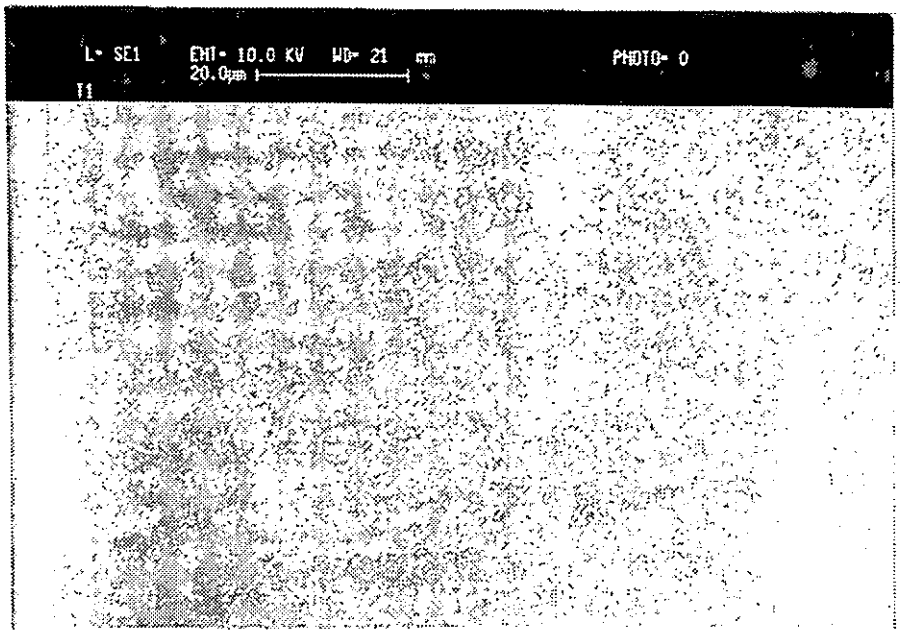

Fig. 10.2 Scanning electron micrograph of oxygen plasma treated film (Treatment condition: 10 min, 300 w, 0.3 torr)

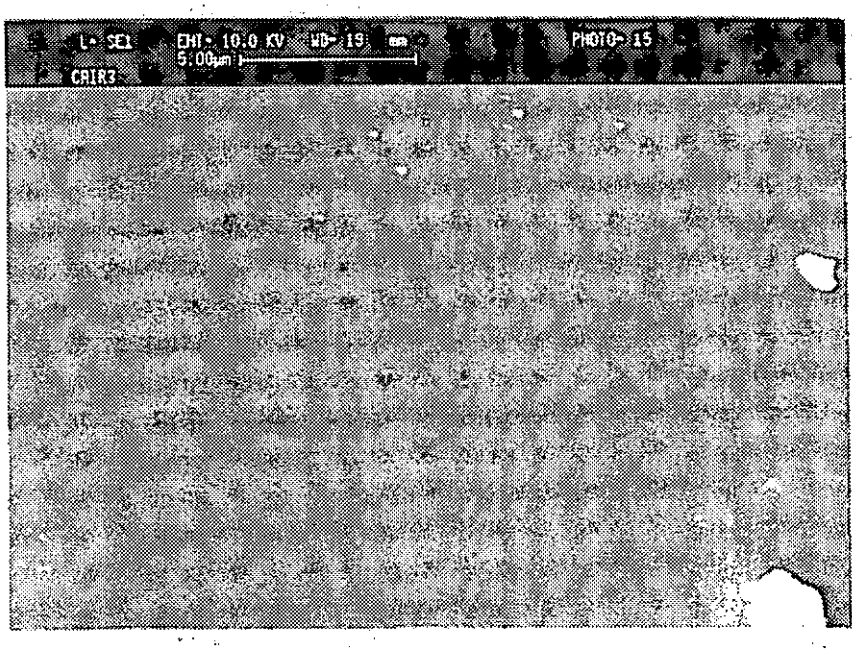

Fig. 10.3 Scanning electron micrograph of air corona discharge treated material (Treatment level: 0.4 J mm^{-2})

10.2 XPS Analysis

10.2.1 Effect of plasma treatment

10.2.1.1 Elemental composition studies

The elemental composition for PEEK films before and after plasma treatment obtained from the XPS survey spectra are given in Table 10.1

Table 10.1 Atomic analysis per 100 carbon atoms from survey spectra of PEEK films before and after plasma treatment

Treatment gas*	Oxygen	Nitrogen
Molecular structure	15.8	0
Untreated	17.6	0
Oxygen	38.1	0
Ammonia	16.3	9.1
Air	31.0	2.2
Argon	30.2	9.0

*Treatment condition: 1 min, 500 w, 0.3 torr

The results show that the amount of oxygen in untreated material is close to what is expected, and all plasma treatment significantly changes the surface element composition of PEEK films. Oxygen plasma treatment increase the amount of oxygen on the surface but does not introduce nitrogen onto the surface, while ammonia plasma seems only introduce nitrogen onto the surface and not affect the surface oxygen concentration. Both air and argon plasma not only increase the oxygen concentration on the surface but also introduce some amount of nitrogen onto the surface.

10.2.1.2 C_{1s} and O_{1s} spectra

It has been found that plasma treatment changes the shapes of C_{1s} and O_{1s} peaks of PEEK films, as shown in Fig. 10.4 and Fig. 10.5

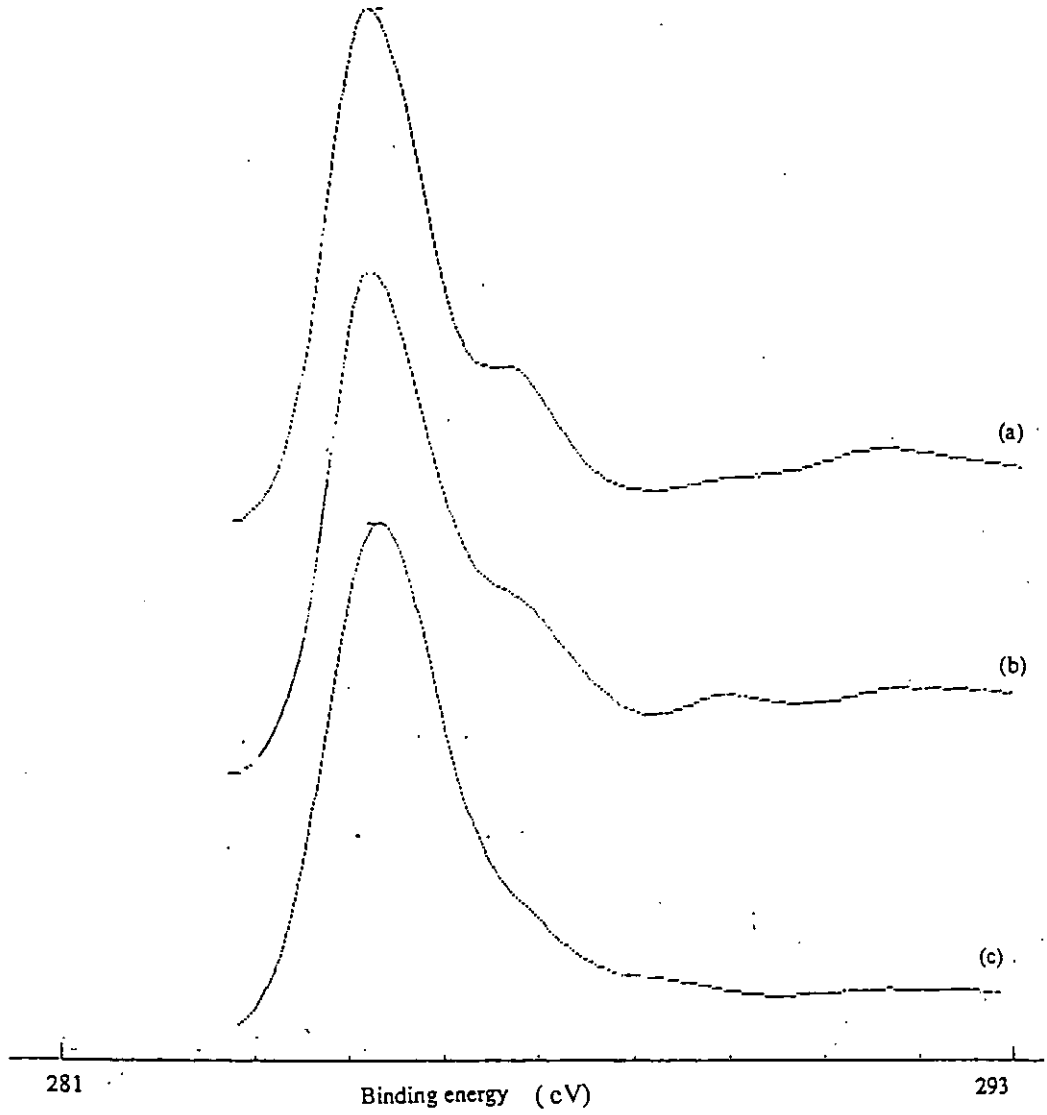

Fig. 10.4 C_{1s} spectra of untreated and plasma treated films

(a) Untreated;

(b) Oxygen plasma treated (Treatment condition: 1 min, 500w, 0.3 torr);

(c) Ammonia plasma treated (Treatment condition: 1 min, 500 w, 0.3 torr)

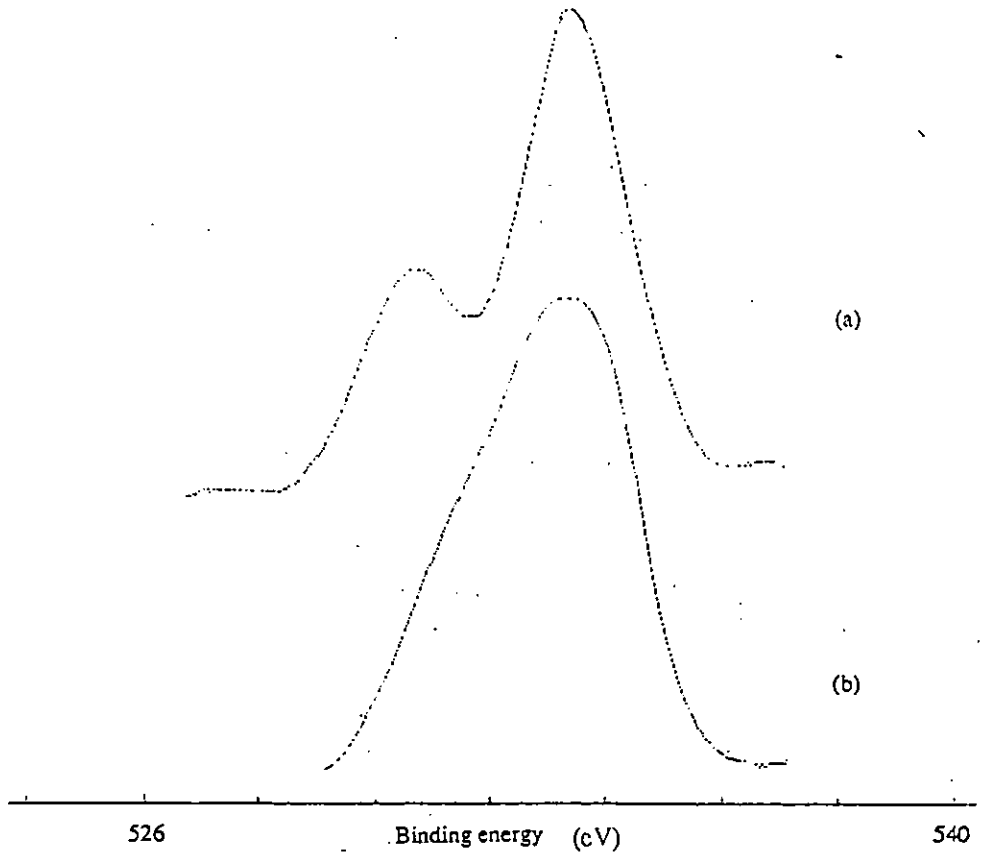

Fig. 10.5 O_{1s} peaks of untreated and plasma treated films

(a) Untreated

(b) Oxygen plasma treated (Treatment condition: 1 min, 500 w, 0.3 torr)

Fig. 10.4 shows the C_{1S} peaks of untreated and plasma treated films. Two noteworthy features are apparent:

(a) The higher binding energy part of the C_{1S} peak becomes larger after plasma treatment, suggesting that the increased oxygen and (or) nitrogen content of plasma treated films may results from the formation of additional functional groups on the surface of PEEK.

(b) The intensity of the π-π^* shake-up satellite at 291.8 eV[131] is reduced by plasma treatment. The results indicate that the amount of aromatic groups on the PEEK surface was reduced by the plasma treatment. In other words, the aromatic structure of the polymer at the surface was destroyed by various plasma treatment. This conclusion is quite consistent with the results obtained by Pawson *et al.* [91]

Fig. 10.5 shows the O_{1S} peaks of untreated and plasma treated PEEK films. From the polymer repeat unit, untreated material has two different oxygen containing groups. one is C=O (at 531.2 eV), the other is C-O-C (at 533.5 eV), and the ratio between them is 1:2, thus the XPS result in Fig. 10.5 is in good agreement with the anticipated result. However, after plasma treatment, the lower energy part of the O_{1S} peak forms a single peak with the higher energy part (as shown in Fig. 10.5), suggesting that the original chain structure of the PEEK film has been changed.

There are four peaks which occur in the high resolution C_{1S} spectra of PEEK, these are illustrated for the untreated and Oxygen plasma treated PEEK in Fig. 10.6. Details of the relative amounts of these, obtained form curve-fitting appear in Table 10.2

Table 10.2 Relative intensities (%) of components in high resolution C_{1S} spectra for plasma treated films

Sample	Binding energy (eV)			
	285.0	286.7	288.0	289.3
Molecular structure	75	21	5	0
Untreated	76	19	5	0
Oxygen plasma treated	71	20	4	6
Ammonia plasma treated	71	20	6	2

Plasma treatment condition: 1 min, 500 w, 0.3 torr

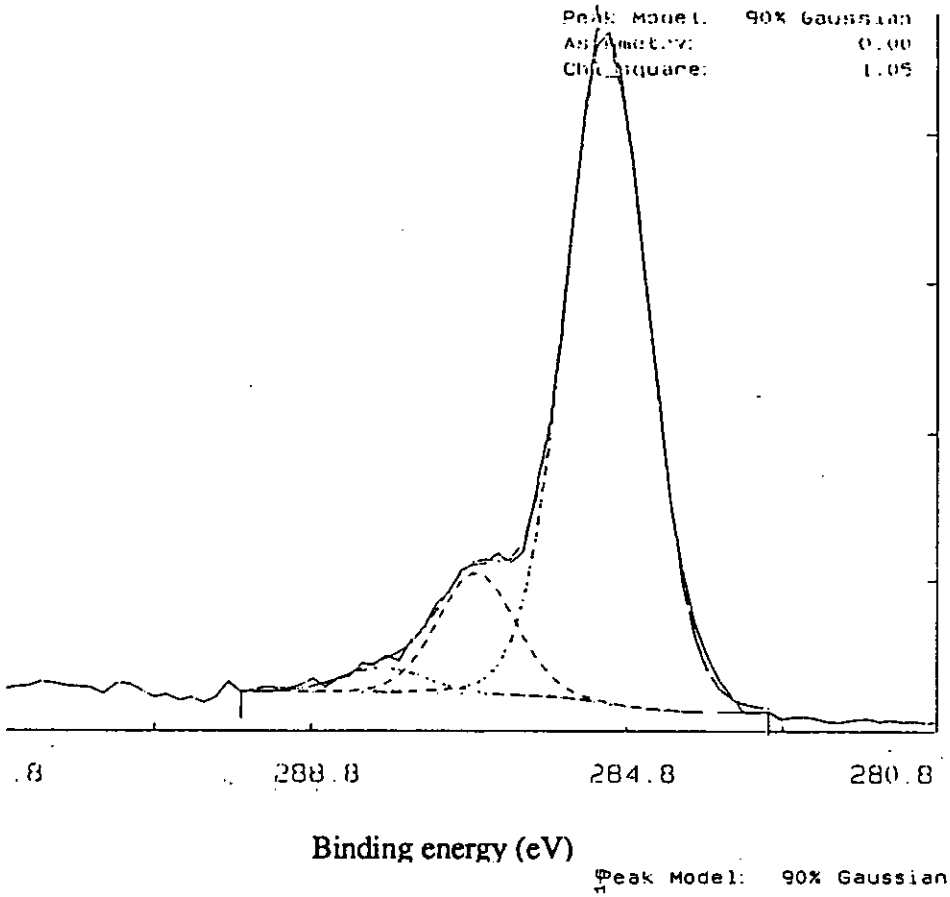

(a)

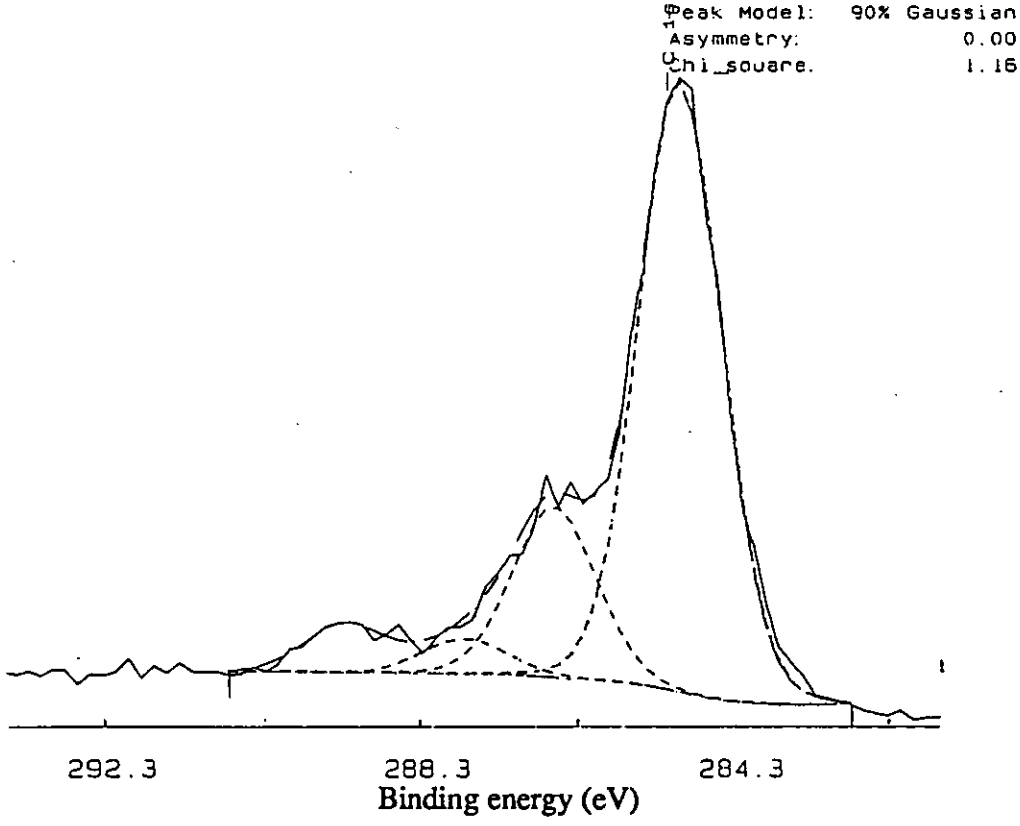

(b)

Fig. 10.6 XPS high resolution C_{1s} spectra of PEEK films before and after oxygen plasma treatment

(a) Untreated

(b) Oxygen plasma treated (Treatment condition: 1 min, 500 w, 0.3 torr)

The assignments of the three peaks of lowest binding energy are as given by Beamson and Briggs[132] and Pawson *et al.* [91], i.e. 285.0 eV aromatic carbon not bonded to oxygen, 286.7 eV aromatic carbon bonded to oxygen and 288.0 eV carbonyl. The peak at 289.3 eV which is produced by both oxygen and ammonia plasma is due to COO units in either an ester or an acid; this evident from the spectra of polymethylmethacrylate and polymethacrylic acid assigned by Beamson and Briggs[132].

10.2.1.3 Chemical derivatisation

To confirm the introduction of hydroxyl and carboxylic groups onto the PEEK surface by plasma treatment, vapour phase chemical derivatisation technique was employed. The reagent used for hydroxyl groups is trifluoroacetic anhydride (TFAA), while that for carboxylic groups is 2,2,2-trifluoroethanol (TFE). Both reagents have been successfully used by many researchers[68,70,72-74,133-138].

The reaction between TFAA and hydroxyl group is

$$-OH + (CF_3CO)_2O \rightarrow -OCOCF_3 + CF_3COOH\uparrow$$

One hydroxyl group will produce three fluorine atoms on the PEEK surface (the relative atomic sensitivity of F_{1S} is very high). Hence, if [F]% is the concentration of fluorine on the PEEK surface after the derivatisation, then the concentration of hydroxyl group on the PEEK surface before the derivatisation is [F]% divided by 3.

Table 10.3 gives the elemental composition of some plasma treated PEEK after TFAA derivatisation. From the concentration of fluorine, the concentration of -OH groups that existed on the plasma treated PEEK surface can be easily calculated, the results are shown in Table 10.5.

Table 10.3 Atomic analyses per 100 carbon atoms from survey spectra of plasma treated PEEK after TFAA derivatisation

Treatment gas*	O	N	F
Oxygen	30.1	0	9.9
Argon	32.0	0.7	9.6
Air	35.3	3.3	13.7

* Treatment condition: 1 min, 500 w, 0.3 torr

The reaction between TFE and acid groups is

$$-COOH + CF_3CH_2OH \rightarrow CO_2CH_2CF_3 + H_2O\uparrow$$

Similar to TFAA derivatisation, one carboxylic group will produce three fluorine on the PEEK surface after TFE derivatisation reaction. Therefore, the concentration of fluorine on the derivatised surface divided by 3 is the concentration of carboxylic group on the underivatised surface. The elemental composition of some plasma treated PEEK after TFE derivatisation are shown in Table 10.4. The concentrations of calculated carboxylic groups on plasma treated surfaces from the data in Table 10.4 are listed in Table 10.5.

Table 10.4 Atomic analyses per 100 carbon atoms from survey spectra of plasma treated PEEK after TFE derivatisation

Treatment gas*	O	F
Oxygen	35.6	8.7
Argon	32.5	4.6
Air	32.0	7.5

* Treatment condition: 1 min, 500 w, 0.3 torr

Table 10.5 Concentrations of hydroxyl and carboxylic groups on plasma treated surfaces

Treatment gas*	C-C	-OH	-COOH
Oxygen	100	3.3	2.9
Argon	100	3.2	1.5
Air	100	4.7	2.5

* Treatment condition: 1 min, 500 w, 0.3 torr

As untreated material does not have any hydroxyl or carboxyl groups, the data listed in Table 10.5 confirm that plasma treatment introduce some amount of -OH and COOH onto the PEEK surface.

10.2.2 Effect of corona discharge treatment

10.2.2.1 Elemental composition studies

Similar to plasma treatment, corona discharge treatment also introduced some oxygen and nitrogen onto the surface of PEEK. As shown in Table 10.6, the oxygen concentration per 100 carbon atoms on the untreated PEEK surface is 17.6, and no nitrogen on that surface, but after corona discharge treatment, oxygen concentration was increased to more than 23, and some nitrogen atoms can be found on the surface.

Table 10.6 Atomic analyses per 100 carbon atoms from survey spectra of PEEK films before and after corona discharge treatment

Treatment gas*	O	N
Molecular structure	15.7	0
Untreated PEEK	17.6	0
Air	25.6	1.0
Ammonia	23.7	4.4
Oxygen	27.4	3.8
Argon	23.1	1.5

* Treatment level: 0.4 J mm^{-2}

10.2.2.2 C_{1s} and O_{1s} spectra

Corona discharge treatments also change the shape of C_{1s} and O_{1s} peaks for PEEK films, as shown in Fig. 10.7 and Fig. 10.8. The effects are quire similar to those of plasma treatment.

For C_{1s} peak, the π-π^* shake-up signal was reduced after treatment, and for O_{1s} peak, the dual peaks simplified as one. The results suggest that corona discharge treatments not only destroy some of the aromatic structure on the surface but also change the relative amount between C-O and C=O bonds.

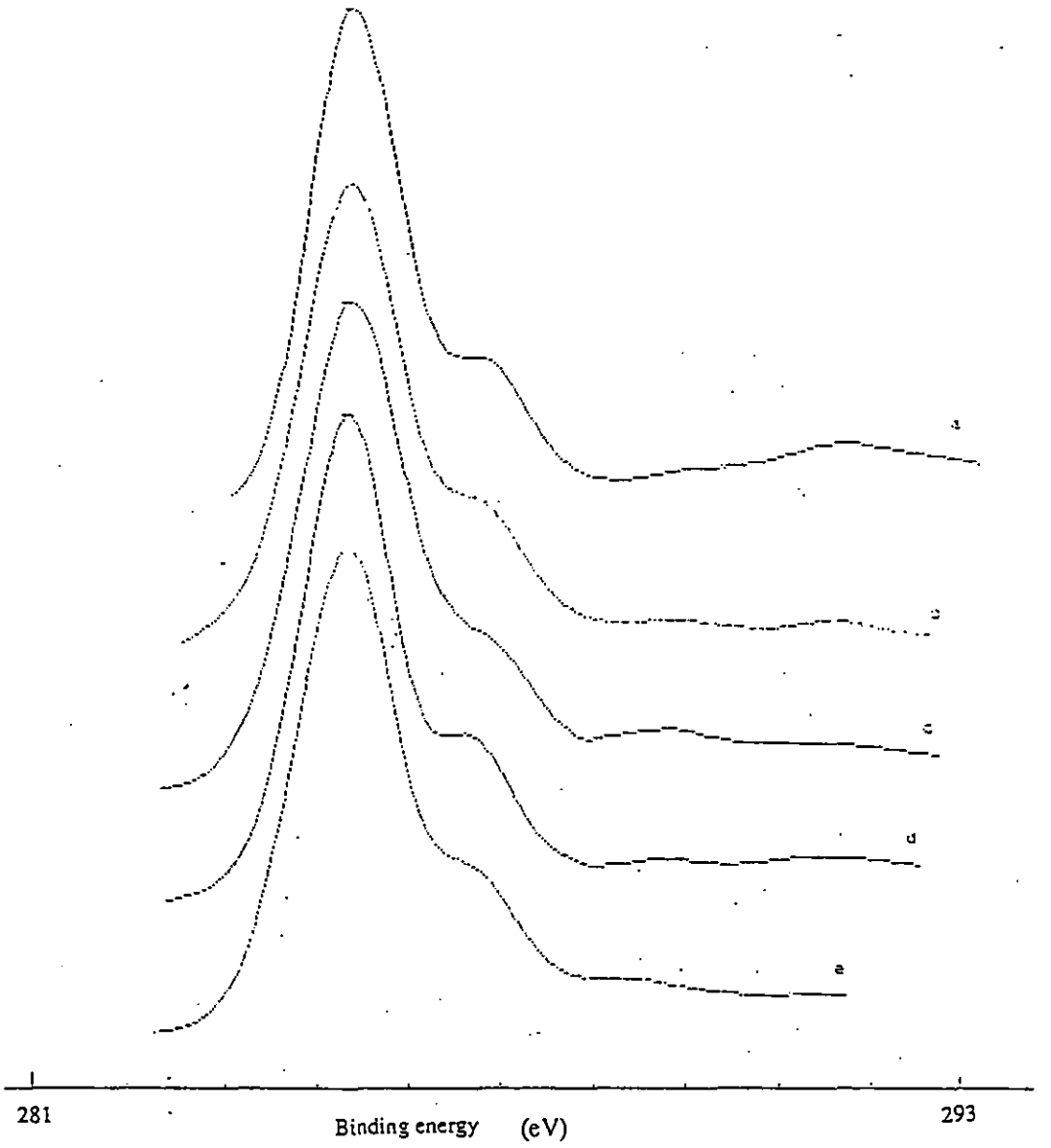

Fig. 10.7 Effects of corona discharge treatment on the C_{1s} peak for PEEK

(a) Untreated

(b) Air corona (treatment level: 0.4 J mm^{-2})

(c) Oxygen corona (treatment level: 0.4 J mm^{-2})

(d) Argon corona (treatment level: 0.4 J mm^{-2})

(e) Ammonia corona (treatment level: 0.4 J mm^{-2})

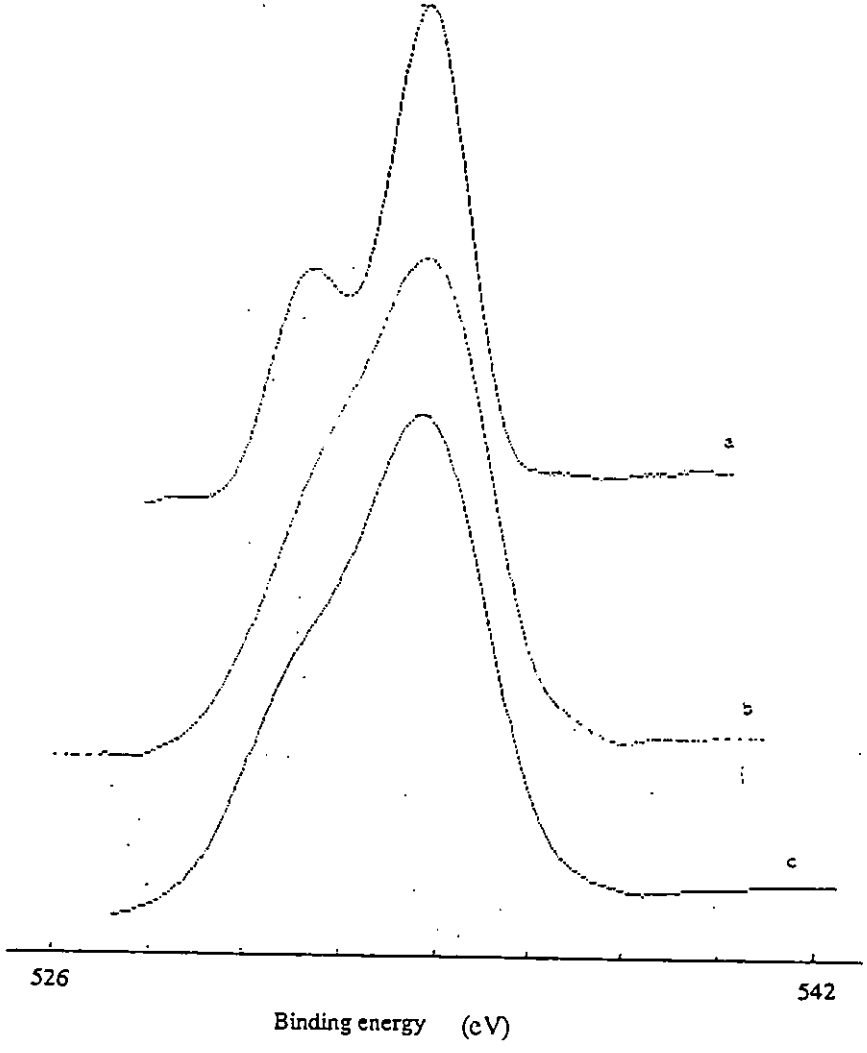

Fig. 10.8 Effects of corona discharge treatment on the O_{1s} peak for PEEK
(a) Untreated
(b) Oxygen corona (treatment level: 0.4 J mm^{-2})
(c) Air corona (treatment level: 0.4 J mm^{-2})

High resolution analyses confirm that corona discharge treatments change the surface chemical structure of PEEK films. The results are shown in Table 10.7. Table 10.7 lists the relative intensities (%) of different groups on the PEEK surface before and after corona discharge treatments. As it can be seen, the corona treatments introduce some acid groups onto the PEEK surface.

Table 10.7 Relative intensities (%) of components in high resolution C_{1s} spectra for corona discharge treated films

Treatment gas*	Binding energy (eV)			
	285.0 C-C	286.7 C-O	288.0 C=O	289.3 COOH
Molecular Structure	73.7	21.0	5.3	0
Untreated film	76.5	18.6	4.9	0
Air	76.4	22.0	2.3	2.8
Ammonia	76.5	19.4	5.3	4.1

* Treatment level: 0.4 J mm^{-2}

10.2.3 Effects of solvent washing on the treated surfaces

It has been found that some of the oxygen and (or) nitrogen atoms introduced by the plasma and corona discharge treatment can be removed by the commonly used solvents (which are not PEEK soluble, as discussed in Section 12.4.1). The results are shown in Table 10.8-10.10

Table 10.8 shows the effect of acetone and IPA washing on the surface element composition of plasma treated films. Several conclusions may be drawn from this table:

(a) Both acetone and IPA washing reduce the amount of oxygen on the oxygen plasma treated surface, but not back to that of the untreated material.

(b) Acetone and IPA washing has very little effect on the oxygen concentration on the argon plasma treated surface, however, they remove all the nitrogen introduced by the argon plasma treatment.

(c) For air plasma treated films, acetone and IPA washing slightly reduce the amount of oxygen on the treated surface, but removes all the nitrogen from the treated surface.

(d) Acetone and IPA washing has little effect on the oxygen amount on the ammonia plasma treated surface, but reduce the amount of nitrogen introduced by the treatment.

Table 10.8 Effects of solvent washing on the surface element composition per 100 carbon atoms of plasma treated films

Treatment gas*	Solvent washing	Oxygen	Nitrogen
Molecular structure		15.8	0
Untreated		17.6	0
Oxygen	Before	38.1	0
	Acetone washing	23.5	0
	IPA washing	35.4	0
Ammonia	Before	16.3	9.1
	Acetone washing	17.2	5.7
	IPA washing	15.3	3.9
Argon	Before	30.2	9.0
	Acetone washing	33.3	0
	IPA washing	32.5	0
Air	Before	31.0	2.2
	Acetone washing	28.7	0
	IPA washing	27.9	0

* Treatment condition: 1 min, 500 w, 0.3 torr

Table 10.9 gives the results of surface elemental composition on corona discharge treated PEEK surfaces before and after solvent washing. As it can be seen, both acetone and IPA washing almost recover the oxygen and nitrogen amount on the corona discharge treated surfaces (within the XPS detecting depth) back to those of the untreated material, no matter which gas was injected into the corona discharge. This result is different with that of plasma treated samples.

To further study the effects of solvents, high resolution analysis of C_{1s} spectra for some treated samples was carried out, the results are shown in Table 10.10. Two noteworthy features are obvious:

One is that acetone and IPA washing increase the aromatic C-C bond on both plasma and corona treated surfaces

Table 10.9 Effects of solvent washing on the surface element composition per 100 carbon atoms of corona discharge treated films

Treatment gas*	Solvent washing	Oxygen	Nitrogen
Molecular structure		15.8	0
Untreated		17.6	0
Air	Before	25.6	1.0
	Acetone washing	17.4	0
	IPA washing	17.5	0
Ammonia	Before	23.7	4.4
	Acetone washing	22.2	0
	IPA washing	16.9	1.2
Oxygen	Before	27.4	3.8
	Acetone washing	16.1	0
	IPA washing	18.3	0
Argon	Before	23.1	1.5
	Acetone washing	15.5	0
	IPA washing	15.3	0

Treatment level: 0.4 J/mm^{-2}

Table 10.10 Effect of solvent on the surface chemical composition of plasma and corona discharge treated PEEK films analysed by high resolution C_{1s} spectra

Sample	Solvent washing	Binding energy (eV)			
		285.0 C-C	286.7 C-O	288.0 C=O	289.3 -COO
Molecular structure		73.7	21.0	5	0
Untreated		76.5	18.6	4.9	0
O_2 plasma treated	Before	70.7	19.7	4.0	5.6
	Acetone washing	78.5	18.7	1.8	1.1
	IPA washing	73.2	19.2	4.6	3.0
NH_3 plasma treated	Before	71.5	20.2	6.3	2.0
	Acetone washing	76.3	18.2	5.5	0
Air corona treated	Before	76.4	18.5	2.3	2.8
	Acetone washing	78.0	22.0	0	0

Plasma treatment condition: 1 min, 500 w, 0.3 torr

The other is that acetone and IPA washing reduce the amount of -COOH group introduced by the plasma and corona discharge treatment. The extent depends on the treatment gas.

10.3. TOF-SIMS Analysis

10.3.1 Untreated PEEK

(a) Positive ion spectra

The positive ion spectra for untreated PEEK is displayed in Fig. 10.9

Below a.m.u. 100 a series of peak at a.m.u. 39, 51, 77 and 91 are typical of polymers containing aromatic groups[139], all other peaks in this region are due to carbon- and hydrogen- containing ions, which are found in the positive ion spectra of nearly all polymers[140]. Our results in this region are quite similar to those obtained by Pawson *et al.* [91]

As suggested by Pawson *et al.* [91], the peaks which are unique to PEEK are shown in the region between a.m.u. 100 and 300. These characteristic peaks are at a.m.u. 104, 105, 195-197, 213-215 and 287-289 which correspond to the following structure and polymer repeat unit $(M\pm H)^+$ (a.m.u. 287-289).

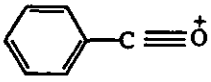
a.m.u. 104

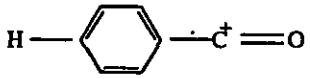
a.m.u. 105

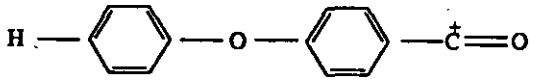
a.m.u. 197

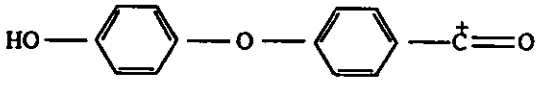
a.m.u. 213

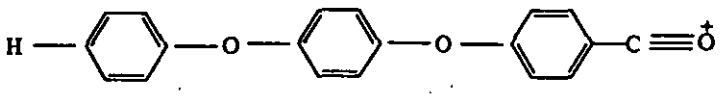
a.m.u. 289

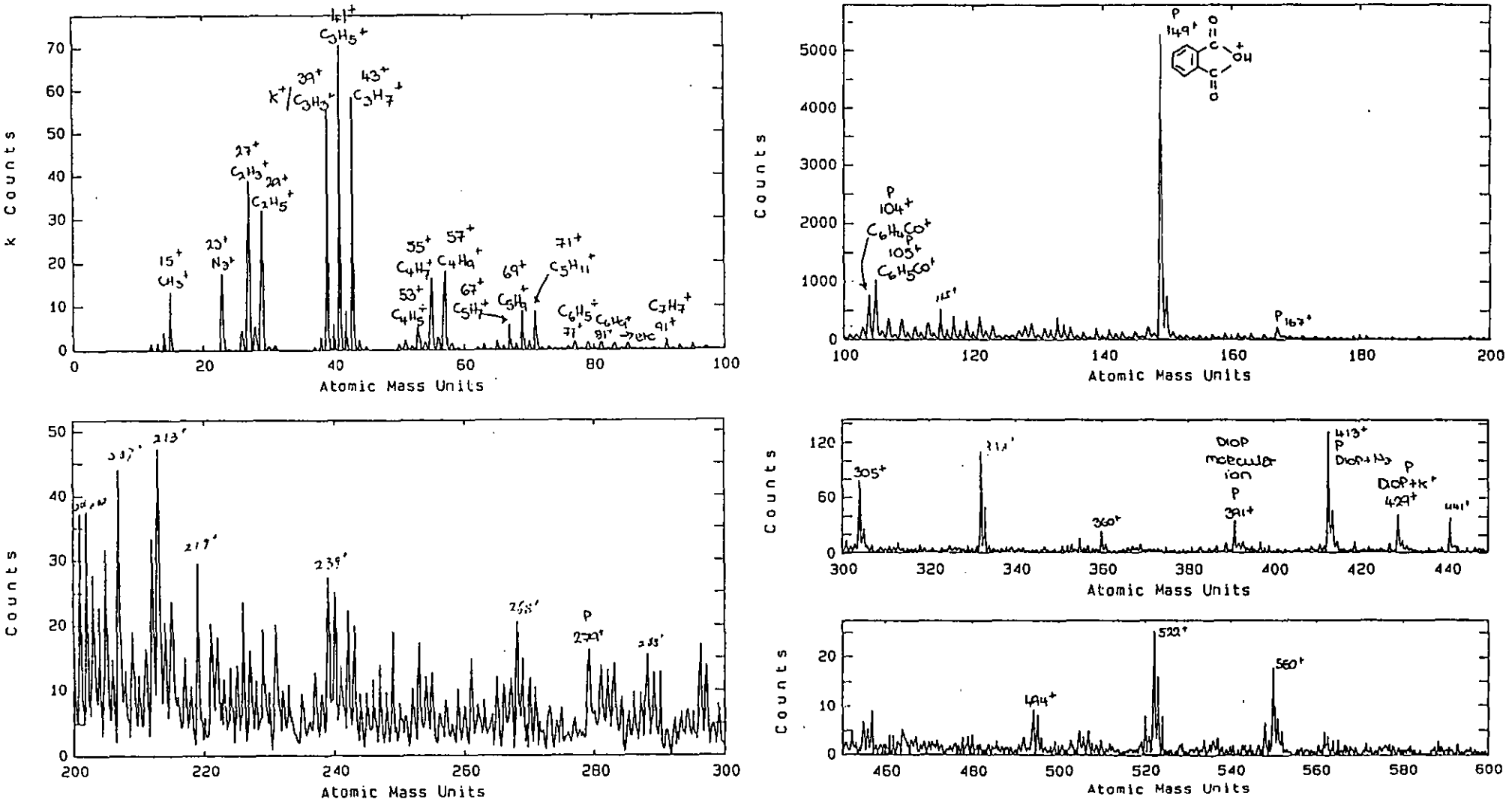

Fig. 10.9 Positive ion spectrum of untreated PEEK

In Fig. 10.9, peaks at a.m.u. 104, 105, 213 and a peak with low intensity at 288 can be found, but peaks at a.m.u. 195-197 are missing.

In this mass region there is a very strong signal at a.m.u. 149, which can be assigned to the structure

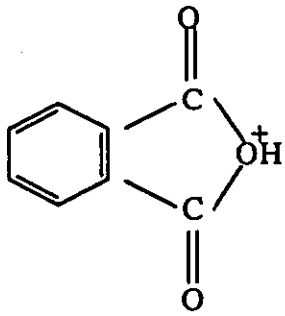

a.m.u. 149

It is not known where this structure comes from.

There are also other weak signals appear in this region. They are the peaks at a.m.u. 201, 202, 207, 219, 239 and 268. Assigning these signals is very difficult. They must be originated from the polymer, though it is not possible to draw ion structures for these peaks based directly on the polymer repeat unit. Therefore, these ions must originate from large ions which have undergone rearrangement and fragmentation prior to mass analysis. However, these peaks did not appear in the spectra obtained by Pawson *et al.* [91], instead they found peaks at a.m.u. 139 and 163 from unknown origin.

Above a.m.u. 300, peaks appear at a.m.u. 305, 332, 391, 413, 429, 441, 494, 522 and 550 with very low intensities. It is also not possible to assign these peaks to any ion structures. In the following sections, the spectrum above a.m.u. 300 will be omitted.

(b) Negative ion spectra

According to ref. 140, in the negative ion spectra of oxygen-containing polymers, rearrangement reactions are not considered to play a particularly important role, and for this reason it is often asserted that negative ion spectra are more reliable than positive spectra for elucidating polymer structure. The negative ion spectra of untreated PEEK are displayed in Fig. 1.10.

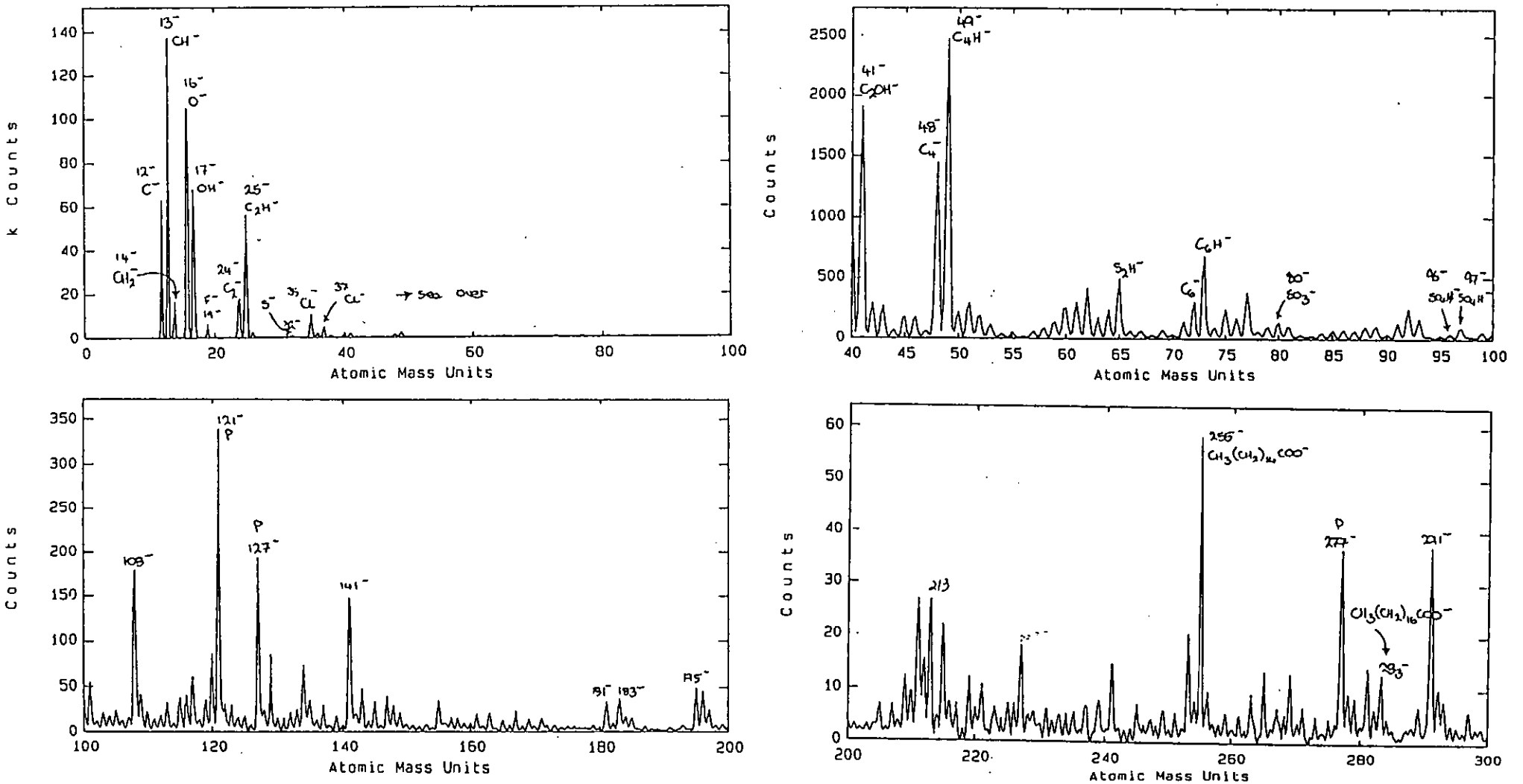

Fig. 10.10 Negative ion spectrum of untreated PEEK

Many peaks appear below a.m.u. 100, however, ions below a.m.u. 60 are not usually considered valuable in a diagnostic sense. These ions correspond to O^- and OH^- (a.m.u. 16 and 17) and C_n^- and $C_nH_m^-$ clusters[140]

Weak signal at a.m.u. 19 is assigned to F^-, which is thought to be indicative of the fluorine-terminated end groups originated from the polymerisation process. This assumption was supported by the weak peak at a.m.u 97, which is assigned to the structure

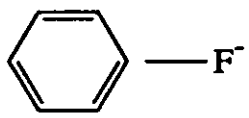

a.m.u. 97

This result is similar to that obtained by Pawson *et al.* [91]

Above a.m.u 100, our results are quite different with those obtained by Pawson *et al.*[91]. They only found strong signal at a.m.u. 108 and peaks with low intensities at a.m.u. 197 and a.m.u. 213. The latter two signals can be assigned to two structures respectively;

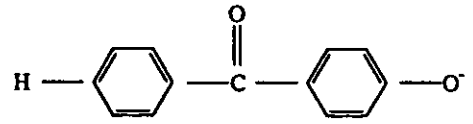

a.m.u.197

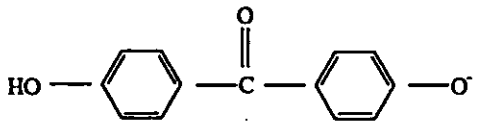

a.m.u. 213

while the former signal could not be assigned. In Fig. 10.10 can be seen not only those peaks but many other signals as well. They are the strong signals at a.m.u. 121, 127, 141, 255, 277 and 291, and the weak signals at a.m.u 181, 183. It is also not possible to assign these peaks.

10.3.2 Effect of plasma treatment

10.3.2.1 Oxygen plasma treatment

(a) Positive ion spectrum (Fig. A2.1)

Compared with the positive ion spectrum of untreated, the following noteworthy features are apparent:

Below a.m.u. 100, a new peak appeared at a.m.u. 18. The origin of this peak has been the subject of speculation[139,141]. It has been suggested that this peak arises from either adsorbed water at the modified surface or, alternatively, from an oxygen functionality formed in the polymer surface during plasma treatment. However, work carried out by Briggs (cited in ref. 91) has led to the unexpected conclusion that in some plasma-treated polymer surfaces the peak at a.m.u. 18 arises from NH_4^+. In addition to this new peak, the relative intensities of peaks at a.m.u. 39, 41 and 43 were reduced.

Between a.m.u. 100-200, a new weak signal appeared at a.m.u. 121

Between a.m.u. 200-300. oxygen plasma treatment introduced new strong signals at a.m.u. 219 and 242 and removed all other signals in this region except the peak at a.m.u. 213, which was enhanced.

(b) Negative ion spectrum (Fig. A2.2)

The differences arise from oxygen plasma treatment can be summarised as the following:

Below a.m.u. 100, the intensities of peaks at a.m.u. 16 (O^-), 17 (OH^-) and 41 (C_2OH^-) were significantly enhanced by the treatment suggesting that oxygen plasma treatment introduced some oxygen containing groups onto the PEEK surface. Other changes of the signals in this region were the slightly enhancing of some weak signals at a.m.u. 45, 57, 59, 77, 93, 95, 97.

Between a.m.u. 100-200, signals at a.m.u. 127, 141, 181, 183, 195-197 disappeared after oxygen plasma treatment, while signals at a.m.u. 108 and 121 still remained there.

Between a.m.u. 200-300, a strong signal appeared at a.m.u. 203, while peaks at a.m.u 227, 253 and 255 disappeared after the treatment. In addition the signal at a.m.u. 211 was enhanced, while the peak at a.m.u. 291 remained little changed.

Hence, both positive and negative ions results confirmed our previous results that oxygen plasma treatment changes the surface chemical structure of PEEK.

10.3.2.2 Ammonia plasma treatment

(a) Positive ion spectrum (Fig. A2.3)

Below a.m.u. 100, similar to oxygen plasma treatment, after ammonia plasma treatment, a new peak appeared at a.m.u. 18, and the relative intensities of peaks at a.m.u. 39, 41 and 43 were reduced.

Between a.m.u. 100-200, a new weak signal appeared at a.m.u. 133 after treatment.

Between a.m.u. 200-300, just like oxygen plasma treatment, ammonia plasma also introduced a new peak at a.m.u 219, however, it introduced another new peak at a.m.u 211, instead of at a.m.u 242, which was the case of oxygen plasma treatment. In addition to the introduction of new peaks, ammonia plasma treatment removed all other peaks shown in the untreated PEEK spectrum.

(b) Negative ion spectrum (Fig. A2.4)

Below a.m.u. 100, ammonia plasma treatment produced new peaks at a.m.u 15 (NH^-), 26 (CN^-), 42 (CNO^-), 66 and 71. The latter two signals are difficult to be assigned. The intensities of peaks at a.m.u. 16 (O^-), 17 (OH^-) and 41 (C_2OH^-) were enhanced just like the oxygen plasma treatment effect.

Between a.m.u. 100 and 200, the spectrum become much complicated after ammonia plasma treatment. Strong new signals appeared at a.m.u 115, 131 and 185, while signals at a.m.u 108, 127, 141, 181, 183, 195-197 disappeared (this is similar to the effect of oxygen plasma treatment)

Between a.m.u. 200-300, a new peak show at a.m.u. 203, and peaks at 227 was much enhanced, while the intensities of other peaks were reduced.

Summarised the positive and negative ions results, it can be concluded that ammonia plasma treatment also changes the surface chemical structure of PEEK and incorporates some nitrogen and oxygen containing groups in the surface layer. This result is in good agreement with the XPS results.

10.3.3 Effect of solvent washing on the plasma treatment effects

10.3.3.1 Oxygen plasma treated sample

(a) Positive ion spectrum (Fig. A2.5)

Compared with unwashed sample, acetone washing caused the following changes

Below a.m.u. 200, signal at a.m.u. 18 was significantly reduced.

Between a.m.u. 200-300, signals at a.m.u. 213 and 219 introduced by oxygen plasma treatment were reduced greatly, however, the peak at a.m.u. 242 remained unchanged. In addition, a relatively strong new signal appeared at a.m.u. 214, and a weak signal shown at a.m.u. 288, which represents the polymer repeat unit of PEEK chains

(b) Negative ion spectrum(Fig. A2.6)

Below a.m.u. 100, the intensities of peaks at a.m.u. 16 (O^-), 17 (OH^-) and 41 (C_2OH^-) were reduced significantly. The signals enhanced by oxygen plasma treatment at a.m.u. 45, 57, 59, 77, 93, 95 and 97 were also reduced.

Between a.m.u. 100-200, signals at a.m.u. 127, 141, 181, 183, 195-197 removed by oxygen plasma treatment reappeared after washing but with different intensities.

Between a.m.u. 200-300, peak at a.m.u. 203 introduced by oxygen plasma treatment disappeared after washing, while a new peak appeared at a.m.u. 281. In addition, the peaks at a.m.u. 227-253, 255, which were removed by the plasma treatment, reappeared after washing. The signal at a.m.u. 211, which was enhanced by the plasma treatment, was reduced by washing.

Therefore, both positive ions and negative ions results suggest that changes caused by oxygen plasma treatment are lost to some extent by acetone washing.

10.3.3.2 Ammonia plasma treated samples

(a) Positive ion spectrum (Fig. A2.7)

Below a.m.u. 100, acetone washing did not make much difference to the spectrum of ammonia plasma treated PEEK.

Between a.m.u. 100-200, acetone removed the peaks at a.m.u. 104 and 133. The latter peak was introduced by the ammonia plasma treatment. However, acetone washing introduced two new weak signals at a.m.u. 107 and 109.

Between a.m.u. 200-300, the peaks at a.m.u. 211, which was introduced by ammonia plasma treatment, disappeared after acetone washing. while another peak introduced by the treatment, which is at a.m.u 219, remained unchanged.

(b) Negative ion spectrum (Fig. A2.8)

Below a.m.u. 200, acetone washing only reduced the peak at a.m.u. 26 (CN^-) slightly, while other peaks introduced by the plasma treatment remained unchanged.

Between a.m.u. 200-300, the signal at a.m.u. 203, which was introduced by the treatment, reduced significantly after acetone washing. While the signal at a.m.u. 227, which was greatly enhanced by the treatment, also reduced significantly. Acetone washing removed the peaks at a.m.u. 213, 277 and 291, which existed in both untreated and ammonia plasma treated PEEK spectra. In addition, acetone washing enhanced the peak at a.m.u. 255, which was reduced significantly by the plasma treatment.

Therefore, both positive and negative ions results suggest that acetone washing can also bring back to some extent the chemical structures changed by the ammonia plasma treatment.

CHAPTER 11 MODELLING OF THE PLASMA AND CORONA DISCHARGE TREATED SURFACES

11.1 Modelling The Treated Surfaces

PEEK is a linear aromatic polymer, with two ether groups, one carbonyl group and three benzene rings in its repeat unit, as shown in Fig. 11.1

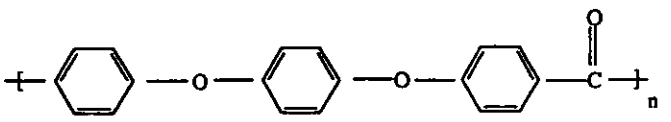

Fig. 11.1 Chemical structure of PEEK

When PEEK is exposed to plasma or corona discharge, the plasma and corona species, which consists of atoms, molecules, ions, free radicals, free electrons and metastable species and etc.[108], attack the benzene rings, the ether bonds and the carbonyl bonds. The effects of these attacks can be the following and, of course, several may occur simultaneously:

(a) Opening of some benzene rings with or without producing small molecules

(b) Chain scission at the ether and carbonyl site, forming fragments of various size.

(c) The products of the above events react with each other or with the treatment gas, causing the introducing of some oxygen and nitrogen containing functional groups into the polymer chains and further scission or cross-linking of the molecular chains.

(d) The incorporation of oxygen and nitrogen containing groups directly into the benzene rings.

To model the treated surfaces, the surface characterisation results given in the last Chapter are summarised here to evaluate the above postulations.

Firstly, both XPS and TOF-SIMS analysis revealed that both plasma and corona discharge treatment change the chemical structure of the PEEK surface. XPS studies have found that all the plasma and corona treatments reduced the π-π^* shake-up signal, which represents the aromatic rings, hence confirmed that some of the aromatic rings on the surface were opened after treatment.

Secondly, both XPS and TOF-SIMS studies have shown that all treatments introduced oxygen and (or) nitrogen containing functionality groups to the PEEK surface, like -OH, -COOH and etc.

Thirdly, XPS and TOF-SIMS studies have revealed that both acetone and IPA washing can significantly reduce the oxygen and (or) nitrogen concentration on the treated surfaces confirming that treatment may produce some small molecules or small fragments on the treated surfaces which are soluble in the ordinary solvents.

Based on these results, it is believed that the treated PEEK surfaces can be modelled as a modified layer. This layer is mainly consisted of plasma (or corona discharge) produced products with varying molecular weight. According to XPS and TOF-SIMS results, those products may have higher polarity (more functionality groups) compared with the untreated material's molecules. The molecules in the modified layer can be divided into two categories subject to their washability by the solvents (such as acetone), namely, low molecular weight molecules (LMWM) which can be washed away by solvent, and high molecular weight molecules (HMWM) which can not be removed by simply solvent washing.

11.2 FTIR Studies on The Low Molecular Weight Molecules (LMWM) Produced by The Treatment

To characterise the LMWM produced by the treatment, both oxygen plasma and ammonia plasma treated films were immersed in acetone for one week five minutes after the treatment. The solvents were then studied by FTIR.

Table 11.1 compares the signals appeared in the spectra of acetone before and after immersing of plasma treated films. It was found that there is a new signal at about 3500 cm^{-1} after immersed of either oxygen plasma or ammonia plasma treated films. This signal could be assigned to hydroxyl or carboxylic acid groups. In the case of ammonia plasma treated materials, this could be amine groups.

Table 11.1 Spectra comparison of acetone before and after immersion of plasma treated films

Pure acetone	After immersion of oxygen plasma treated films	After Immersion of ammonia plasma treated films
	~3493 cm^{-1}	~3572 cm^{-1}
~3005 cm^{-1} ($-CH_3$)	~3005 cm^{-1}	~3005 cm^{-1}
~1713 cm^{-1} (-C=O)	~1711 cm^{-1} (-C=O)	~1713 cm^{-1} (-C=O)
~1422 cm^{-1}	~1424 cm^{-1}	~1422 cm^{-1}
~1364 cm^{-1}	~1366 cm^{-1}	~1364 cm^{-1}
~1223 cm^{-1}	~1225 cm^{-1}	~1223 cm^{-1}
~1093 cm^{-1}	~1094 cm^{-1}	~1094 cm^{-1}

After subtracting pure acetone spectrum, the spectra for acetone immersed of oxygen plasma treated materials and ammonia plasma treated films are shown in Fig. 11.1 and Fig. 11.2 respectively.

As it can be seen, after subtraction, there are two new signals at ~3500 cm^{-1} and 1649 cm^{-1} in the spectra for acetone rinsed of either oxygen plasma or ammonia plasma treated films. The assigning of the former signal was discussed above, while its broad range may indicate the existence of intermolecular hydrogen bonding [142]; The latter signal is difficult to be assigned, but according to ref .143, it could be due to the enolisation between the ester C=O and the enolic hydroxyl group.

Other signals appeared in the subtracted spectra are similar to those of pure acetone but with a slightly different absorbing frequency. For instance the C=O signal, for acetone after extraction of oxygen plasma treated films, this signal appears at about ~1707 cm^{-1} in stead of at ~1713 cm^{-1}, which is the case of pure acetone. This could be due to the conjugation of -C=O group with other groups, like -C=C- . Therefore, acetone washing may wash out LMWM with hydroxyl, carboxyl, carbonyl, amine, ketone and etc. groups from the plasma treated surfaces. These groups could play a very important role on the surface properties. The role played by LMWM will be discussed in next Chapter.

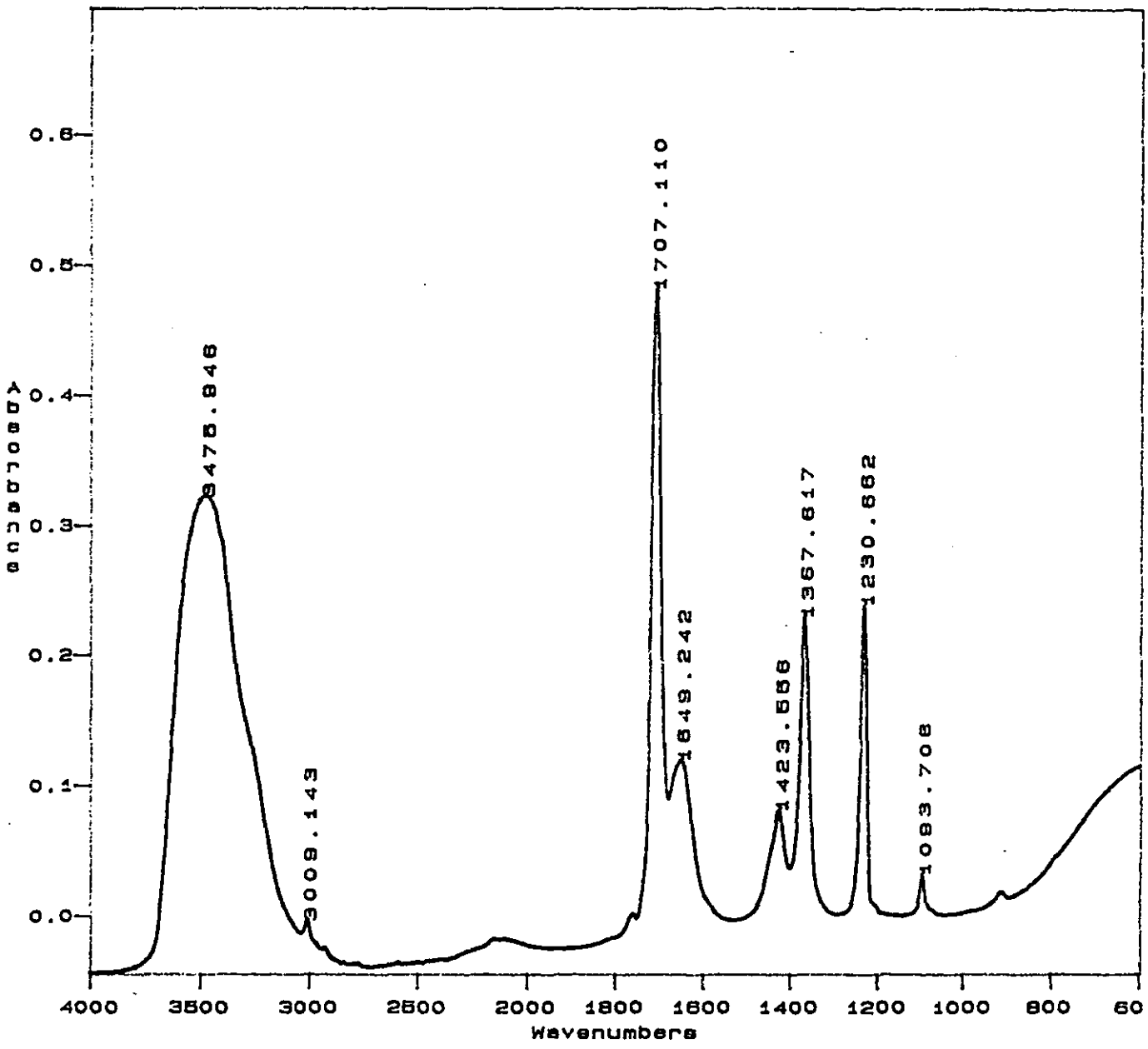

Fig. 11.1 Spectrum for acetone immersed with oxygen plasma treated films after subtracting the spectrum for pure acetone

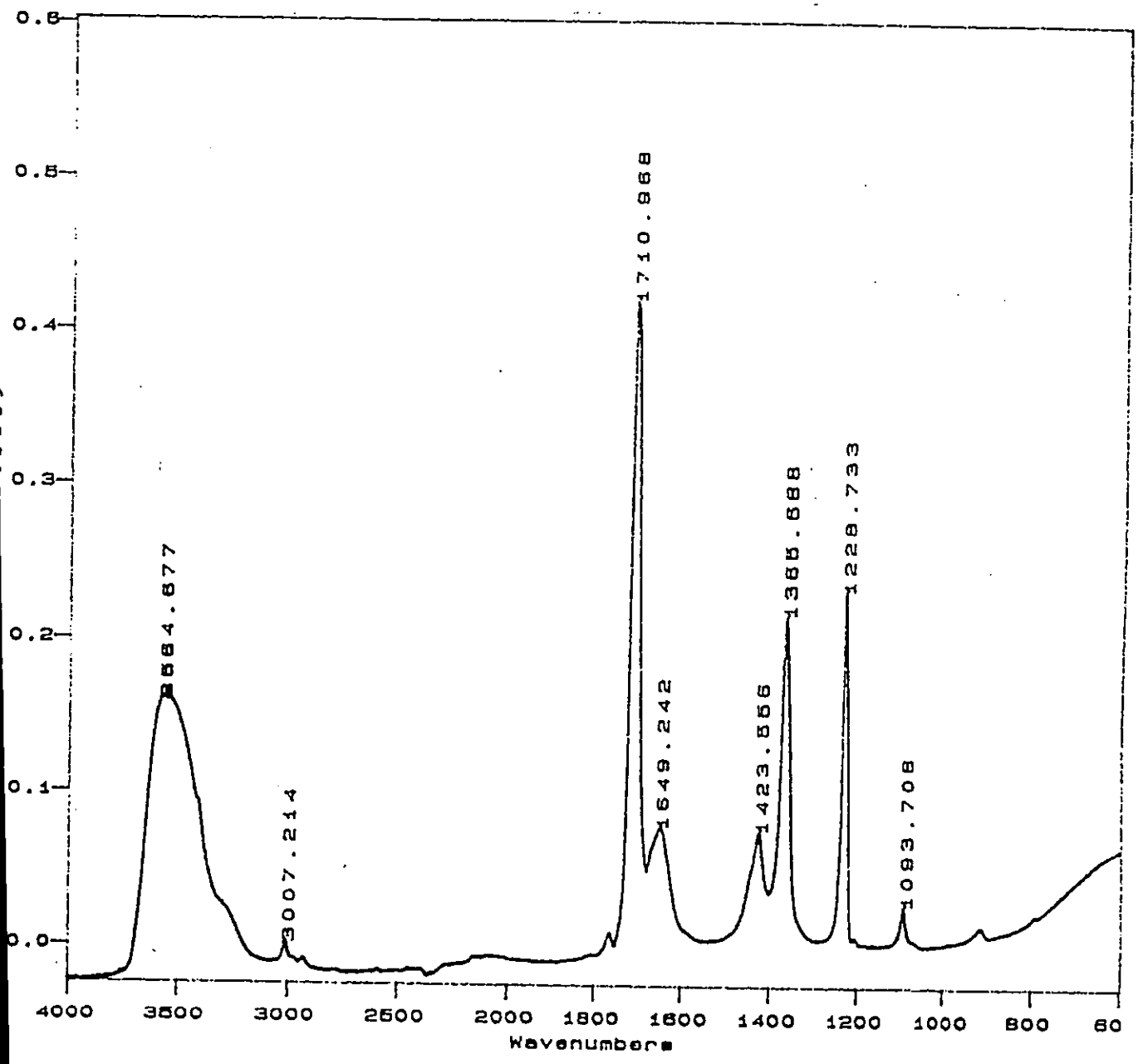

Fig. 11.2 Spectrum for acetone immersed with ammonia plasma treated films after subtracting the spectrum for pure acetone

CHAPTER 12 STUDIES ON THE MECHANISMS OF BONDABILITY ENHANCEMENT

Adhesion is a surface phenomenon and, therefore, the bond strength is governed by surface properties. The results in Chapter 8, 9 and 10 have shown that both plasma and corona discharge treatment significantly changes the bondability, wettability and surface chemical compositions of PEEK films. This Chapter try to correlate the adhesion of the treated materials to their surface properties. Before making the correlation, the adhesion theories available were reviewed and their relevance to this work were analysed.

12.1 Adhesion Theories

There are five adhesion theories which have been proposed, namely:

(a) Weak boundary layers
(b) Mechanical interlocking
(c) Diffusion theory
(d) Electronic theory
(e) Adsorption theory

Some years ago many works searched for "the mechanism of adhesion", but more recently it has become generally accepted that, whilst the adsorption theory has the widest applicability, each of the others may be appropriate in certain circumstances and often make a contribution to the intrinsic adhesion forces which are acting across the interface[144]. These theories will be discussed respectively in the following sections.

12.1.1 Weak boundary layer

An adhesive bond will fracture at its weakest link. Thus, if a cohesively weak layer exists on the adherend surface, the adhesive bond may fracture within this weak boundary layer at low applied stress. For polymers, the WBL maybe common because of their tendency to reject foreign substance to their surfaces by the process of diffusion. An important foreign substance which might be a general source of WBL is

low molecular mass polymer. In addition, WBL also could occur as the consequence of contamination.

However, solvent washing, abrasion or blasting can hardly improve the adhesive joint strength of neat PEEK or its composites [6,7,100-103]. The results indicate that the low joint strength of PEEK is not due to the existence of WBL if it exists on the untreated surface.

12.1.2 Mechanical interlocking

This theory essentially proposes that mechanical keying, or interlocking, of the adhesive into the irregularities of the substrate surface is the major source of intrinsic adhesion[145]. Hence, in order to get maximum bond properties, the adherends must be roughened in some way.

Nevertheless, the results in Chapter 10 show that both plasma and corona discharge treatment have very little effects on the surface topography of the PEEK films studied. Therefore, the bondability enhancement in this work is thought to be due to other mechanisms.

12.1.3 Diffusion theory

In essence, the theory states that during the adhesive bonding operation, segments or potions of the polymer in the adhesive diffuse into the polymeric substrate and vice versa. This requires that the macromolecules or chain segments of the polymers (adhesive and substrate) possess sufficient mobility and are mutually soluble. Voyutskii [23] in particular have been the strong advocates of the diffusion mechanism.

If the above requirements are met then the diffusion of an adhesive into a substrate will increase as the period of contact, temperature, pressure are increased. Further, diffusion will decrease if molecular weight and crosslinking are increased.

To consider the possibility of diffusion then several facts have to be considered. Firstly, PEEK has a T_g value above the curing temperature of the epoxy adhesive employed. Secondly, PEEK and the adhesive employed are not identical polymers. Hence it is unlikely that interdiffusion across the interface could occur in our case.

The modified layer produced by the plasma and corona discharge treatment (as modelled in last Chapter), however, could possibly possess sufficient mobility and has similar solubility with the adhesive. Hence, adhesive could diffuse into the treated surface to some extend, but according to Anand [146], even in the case of autohesion of elastomers, which was shown as the direct experiment evidence for interdiffusion, the contribution of diffusion to the intrinsic adhesion is minimal compared to that from the formation of interfacial secondary bonds.

Therefore, the interdiffusion between the adhesive and the treated PEEK films is not thought to be the main mechanism of bondability enhancement.

12.1.4 Electronic theory

The chief proponents of this theory have been Deryaguin and his co-workers [147]. They proposed that adhesion is due to electrostatic forces, arising from the transfer of electrons from one material of an adhesive joint to another. The controversy this theory has caused is due to this statement that such electrostatic forces are an important cause, rather than merely a result, of high joint strength. Kinloch [148] made a thorough review on this theory in his book and concluded that, for typical adhesive/substrate interfaces, any electrical double layer generated does not contribute significantly to the intrinsic adhesion. Further, any electrical phenomena observed during the joint fracture process probably arise from the failure event, rather than cause the adhesion between the materials. Hence this theory is also thought irrelevant to the present work.

12.1.5 Adsorption theory

The adsorption theory of adhesion is the most widely applicable theory and proposes that, provided sufficiently intimate molecular contact is achieved at the interface, that material will adhere because of the interatomic and intermolecular forces which are established between the atoms and molecules in the surfaces of the adhesive and substrate [149]. As both plasma and corona discharge treatment significantly improve the wettability of PEEK and also introduce some functional groups on to the surface, which can contribute to the enhancement of the adhesion of the treated surfaces. It is believed that this theory is most relevant to the bondability enhancement of PEEK by means of plasma and corona discharge treatment. A detailed study has been made on the contributions of various surface properties to the bondability of the treated PEEK, the results are shown in the following sections.

12.2 Interfacial Contact

The establishment of intimate molecular contact between adhesive and adherend surfaces is the basic requirement for developing strong adhesive joints though sometimes insufficient [150]. This means that the adhesive needs to be able to spread the adherend surface and needs to displace air and other contaminants that may be present on the surface.

An adhesive which conforms ideally to these conditions should[150]

(a) when liquid exhibit a zero or near zero contact angle
(b) at some time during the bonding operation have a viscosity that should be relatively low, e.g. no more than a few centipoises
(c) be brought together with the substrate in a rate and manner that should assist in the displacement of any trapped air

The adhesive employed is believed to satisfy the condition (b) and (c) as this adhesive has been successfully used commercially and the curing condition employed was suggested by the supplier.

In order to assess the condition (a), let us consider the wetting equilibrium of an liquid on a solid (Young's equation), which is shown in Equation 12.1

$$\gamma_{SV} = \gamma_{LS} + \gamma_{LV}\cos\theta \qquad (12.1)$$

When $\theta>0°$ the liquid is non spreading, but when $\theta=0°$ the liquid wets the solid completely and spontaneously, and spreads over the surface at a rate depending on the liquid viscosity and solid surface roughness. Thus for spontaneous wetting to occur, the following condition must be satisfied:

$$\gamma_{SV} \geq \gamma_{LS} + \gamma_{LV} \qquad (12.2)$$

This criterion may also be expressed by defining a parameter termed the equilibrium spreading coefficient λ_{LS}, where [151]

$$\lambda_{LS} = \gamma_{SV} - \gamma_{LS} - \gamma_{LV} = (\gamma_S - \pi_e) - \gamma_{LS} - \gamma_{LV} \qquad (12.3)$$

Hence, a liquid will spread spontaneously and completely on a solid surface when λ_{LS} ≥0. It is also possible of course, to make a liquid spread across a solid surface when θ >0°, but this would require the application of pressure or forces to the liquid to spread it forcibly over the substrate [151].

Substituting Equation 7.4 into Equation 12.3 then

$$\lambda_{LS} = 2(\gamma_S^d \gamma_L^d)^{\frac{1}{2}} + 2(\gamma_S^p \gamma_L^p)^{\frac{1}{2}} - 2\gamma_L \qquad (12.4)$$

Assuming that the surface free energy of the adhesive does not change significantly after it solidified and employing Equation 12.4, the spreading coefficient of the adhesive on untreated and treated PEEK films can be calculated, the results are shown in Table 12.1

As it can be seen from Table 12.1, the adhesive shown positive λ_{LS} results for the PEEK films before and after various plasma and corona discharge treatment. Therefore, the adhesive employed in this project can spread on both untreated and treated surfaces and form intimate interfacial contact.

Table 12.1 Spreading coefficient of the adhesive on untreated and treated PEEK films

Sample	Spreading coefficient (mJm^{-2})
Untreated	4.0
Oxygen plasma treated	23.5
Ammonia plasma treated	16.9
Sulfur dioxide plasma treated	16.1
Air corona treated	19.4
Ammonia corona treated	15.6
Sulfur dioxide corona treated	16.7

*Plasma treatment condition: 1 min, 500 w, 0.3 torr

Corona discharge treatment level: 0.4 J mm^{-2}

(The surface free energy for the adhesive employed (curing in the air) is γ_L=33.1 mJm^{-2} γ_L^p=11.9±2.8 mJm^{-2} γ_L^d=21.2±3.7 mJm^{-2})

12.3 Interfacial Interactions

As shown in Chapter 10, XPS and TOF-SIMS analysis have found that both plasma and corona discharge treatment introduced some functional groups onto the PEEK

surfaces such as hydroxyl, carboxyl, amine and etc. Those functional groups might play dual role when the treated surfaces are forming joints with the epoxy adhesive. One is to change the van der Waals forces across the interface, the other is possibly forming chemical bonds with the adhesive.

In this Chapter, the contribution of the functional groups to the van der Waals forces, and further to the adhesion enhancement was assessed by the thermodynamic work of adhesion (W_A). while the possible formation of chemical bonds across the interface was investigated by TOF-SIMS.

12.3.1 Thermodynamic work of adhesion

The work required to separate reversibly a unit area of the interface between two bulk phases from their equilibrium separation to infinity is the thermodynamic work of adhesion W_A, If only considering the secondary force interactions in the interface between the adhesive and the substrate, W_A can be related to the surface and interfacial free energies by the Dupre Equation (modified by Wake [152]), as shown in Equation 12.5

$$W_A = \gamma_S + \gamma_A - \gamma_{SA} \qquad (12.5)$$

Where the subscripts S and A represent substrate and adhesive respectively.

By using Equation 7.4 to eliminate the interfacial free energy, Equation 12.5 may be derived as Equation 12.6

$$W_A = 2(\gamma_A^d \gamma_S^d)^{\frac{1}{2}} + 2(\gamma_A^p \gamma_A^p)^{\frac{1}{2}} \qquad (12.6)$$

Employing Equation 12.6, the thermodynamic work of adhesion for PEEK film/adhesive joints was calculated, the results are listed in Table 12.2

As shown in Table 12.2, both plasma and corona discharge treatment increase the work of adhesion for PEEK/epoxy adhesive joints. The results imply that the van der Waals forces across the interfaces between treated materials and adhesive are stronger than those across the interface between untreated films and the adhesive. Hence the chemical functional groups introduced by both plasma and corona discharge treatment can enhance the interfacial attraction between PEEK films and the adhesive.

Table 12.2 Thermodynamic work of adhesion for PEEK/adhesive joints

Treatment condition*	Work of adhesion (mJm^{-2})
Untreated	70.2
Oxygen plasma	89.7
Ammonia plasma	83.1
Sulfur dioxide plasma	82.3
Air corona	85.6
Ammonia corona	81.2
Sulfur dioxide corona	82.9

*Plasma treatment condition: 1 min, 500 w, 0.3 torr
Corona discharge treatment level: 0.4 J mm^{-2}

12.3.2 TOF-SIMS analysis

12.3.2.1 Sample preparation

Untreated, oxygen plasma treated and ammonia plasma treated PEEK (labelled as EUPK, EOPK and ENHPK respectively) after being exposed to the atmosphere for less than 5 min, were dipped twice in 2% MY750 epoxy acetone solution, then put into an oven for 3 hours at 120°C. Before SIMS analysis, the epoxy coated samples were immersed in acetone for 24 hours, then rinsed five times in pure acetone, and then hang-dry in an air circulated clean container. The idea of preparing such kind samples is based on the following assumption: If strong interfacial attractions or interdiffusion can occur between the epoxy resin and PEEK, then after coating PEEK with epoxy resin, the coating will not be removed by acetone. The choose of 120°C for 3 hour curing condition is to ensure that all the functional groups introduced by the plasma treatment have the chance to react with the epoxy resin.

12.3.2.2 Characteristic signals of epoxy resin[153]

The chemical structure of MY-750 is

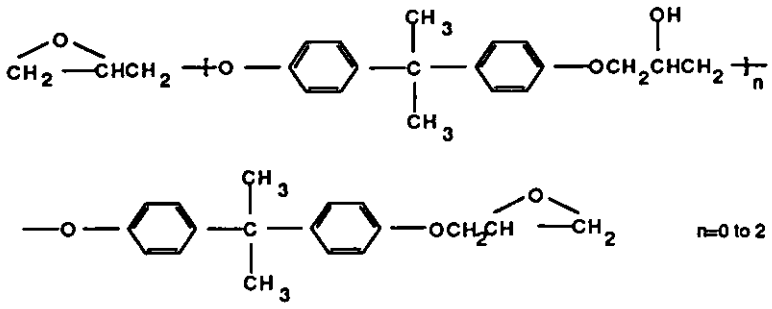

(a) Positive ion signals

The characteristic signals assigned to fragments containing a terminal epoxy group appear at a.m.u. 57, 191, 252 and 269, which correspond to the following structure

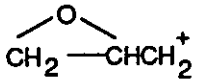

a.m.u. 57

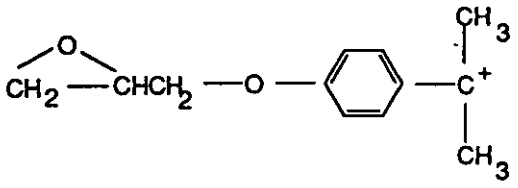

a.m.u. 191

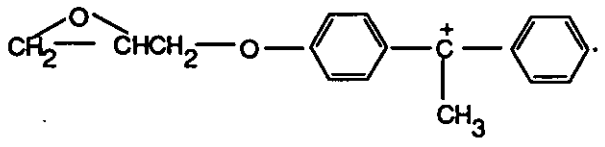

a.m.u. 252

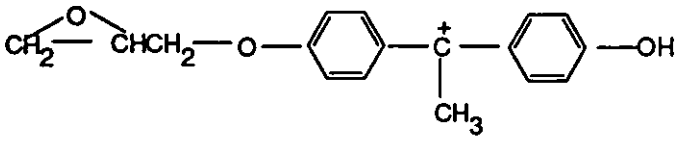

a.m.u. 269

The positive ion signals specifically diagnostic of the bisphenol-A component show at a.m.u. 135 and 213 corresponding to structures

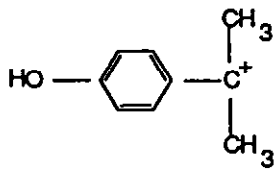

a.m.u. 135

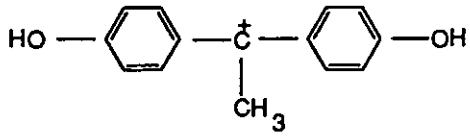

a.m.u. 213

As untreated PEEK also show peaks at a.m.u. 57 and 213, the characteristic positive signals of epoxy resin in this work appear at a.m.u. 135, 191, 252 and 269.

(b) Negative ion signals

The signal characterising the fragment containing the epoxy group at a.m.u. 283 correspond to the structure

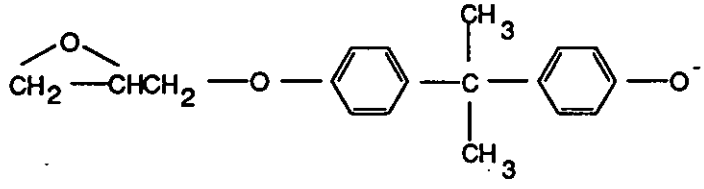

a.m.u. 283

while the signal at a.m.u. 71 (assigned to O=CH-CH=CH-O$^-$) is thought to be one of the characteristic of the terminal epoxy group.

The characteristic signals of the bisphenol-A part of the molecule appear at a.m.u. 93, 117, 133 and 211 corresponding to the structures

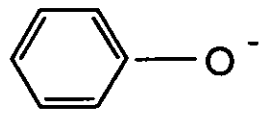

a.m.u. 93

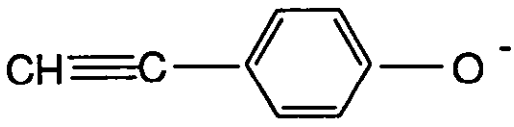

a.m.u. 117

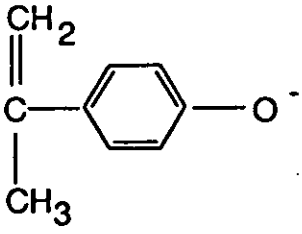

a.m.u. 133

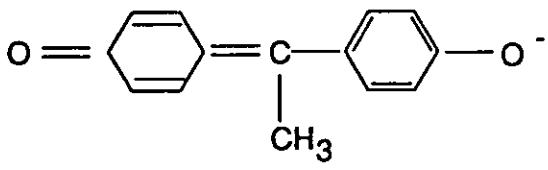

a.m.u. 211

However, the signals at a.m.u. 71, 93 and 211 also can appear in the PEEK spectra, therefore, the characteristic negative signals of epoxy resin in our case are those at a.m.u. 117, 133 and 283.

12.3.2.3 EUPK

In both positive and negative ion spectra of EUPK (Fig. 12.1 and Fig. 12.2), cannot be found any characteristic signals for the epoxy resin, suggesting that the epoxy resin coating can be thoroughly removed by acetone. The results indicate that there is no strong interfacial attractions or interdiffusion between untreated PEEK and the MY-750 epoxy resin.

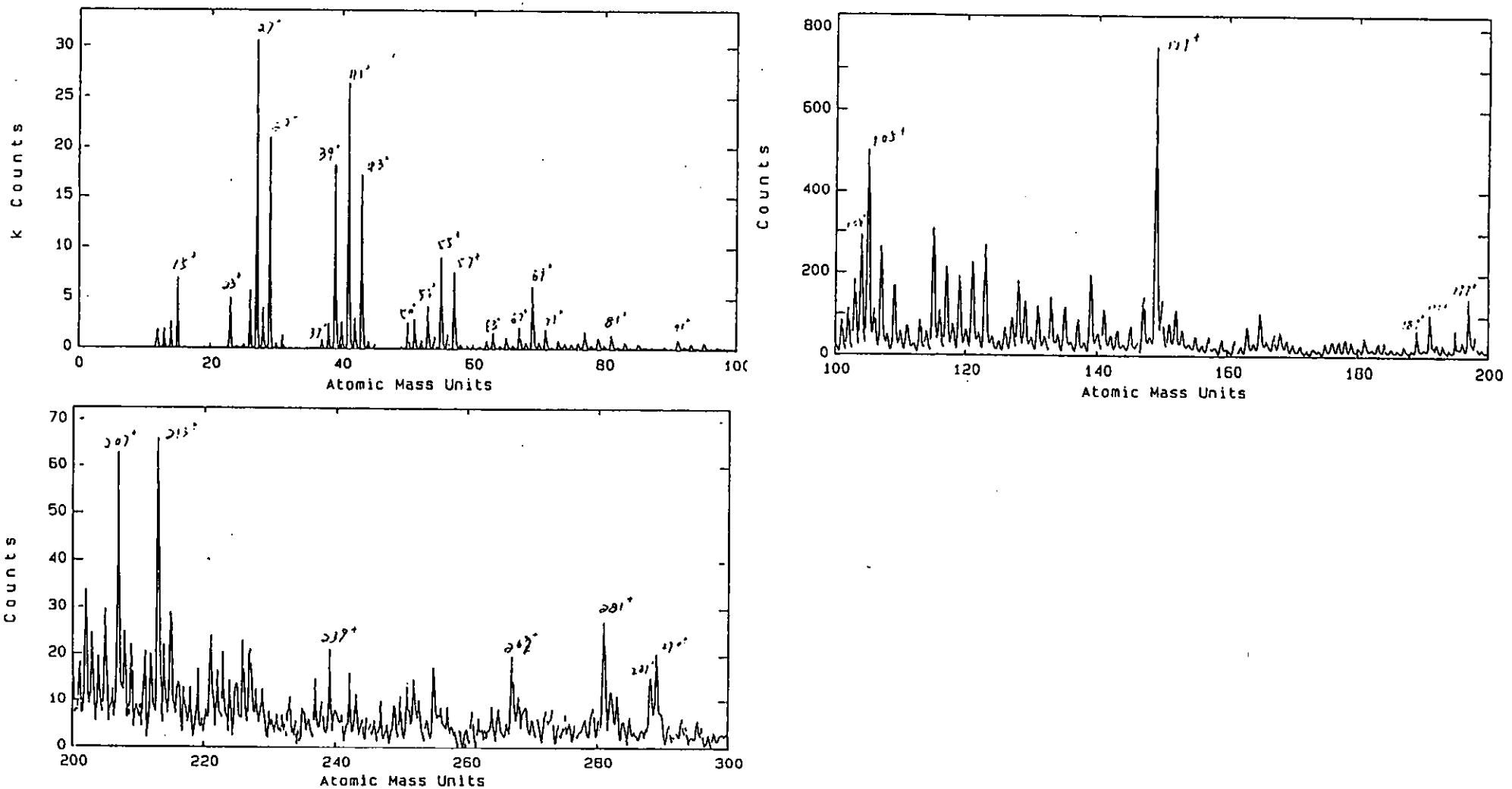

Fig. 12.1 Positive ion spectrum of EUPK

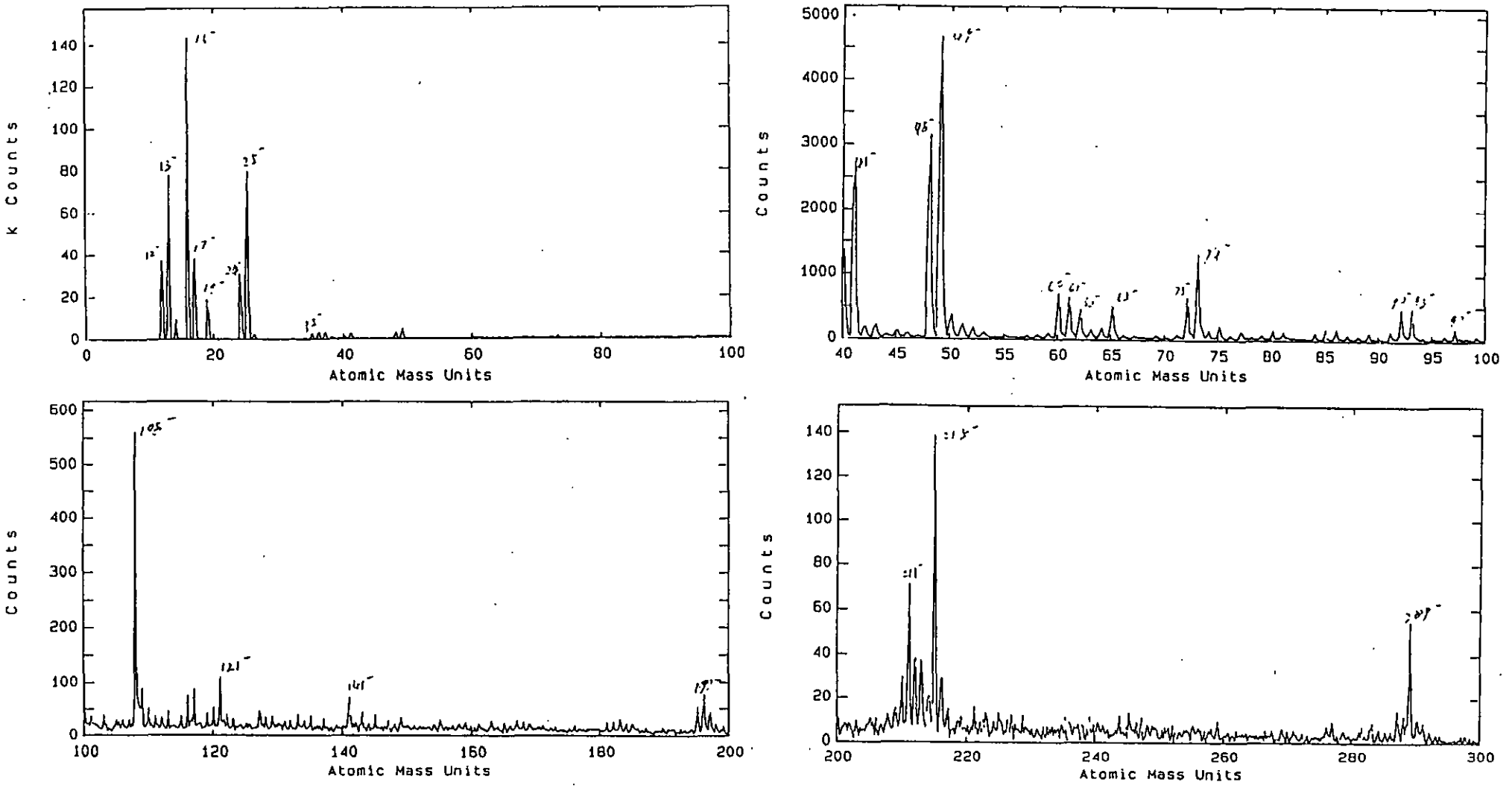

Fig. 12.2 Negative ion spectrum of EUPK

12.3.3.4 EOPK

Comparing the positive and negative ion spectra of EOPK (Fig. 12.3 and Fig. 12.4) with those of oxygen plasma treated PEEK after acetone washing (Fig. A2.5 and Fig. A2.6), the following observations are revealed:

(a) In the positive ion spectra, new peaks appear at a.m.u. 135, 191, 252 and 269, while the signal at a.m.u. 213 is enhanced. All these signals are the characteristic peaks of the epoxy resin. However, the peak at a.m.u. 214, which also exist in the uncoated sample spectra, disappears from the spectra, and the signal at a.m.u. 242, which is introduced by the oxygen plasma treatment, becomes very weak. In addition, the coated sample also show some new weak signals at a.m.u. 107, 115 and 165.

(b) In the negative ion spectra, new peaks appear at a.m.u. 117, 133 and 283, and the peaks at a.m.u. 211 become much strong. Also all these signals are attributed to the epoxy resin. The strong signals at a.m.u 213, 227, 253, 255, 277, 281 and the weak signal at a.m.u. 291 shown in the uncoated PEEK spectra disappeared from the spectrum of EOPK. In addition, the intensity of the peak at a.m.u. 41 (C_2OH^-) is stronger than that appeared in the uncoated sample.

Therefore, both positive and negative ion spectra suggest that acetone can not remove the MY-750 epoxy resin coated on the oxygen plasma treated PEEK surfaces. The results also imply that chemical reaction could occur between epoxy resin and the function groups introduced by the oxygen plasma treatment.

12.3.2.5 ENHPK

The differences between the positive and negative ion spectra (Fig. 12.5 and Fig. 12.6) and their uncoated counterparts (Fig. A2.7 and Fig. A2.8) can be summarised as the following:

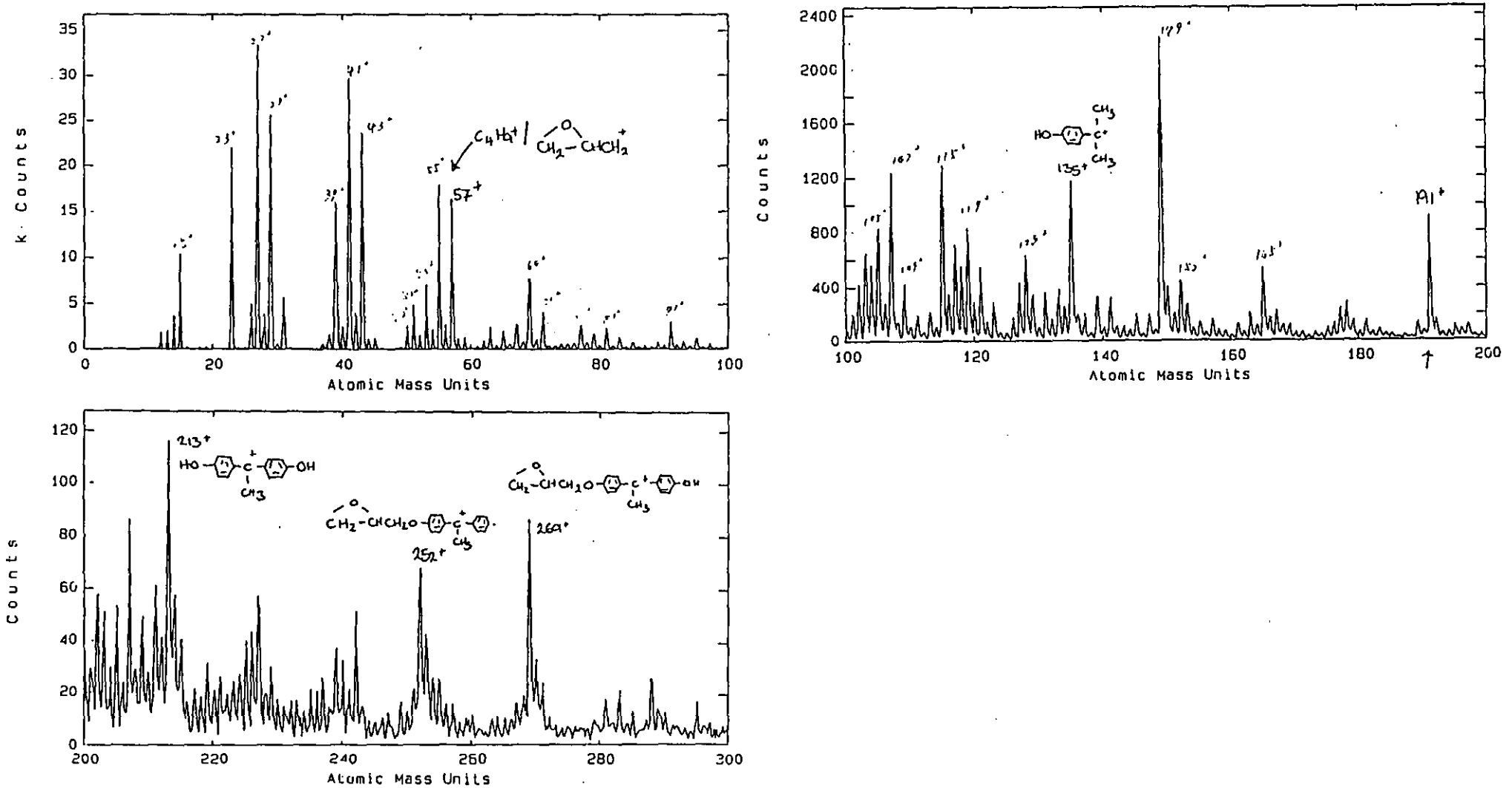

Fig. 12.3 Positive ion spectrum of EOPK

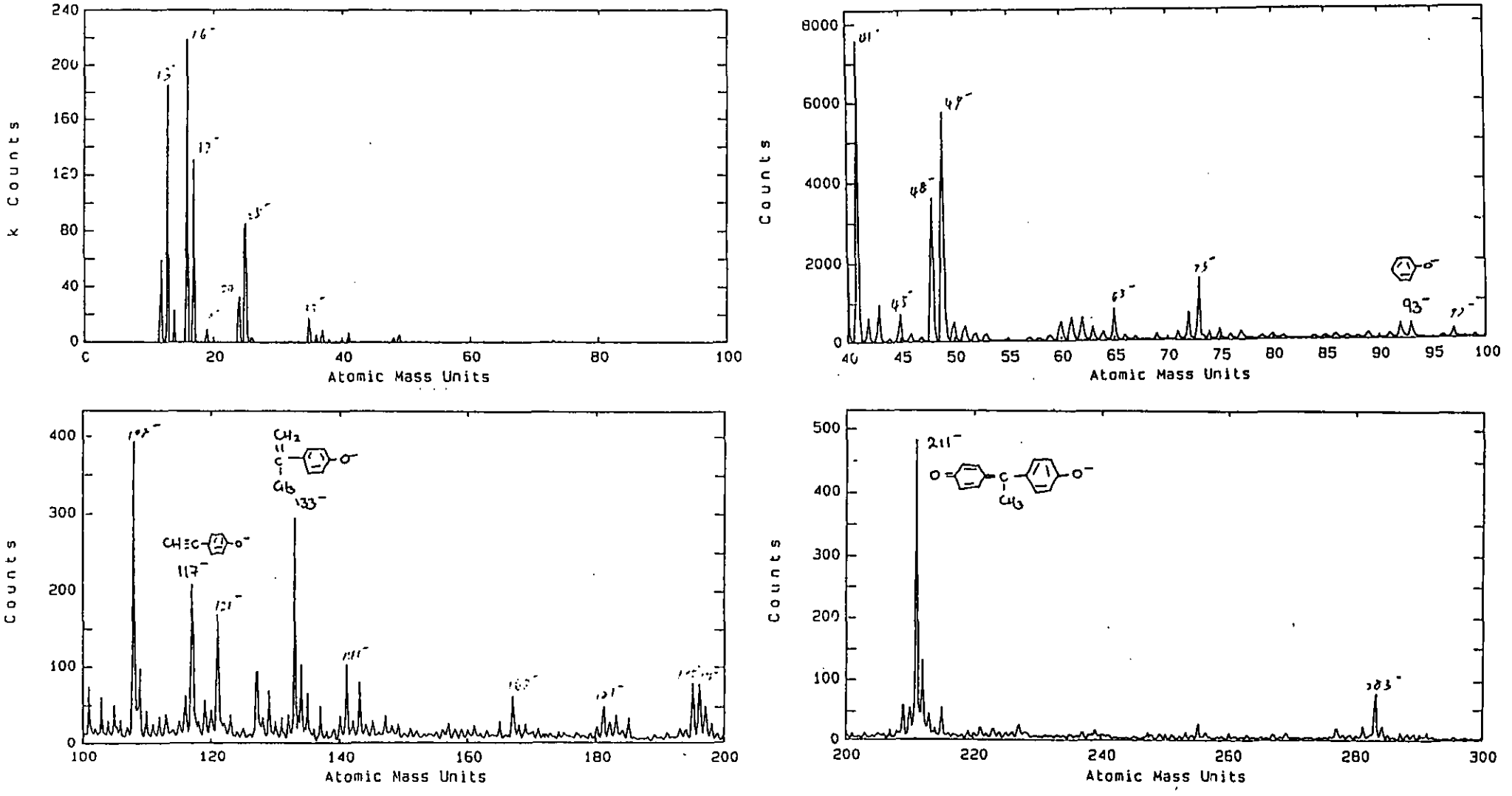

Fig. 12.4 Negative ion spectrum of EOPK

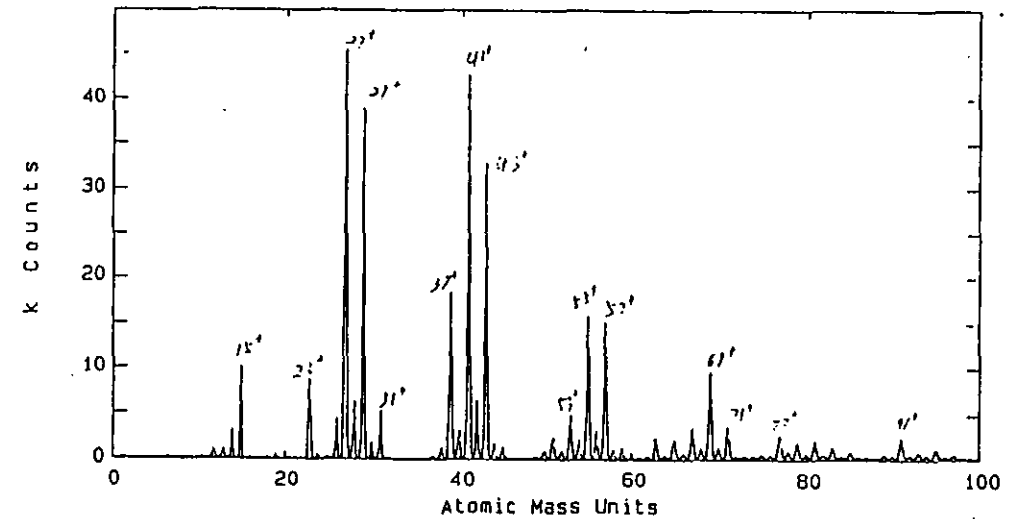

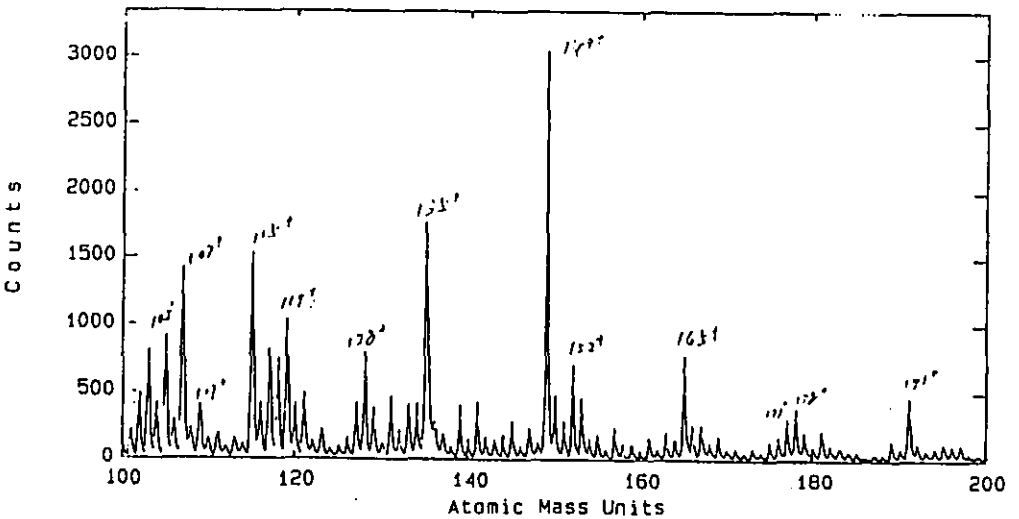

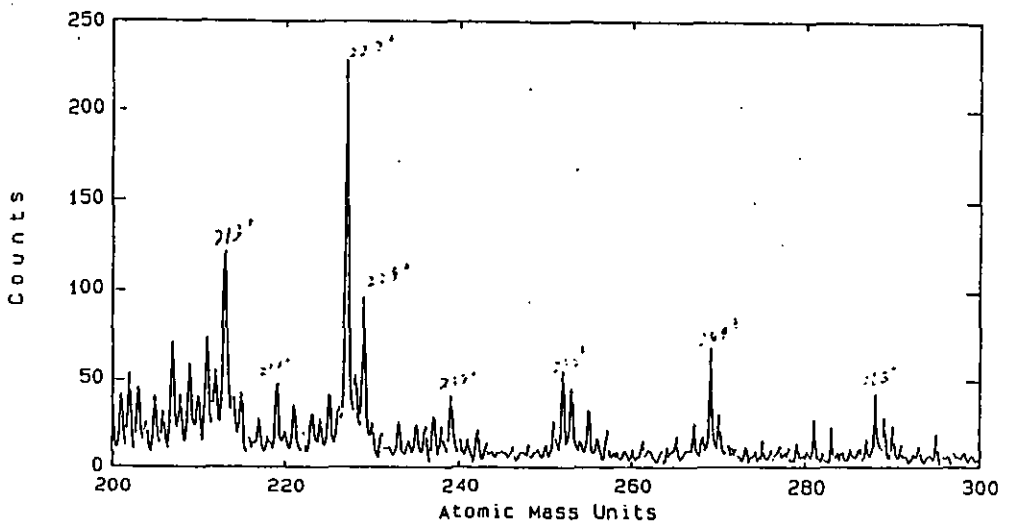

Fig. 12.5 Positive ion spectrum of ENHPK

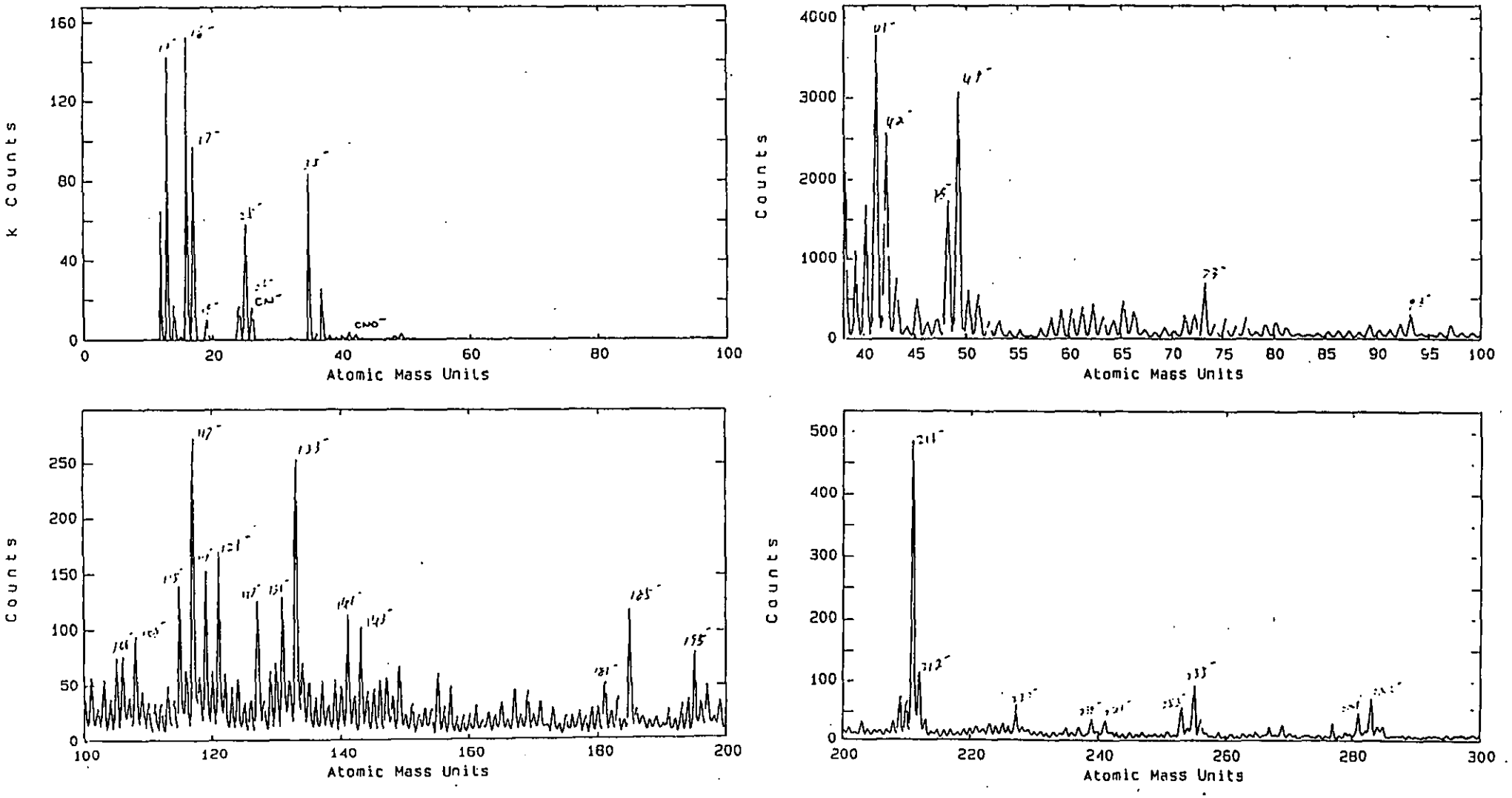

Fig. 12.6 Negative ion spectrum of ENHPK

(a) Many new peaks appear in the positive ion spectra of ENHPK. Some of these new peaks are the characteristic signals of the epoxy coating, i.e. signals at a.m.u. 135, 191, 213, 252 and 269. Other new strong signals appear at a.m.u. 107, 115, 165 and 227, while some new weak signals appear at a.m.u. 119, 128, 152, 177, 178, 229 and 288. However, the strong signal at a.m.u. 219 for uncoated sample are not present. The new signals could be attributed to chemical reactions between the epoxy resin and the nitrogen or oxygen containing groups introduced by the ammonia plasma treatment, but it is not possible to work out the details of these reactions.

(b) Also some new peaks appeared in the negative spectra of ENHPK, i.e. signals at a.m.u. 48, 73, 93, 117, 133, 195, 211 and 283. Among these new peaks, those at a.m.u. 93, 117, 133, 211 and 283 are the characteristic signals of the epoxy resin, while the peaks at a.m.u. 48, 73, 195 could be due to the chemical reactions between epoxy and nitrogen or oxygen containing function groups.

The signals represent the nitrogen containing groups in the low mass region became much weak, these peaks are at a.m.u. 15 (NH^-), 26 (CN^-) and 42 (CNO^-). These results also suggest that chemical reactions have occurred between these groups and the epoxy groups. In addition, the signal at a.m.u. 66, 79, 81 and 203 disappeared from the spectrum, and the signals at a.m.u. 115, 121, 131, 241 and 255 became much weak, but signal at a.m.u. 49 became much stronger.

Summarising the TOF-SIMS results and discussions it is believed that the functional groups introduced by the plasma treatment can form strong interfacial attractions with their counterparts of the epoxy adhesive, possibly forming some chemical bonds.

12.4 Role of Low Molecular Weight Molecules

As discussed in Chapter 10 and Chapter 11, both plasma and corona discharge treatment produce some LMWM on the treated PEEK surfaces, which are highly oxidised or nitrogenated. These small molecules may have several effects in the formation of joints, i.e.

(a) Weak boundary layer

Assuming plasma and corona discharge treatment produce large amount of low molecular weight molecules on the treated surfaces, WBL will be formed on the treated surface, and then plasma and corona treatment could not significantly enhance

the joint strength of PEEK materials. Since the results shown in chapter 8 suggest the opposite treatment effects, the LMWM small molecules produced by the treatment is believed not forming WBL on the treated surfaces.

(b) Primer (or coupling agent)

As the LMWM produced by the treatment contains some functional groups, like -OH, -COOH and etc., which could react directly or indirectly with the epoxy group, it can play the role similar to that of the primer or coupling agent, thereby enhancing the adhesive joint strength of the treated materials.

(c) Dissolving in the adhesive

During the adhesive joint forming process, the LMWM produced by the treatment could dissolve into the adhesive. However, as the concentration of these small molecules is very low, the effect of their dissolution in the adhesive on the mechanical properties of the adhesive is thought to be negligible.

Before investigating the effects of solvents, it is necessary to know the mass uptake of the solvents used on the treated surfaces.

12.4.1 Mass uptake of solvents by plasma and corona discharge treated PEEK surfaces

PEEK does not adsorb ordinary solvents, like acetone and water. Cogswell and Hopprich [154] have found no changes in weight when immersing APC-1(a PEEK composites) in acetone for 7 days at 23°C. Also very little effect of moisture on the properties of PEEK was seen [154-157]. Less than 0.1% weight gain was detected when PEEK films were either immersed in deionized water at 20 and 70°C[155] or conditioned in air at about 70% RH for 7 days[156].

However, as both plasma and corona discharge treatment change the surface properties of PEEK, solvent washing could affect the weight of treated materials. Table 12.3 listed the results of mass uptake of the solvents employed in this work on the plasma and corona discharge treated films. The results reported are the percentage absorption of treated films after 10 min immersion in the solvents.

Although the results are highly scattered, it is clear that very small amount of LMWM were present on the treated surfaces.

In addition, XPS results shown that the surface O/C ratio of treated films decreased after washing (see section 10.2.3), hence it is very unlikely that the treated surface adsorb any solvent used, since the adsorption will increase the surface O/C ratio (the O/C ratio for both acetone and IPA is 0.333).

Table 12.3 Mass uptake of solvents on plasma and corona discharge treated PEEK films

Solvent	Absorption (%)			
	Oxygen plasma treated PEEK		Air corona treated PEEK	
	Average	Range	Average	Range
Acetone	-0.260	0.181 -- (-0.352)	0.230	0 -- 0.415
IPA	-0.250	-0.737 -- 0	0	0 -- 0
Water	-0.024	0.072 -- 0	-0.008	-0.490 -- 0.263

Plasma treatment condition: 1 min, 500 w, 0.3 torr
Corona discharge treatment level: 0.4 J mm^{-2}

12.4.2 Effect of solvent washing on the wettability of plasma and corona discharge treated surfaces

Table 12.4 shows the effect of solvent washing on the surface free energy and polarity of both plasma and corona discharge treated films. Water, acetone and IPA washing lower the surface free energy of the treated films significantly, but do not reverse them to the value of the untreated. Analysing the results illustrated in Table 12.4, it can be seen that different solvents show different effects on the components of the surface free energy. Water washing causes less changes in the polar and dispersion components compared with acetone and IPA washing. This could be either due to the LMWM produced by the treatment having different solubility in different solvents or to the relatively low polarity of acetone and IPA (During the washing period, they not only remove the LMWM, but can also cause some polar groups to reorient into the bulk or subsurface). Solvent washing show similar effect on the surface polarity of treated films.

Table 12.4 Effect of solvent washing on the surface free energy, surface polarity and contact angle hysteresis of plasma and corona discharge treated films

Treatment condition*	Solvent	Surface free Energy (mJm^{-2}) γ_S^p	γ_S^d	γ_S	Surface Polarity	Contact angle hysteresis θ_a	θ_r
Untreated		7.2±3.9	31.5±8.3	38.7	0.186	73	32
Oxygen plasma	Before	42.0±18.3	23.9±14.0	66.0	0.638	<5	<5
	Water	11.8±4.4	33.3±7.5	45.1	0.262	63	<5
	Acetone	4.3±2.3	39.3±7.0	43.6	0.098	76	11
	IPA	4.8±2.3	37.1±6.5	41.9	0.114	76	7
Ammonia plasma	Before	32.4±11.6	22.7±9.8	55.1	0.587	37	<5
	Water	23.6±9.8	25.2±10.3	48.9	0.483	48	<5
	Acetone	15.9±5.2	31.6±7.4	47.5	0.336	57	<5
	IPA	16.8±5.5	30.8±7.5	47.6	0.353	56	<5
SO_2 plasma	Before	26.3±11.2	26.0±11.3	52.3	0.503	43	<5
	Water	4.8±2.5	36.5±6.9	41.3	0.116	76	5
	Acetone	5.3±4.7	31.8±11.6	37.1	0.143	76	5
	IPA	5.3±3.0	35.4±7.9	40.7	0.131	75	5
Air corona	Before	34.5±14.3	24.0±12.0	58.5	0.590	30	<5
	Water	13.7±4.7	29.7±7.0	43.4	0.316	62	8
	Acetone	6.0±2.5	36.7±6.3	42.7	0.141	73	42
	IPA	10.8±3.3	33.5±5.9	44.3	0.245	65	36
Ammonia corona	Before	25.9±8.7	25.7±8.7	51.6	0.502	45	<5
	Water	13.7±3.8	30.5±5.8	44.2	0.310	62	5
	Acetone	11.2±4.4	33.0±7.7	44.2	0.253	64	41
	IPA	8.0±1.1	35.3±2.3	43.4	0.185	71	34
SO_2 corona	Before	24.6±8.3	28.0±9.0	52.6	0.467	45	<5
	Water	21.2±8.6	25.4±9.5	46.6	0.454	52	<5
	Acetone	4.9±2.3	36.5±6.4	41.4	0.118	76	27
	IPA	8.6±3.4	37.5±7.2	46.1	0.187	67	5

* Plasma treatment condition: 1 min, 500 w, 0.3 torr
Corona discharge level: 0.4 J mm^{-2}

Table 12.4 also shows the effects of solvents on the contact angle hysteresis for plasma and corona discharge treated films. Solvents have different effects on the plasma treated films. For oxygen plasma treated materials, acetone and IPA washing recovers the advancing contact angle completely, but only changes the receding angle slightly.

Water washing, on the other hand, increases the advancing angle significantly (though not fully back to that of the untreated sample), and does not affect the receding angle. For ammonia and sulfur dioxide plasma treated films, water, acetone and IPA washing only changes the advancing contact angle to some extent, but does not affect the receding contact angle. Nevertheless, solvents have the same effects on all gas corona discharge treated samples. After acetone and IPA washing, the values of the advancing and receding contact angles of water became approximately the same as those of the untreated PEEK surface, suggesting that acetone and IPA washing recovers the topmost layer of the treated surface back to that of the untreated surface. However, water washing only affects the advancing contact angle of the corona treated surfaces, which also implies that water washing removes only the LMWM, but does not cause the reorientation of the polar groups away from the surface to the bulk.

The different changes in surface properties caused by solvent washing for different condition treated films are believed to be due to the fact that different treatment conditions produce different molecule size and different amount of LMWM on the PEEK surface.

Table 12.5 Effect of water immersion on the surface free energy, surface polarity and contact angle hysteresis of acetone washed oxygen plasma treated materials

Water Immersion (1 hour)	Temperature (°C)	Surface free Energy (mJm^{-2}) γ_S^p	γ_S^d	γ_S	Surface Polarity	Contact angle hysteresis θ_a	θ_r
Before	RT	4.3±2.3	39.3±7.0	43.6	0.098	76	11
After	RT	12.1±4.0	33.0±6.6	45.1	0.269	63	<5
	100 °C	19.3±7.3	28.4±8.9	47.7	0.405	53	<5

* Oxygen plasma treatment condition: 1 min, 500 w, 0.3 torr
  Acetone dipping five times

Owing to its high polarity, water could recover the reorientation process in the acetone washing period if it occurred. Table 12.5 gives the results of water immersion on the surface properties of acetone washed oxygen plasma treated materials. The results show that water do recover the surface free energy, surface polarity and contact angle hysteresis to some extent. Increasing temperature facilitates this recovering process, hence confirming that surface reorientation do occur during the washing period.

12.4.3 Effect of solvent washing on the bondability of plasma and corona discharge treated materials

Table 12.6 shows the effect of solvent washing on the lap shear joint strength of plasma and corona treated films. Acetone and IPA washing does not appear to have much effect on the shear joint strengths of plasma and corona treated films, indicating that LMWM on the treated surfaces do not play a very important role on the bondability of treated materials. However, acetone and IPA washing lowers slightly the T-peel joint strengths of oxygen plasma treated samples, but not that for the ammonia plasma treatments (as shown in Table 12.7).

Table 12.6 Effect of solvent washing on the lap shear joint strength of plasma and corona discharge treated films

Treatment condition	Solvent	Lap shear strength (MPa)	Failure locus
Untreated		16.9±1.3	I+C
Oxygen plasma	Before	34.0±1.4	C+M
	Acetone	33.8±1.4	C+M
	IPA	35.8±0.5	C+M
Ammonia plasma	Before	32.2±2.1	C+M
	Acetone	32.3±1.6	C+M
	IPA	33.7±1.7	C+M
Sulfur dioxide plasma	Before	32.8±0.9	C+M
	Acetone	31.7±0.5	C+M
	IPA	31.9±0.5	C+M
Air corona	Before	28.5±1.8	C+M
	Acetone	28.2±2.4	C+M
	IPA	29.6±0.9	C+M
Ammonia corona	Before	28.0±0.7	C+M
	Acetone	31.1±1.2	C+M
	IPA	28.3±1.5	C+M
Sulfur dioxide corona	Before	31.9±1.2	C+M
	Acetone	31.1±0.7	C+M

* Plasma treatment condition: 1 min, 500 w, 0.3 torr
Corona discharge level: 0.4 J mm^{-2}

Table 12.7 Effect of solvent washing on the T-peel joint strength of plasma treated films

Treatment condition	Solvent	T-peel strength (N/mm)	Failure locus
Untreated		0	I
Oxygen plasma	Before	4.64±0.02	C+M
	Acetone	3.12±0.18	C
	IPA	3.76±0.14	C
Ammonia plasma	Before	4.05±0.11	C
	Acetone	3.99±0.16	C
	IPA	3.95±0.27	C

* Plasma treatment condition: 1 min, 500 w, 0.3 torr

CHAPTER 13 SURFACE DYNAMICS AND ADHESION

As discussed in Chapter 11, the plasma and corona discharge treated surfaces can be modelled as a modified layer consisting of various size molecules with some functional groups introduced by the treatment. Since the chemical composition of this modified layer is different with the bulk of PEEK films, the treated surfaces are in a thermodynamically unstable state. For other polymers, it has been found that the plasma treated surfaces are not stable[158-164], i.e. the improved surface properties tend to change with the time and temperature. However, for PEEK, it is not known whether the treated surfaces are stable are not.

In this work, the surface dynamics of the treated surfaces in atmosphere, hot or humid environment were investigated. The results of three months atmospheric exposure, heat treatment and water immersion are reported.

13.1 Theoretical Analysis

Because the properties of the modified layer are different from those of the bulk material, the modified layer has two interfaces (or interphases) with its surroundings, one is between the modified layer and the bulk material, the other is between the treated surface and its environment, like air, solvent etc. The composition and structure of this layer tend to change to minimise its interfacial tension.

In the interface between the treated surface and its environment, the modified layer will restructure according to the environment to lower the interfacial tension. In the polar environment, the molecules modified by the treatment will stay in the surface because they have higher polarity than the bulk molecules, in addition, the polar groups will reorient to the surface to minimise the interfacial tension. In the non-polar environment, the molecules modified by the treatment tend to migrate away from the surface while the molecules with low polarity tend to move to the top surface. In addition the polar groups will reorient away the surface.

In the interface (or interphase) between the modified layer and the bulk, in order to lower the interfacial tension, the molecules produced by the treatment tend to migrate

into the bulk. Among them the LMWM might migrate rapidly and cost less energy, while the HMWM are expected to diffuse very slowly and needs more energy. At the same time, the PEEK molecules have a tendency to migrate to the surface layer, but because of the high T_g of PEEK, this migration would take place at an extremely low rate and may not occur at all.

In the above restructuring processes, the polar groups in the molecules, like hydroxyl, carboxyl, amine, and etc. could form internal hydrogen bonds, hence hinder the further migration of the molecules and the orientation of the polar groups, and stabilise the composition and structure of the modified layer.

13.2 Atmospheric Exposure

Treated films were exposed to the laboratory atmosphere and tested at different time intervals. The results of wettability and bondability studies are reported here.

13.2.1 Surface free energy

Fig. 13.1 shows the effects of atmospheric exposure on the surface free energy and its components for ammonia plasma treated materials. Several noteworthy features are apparent, namely:

Firstly, the polar component value decreased in the first two months' exposure, then reached a value approximately equal to that of the untreated film, and remained more or less unchanged after longer exposure (The equilibrium value is similar to that of the untreated film (7.2 mJm^{-2})).

Secondly, the value of the dispersion component show a different trend, it changed little in the exposure period.

Thirdly, the total surface free energy of the ammonia treated material also decreased with the time of exposure. After two months, it reached an equilibrium value and remained unchanged thereafter. This value is slightly lower than that of the untreated film (38.7 mJm^{-2}).

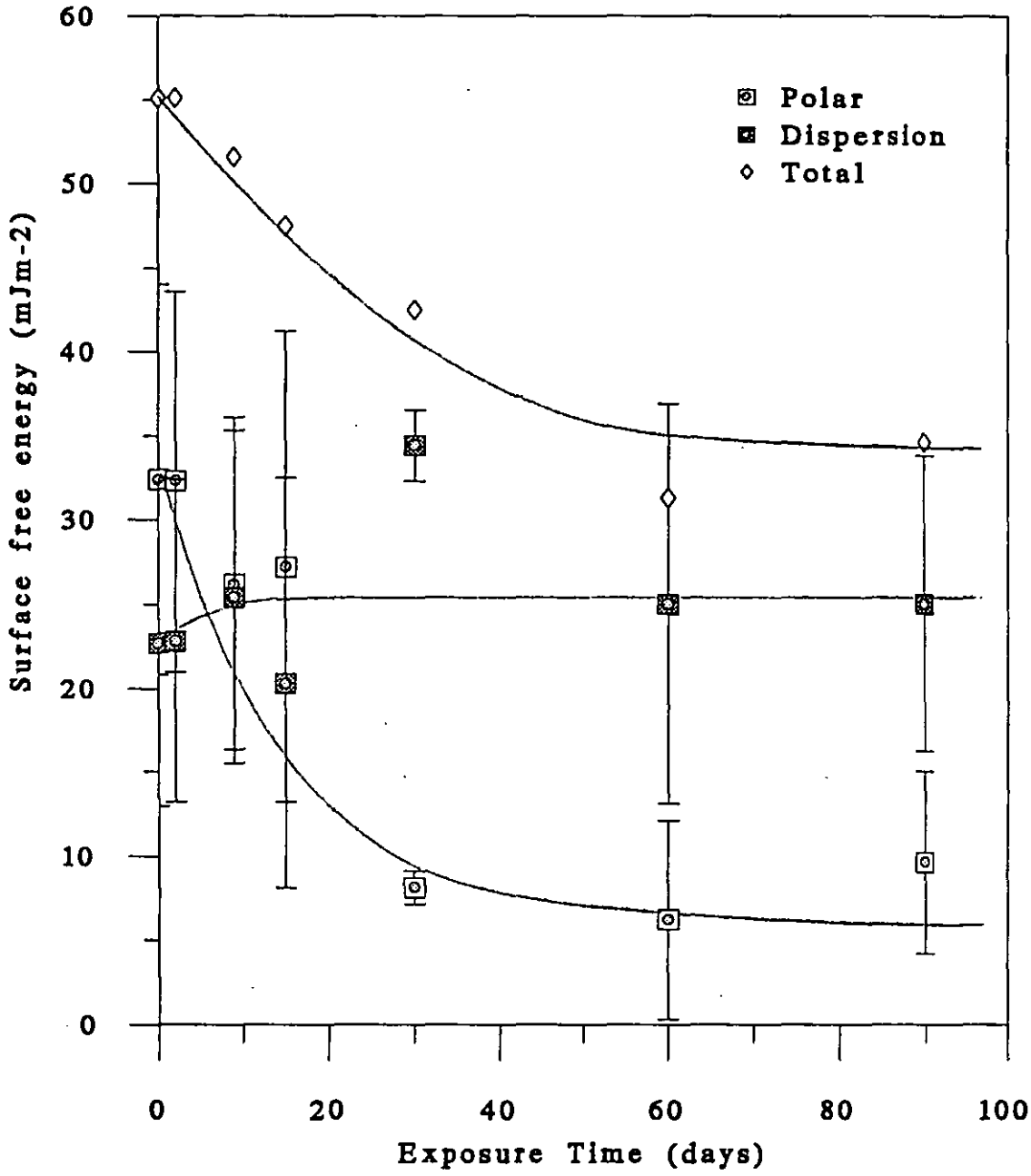

Fig. 13.1 Effect of exposure to atmospheric environment on the surface free energy of ammonia plasma treated films

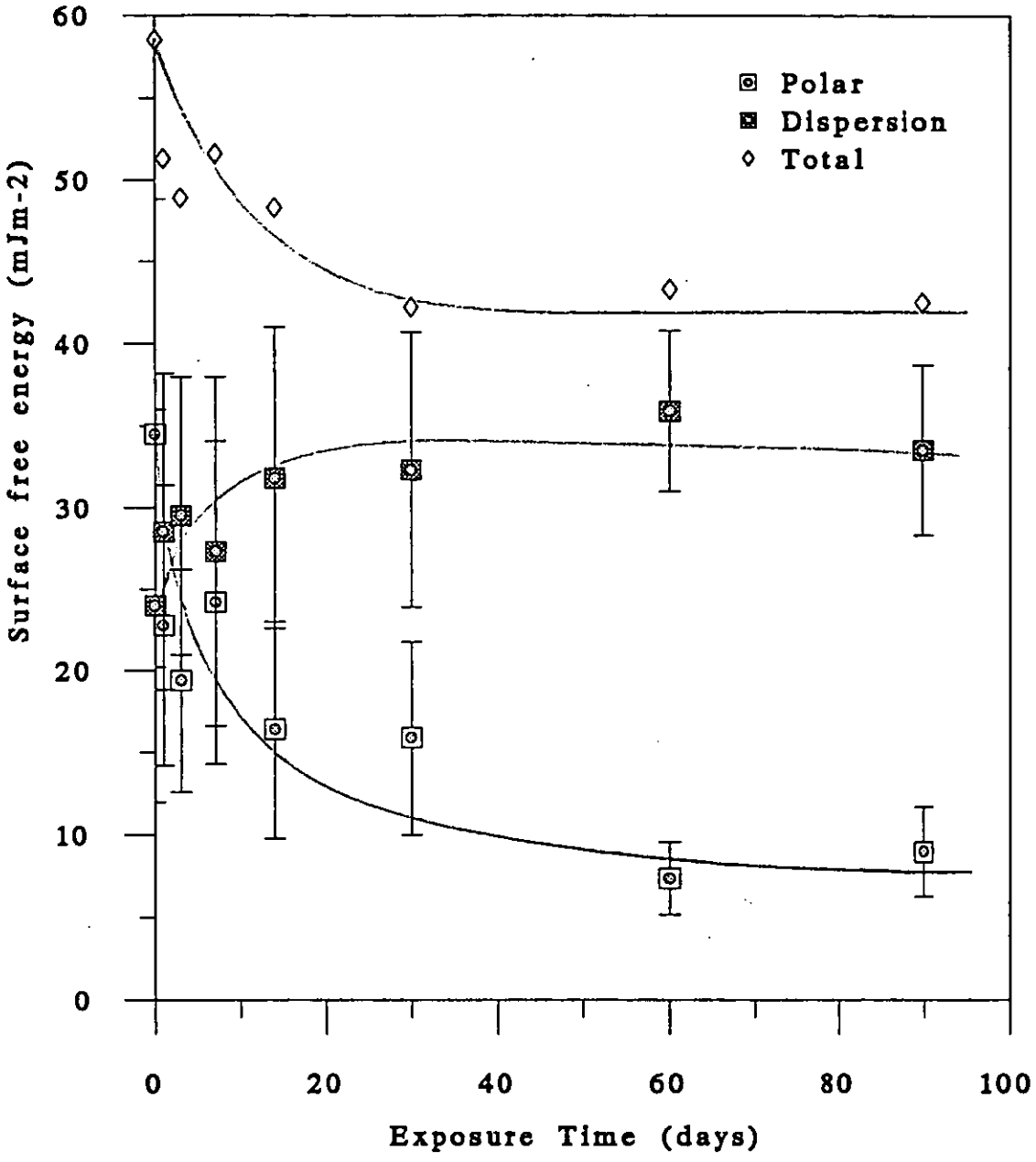

Fig. 13.2 Effect of exposure to atmospheric environment on the surface free energy of air corona discharge treated films

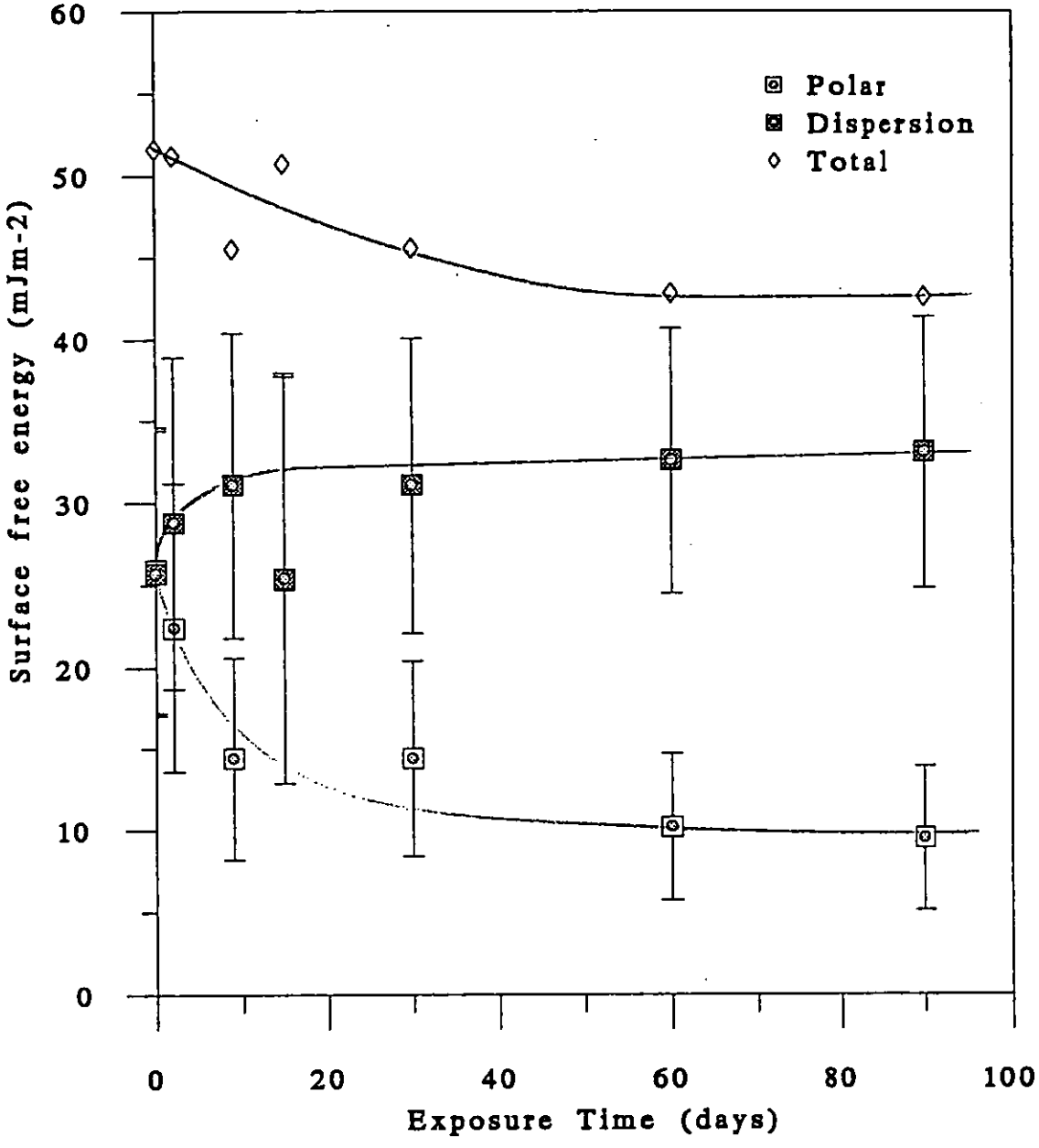

Fig. 13.3 Effect of exposure to atmospheric environment on the surface free energy of ammonia corona discharge treated films

Exposure to the atmospheric environment showed a similar effects on the surface free energy and its components for air corona and ammonia corona discharge treated materials, as shown in Fig. 13.2 and Fig. 13.3. However, the value of the dispersion component increased very quickly in the early exposure period, and then changed little at longer exposure. The plateau value is similar to that of the untreated (31.5 mJm^{-2}). In addition, the equilibrium value of the total surface free energy after exposure is slightly higher than that of the untreated.

Hence, the results imply that the surface layer characterised by contact angle measurement (less than 10 nm[25]) of treated films has changed during the exposing period. The results also show that the decrease of the surface energy is mainly caused by the decrease of its polar components. The next section will show the effects of atmospheric exposure on the surface polarity of treated materials.

13.1.2 Surface polarity

The surface polarity of both plasma and corona discharge treated films significantly decreased in the first two months exposure period, then remained constant with a value similar to that of the untreated films, as shown in Fig. 13.4 -13.6.

Therefore the surface polarity results suggest that most of the polar groups introduced by the treatment disappear from the surface layer characterised by contact angle measurement after more than two months atmospheric exposure.

13.1. 3 Contact angle hysteresis

With respect to contact angle hysteresis, the results are very intriguing. Atmospheric exposure tended to increase the hysteresis, i.e. the advancing contact angle of water for both plasma and corona treated PEEK increased very quickly in the early exposure period then reached their equilibrium values and remained unchanged, as shown in Fig. 13.7. For air corona, ammonia corona and plasma treated samples, those values are about the same as the advancing contact angle of water for untreated PEEK (about 73°), while for oxygen plasma treated films the equilibrium value is more than 20° lower than that of untreated film. In addition, the rate to reach their equilibrium is also different, the trend being: oxygen plasma > ammonia plasma > air corona = ammonia corona. Nevertheless, the receding contact angle did not change with the exposure time (as shown in Fig. 13.8). Comparing these values with the receding contact angle of water for untreated sample, it is found that these values (about 5°) are much lower

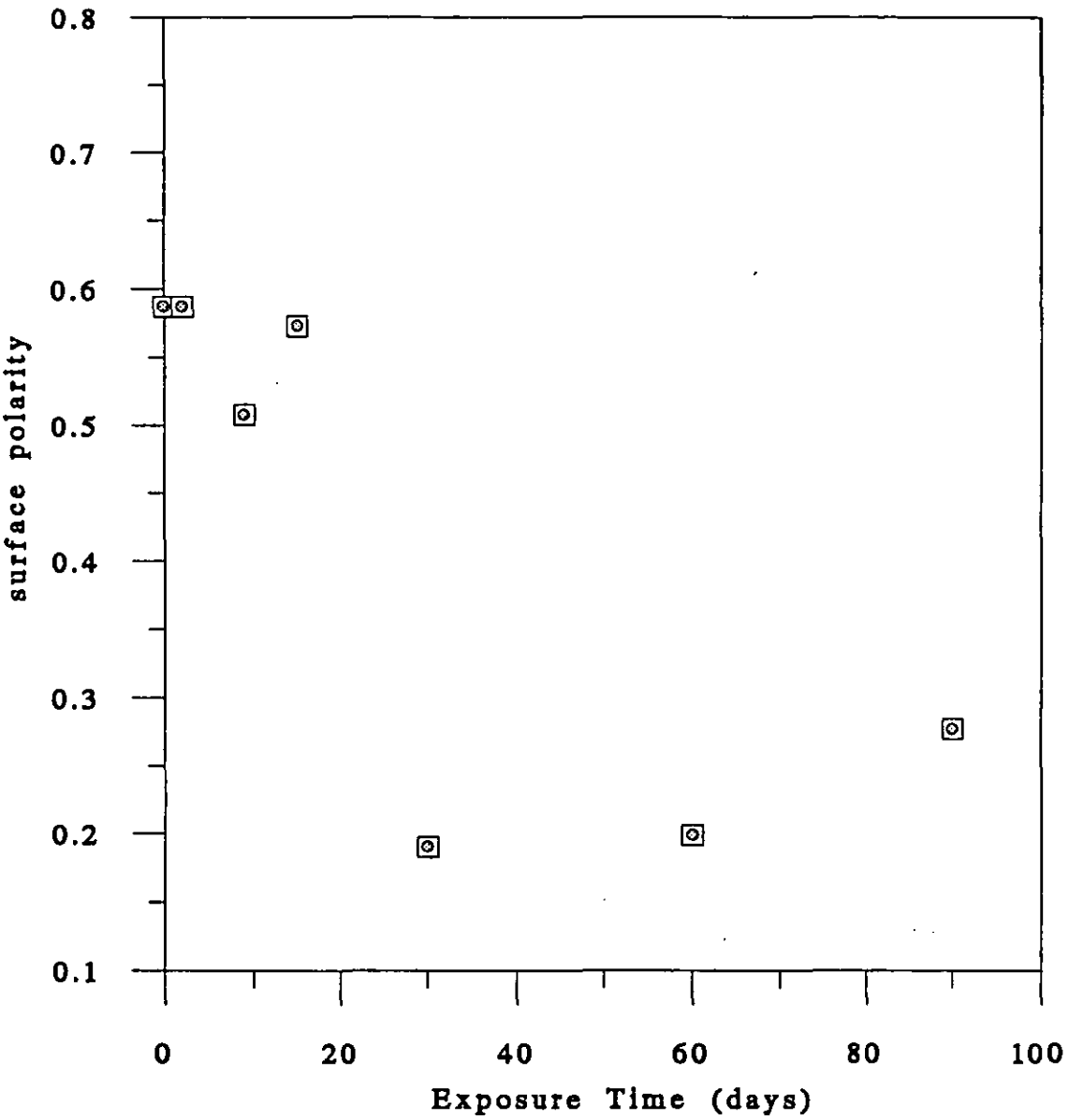

Fig. 13.4 Effect of exposure to atmospheric environment on the surface polarity of ammonia plasma treated films

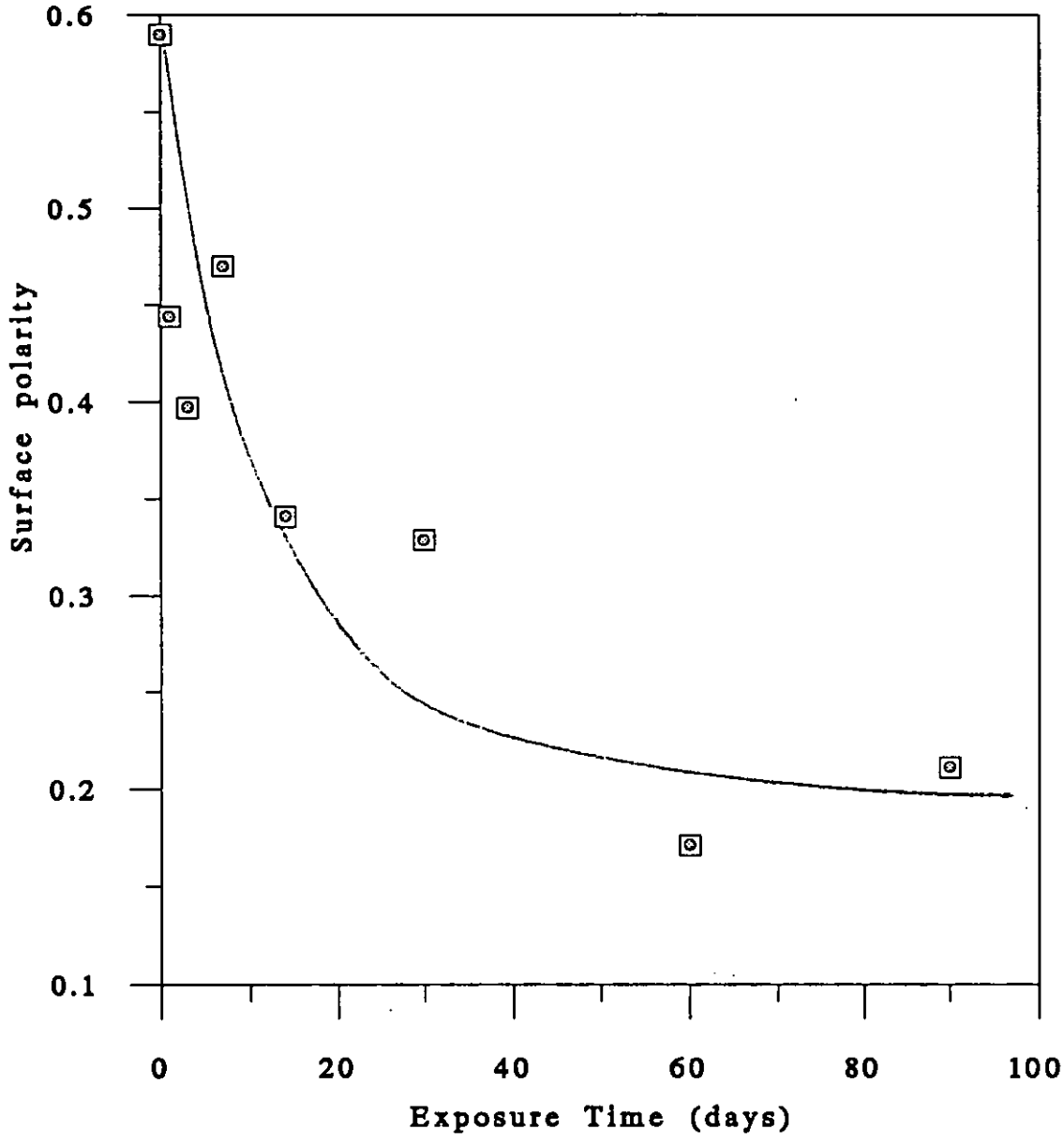

Fig. 13.5 Effect of exposure to atmospheric environment on the surface polarity of air corona discharge films

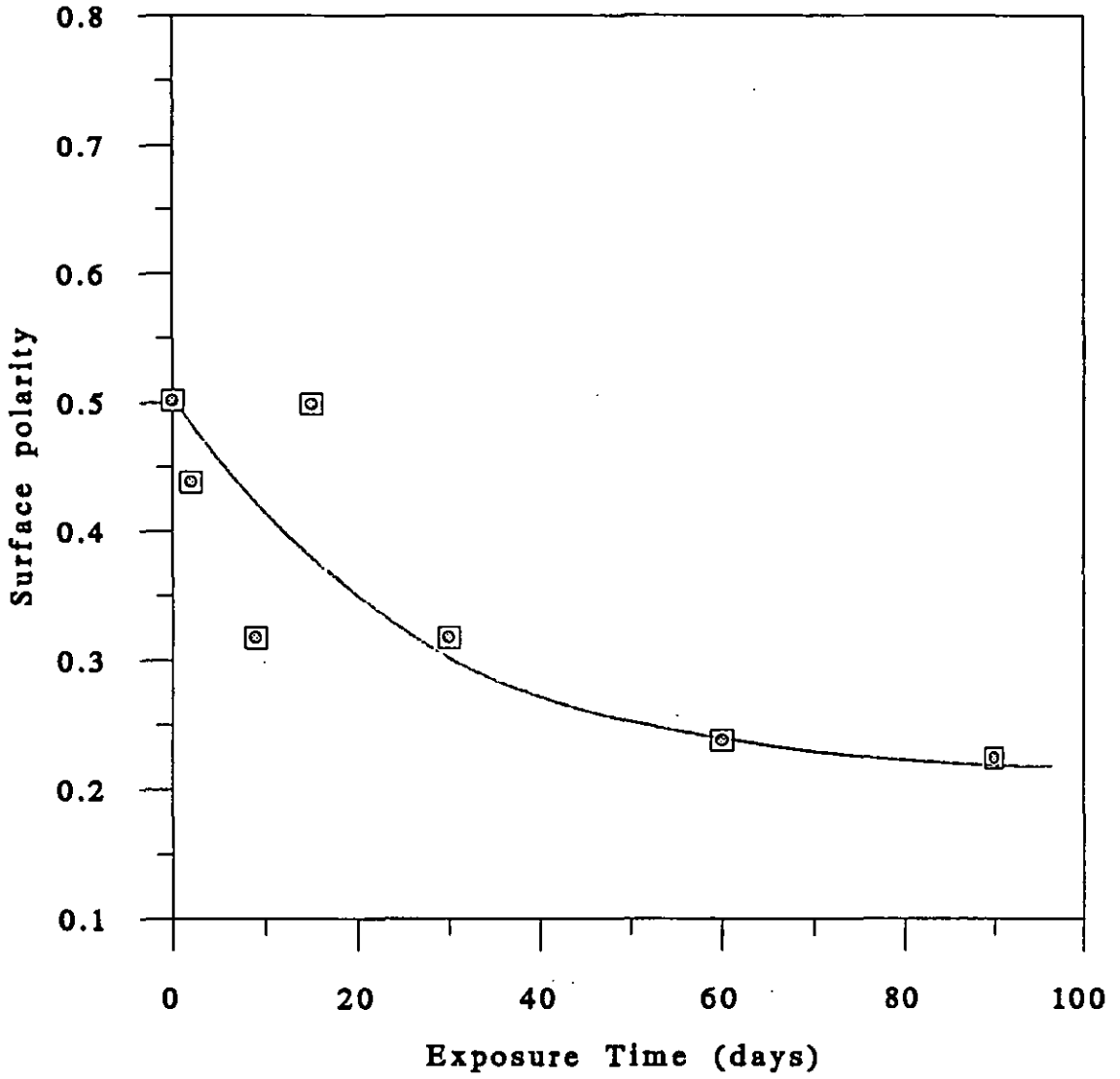

Fig. 13.6 Effect of exposure to atmospheric environment on the surface polarity of ammonia corona discharge treated films

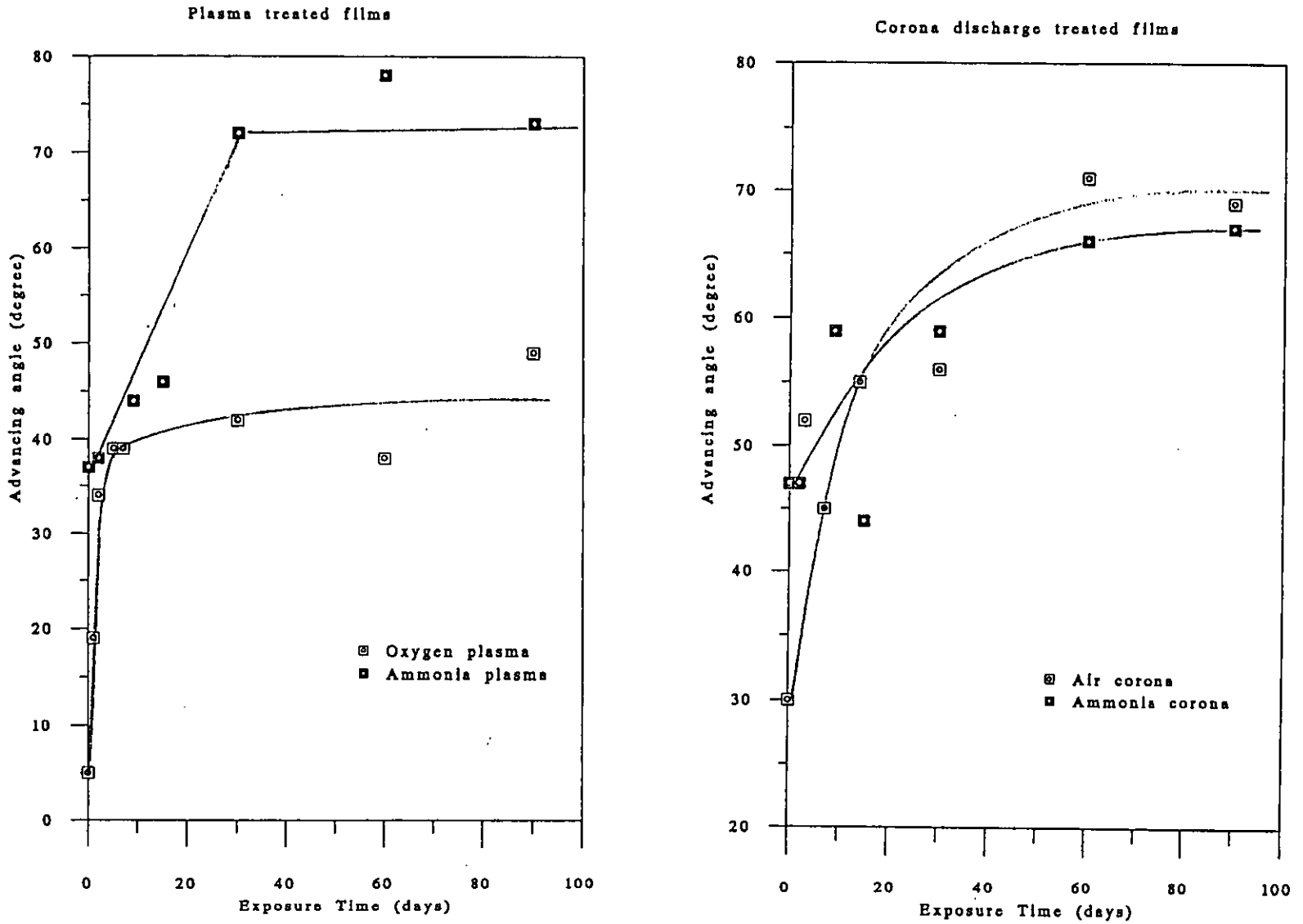

Fig. 13.7 Effect of exposure to atmospheric environment on the advancing contact angle of plasma and corona discharge treated films

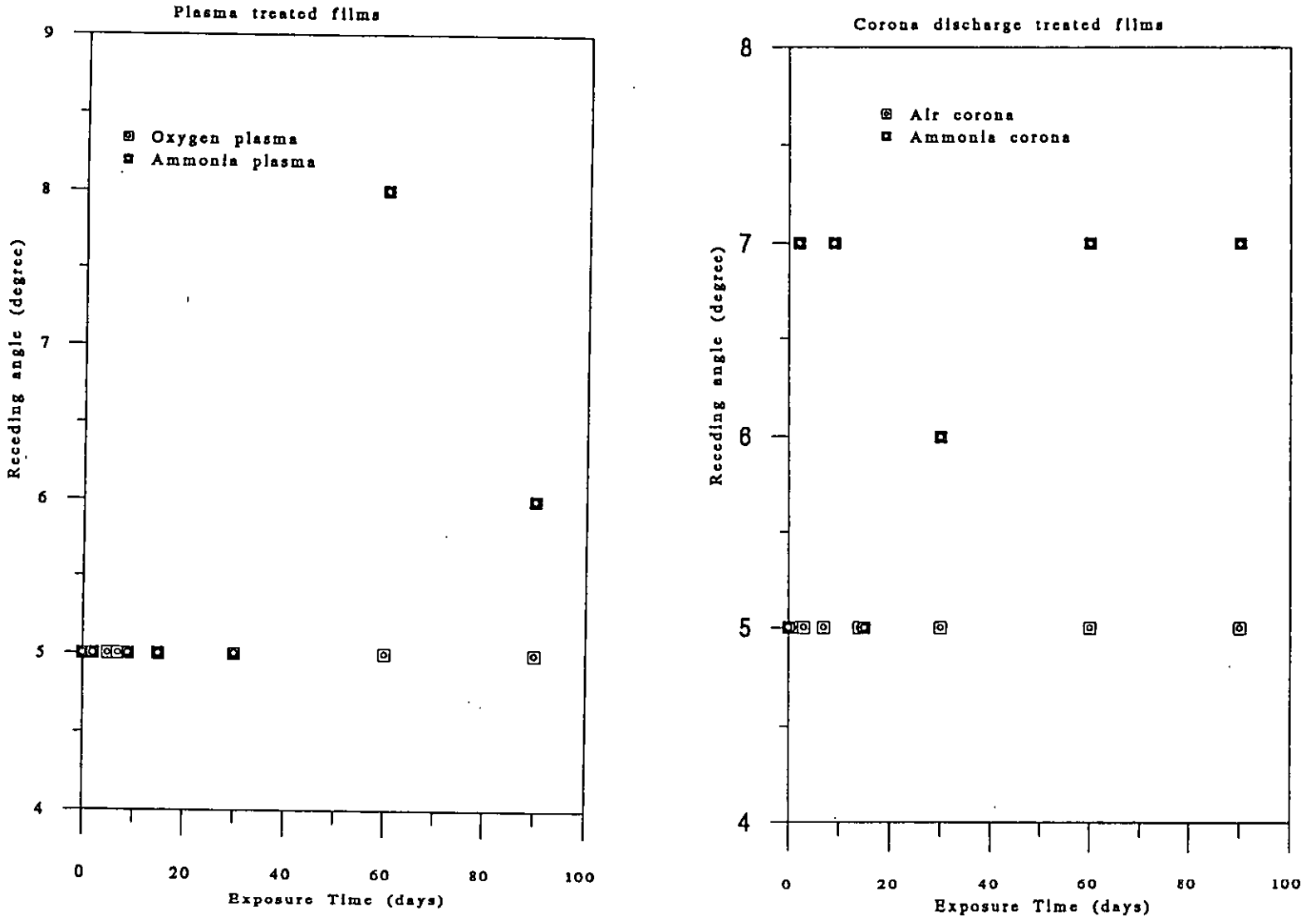

Fig. 13.8 Effect of exposure to atmospheric environment on the receding contact angle of plasma and corona discharge treated films

than that for the untreated (about 32°), suggesting that the treated surfaces did not fully reverse back to that of the untreated PEEK after atmospheric exposure.

Contact angle hysteresis is mainly influenced by two aspects, one is the surface heterogeneity[125], the other is surface roughness[126,127]. Wu[128] suggested that any hysteresis on an optically smooth surface must arise from surface heterogeneity. Since SEM studies have revealed that the materials used in this work are very smooth, both plasma and corona discharge treatment and subsequent atmospheric exposure do not change the surface topography of materials employed[165]. Thus, it is believed that the changes of contact angle hysteresis are induced by the altering of the surface heterogeneity.

The hysteresis results obtained are the typical behaviour of heterogeneous surfaces composed by a high energy and a low energy part [125,129,130]. The advancing angles tend to reflect the lower free energy part; while the receding angles tend to reflect the higher energy part of the heterogeneous surface. Morra *et al.* [166] suggested that if one starts with a wettable surface and introduces a hydrophobic component, one must expect a sudden increase of the advancing angle, which already at low fractional coverage reaches the typical values of the less wettable part. The receding angle remains constant at the low value of the more wettable part and starts to increase at coverage close to unity. Considering our data it is believed that both plasma and corona discharge treatment produced heterogeneous surfaces with varying surface free energy (different wettability) domains. Atmospheric exposure increases the fraction of the surface covered by the low energy domain to some extent with some high energy region produced by the treatment still remained on the surface.

13.2.4 Adhesion studies

Atmospheric exposure show different effects on the joint strength of various plasma and corona discharge treated materials, as shown in Fig. 13.9-13.12. Fig. 13.9 shows the effect of exposure on the T-peel joint strength of oxygen plasma treated films. The joint strength remained unchanged in the first month of the exposing period, then reduced slightly. The air corona treated sample behaved the same as the oxygen plasma treated sample (as shown in Fig. 13.10). Whereas the joint strength of both ammonia plasma and ammonia corona treated materials remained unchanged in the whole exposing period. The results may suggest that different treatment conditions produce different surface structures which restructure differently during the atmospheric exposure period.

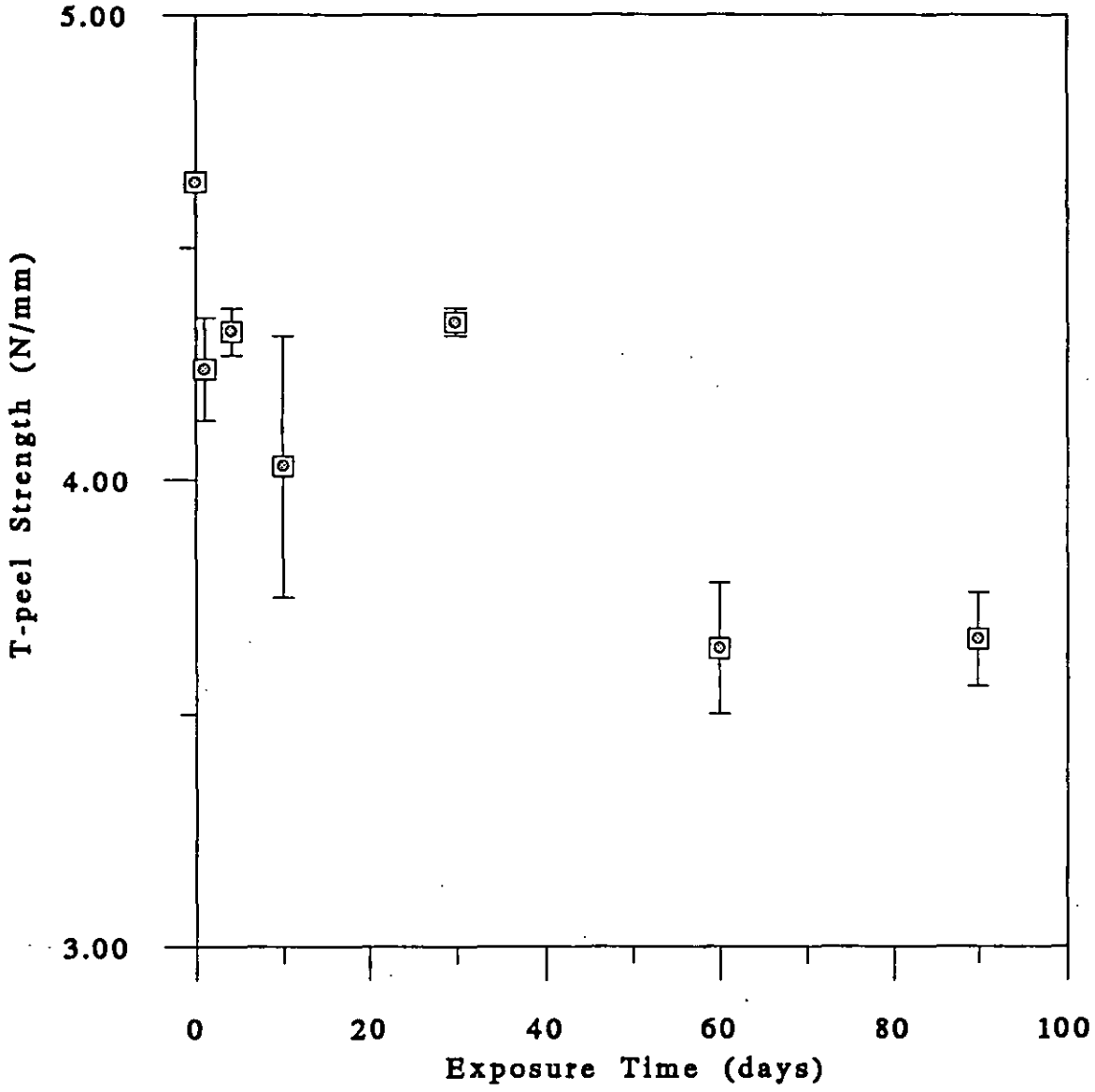

Fig. 13.9 Effect of exposure to atmospheric environment on the T-peel joint strength of oxygen plasma treated films

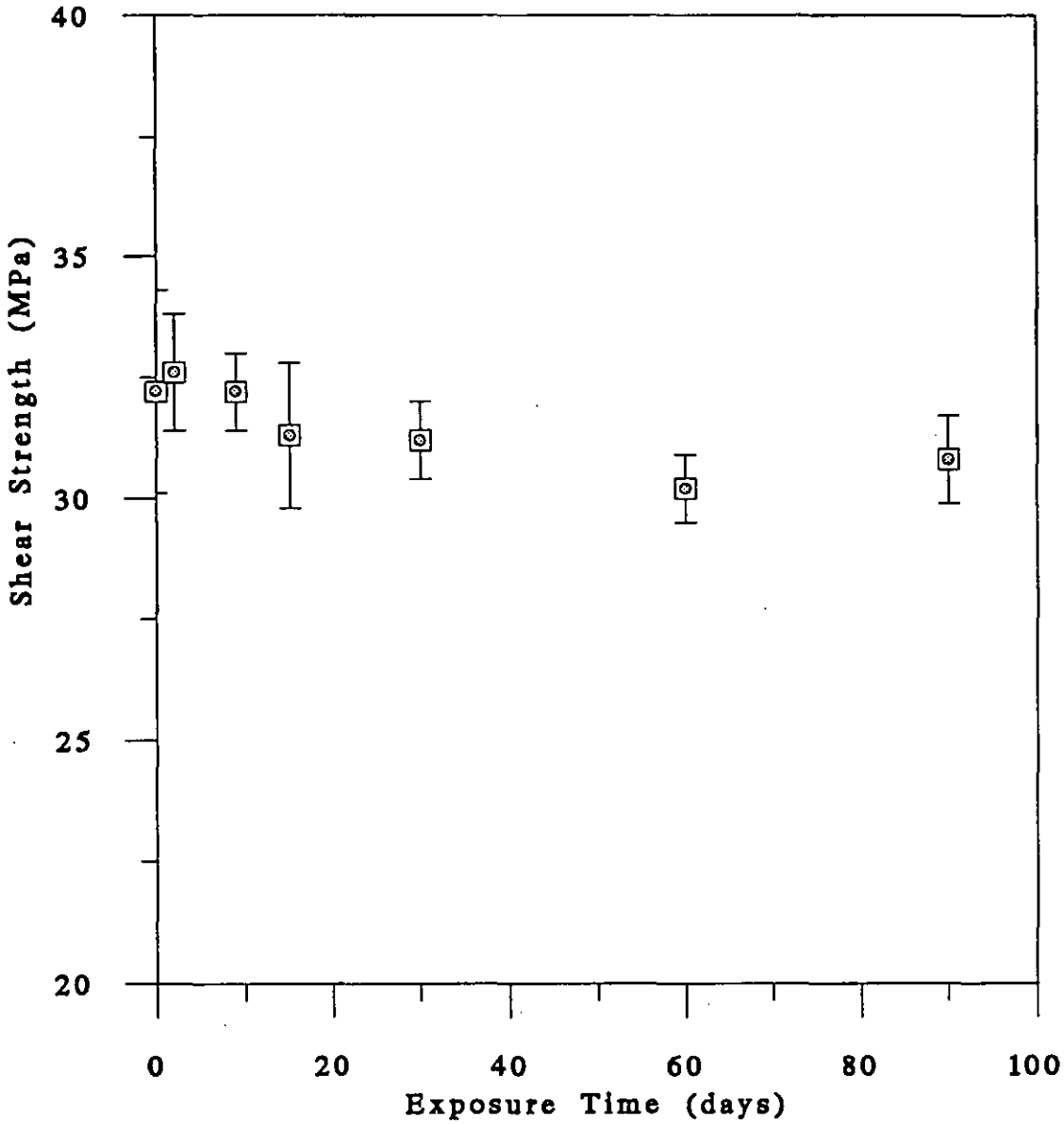

Fig. 13.10 Effect of exposure to atmospheric environment on the lap shear joint strength of ammonia plasma treated films

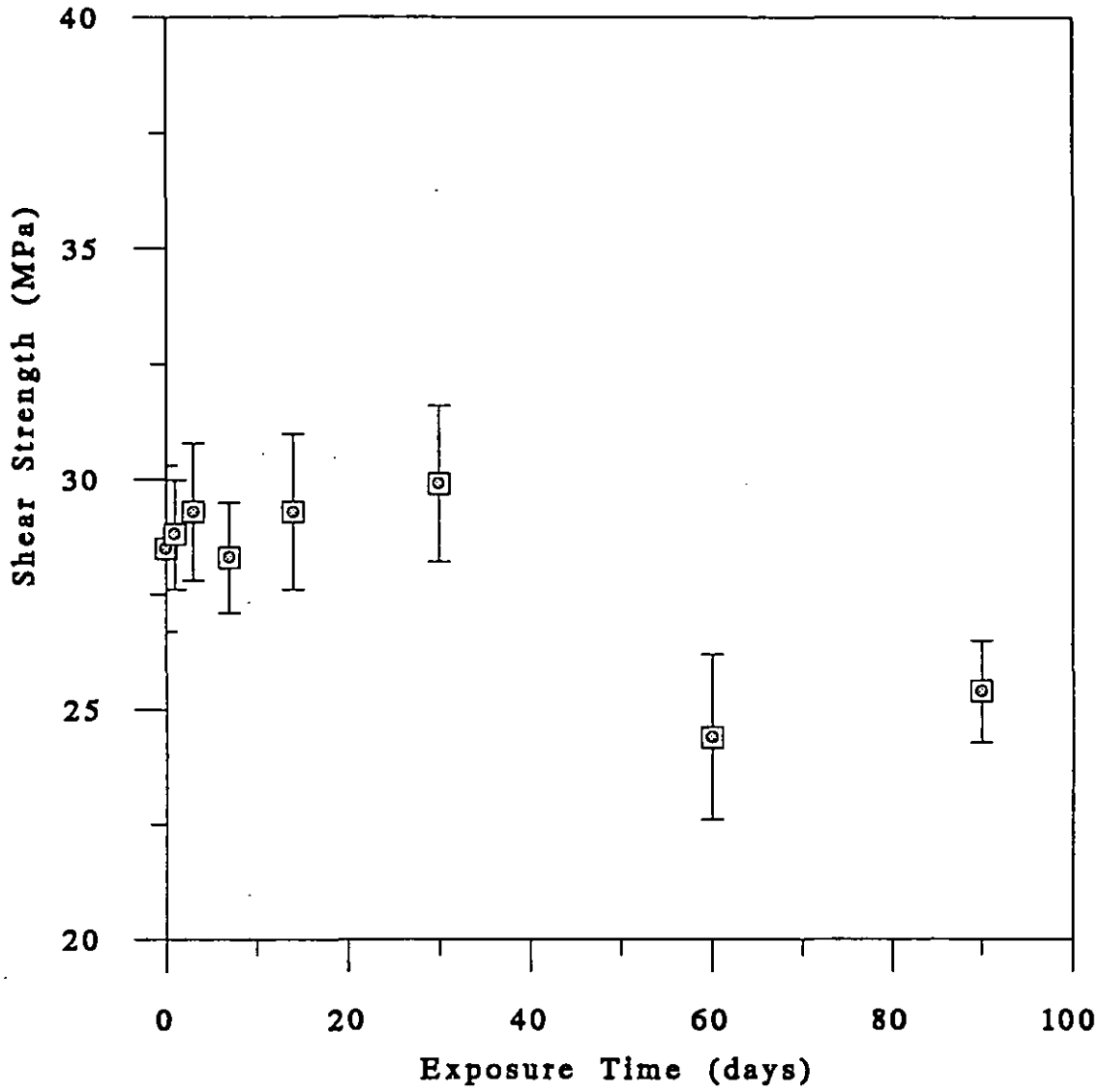

Fig. 13.11 Effect of exposure to atmospheric environment on the lap shear joint strength of air corona discharge treated films

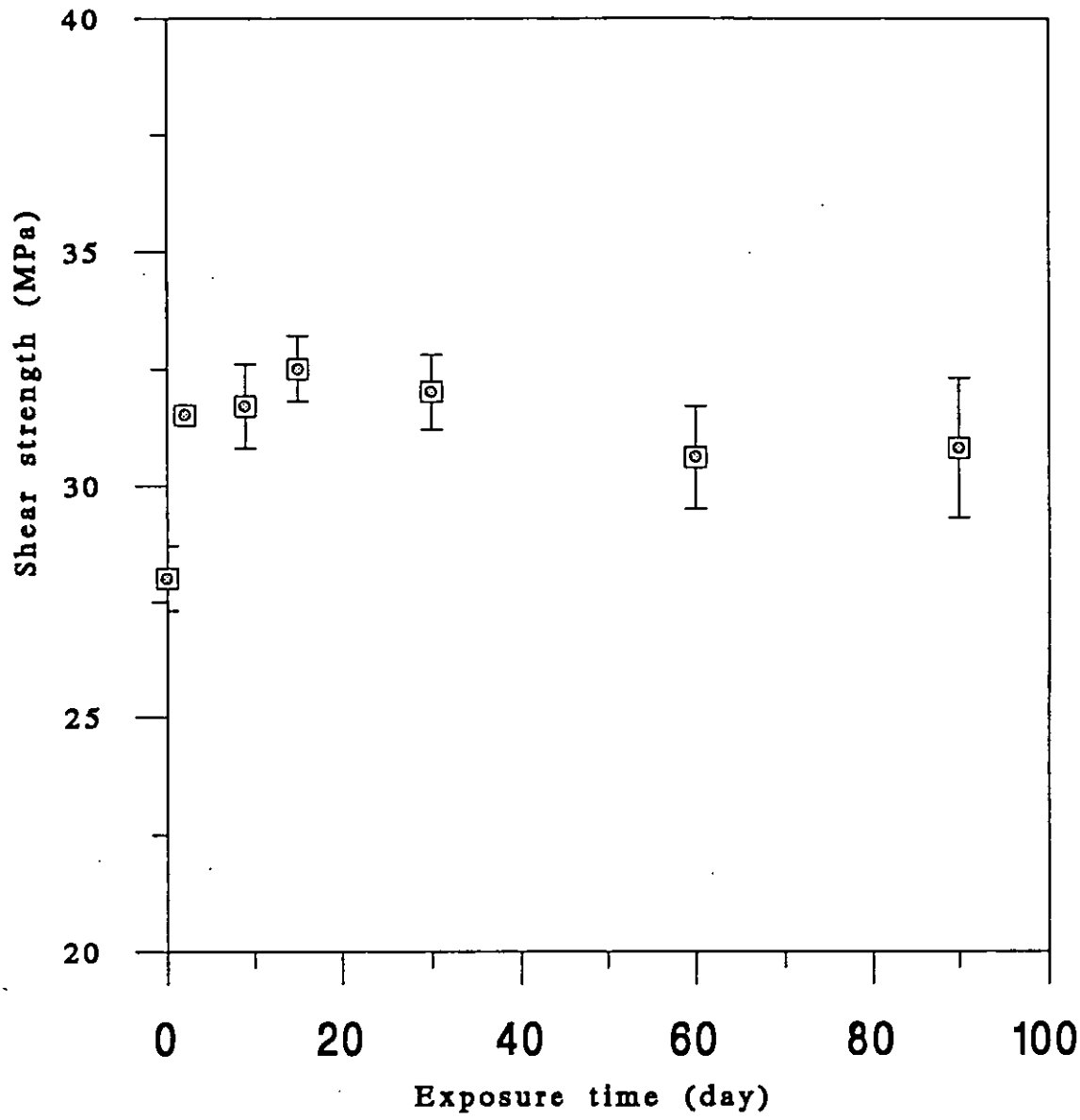

Fig. 13.12 Effect of exposure to atmospheric environment on the lap shear joint strength of ammonia corona discharge treated films

During the atmospheric exposure period, because air has very low polarity, the modified layer tends to restructure and lower their interfacial tension. The changes in the surface energy, surface polarity and the contact angle hysteresis, therefore, could be due to the following restructuring process occurring within the contact angle sampling depth on the treated PEEK surfaces.

(a) LMWM migrate away from the topmost layer towards the bulk to minimise the interfacial tension between the treated surface and the air. This process could proceed very fast, thus lowering the surface free energy, its polar component and the surface polarity significantly in the early exposing period.

In the mean time the LMWM migrate into the bulk, the HMWM expose to the atmosphere, due to the fact that they were less affected by the plasma and corona treatment, their dispersion component of the surface energy are more close to the untreated PEEK. Hence the dispersion component of corona discharge treated films have increased after exposing.

XPS studies [113] on the atmospheric exposure of oxygen plasma treated PEEK has confirmed the removal of some small molecules within its sampling depth, i.e. about 2.5 nm. It was found that the O/C ratio of the treated surface dropped from 35/100 to a steady value 28/100 in about two days. At the same time the amount of oxygen containing polar groups also decreased while the amount of species containing benzene rings increased.

(b) The polar groups in the molecules orient away from the topmost layer to the subsurface, driven by the thermodynamically requirement. This process may also be very fast, and contribute to the lowering of the polar part of the surface energy and surface polarity in the early exposing period.

(c) The migration of the HMWM away from the topmost layer may take long time to reach completion and may not be observed within the examination period. This process causes the surface energy and its components to change only very slowly.

(d) The polar groups of the molecules may form internal hydrogen bond among each other or with the bulk molecules, thus hindering the restructuring in the modified layer. After a certain period, both the thermodynamic driving force and the obstructing force of the internal hydrogen bond could reached an equilibrium, thereby preventing further

changes in surface properties. Hence the aged surfaces are different to the surface of untreated PEEK, as confirmed by the above results.

The extent of the above restructuring processes depend on the chemical structure produced by the plasma and corona treatment. Oxygen plasma treatment may cause more oxidation on the surface, as confirmed by the XPS and TOF-SIMS analysis (Chapter 10 and Ref. 97), and there are more functional groups on the oxygen plasma treated PEEK surface. After atmospheric exposure, because of the obstructing force of internal hydrogen bonds, more functional groups remain on the top surface layer, giving rise to lower advancing contact angle of water compared with the aged surfaces from other treatments.

As shown in Section 12.2, the LMWM that are easily removed from the surface are not associated with bondability, therefore the bondability of treated materials was speculative as only decided by the composition of HMWM. The HMWM produced by oxygen plasma and air corona may be not big enough to hinder their mobility, some of them could migrate out of the modified layer in the long term exposure period, hence these treated materials would lose some of their bondability correspondingly. This decaying process could be stopped by the forming of internal hydrogen bond. For the ammonia plasma and corona treated PEEK, the HMWM may be too big and unable to move, hence their bondability is not affected by the atmospheric exposure.

In addition, if we relate the joint strength results to the wettability results, it can be seen that no direct relationship exist between bondability and wettability. This could be due to two reasons, one is that the adhesive employed can wet the substrate even when they are not treated, so intimate interfacial contact can be formed in any case, the other is that the treated surfaces can form strong interfacial attractions with the adhesive, as the results in Section 12.3.2 suggest.

13.3 Temperature Effect

As discussed in the previous section, the surface restructuring processes mainly involve the molecular migration and reorientation. Increasing the temperature can increase the molecular mobility, hence it may facilitate the restructuring process occurring in the modified layer produced by the plasma and corona treatment. This section is dealing with the effects of temperature on the surface dynamics of treated PEEK.

13.3.1 Wettability studies

Fig. 13.13 and Fig. 13.14 show the temperature effect on the surface free energy of oxygen plasma and air corona discharge treated PEEK films respectively. As it can be seen, the polar component and the total surface free energy decrease with the increase of temperature until the T_g of PEEK (about 143°C) is reached, and then remains constant values which are similar to those of the untreated material. However, the dispersion component of the surface free energy increased with the temperature and reached its plateau at temperature much lower than the T_g of PEEK.

Fig. 13.15 and Fig. 13.16 shows the temperature effect on the surface polarity of oxygen plasma and air corona discharge treated films respectively. The results suggest that increasing the temperature has the similar effect on the surface polarity as increasing atmospheric exposure time. i.e. surface polarity decreased with increasing temperature and then reached an equilibrium value at temperature around T_g of PEEK.

Table 13.1 shows the effect of 1 hour heat treatment at temperature of 180°C on the surface free energy and polarity of other plasma and corona discharge treated films. It can be seen that the heat treatment changes the surface free energy and its components, surface polarity of the treated films to values which are similar to those of the untreated materials.

Fig. 13.17 and Fig. 13.18 show the temperature effect on the contact angle hysteresis of oxygen plasma treated and air corona treated materials respectively. Increasing temperature tends to increase the advancing and receding contact angle simultaneously but with different rate. The advancing angle reaches its equilibrium value about T_g, while the receding angle continues to increase even when the temperature is above T_g.

Table 13.1 also shows the temperature effect of 1 hour heat treatment at temperature of 180°C on the contact angle hysteresis of plasma and corona treated films. As it can be seen, the heat treatment reverses the advancing angles of plasma and corona treated samples back to that of the untreated, but gives varied receding angle results. Suggesting that the consequence of surface reorganisation process is not the same for different condition treated materials.

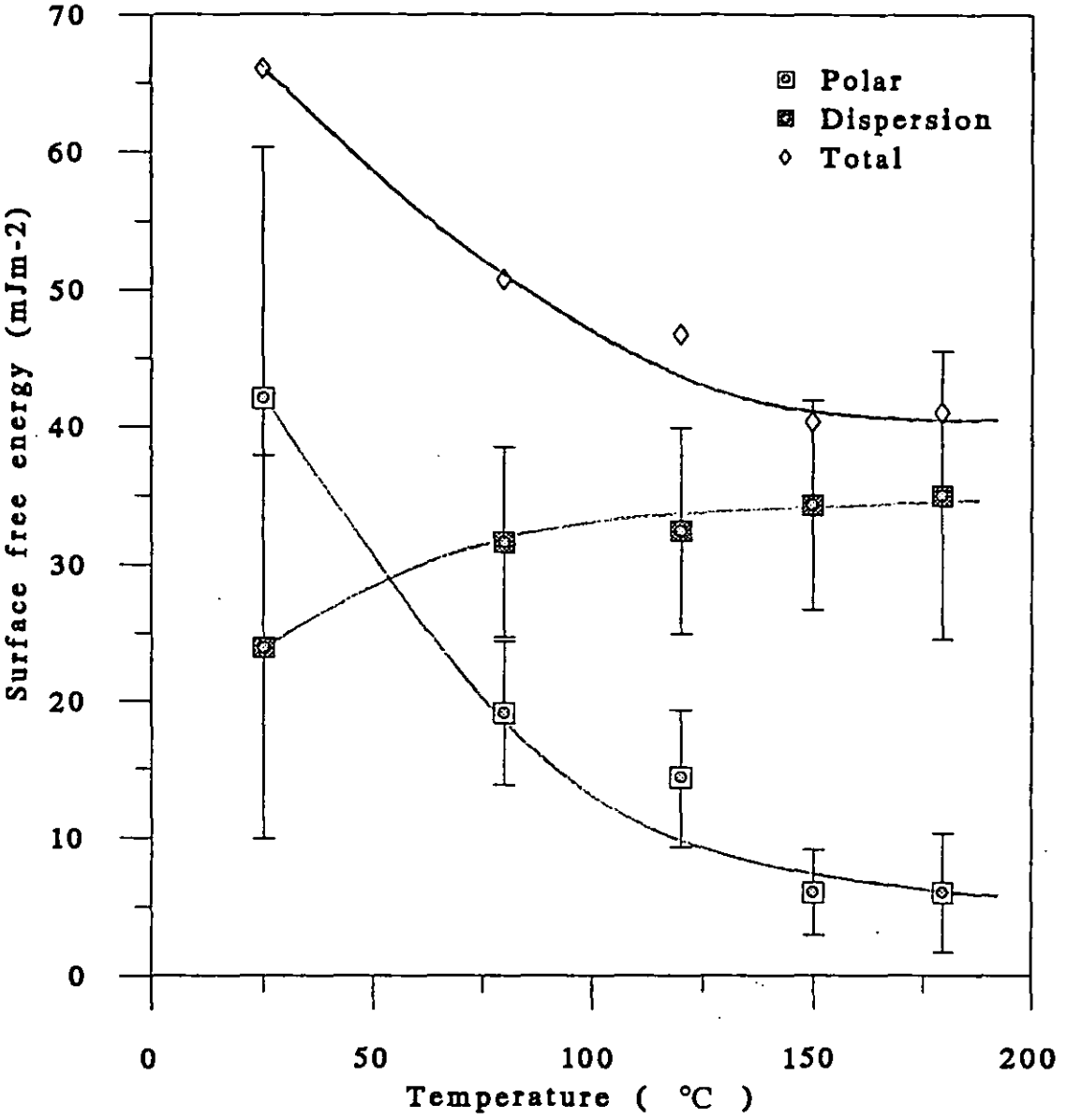

Fig. 13.13 Effect of heat treatment temperature on the surface free energy of oxygen plasma treated films

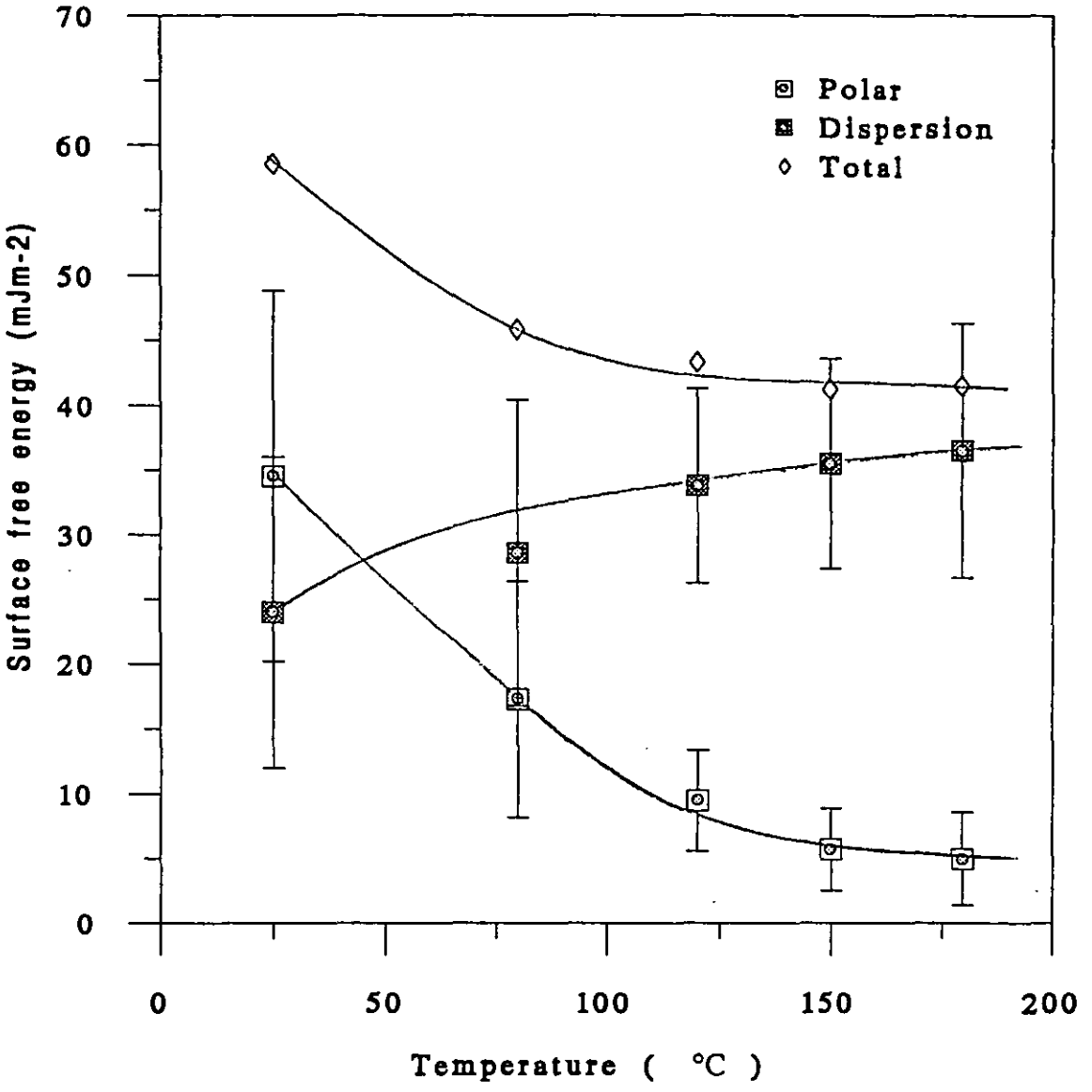

Fig. 13.14 Effect of heat treatment temperature on the surface free energy of air corona discharge treated films

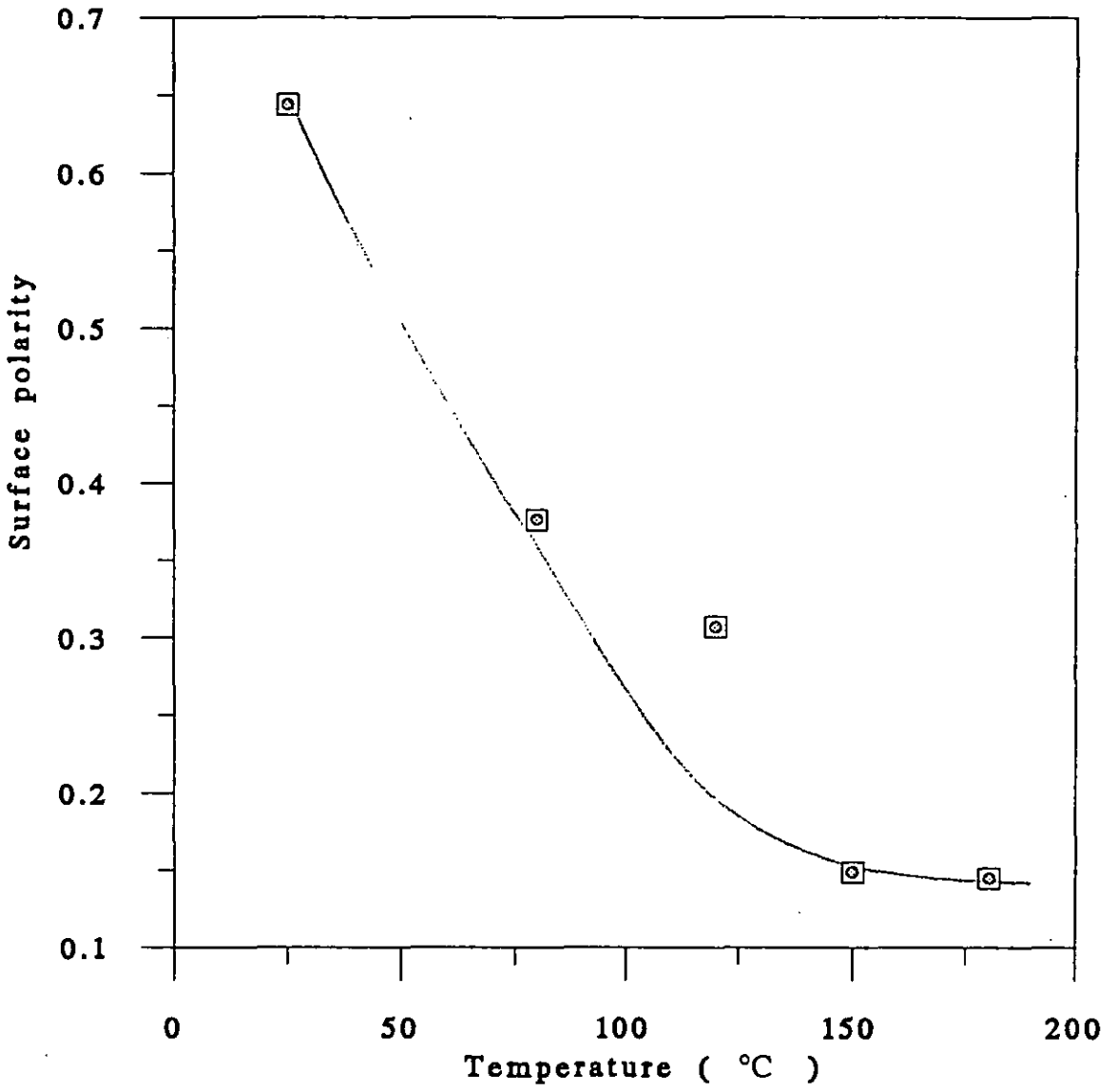

Fig. 13.15 Effect of heat treatment temperature on the surface polarity of oxygen plasma treated films

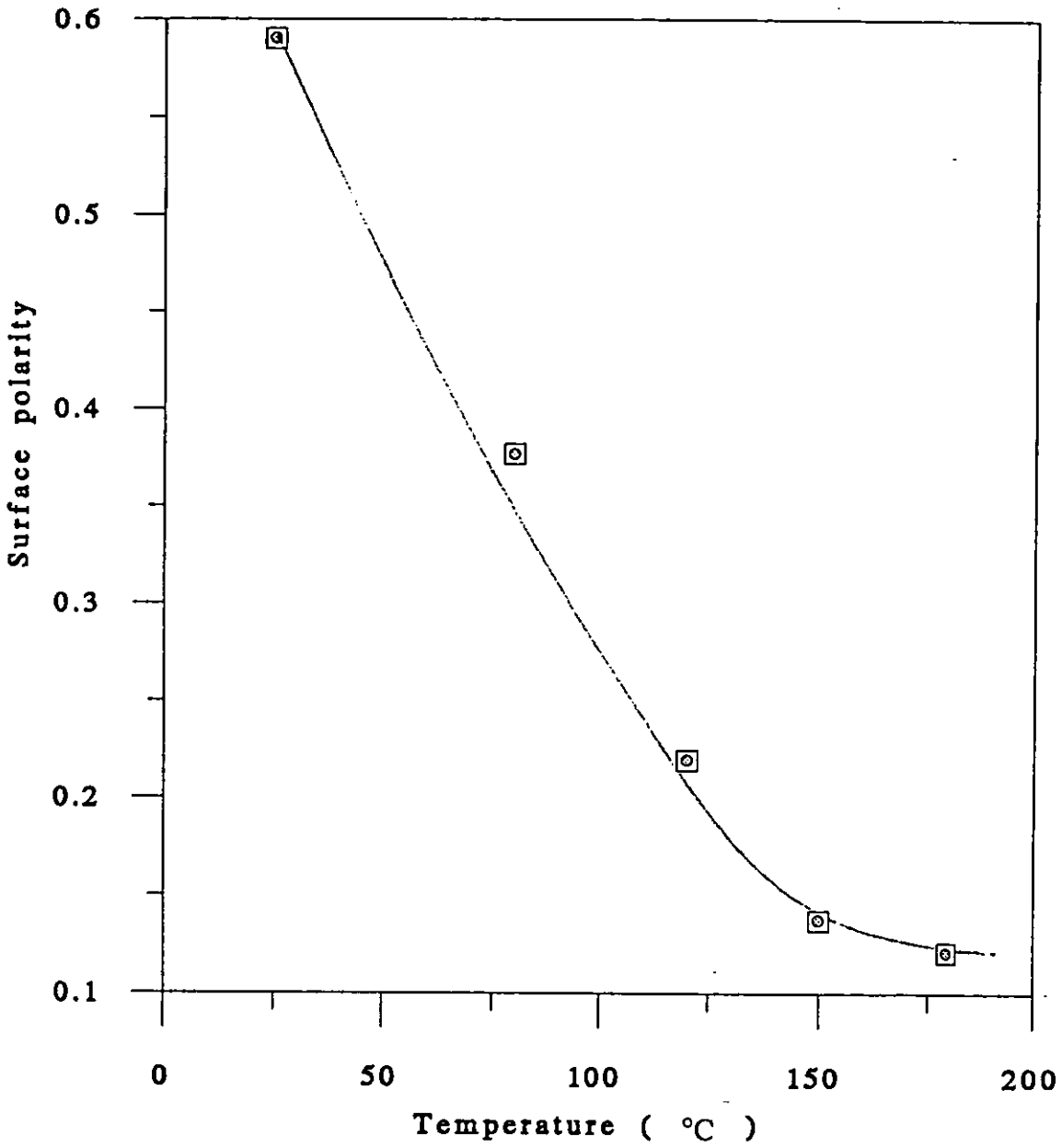

Fig. 13.16 Effect of heat treatment temperature on the surface polarity of air corona discharge treated films

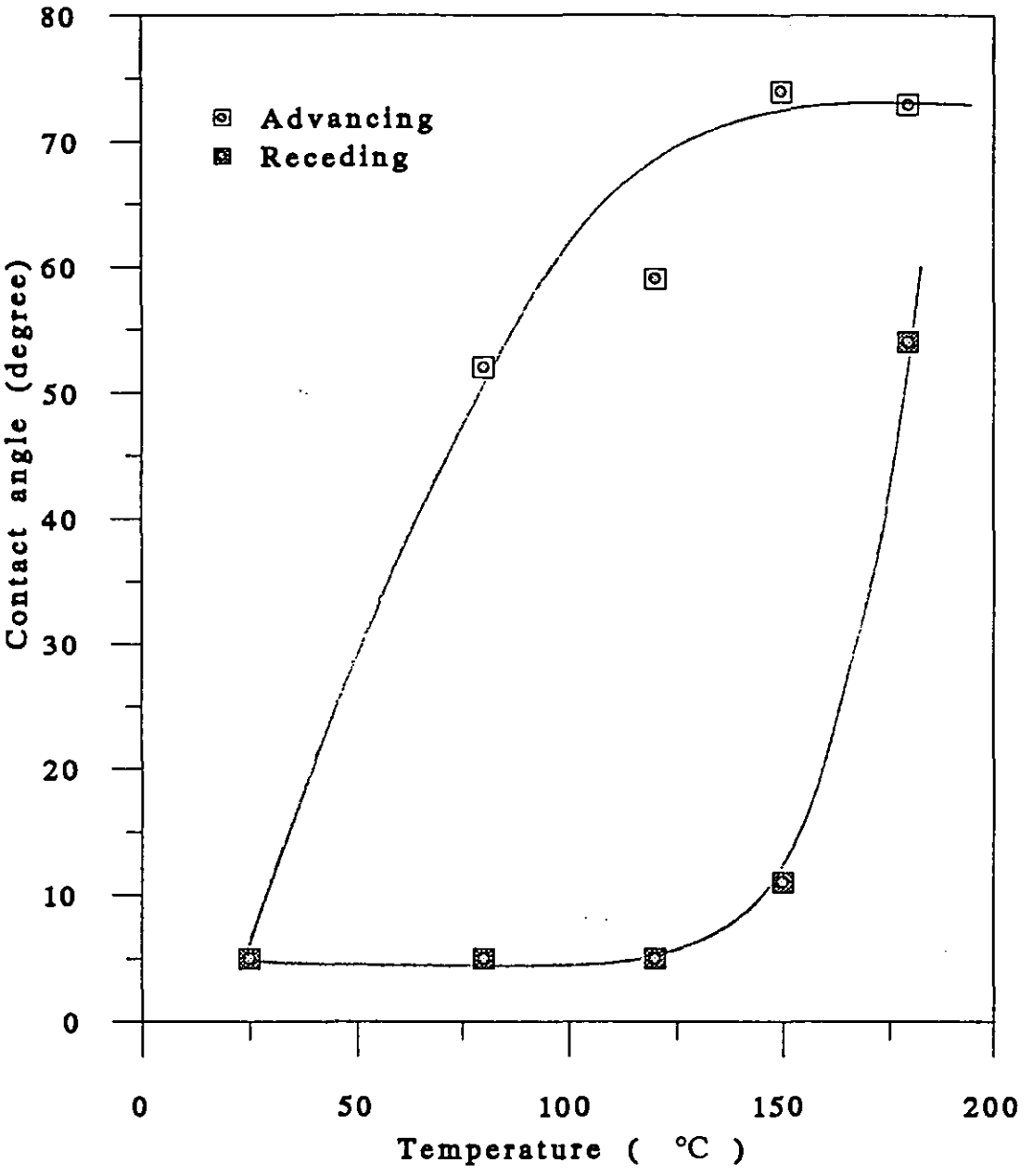

Fig. 13.17 Effect of heat treatment temperature on the contact angle hysteresis of oxygen plasma treated films

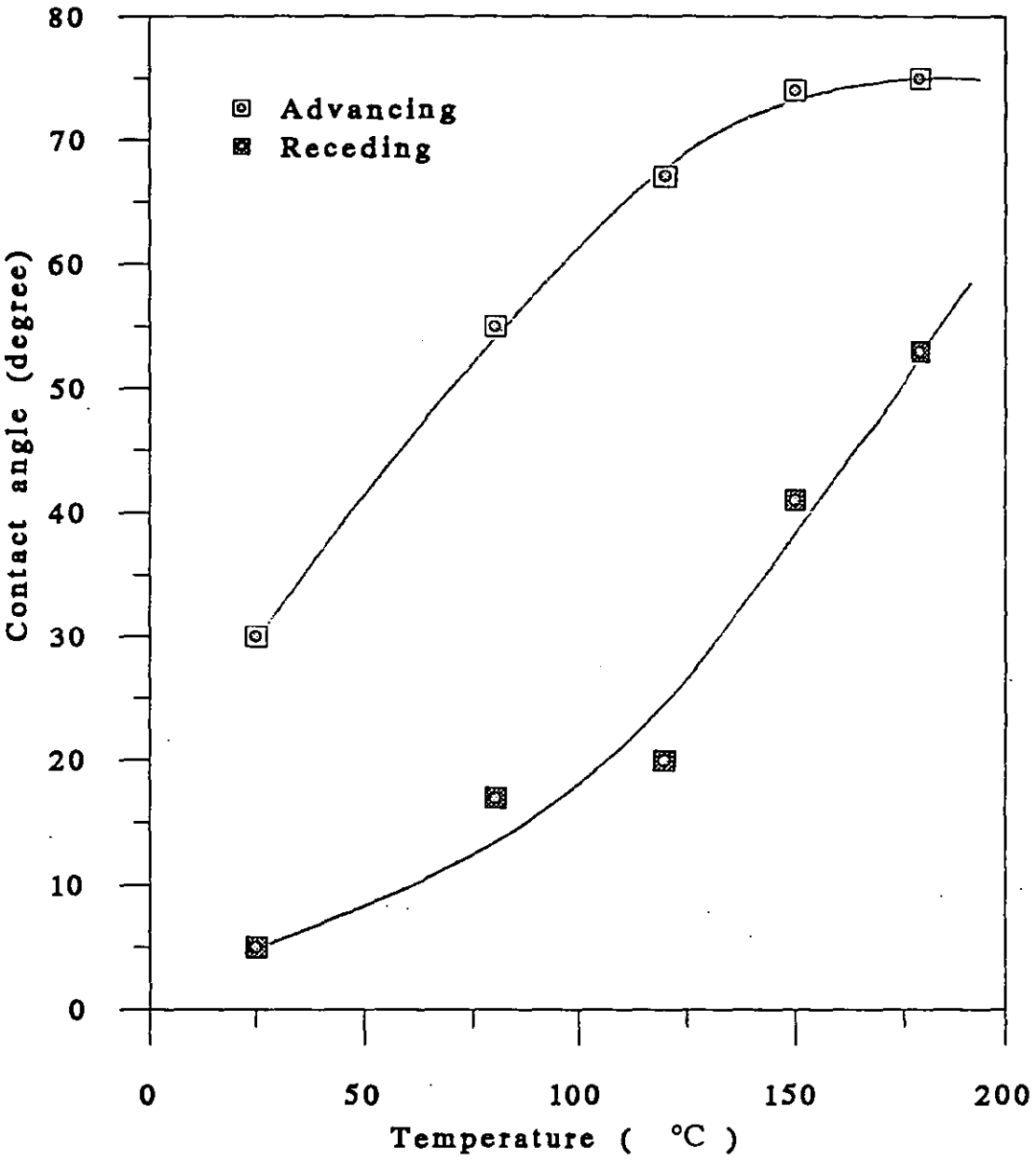

Fig. 13.18 Effect of heat treatment temperature on the contact angle hysteresis of air corona discharge treated films

Table 13.1 Effect of 1 hour heat treatment at temperature of 180°C on the wettability of some plasma and corona discharge treated films

Treatment condition	Heat treatment	Surface free energy (mJm^{-2}) γ_s^p	γ_s^d	γ_s	Surface polarity	Contact angle hysteresis θ_a	θ_r
Untreated	Before	7.2±3.9	31.5±8.3	38.7	0.186	73	32
	After	2.3±2.6	34.8±10.3	37.1	0.06	84	49
O_2 Plasma	Before	42.0±18.3	23.9±14.0	66.0	0.638	<5	<5
	After	6.0±4.3	35.0±10.5	41.0	0.145	73	54
NH_3 Plasma	Before	32.4±11.6	22.7±9.8	55.1	0.587	41	<5
	After	9.4±5.0	25.9±8.3	35.3	0.266	72	--
SO_2 Plasma	Before	26.3±11.2	26.0±11.3	52.3	0.503	43	<5
	After	6.6±4.7	32.3±10.6	38.9	0.171	73	44
Air Corona	Before	34.5±14.3	24.0±12.0	58.5	0.590	30	<5
	After	5.0±3.6	36.5±9.8	41.5	0.121	75	53
NH_3 Corona	Before	25.9±8.7	25.7±8.7	51.6	0.502	45	<5
	After	5.4±4.2	34.1±10.7	39.5	0.136	75	37
SO_2 Corona	Before	24.6±8.3	28.0±9.0	52.6	0.518	46	<5
	After	6.6±5.2	31.7±11.5	38.3	0.172	76	47

Plasma treatment condition: 1 min, 500 w, 0.3 torr

Corona discharge treatment level: 0.4 J/mm^2

Therefore, the above results indicate that heat treatment can be used as an accelerated test for the atmospheric exposure experiment when studying the surface dynamics of the plasma and corona treated PEEK films.

13.3.2 TOF-SIMS analysis

Both oxygen plasma and ammonia plasma treated films were studied by TOF-SIMS. Samples were prepared by post treating the films for 1 hour at temperature of 150°C

13.3.2.1 Positive ion spectra (Fig. 13.19 and Fig. 13.20)

Below a.m.u. 200, heat treatment has very little effect on the spectra of both oxygen plasma and ammonia plasma treated films, except for the peak at a.m.u. 18 (which was introduced by the treatment). For oxygen plasma treated sample, this signal was reduced, while for ammonia plasma treated sample this signal was removed.

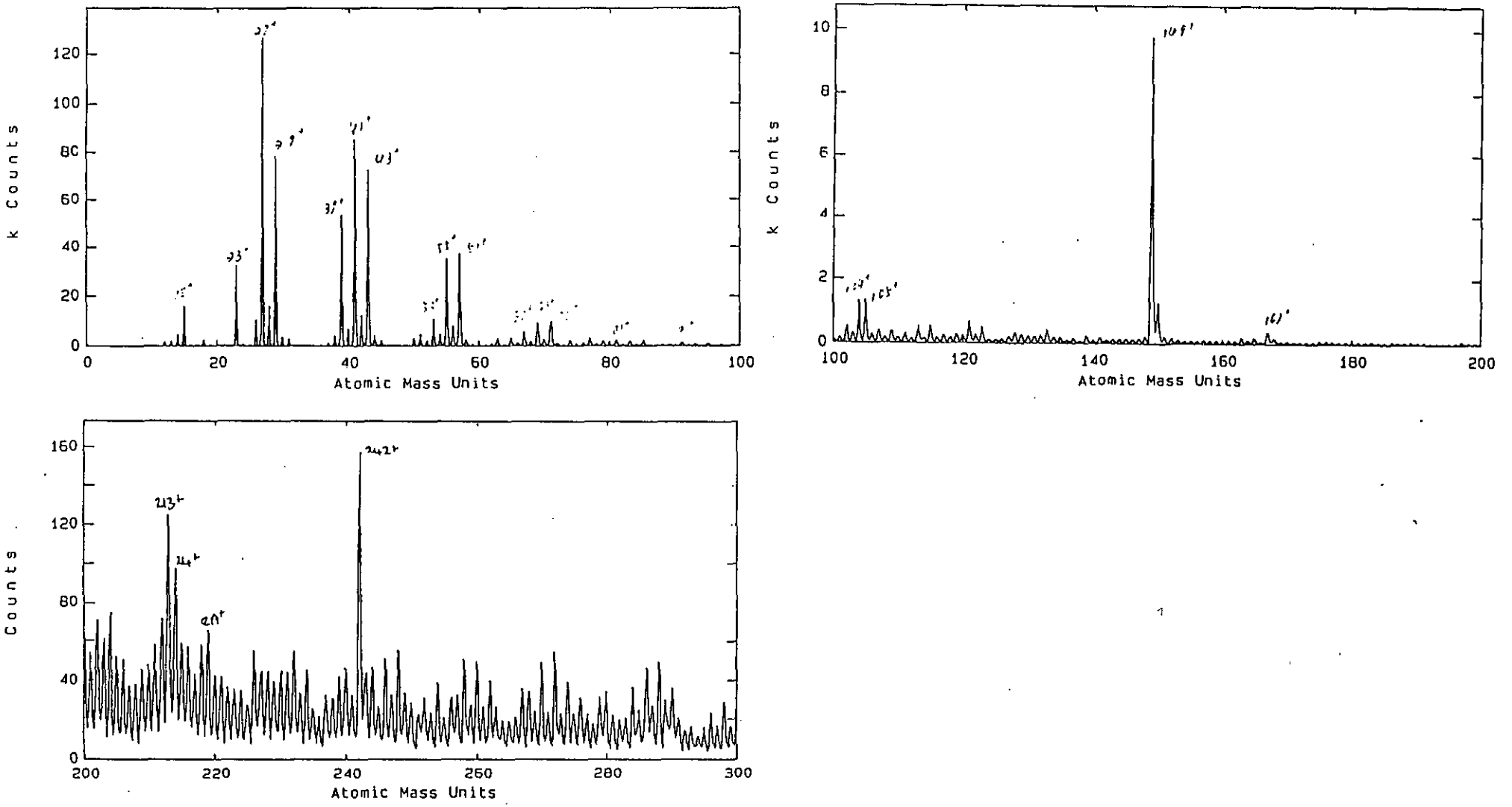

Fig. 13.19 Positive ion spectrum for oxygen plasma treated PEEK film after 1 hour heat treatment at temperature of 150°C (Plasma treatment condition: 1 min, 500 w, 0.3 torr)

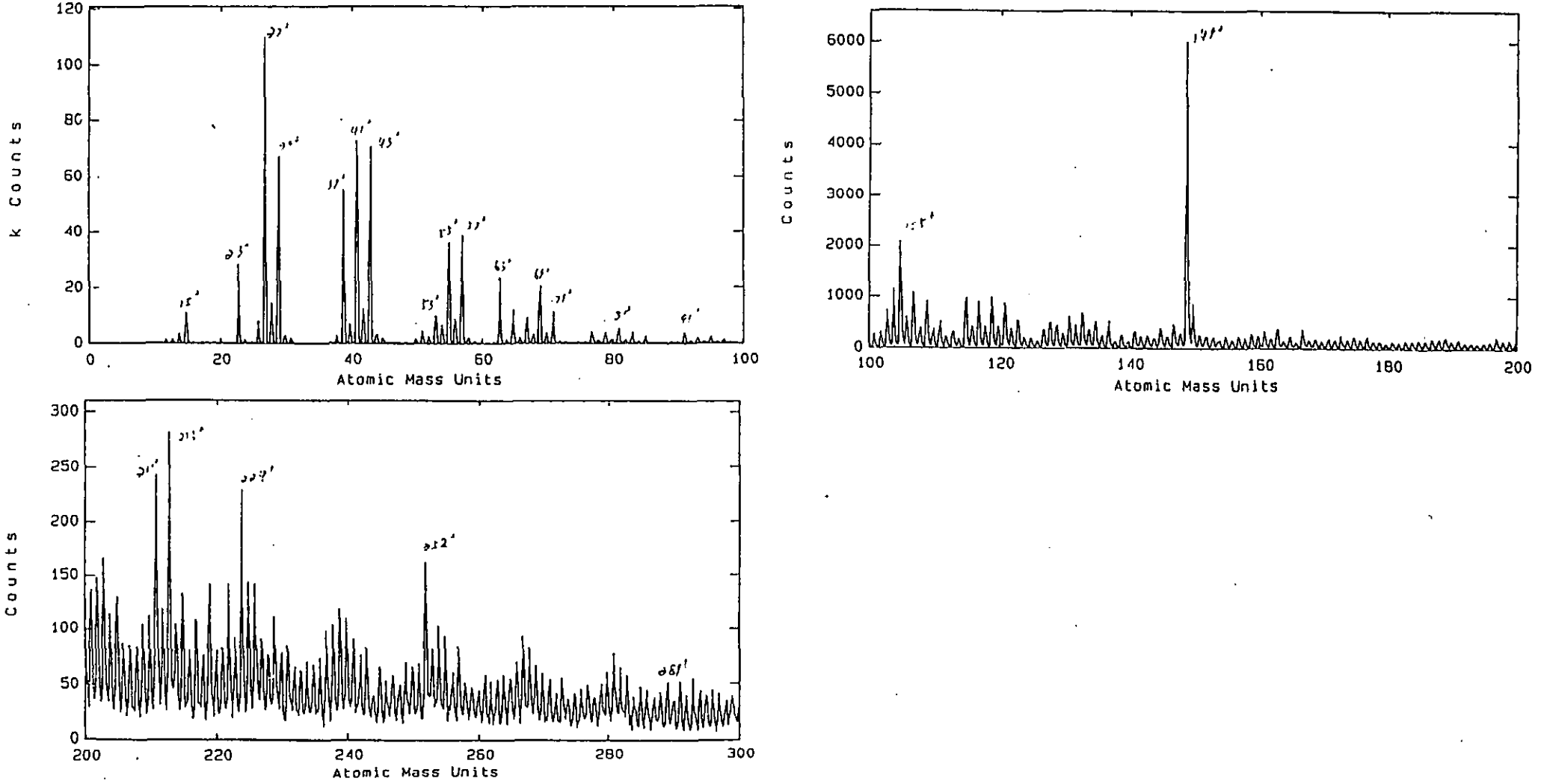

Fig. 13.20 Positive ion spectrum for ammonia plasma treated PEEK film after 1 hour heat treatment at temperature of 150°C (Plasma treatment condition: 1 min, 500 w, 0.3 torr)

Between a.m.u. 200-300, the peak at a.m.u. 219, which was introduced by both plasma treatment, disappeared after heat treatment.

For oxygen plasma treated films, two other signals which were introduced or enhanced by the treatment, i.e. at a.m.u. 213 and 242, were reduced after heat treatment. For ammonia plasma treated films, the peak at a.m.u. 213, which was removed by the plasma treatment, reappeared after heat treatment, in addition, new peaks at a.m.u. 224 and 252 appeared after heat treatment, none of which being present in the untreated PEEK spectrum.

13.3.2.2 Negative ion spectra

(a) Oxygen plasma treated films (Fig. 13.21)

Below a.m.u. 100, the intensities of the peaks at a.m.u. 45, 57, 59, 77, 93 and 97, which have been enhanced slightly by the plasma treatment, are slightly reduced, but not to the level of the untreated sample.

In this mass region, the peak at a.m.u. 19, which had been assigned to F^-, was enhanced after heat treatment.

Between a.m.u. 100-200, the signal at a.m.u. 141, which was removed by oxygen plasma treatment, reappeared after heat treatment, but other peaks which were removed by the plasma treatment were still missing after heat treatment. On the other hand, the signal at a.m.u. 108 was enhanced by heat treatment.

Between a.m.u. 200-300, new peaks appear at 215, 255, 259 and 283 after heat treatment. Among these, the peak at a.m.u. 255 also appeared in the untreated PEEK spectrum but with a much strong intensity. The peak at a.m.u. 219, which was introduced by the plasma treatment, disappeared after the heat treatment.

(b) Ammonia plasma treated films (Fig. 13.22)

Below a.m.u. 100, after heat treatment, the intensities of peaks at a.m.u. 26 (CN^-), 66 and 71 (all of them were introduced by the ammonia plasma treatment), were reduced, while others remained virtually unchanged.

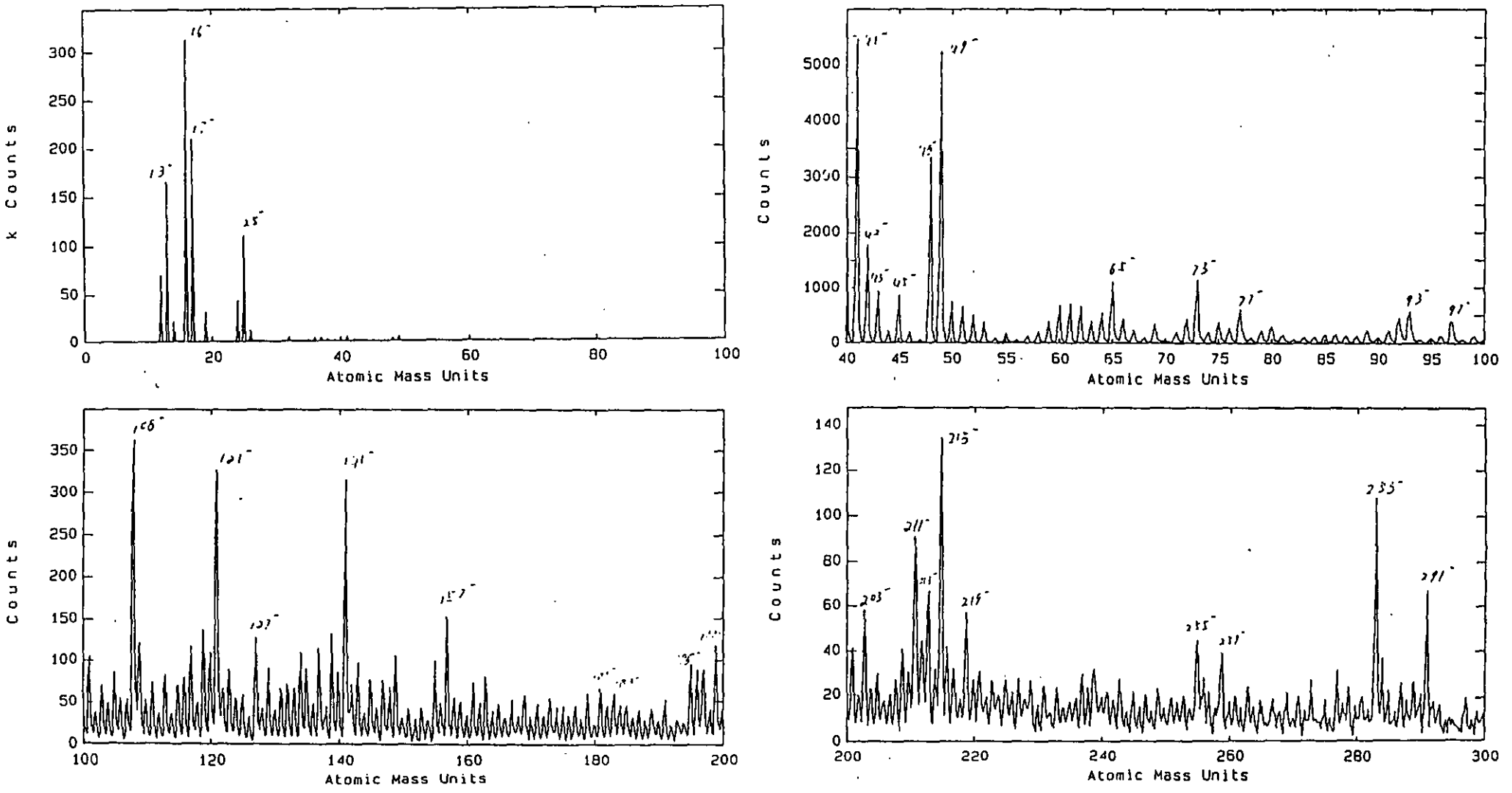

Fig. 13.21 Negative ion spectrum for oxygen plasma treated PEEK film after 1 hour heat treatment at temperature of 150°C (Plasma treatment condition: 1 min, 500 w, 0.3 torr)

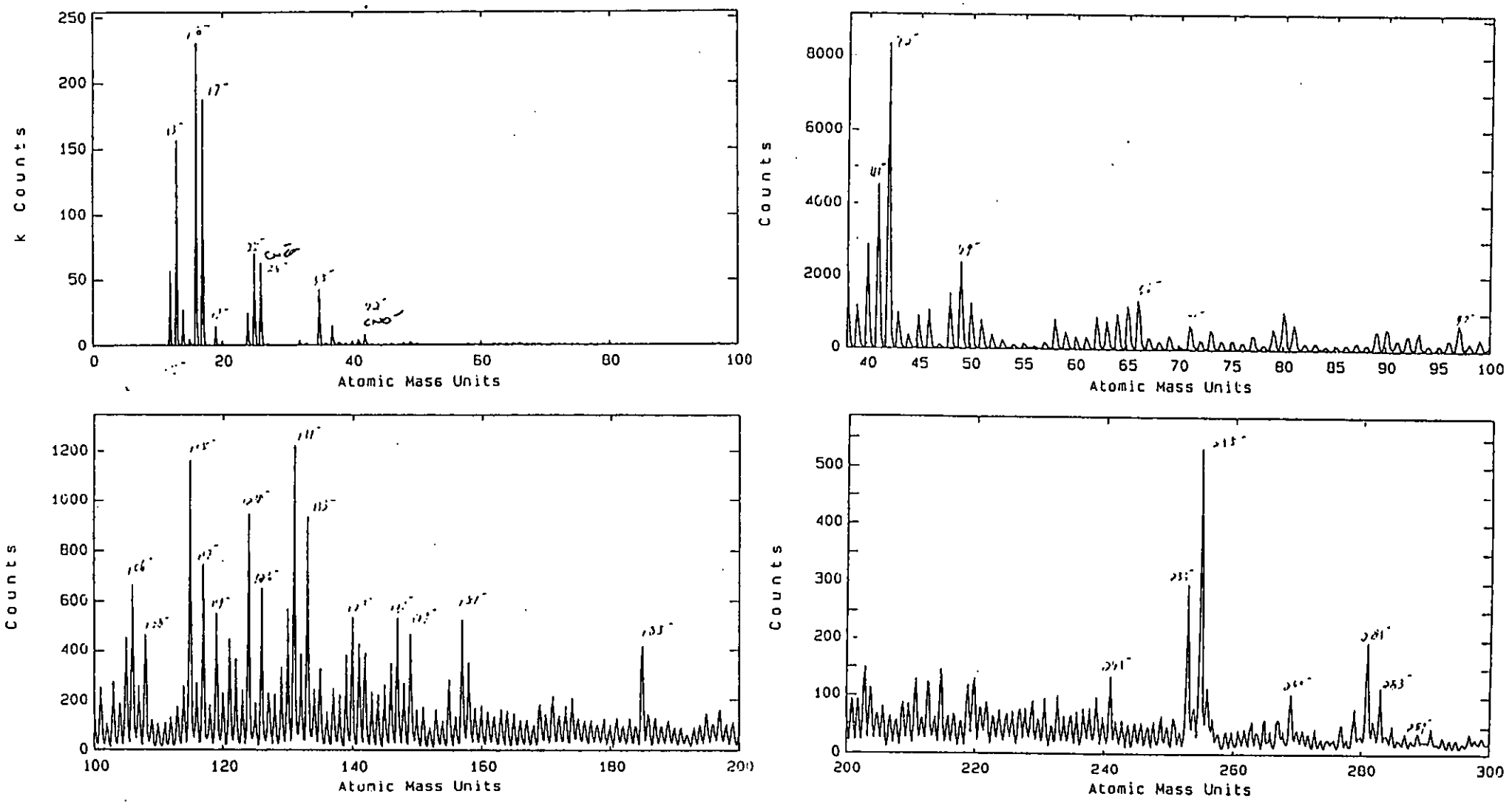

Fig. 13.22 Negative ion spectrum for ammonia plasma treated PEEK film after 1 hour heat treatment at temperature of 150°C (Plasma treatment condition: 1 min, 500 w, 0.3 torr)

Between a.m.u. 100-200, the heat treatment has very little effect on the spectrum of ammonia plasma treated PEEK.

Between a.m.u. 200-300, after the heat treatment, peaks at 203, 213, 227, 277 and 291 disappeared. Among them, the peak at a.m.u. 203 was introduced by the plasma treatment, while the peak at a.m.u. 227 was much enhanced by the plasma treatment. The intensity of the peak at 255 was much enhanced.(there is also a strong signal at a.m.u. 255 in the spectra of untreated PEEK). Some new weak signals appeared at a.m.u. 269, 281 and 283. Those signals also exist in the untreated PEEK spectrum but not the ammonia plasma treated spectrum.

Therefore, both positive and negative ions results show that heat treatment can also recover to some extent the chemical structures changed by both oxygen and ammonia plasma treatment back to those of the untreated PEEK.

13.3.4 Adhesion studies

Fig. 13.23 and Fig. 13.24 show the temperature effect on the lap shear joint strengths of both oxygen plasma and air corona discharge treated materials respectively. As it can be seen, when the heat treatment temperature is lower than 150°C, i.e. lower than T_g), the heat treatment has very little effect on the joint strength and the failure locus. Only when the heat treatment temperature is above 150°C, does the joint strength decreases, and the failure locus changes, particularly for oxygen plasma treated samples. However, heat treatment for 1 hour at temperature of 180°C only slightly decrease the joint strength of ammonia plasma and sulfur dioxide plasma treated materials, while slightly increase the joint strength of ammonia corona and sulfur dioxide corona treated films (as shown in Table 13.2).

The difference here is thought to be due to different treatment condition produce different size molecules on the surface. The HMWM produced by the oxygen plasma treatment may have relatively small size and could move into the bulk when temperature is over the T_g. While the HMWM produced by other treatment may have relatively large size and it is difficult for them to migrate into the bulk even when temperature is over the T_g. Hence heat treatment does not affect their joint strength.

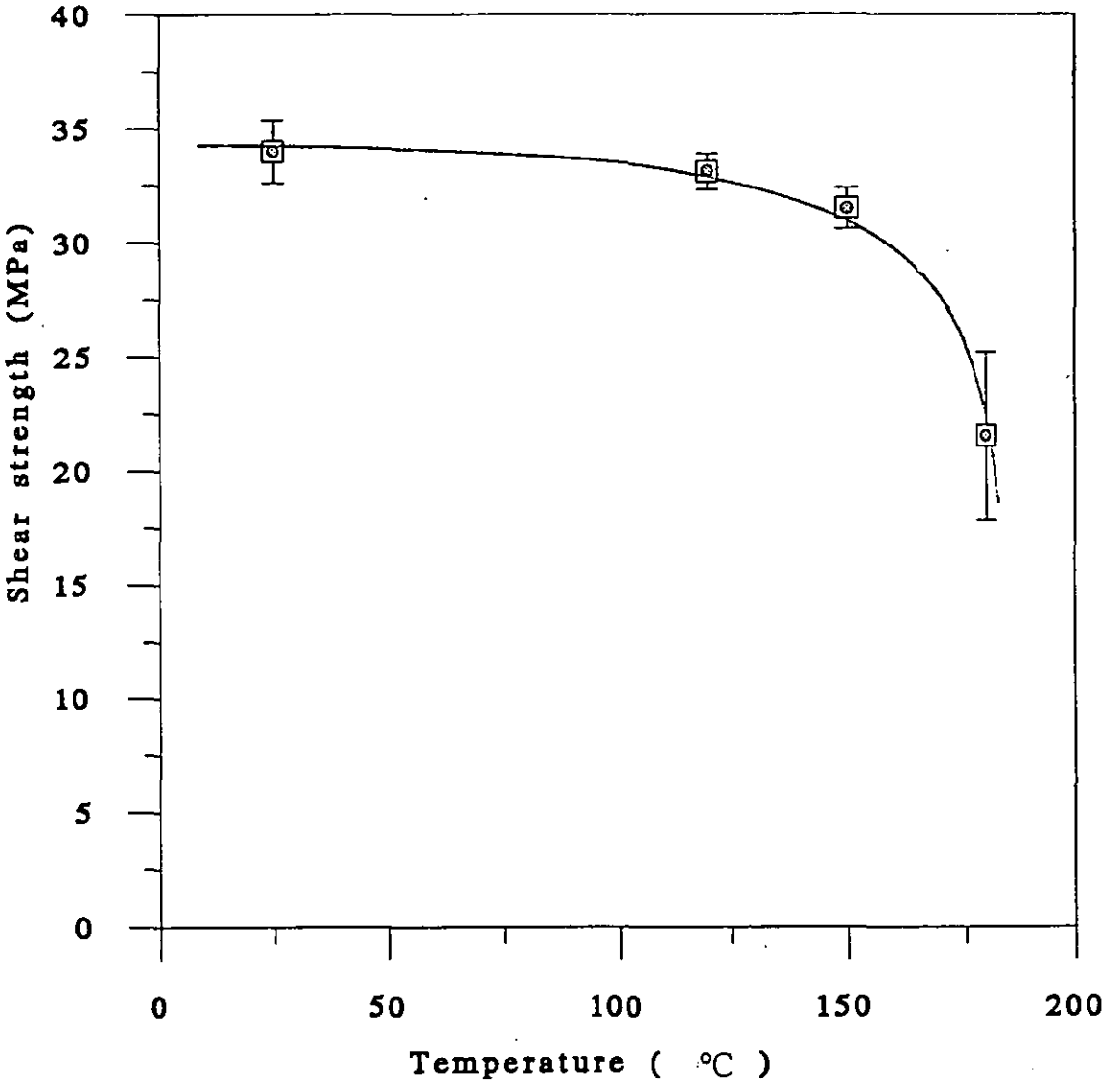

Fig. 13.23 Effect of heat treatment temperature on the lap shear joint strength of oxygen plasma treated films

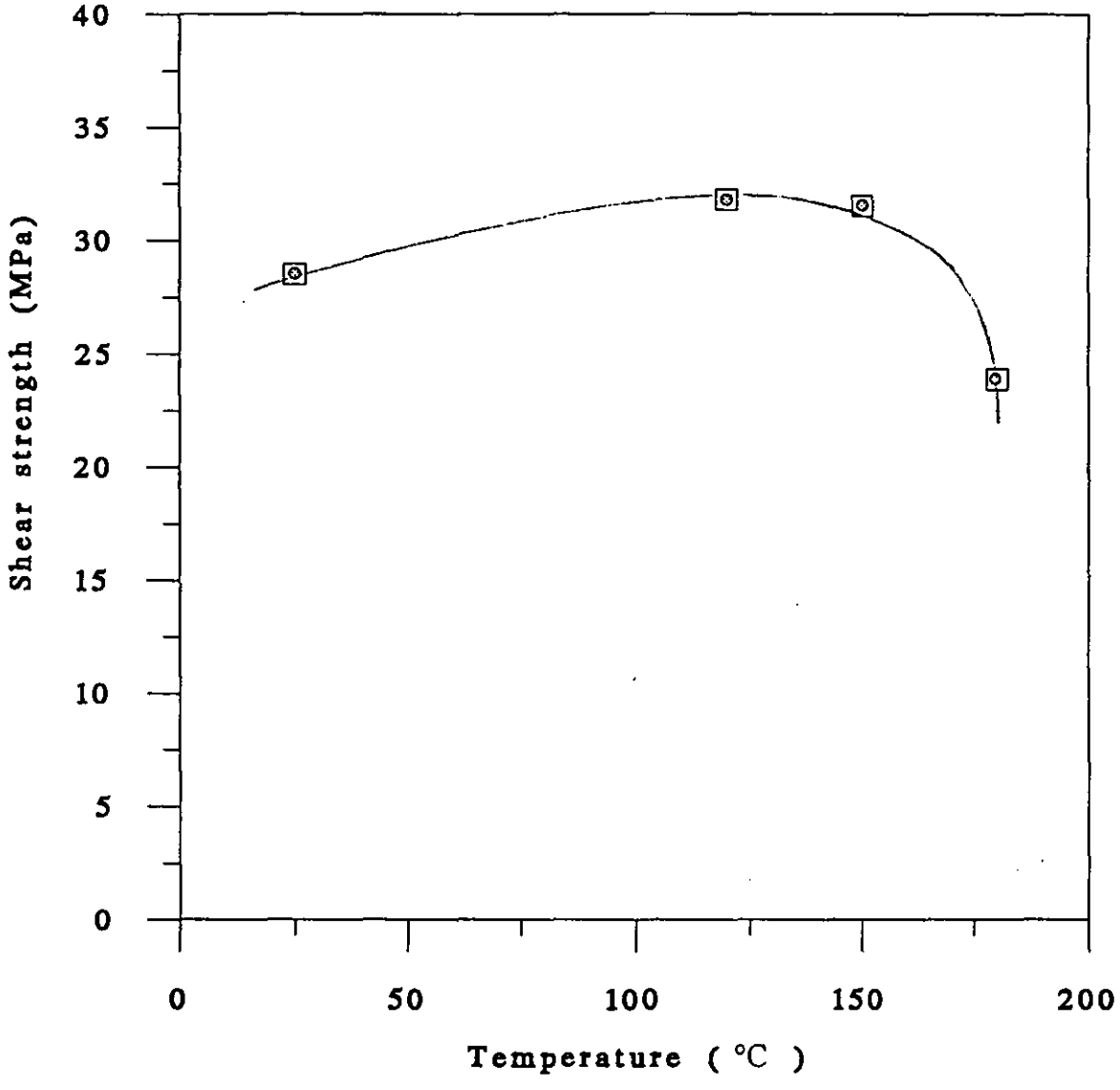

Fig. 13.24 Effect of heat treatment temperature on the lap shear joint strength of air corona discharge treated films

Table 13.2 Effect of heat treatment (1 hour at 180°C) on the lap shear joint strength of some plasma and corona discharge treated PEEK

Treatment method	Heat treatment	Joint strength (MPa)	Locus of failure
Untreated	Before	16.9±1.3	I+C
	After	13.0±3.8	I+C
O_2 plasma	Before	34.0±1.4	C+M
	After	15.2±6.9	I+C+M
NH_3 plasma	Before	32.2±2.1	C+M
	After	26.4±0.7	C+M
SO_2 plasma	Before	32.8±0.9	C+M
	After	28.0±1.2	C+M
Air corona	Before	28.5±1.8	C+M
	After	27.2±4.6	I+C+M
NH_3 corona	Before	28.0±0.7	C+M
	After	32.2±0.1	C+M
SO_2 corona	Before	32.0±1.2	C+M
	After	32.5±1.7	C+M

Plasma treatment condition: 1 min, 500 w, 0.3 torr
Corona discharge treatment level: 0.4 J mm^{-2}

13.4 Effect of Water

As discussed above, the molecules in the modified layer produced by plasma and corona discharge treatment tends to restructure to minimise its interfacial tension. In the non-polar environment, the polar groups would orient into the bulk, as the result shown above, while in the polar environment, the polar groups would stay in the surface or orient to the surface. In addition, polar environment should recover the atmospheric exposed or heat treated sample to some extent, if the molecules have enough mobility. This section will discuss the results of water effect on the surface dynamics of plasma and corona discharge treated films.

Table 13.3 Effects of one week water immersion on the surface free energy, surface polarity and contact angle hysteresis of plasma and corona discharge treated materials

Treatment condition	Water immersion	Surface free energy (mJm^{-2}) γ_s^p	γ_s^d	γ_s	Surface polarity	Contact angle hysteresis θ_a	θ_r
Untreated	Before	7.2±3.9	31.5±8.3	38.7	0.186	73	32
O_2 Plasma	Before	42.0±18.3	23.9±14.0	66.0	0.638	<5	<5
	After	34.8±15.5	25.3±13.3	60.1	0.579	33	<5
NH_3 Plasma	Before	32.4±11.6	22.7±9.8	55.1	0.587	41	<5
	After	35.4±15.2	24.6±12.8	60.0	0.590	27	<5
Air Corona	Before	34.5±14.3	24.0±12.0	58.5	0.590	30	<5
	After	38.5±18.0	21.2±13.5	59.7	0.645	26	<5
NH_3 Corona	Before	25.9±8.7	25.7±8.7	51.6	0.502	45	<5
	After	26.6±9.9	24.3±9.5	50.9	0.523	45	<5

Plasma treatment condition: 1 min, 500 w, 0.3 torr

Corona discharge treatment level: 0.4 J mm^{-2}

Table 13.4 Effects of one week water immersion on the lap shear joint strength of plasma and corona discharge treated materials

Treatment method	Water immersion	Joint strength (MPa)	Locus of failure
Untreated	Before	16.9±1.3	I+C
O_2 plasma	Before	34.0±1.4	C+M
	After	32.5±0.7	C+M
NH_3 plasma	Before	32.2±2.1	C+M
	After	31.4±2.0	C+M
Air corona	Before	28.5±1.8	C+M
	After	29.6±2.2	C+M
NH_3 corona	Before	28.0±0.7	C+M
	After	30.1±2.3	C+M

Plasma treatment condition: 1 min, 500 w, 0.3 torr

Corona discharge treatment level: 0.4 J mm^{-2}

Table 13.3 shows the effects of one week water immersion on the surface free energy and its components for plasma and corona discharge treated films, also listed are the results of surface polarity and contact angle hysteresis. It can be safely stated that one week water immersion has not much effect on either surface free energy and its components or surface polarity. Except for oxygen plasma treated sample, water immersion decreases the surface free energy and surface polarity to some extent. The results of the contact angle hysteresis show the same trend, as shown in Table 13.3.

Table 13.4 shows the results of water immersion on the joint strength and it can be found that the lap shear joint strengths of plasma and corona discharge treated materials are not affected by the water immersion, implying that very little water was absorbed by the treated materials during the immersion period.

Hence water immersion does not change the wettability and bondability of plasma and corona discharge treated materials. This is believed to be due to very little water absorption during the immersion period and that water immersion may affect the modified layer in two ways: one is the dissolution of some LMWM which depending on the treatment condition employed; and the other is the reorientation of the polar groups to the surface. The net effect of these two effects is that for most treated samples, the immersed surfaces still keep their wettability and polarity. The exceptional decrease of the surface energy and the increase of the advancing contact angle for oxygen plasma treated films is thought to be due to that oxygen plasma treatment produces more LMWM than other treatments.

To assess the possibility of reversing the reorientation process occurred during atmospheric exposure and heat treatment. A one hour heat post-treated oxygen plasma modified sample was immersed in distilled water for one hour at room temperature (about 20°C) and 100°C respectively. The surface energy, surface polarity and contact angle hysteresis were studied and the results are shown in Table 13.5. As it can be seen, water immersion at high temperature can recover the surface properties of the aged sample, hence confirming our postulations about the surface orientation and restructuring (or surface dynamics).

Table 13.5 Effect of one hour water immersion on the surface properties of heat post-treated oxygen plasma modified materials

Water immersion	Temperature	Surface free energy (mJm^{-2})			Surface polarity	Contact angle hysteresis	
		γ_s^p	γ_s^d	γ_s		θ_a	θ_r
Before		11.3±4.0	32.4±7.5	43.7	0.259	66	<5
After	RT	13.6±4.2	29.3±6.3	42.9	0.318	63	<5
	100°C	36.0±11.6	20.1±8.8	56.1	0.642	35	<5

Plasma treatment condition: 1 min, 500 w, 0.3 torr

Heat post-treatment: 1 hour at 120°C

CHAPTER 14 CONCLUSIONS AND RECOMMENDATIONS FOR FUTURE WORK

14.1 Conclusions

Several conclusions can be drawn from the above results and discussions:

1. Untreated samples show low peel and shear joint strengths with the failure occurring either at the interface or at the interface and in the adhesive, suggesting that the interface is the weakest part in the untreated PEEK/adhesive joints.

2. Plasma and corona discharge treatment significantly increase both peel and lap shear joint strengths of PEEK. The treatments also change the failure mode of the PEEK/adhesive joints to cohesive or the mix of cohesive and material. The results indicate that plasma and corona discharge treatment can enhance the bondability of PEEK films to a level where the PEEK ruptures.

3. The results of the adhesion studies have shown that both amorphous and crystalline materials gave the same adhesive joint strength immediately after either plasma or corona discharge treatment with the fracture occurred primarily in the adhesive.

4. The initial durability studies have found that the adhesive joint for both plasma and corona discharge treated films does not lose their strength after either 180°C, 1 hour heat treatment or 1 month water immersion. These results and those of the other adhesion studies indicate that plasma and corona discharge treated materials can form strong interfacial attractions with the adhesive employed.

5. To study the mechanism of bondability enhancement, contact angle measurement, SEM, XPS and TOF-SIMS were employed to characterise the plasma and corona discharge treated surfaces. From contact angle studies it has been found that the treatment can significantly increase the wettability and polarity of PEEK films. While SEM analysis does not reveal surface topography changes after the treatment, both XPS and TOF-SIMS investigations show that plasma and corona discharge treatment change the chemical structures of the material surfaces. Some chemical groups, like hydroxyl, acid and etc. are introduced to the treated surfaces, and some low molecular weight molecules (LMWM) are also produced on the treated surfaces, which can be removed, to some extent, by solvents like acetone.

6. Based on the surface characterisation results, the treated surfaces can be modelled as a modified layer consisting of scattering molecular weight molecules with some functional groups introduced by the treatment bonded to their main structures. The distribution of the molecular weight in the modified layer depends on the treatment condition. According to solvent washability, the molecules on the treated surfaces can be classified into two categories, namely low molecular weight molecules (LMWM), which is washable by ordinary solvent, and high molecular weight molecules (HMWM), which are not washable by solvent.

7. The studies of bondability enhancement mechanism have shown that either weak boundary layers, or lack of mechanical interlocking and wetting is the main reason for the weak adhesion of PEEK films. The TOF-SIMS results suggest that chemical bonds can be formed between the treated surfaces and the epoxy resin, hence, it is believed that the lack of intrinsic adhesion is due to the lack of active chemical groups which, if present, can establish strong interatomic and intermolecular forces across the adhesive/PEEK interface. Both plasma and corona discharge treatment introduce such chemical groups onto the surface of PEEK film and so greatly enhance the intrinsic adhesion at the adhesive/substrate interface. Moreover, the results obtained also show that the small molecules produced by the treatment play a little role on the adhesion enhancement, though they reduce the wettability drastically.

8. Surface dynamics studies have revealed that both plasma and corona discharge treated surfaces are in a thermodynamically unstable state. Atmospheric exposure and heat treatment can recover the wettability and surface polarity of the treated surface to those of the untreated material to a large extent which depends on the ageing condition, while water immersion can reverse those ageing effects. However, atmospheric exposure has little effects on the bondability (with the adhesive employed) of the treated films except for the oxygen plasma and air corona discharge treated materials, for which the joint strength is slightly lowered after more than two months exposure. Heat treatment below the glass transition temperature of PEEK does not affect the bondability (with the adhesive employed) of the treated materials, but treatment above that temperature could deteriorate the bondability of oxygen plasma and air corona discharge treated films. The mechanism of the surface dynamics is thought to be due to the reorientation of the chemical groups and the migration of LMWM which depend on the ageing condition.

14.2 Recommendations for Future Work

The present research work has established the techniques required for successful bonding of PEEK. To gain a further understanding of the mechanisms of adhesion and establish critical engineering design data the following suggestions are recommended for future work.

1. Durability Studies

The initial durability studies have shown that the plasma and corona discharge treated PEEK/adhesive joints have a very promising hot/wet performances, but since durability is often the limiting factor in adhesive bonding, this area needs further studies, e.g. exposure for up to one year.

2. Interfacial Interactions

The work carried out so far has revealed that chemical bonds can be formed between the treated surfaces and the epoxy adhesive. But to design the surface chemical composition which is good for adhesion, it needs to know the contributions from various chemical groups introduced by the treatment.

3. Surface Dynamics

The current studies had found that the wettability and chemical composition changes with time and temperature, but not the adhesive joint strength. This could be due to the high curing temperature for the adhesive employed. To gain further understanding of the relation between the adhesive and surface dynamics, different curing temperature adhesive should be investigated.

REFERENCES

1. Engineered Materials Handbook, Vol.2, "Engineering Plastics", ASM International, 144(1988)
2. T. E. Attwood et al, Polymer, 22, 1096(1981)
3. T. C. Stening, C. P. Smith and P.J. Kimber, Modern Plastics International, March, 54(1982)
4. D. J. Willats, SAMPE J., 20, 6(1984)
5. V. Wigotsky, Plast. Eng., 42, 17(1986)
6. A. J. Kinloch and C. M. Taig, J. Adhesion, 21, 291(1987)
7. Szu-I Y. Wu, Ann M. Schuler and Dan V. Keane, 19th International SAMPE Technical Conference, Oct.13-15, 277(1987)
8. S. Wu, Polymer Interface and Adhesion, p 29, Marcel Dekker, Inc., New York and Basel (1982)
9. *ibid.* p 359
10. L. H. Lee, in Fundamentals of Adhesion (L. H. Lee, ed.), p 6, Plenum Press, New York (1991)
11. S. Wu, Polymer Interface and Adhesion, p 360, Marcel Dekker, Inc., New York and Basel (1982)
12. *ibid.* p 406
13. L. Pauling, The Nature of The Chemical Bond, Cornell University Press, New York(1960)
14. R. J. Good, in Treatise on Adhesion and Adhesives, Vol.1 (R. L. Patrick, ed.), p 15, Marcel Dekker, Inc., New York (1967)
15. F. M. Fowkes, in Physicochemical Aspects of Polymer Surfaces, Vol.2 (K. L. Mittal, ed.), p 583, Plenum Press, New York (1983)
16. R. N. Wenzel, Ind. Eng. Chem. 28, 988 (1936)
17. J. R. Evans and D. E. Packham, J. Adhesion, 10, 177(1979)
18. D. E. Packham, in Developments in Adhesives 2 (A. J. Kinloch, ed.), p 315, Applied Science Pub., London (1981)
19. D. E. Packham, in Adhesion Aspects of Polymeric Coatings (K. L. Mittal, ed.), p 19, Plenum Press, New York (1983)
20. P. J. Hine, S. E. Muddarris and D. E. Packham, J. Adhesion, 17, 207(1984)
21. H. E. Bair, S. Matsuoka, R. G. Vadimsky and T. T. Wang, J. Adhesion, 3, 89(1971)
22. T. T. Wang and H. N. Vazirani, J. Adhesion, 4, 353(1972)
23. S. S Voyutskii, Autohesion and Adhesion of High Polymers, Interscience, New York (1963)

24. A. J. Kinloch, Adhesion and Adhesives Science and Technology, p 248, Chapman and Hall Ltd., London (1987)
25. W. A. Zisman, Adv. Chem. Ser., 43, 1(1964)
26. F. M. Fowkes, Ind. Eng. Chem., 56, 40(1964)
27. T. W. Whalen, J. Colloid Interf. Sci., 28, 443(1968)
28. A. W. Neumann, R. J. Good, J. Colloid Interf. Sci., 38, 341(1979).
29. A. W. Neumann, R. J. Good, in Surface and Colloid Science 11 (R. J. Good and R. R. Stromberg, eds.), 31(1979)
30. D. G. Rance, in Industrial Adhesion Problems (D. M. Brewis and D. Briggs, eds.), p 48, Orbital Press, Oxford (1985)
31. S. Wu, Polymer Interface and Adhesion, p 15, Marcel Dekker, Inc., New York and Basel (1982)
32. H. W. Fox, W. A. Zisman, J. Colloid Sci., 5, 514(1950)
33. H. W. Fox, W. A. Zisman, J. Colloid Sci., 7, 109(1952)
34. H. W. Fox, W. A. Zisman, J. Colloid Sci., 7, 428(1952)
35. E. G. Shafrin, and W.A. Zisman, J. Phys. chem., 64, 519(1960)
36. W. A. Zisman in Contact Angle, Wettability, and Adhesion, ACS, Washington D. C., Advances in Chemistry Series, 43, 1(1964)
37. L.A. Girifalco, R. J. Good, J. Phys. Chem., 61, 904(1957)
38. R. J. Good, L. A. Girifalco, G. Kraus, J. Phys. Chem., 62, 1418 (1958)
39. F. M. Fowkes, J. Phys. Chem., 66, 1863(1962)
40. F. M. Fowkes, J. Phys. Chem., 67, 2538(1963)
41. D. K. Owens, R. C. Wendt, J. Appl. Polym. Sci., 13, 1740(1969)
42. D. K. Owens, J. Appl. Polym. Sci., 14, 1725(1970)
43. S. Wu, J. Poly. Sci.: Part C, No.34, 19(1971)
44. S. Wu, in Polymer Science and Technology, Vol.12a, Adhesion and Adsorption of Polymers (L. H. Lee, ed.), p 53, Plenum Press, New York (1980)
45. S. Wu, Polymer Interface and Adhesion, p 178, Marcel Dekker, Inc., New York and Basel (1982)
46. C.A. Ward, A. W. Neumann, J. Colloid Interf. Sci., 49, 286(1974)
47. F. M. Fowkes, in Polymer Science and and Technology, Vol.12a, Adhesion and Adsorption of Polymers (L. H. Lee, ed.), p 43, Plenum Press, New York(1980)
48. F. M. Fowkes, J. Adhesion Sci. Technol. 17(1987)
49. D. H. Kaelble and K. C. Uy, J. Adhesion, 2, 50(1970)
50. F. M. Fowkes, J. Colloid Interf. Sci., 28, 493(1968)
51. J. Schultz, K. Tsutsumi and J. B. Donnet, J. Colloid Interf. Sci., 59, 277(1977)
52. F. M. Fowkes, in Treatise on Adhesion and Adhesives, Vol. 1 (R. L. Patrick, ed.), p 352, Marcel Dekker, New York (1967)

53. C. F. A. Culling, Modern Microscopy, Elementary Theory and Practice, Butterworth, London (1974)
54. O. Johari and A. V. Samudra, in Characterization of Solid Surfaces (P.F. Kane and G. P. Larrabee, eds.), p 107, Plenum Press, New York (1974)
55. J. A. Filbey and J. P. Wightman, in Adhesive Bonding (L. H. Lee, ed.), p 175, Plenum Press, New York (1991)
56. E. A. Ledbury, A. G. Miller, P. D. Peters, E. E. Peterson and B. W. Smith, Proc. 12th Natl. SAMPE Techn. conf. Series, p 935, SAMPE, Azusa, CA (1980)
57. G. D. Davis, in Adhesive Bonding (L. H. Lee, ed.), p 139, Plenum Press, New York (1991)
58. N.J.Harrick, Internal Reflection Spectroscopy, Wiley, New York (1967)
59. N. J. Harrick, in Characterization of Metal and Polymer Surfaces (L. H. Lee, ed.), Vol.2, p 153, Academic Press, New York (1977)
60. P. R. Griffiths and J. A. deHaseth, Fourier Transform Infrared Spectroscopy, wiley, New York (1986)
61. H. A. Willis and V. J. I. Zichy, in Polymer Surfaces (D. T. Clark and W. J. Feast, eds.), p 287, Wiley, London (1978)
62. D. Briggs, in Surface Analysis and Pretreatment of Plastics and Metals (D. M Brewis, ed.), p 84, Applied Science Publishers, London (1982)
63. C. D. Wagner, in Practical Surface Analysis (D. Briggs and M.P. Seah, eds.), p 477, Wiley, Chichester (1983)
64. L. C. Feldman and J. W. Mayer, Fundamentals of Surface and Thin film Analysis, North-Holland, New York (1986)
65. T. A. Carlson, Photoelectron and Auger Spectroscopy, Plenum Press, New York (1974)
66. D. T. Clark, W. J. Feast, W. K. R. Musgrave, I. Ritchie, J. Polym. Sci. Chem. Ed. 13, 857(1975)
67. D. Briggs, in Encyclopedia of Polymer Science and Engineering (J. I. Kroschwitz, ed.), 2nd Ed., 16, 406(1989)
68. D. S. Everhart, C. N. Reilley, Anal. Chem., 53, 665(1981)
69. D. Briggs, C. R. Kendall, Int. J. Adhes. Adhes., Jan, 13(1982)
70. R. A. Dickie, J. S. Hammond, J. E. DeVries, J. W. Holubka, Analy. Chem., 54, 2045(1982)
71. J.S. Hammond, Polym. Prepr. Am. Chem. Soc. Div. Polym. Chem. 21, 149(1980)
72. L. J. Gerenser, J. F. Elman, M. G. Mason, J. M. Pochan, Polymer, 26,1162(1985)
73. J. M. Pochan, L. J. Gerenser, J. F. Elman, Polymer, 27, 1058(1986)
74. A. Chilkoti, B. D. Ratner and D. Briggs, Chem. Mater. 3, 51(1991)

75. J. C. Vickerman, in Secondary Ion Mass Spectrometry (J. C. Vickerman, A. Brown and N. M. Reed, eds.), P 2, Clarendon Press, Oxford (1989)
76. E. Zinner, J. Electrochem. Soc., 130, 199C, 1983
77. A. Benninghoven, Phys. Status Solidi, 34, K169(1969)
78. D. Briggs, Surf. Interface Anal. 4, 151(1982)
79. D. Briggs, Surf. Interface Anal.. 5, 113(1983)
80. D. Briggs and A. B. Watton, Surf. Interface Anal. 4, 109(1982)
81. D. Briggs, M. J. Hearn and B. D. Ratner, Surf. Interface Anal. 6, 184(1984)
82. A. Brown and J. C. Vickerman, Surf. Interface Anal. 6, 1(1984)
83. A. Brown and J. C. Vickerman, Surf. Interface Anal. 8, 75(1986)
84. D. Briggs and M. J. Hearn, Vacuum, 36, 1005(1986)
85. J. Lub, F. C. B. M. van Vroonhoven, D. van Leyen and A. Benninghoven, Polymer, 29, 998(1985)
86. J. Lub, P. N. T. van Velzen, B. Hagenhoff and A. Benninghoven, Surf. Interface Anal., 12, 53(1988)
87. D. Briggs and M. J. Hearn, Surf. Interface Anal., 13, 181(1988)
88. D. Briggs, M. J. Hearn, I. W. Fletcher, A. R. Waugh and B. J. Macintosh, Surf. Interface Anal., 15, 62(1990)
89. D. Briggs, in Practical Surface Analysis, second edition, Vol. 2, (D. Briggs an M. P. Seah, eds.), p367, John Wiley and Sons, Chichester (1992)
90. M. J. Hearn, D. Brigg, S. C. Yoon and B. D. Ratner, Surf. Interface Anal., 10, 384(1987)
91. D. J. Pawson, A. P. Ameen, R. D. Short, P. Denison and F. R. Jones, Surf. Interf. Analy., 18, 13(1992)
92. A. J. Kinloch, Adhesion and Adhesives: Science and Technology, p 248, Chapman and Hall Ltd, London(1987)
93. D. M. Brewis in Industrial Adhesion Problems (D. M. Brewis and D. Briggs, eds.), p 129, Orbital Press, Oxford(1985)
94. G. B. Portelli, in Structural Adhesives: Chemistry and Technology, (S. R. Hartshorn ed.), p407, Plenum Press, New York (1986)
95. J. Comyn, Lectring materials, Loughborough University of Technology, 1995
95a. A. J. Kinloch, Adhesion and Adhesives: Science and Technology, p 216, Chapman and Hall Ltd, London(1987)
96. O. Volkersen, Luftfahrtforschung, 15, 41(1938)
97. S. Wu, Polymer Interface and Adhesion, p 530, Marcel Dekker, Inc., New York and Basel (1982)
98. D. H. Kaelble, Trans. Soc. Rheol., 3, 161 (1959)
99. D. H. kaelble, Trans. Soc. Rheol., 4, 45 (1960)

100. S. Hamdan and J.R. G. Evans, J. Adhesion Sci. Tech. 1(4), 281(1987)
101. G. K. A. Kodokian, A. J. Kinloch, J. Mater. Sci. Lett., 7, 625(1988)
102. E. M. Silverman and R. A. Griese, SAMPE Journal, 25, 34(1989)
103. Tae-Ho Yoon and J. E. Mcgrath, 36th Inter. SAMPE Sym., April 15-18, 428(1991)
104. A. J. Kinloch, Adhesion and Adhesives: Science and Technology, p 141, Chapman and Hall Ltd, London(1987)
105. B. R. Strohmeier, J. Vac. Sci. Tech., A7, 3228(1989)
106. P. Davies, C. Courty, N. Xanthopoulos and H. J. Mathieu, J. Mater. Sci. Lett., 10, 335(1991)
107. J. R. G. Evans, R. Bulpett and M. Ghezl, J. Adhesion Sci. Technol. 1, 291(1987)
108. J. R. Hollahan and A. T. Bell, Techniques and Applications of Plasma Chemistry, John Wiley & Sons, New York (1974)
109. E. M. Liston, J. Adhesion, 30, 199 (1989)
110. S. Wu, Polymer Interface and Adhesion, p 298, Marcel Dekker, Inc., New York and Basel (1982)
111. E.Occhiello, M.Morra, G. L. Guerrini and F. Garbassi, Composites, 23(3), 193(1992)
112. A. D. Katnani, A. Knoll and M. A. Mycek, J. Adhesion Sci. Tech., 3, 441(1989)
113. W. J. Brennan, W. J. Feast, H. S. Munro and S. A. Walker, Polymer, 32, 1527(1991)
114. H. V. Boenig, Fundamentals of Plasma Chemistry and Technology, p 17, Technomic Publishing Co., Inc., Lancaster and Basel (1988)
115. A. J. Kinloch, G. K. A. Kodokian and J. F. Watts, J. of Mater. Sci. Lett., 10, 815(1991)
116. A. J. Kinloch and G. K. A. Kodokian, J. Adhesion, 37, 33(1992)
117. G. K. A. Kodokian and A. J. Kinloch, in "Bonding and Repair of Composites", (Butterworths, Guildford, 1989), P57
117a. L. Mascia, G. E. Carr and P. Kember, Plastics and Rubber Processing and Applications, 9, 133(1988)
118. J. Comyn, D. C. Blackley and L. M. Harding, Int. J. Adhes. Adhes., 13, 163(1993)
119. J. R. Dann, J. Colloid Interf. Sci., 32, 302(1970)
120. F. M. Fowkes and S. Maruchi, Coatings and Plastics Preprints, 37, 605(1977)
121. S. Wu, Polymer Interface and Adhesion, p 260, Marcel Dekker Inc., New York (1982)
122. R. J. Good, J. colloid Interf. Sci., 52, 308(1975)

123. S. Wu, Polymer Interface and Adhesion, p 103, Marcel Dekker Inc., New York (1982)
124. E. Sheng, PhD Thesis, Loughborough University of Technology, 1992
124a. S. Wu, Polymer Interface and Adhesion, p 537, Marcel Dekker Inc., New York (1982)
125. A. W. Neumann and R. J. Good, J. Colloid Interf. Sci., 38, 341(1972)
126. J. D. Eick, R. J. Good and A. W. Neumann, J. Colloid Interf. Sci., 53, 235(1975)
127. J. D. Andrade, D. E. Gregonis and L. M. Smith, Physicochemical Aspects of Polymer Surfaces, Vol. 2, p 911, Plenum, New York/London(1982)
128. S. Wu, Polymer Interface and Adhesion, p 25, Marcel Dekker Inc., New York (1982)
129. R. E. Jr. Johnson and R. H. Dettre, J. Phys. Chem., 68, 1744(1964)
130. L. W. Schwartz and S. Garoff, Langmuir, 1, 219(1985)
131. D. Briggs, D. G. Rance, C. R. Kendall and A. B. Blythe, Polymer, 21, 895(1980)
132. G. Beamson and D. Briggs, High Resolution XPS of Organic Polymers: The Sciencta ESCA 300 Database, John Wiley & Sons Ltd, 1992
133. Y. Tamada and Y. Ikada, Polymer, 34, 2208(1993)
134. A. P. Ameen, R. J. Ward, R. D. Short, G. Beamson and D. Briggs, Polymer, 34, 1795(1993)
135. E. Sheng, I. Sutherland, D. M. Brewis and R. J. Heath, Surf. Interface Anal., 19, 151(1992)
136. A. Chilkoti and B. D. Ratner, Surf. Interface Anal., 17, 567(1991)
137. Y. Yakayama, T. Takahagi, F. Soeda, K. Hatada, S. Nagacka, J. Suzuki and A. Ishitani, J. Polym. Sci. Poly. Chem. ed., 26, 559(1988)
138. I. Sutherland, E. Sheng, D. M. Brewis and R. J. Heath, J. Mater. Chem., 4, 683(1994)
139. D. Briggs, A. Brown and J. C. Vickerman, Handbook of Static Secondary Ion Mass Spectroscopy, Wiley, Chichester (1989)
140. J. Lub, F. C. M. van Vroonhoven, D. van leyen and A. Benninghoven, Polymer, 29, 998(1988)
141, F. Garbassi, E. Occhiello, F. Polato and A. Brown, J. Mater. Sci., 22, 1450(1987)
142. R. M. Silverstein, G. C. Bassler and T. C. Morrill, Spectrometric Identification of Organic Compounds, Fifth edition, p 110, John Wiley & Sons, Inc. New York (1991)
143. ibid p120
144. A. J. Kinloch, Adhesion and Adhesives Science and Technology, p 248, Chapman and Hall Ltd., London(1987)
145. *ibid.* p 57
146. J. N. Anand, J. Adhesion, 5, 265(1973)

147. B. V. Deryaguin and V. P. Smilga, J. Appl. Phys. 38 (12), 4609 (1967)
148. A. J. Kinloch, Adhesion and Adhesives Science and Technology, p 74, Chapman and Hall Ltd., London(1987)
149. *ibid.* p 248
150. *ibid.* p 149
151. *ibid.* p 20
152. W. C. Wake, Adhesion and The Formulation of Adhesives, p 54, Applied Science Pub., London (1982)
153. Handout from CSMA
154. F. N. Cogswell and M. Hopprich, Composites, 14, 251 (1983)
155. E. J. Stober, J. C. Seferis and J. D. Keenan, Polymer, 25, 1845(1984)
156. T. Sasuga and M. Hagiwara, Polymer, 26, 501(1985)
157. A. Arzak, J. I. Eguiazabal and J. Nazabal, J. Mater. Sci., 28, 3272(1993)
158. H. Yasuda, A. K. Sharma and T. Yasuda, J. Polym. Sci. Polym. Phys. Ed., 19, 1285(1981)
159. T. Yasuda, T. Okuno, K. Yoshida and H. Yasuda, J. Polym. Sci. Polym. Phys. Ed., 26, 1781(1988)
160. Y. Iriyama, T. Yasuda, D. L. Cho and H. Yasuda, J. Appl. Polym. Sci., 39, 249(1990)
161. H. Iwata, A. Kishida, M. Suzuki, Y. hata and Y. Ikada, J. Polym. Sci. Polym. Chem., 26, 3309(1988)
162. M. Morra, E. Occhiello, L. Gila and F. Garbassi, J. Adhesion, 33, 77(1990)
163. D. Briggs, D. G. Rance, C. R. Kendall and A. R. Blythe, Polymer, 21, 895(1980)
164. A. Blythe, D. Briggs, C. R. Kendall, D. G. Rance and V. J. I. Zichy, Polymer, 19, 1273(1978)
165. Report for DRA, Research Agreement CB/RAE/9/4/2170/127/MA
166. M. Morra, E. Ochiello and F. Garbassi, J. Colloid Interf. Sci., 132, 504(1989)

Appendix 1 Calculation of Crystallinity From DSC Results

The DSC thermograms of crystallised PEEK show double-melting peaks. The peaks have been proposed to be related to a melting and recrystallization phenomenon of one initial crystal morphology, which is characteristic of the previous crystallisation history[1-3] or to be associated with distinct morphologies or crystals[4-6]. In this work, the crystallinity was calculated according to the former theory and the "peak area" method (as reviewed in ref. 7) was employed.

According to the "peak area" method, the weight per cent crystallinity $X(T_1)$ is given by the following equation

$$X(T_1)=\Delta A/\Delta H_f(T_2) \times 100$$

Where ΔA is the area of the melting endotherm above the baseline between T_1 and T_2; T_1 and T_2 are the temperature at the onset and completion of melting, $\Delta H_f(T_2)$ is the enthalpy of melting of fully crystalline polymer at T_2, by carefully choosing T_1 and T_2, the area under the endotherms of DSC curve can be obtained. By approximating T_2 to T_m, the value of $\Delta H_f = 130$ J g^{-1} given by Blundell and Osborn[2] can be used.

The results of peak area listed in Table 8.6 are the average of two sets of DSC curves. The original data are shown in Table A-1, and a set of the DSC curves are shown in Fig. A1.1-A1.4.

Table A-1 Annealing time and DSC peak area

Annealing time (hour)	Peak area (J/g)		
	Curve 1	Curve 2	Average
0.5	37.97	42.58	40.28
1.0	40.32	42.09	41.21
2.0	42.23	--	42.23
4.0	44.58	44.34	44.46

Reference

1. D. J. Blundell and B. N. Osborn, polymer, 24, 953(1983)

2. Y. C. Lee and R. S. Porter, Macromolecules, 20, 1336(1987)

3. D. C. Blundell, Polymer, 28, 2248(1987)

4. P. Cebe and S. D. Hong, Polymer, 27, 1183(1986)

5. S. Z. D. Cheng, M. Y. Cao and B. Wunderlich, Macromolecules, 19, 1868(1986)

6. D. C. Bassett, R. H. Olley and I. A. M. Al Rahell, Polymer, 29, 1745(1988)

7. D. J. Blundell, D. R. Beckett and P. H. Wilcocks, Polymer, 22, 704(1981)

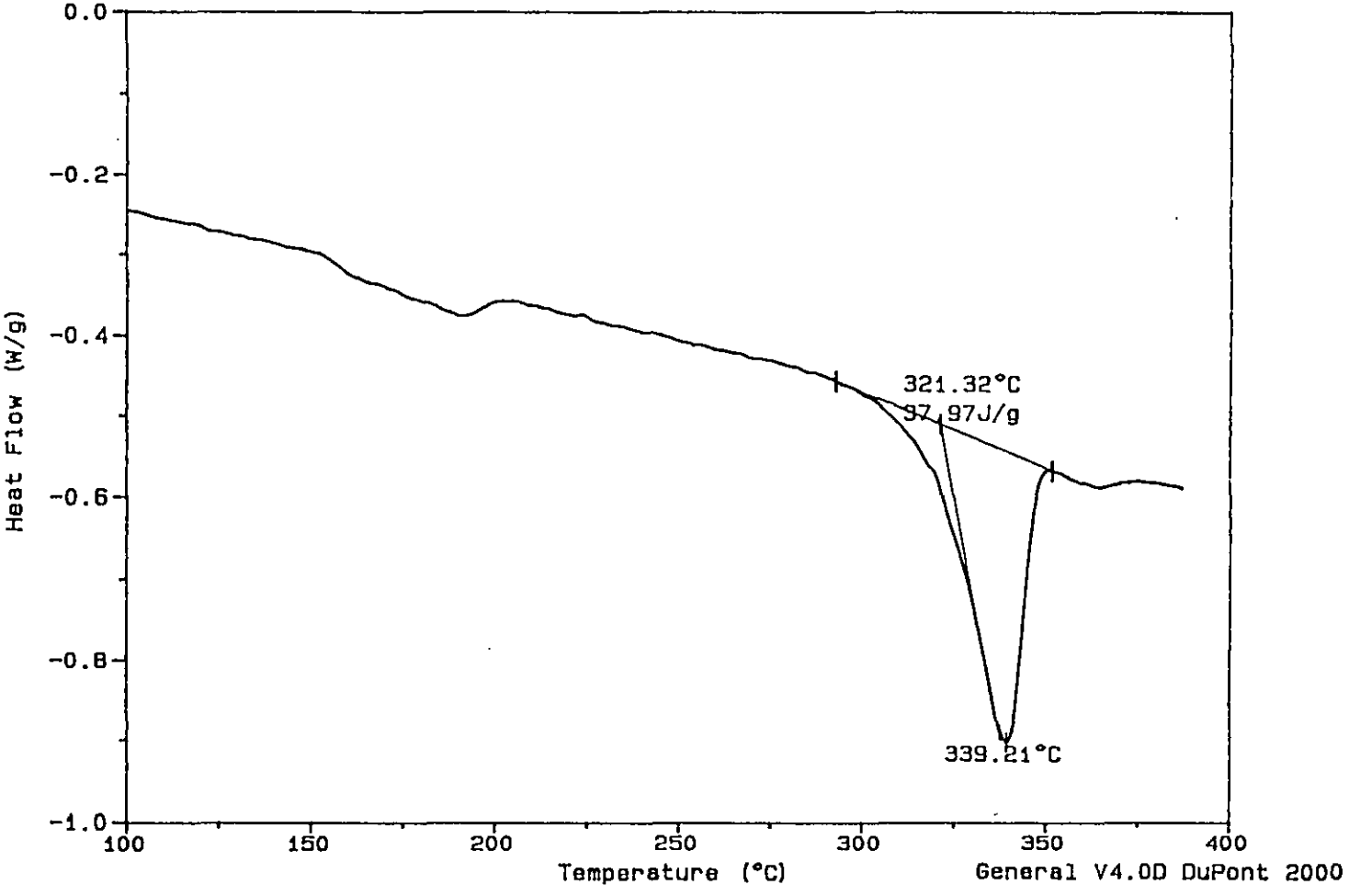

Fig. A1.1 DSC curve of PEEK film annealed at the temperature of 180°C for 0.5 hour

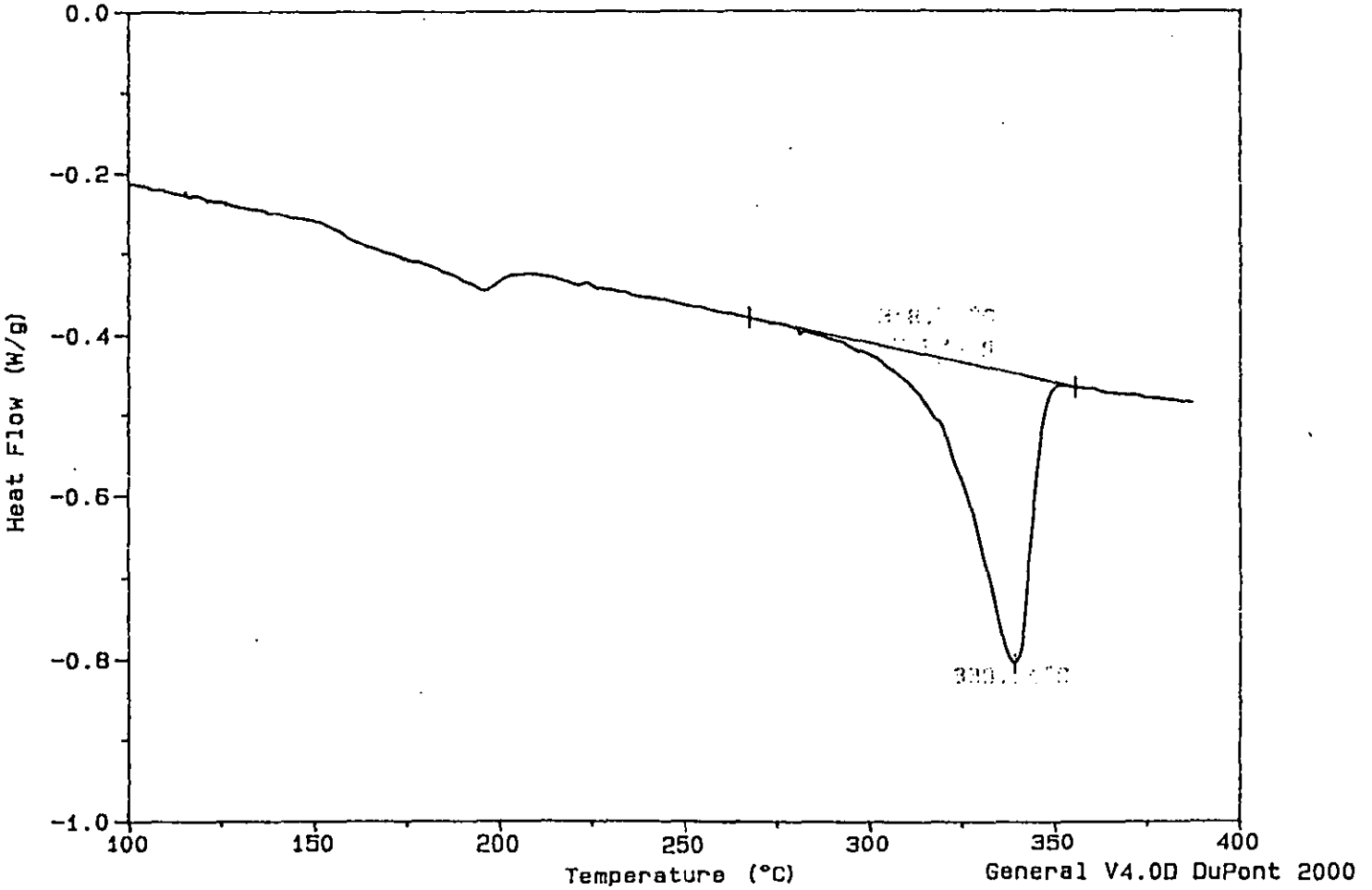

Fig. A1.2 DSC curve of PEEK film annealed at the temperature of 180°C for 2 hours

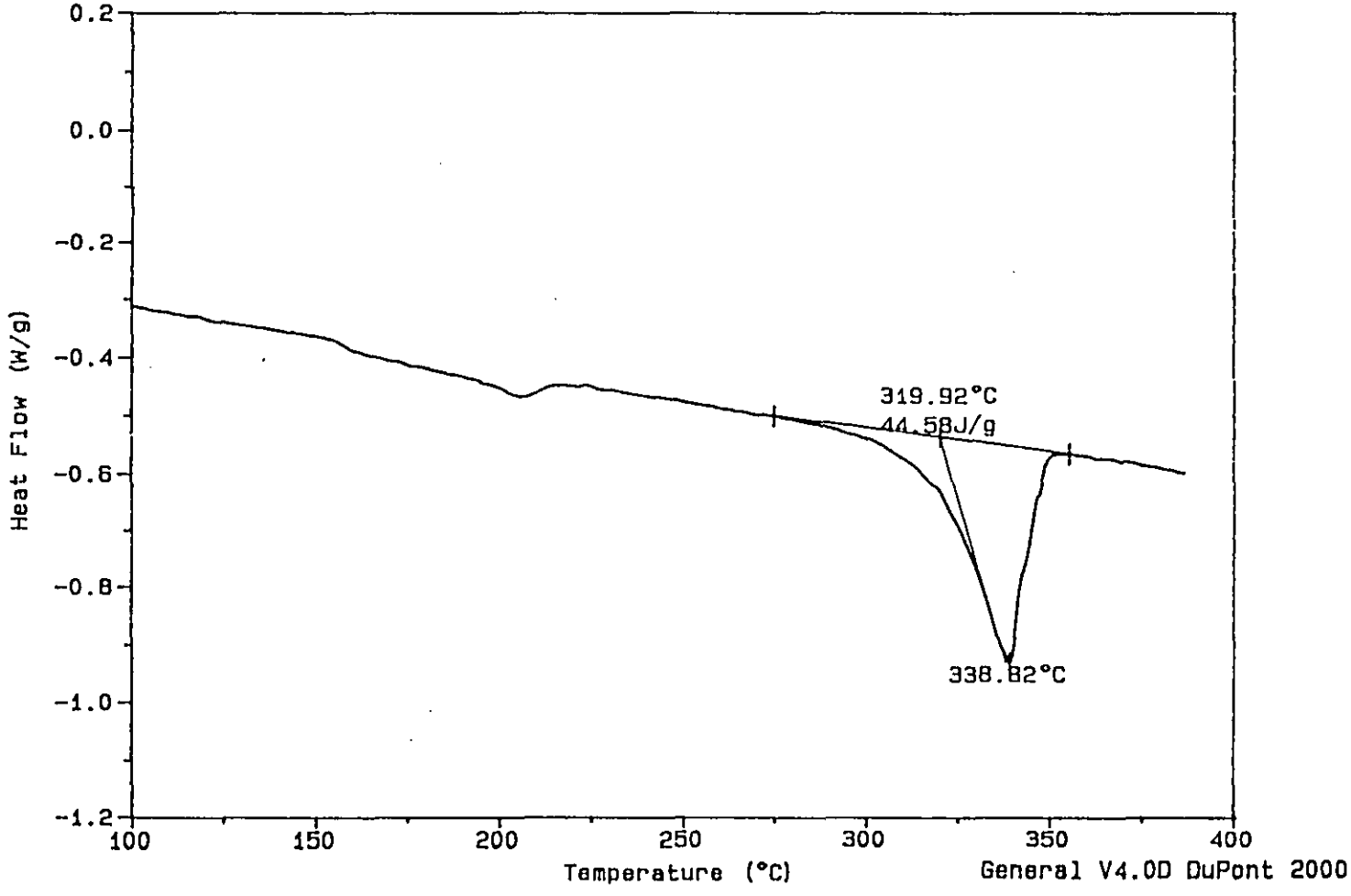

Fig. A1.3 DSC curve of PEEK film annealed at the temperature of 180°C for 4 hours

Appendix 2 TOF-SIMS Spectra of Some Plasma Treated PEEK Films

Fig. A2.1 Positive ion spectrum of oxygen plasma treated film (Treatment condition: 1 min, 500 w, 0.3 torr)

Fig. A2.2 Negative ion spectrum of oxygen plasma treated film (Treatment condition: 1 min, 500 w, 0.3 torr)

Fig. A2.3 Positive ion spectrum of ammonia plasma treated film (Treatment condition: 1 min, 500 w, 0.3 torr)

Fig. A2.4 Negative ion spectrum of ammonia plasma treated film (Treatment condition: 1 min, 500 w, 0.3 torr)

Fig. A2.5 Positive ion spectrum of oxygen plasma treated film after acetone washing (Treatment condition: 1 min, 500 w, 0.3 torr)

Fig. A2.6 Negative ion spectrum of oxygen plasma treated film after acetone washing (Treatment condition: 1 min, 500 w, 0.3 torr)

Fig. A2.7 Positive ion spectrum of ammonia plasma treated film after acetone washing (Treatment condition: 1 min, 500 w, 0.3 torr)

Fig. A2.8 Negative ion spectrum of ammonia plasma treated film after acetone washing (Treatment condition: 1 min, 500 w, 0.3 torr)

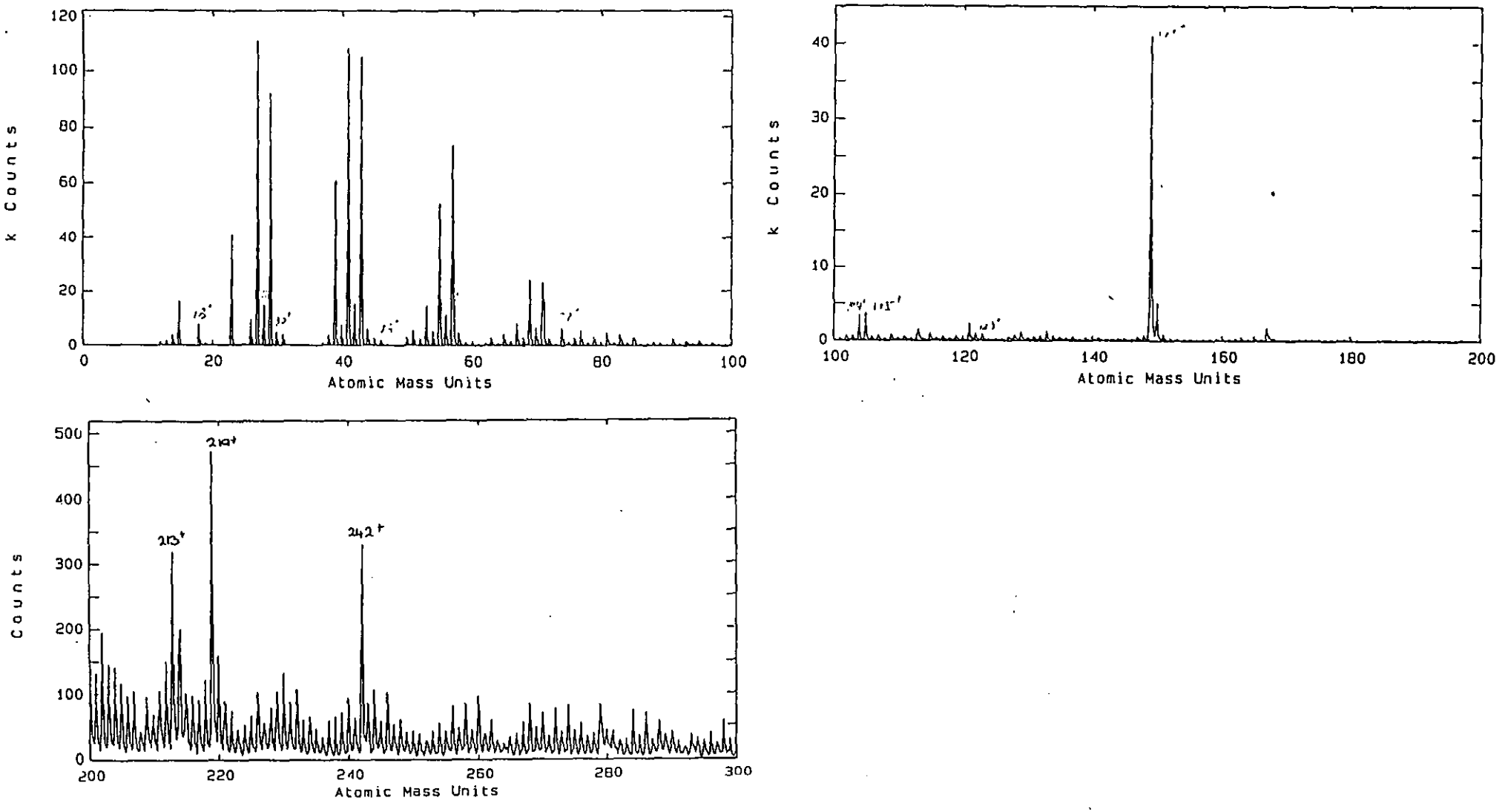

Fig. A2.1 Positive ion spectrum of oxygen plasma treated PEEK (Treatment condition: 1 min, 500 w, 0.3 torr)

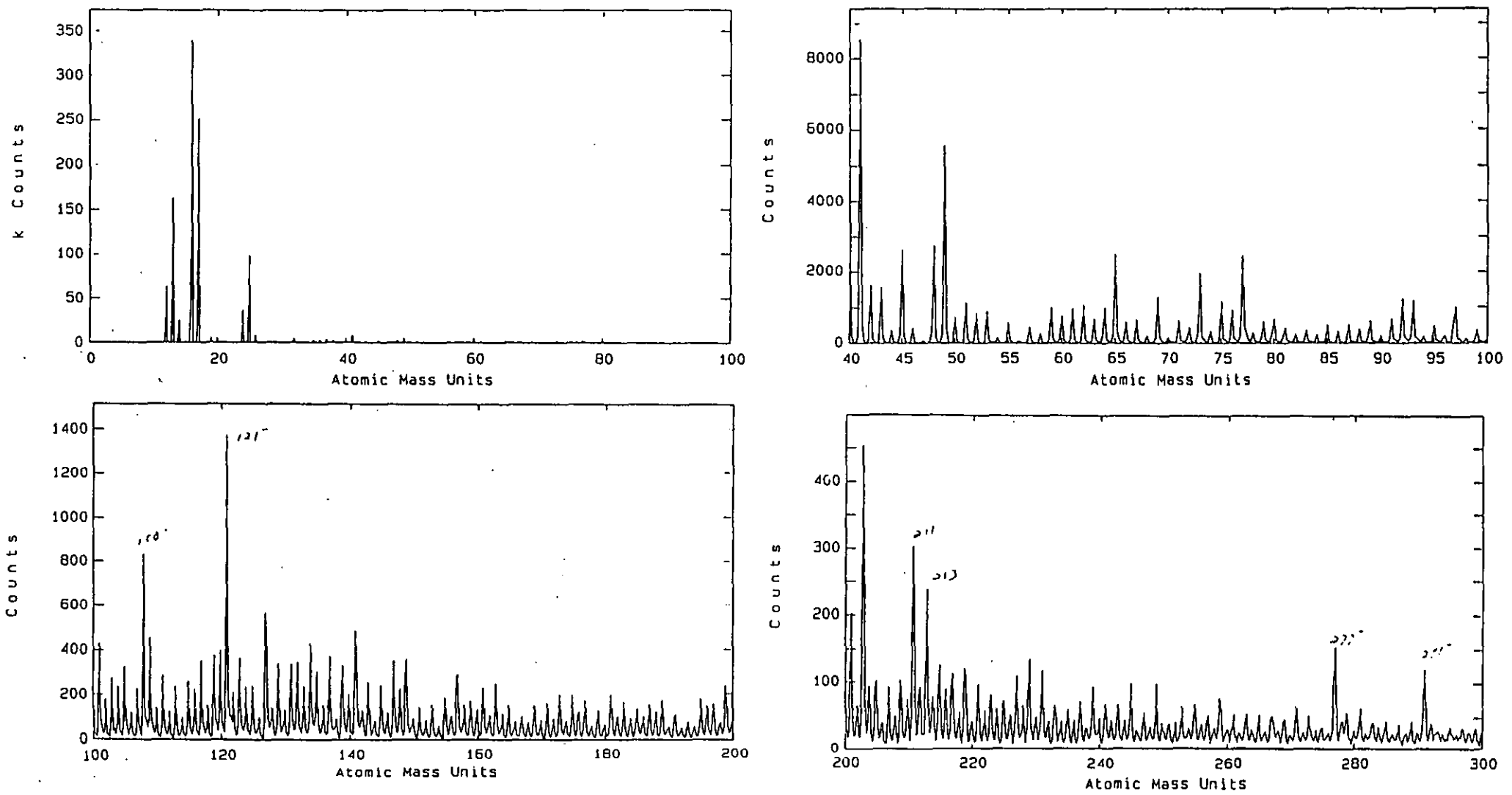

Fig. A2.2 Negative ion spectrum of oxygen plasma treated PEEK (Treatment condition: 1 min, 500 w, 0.3 torr)

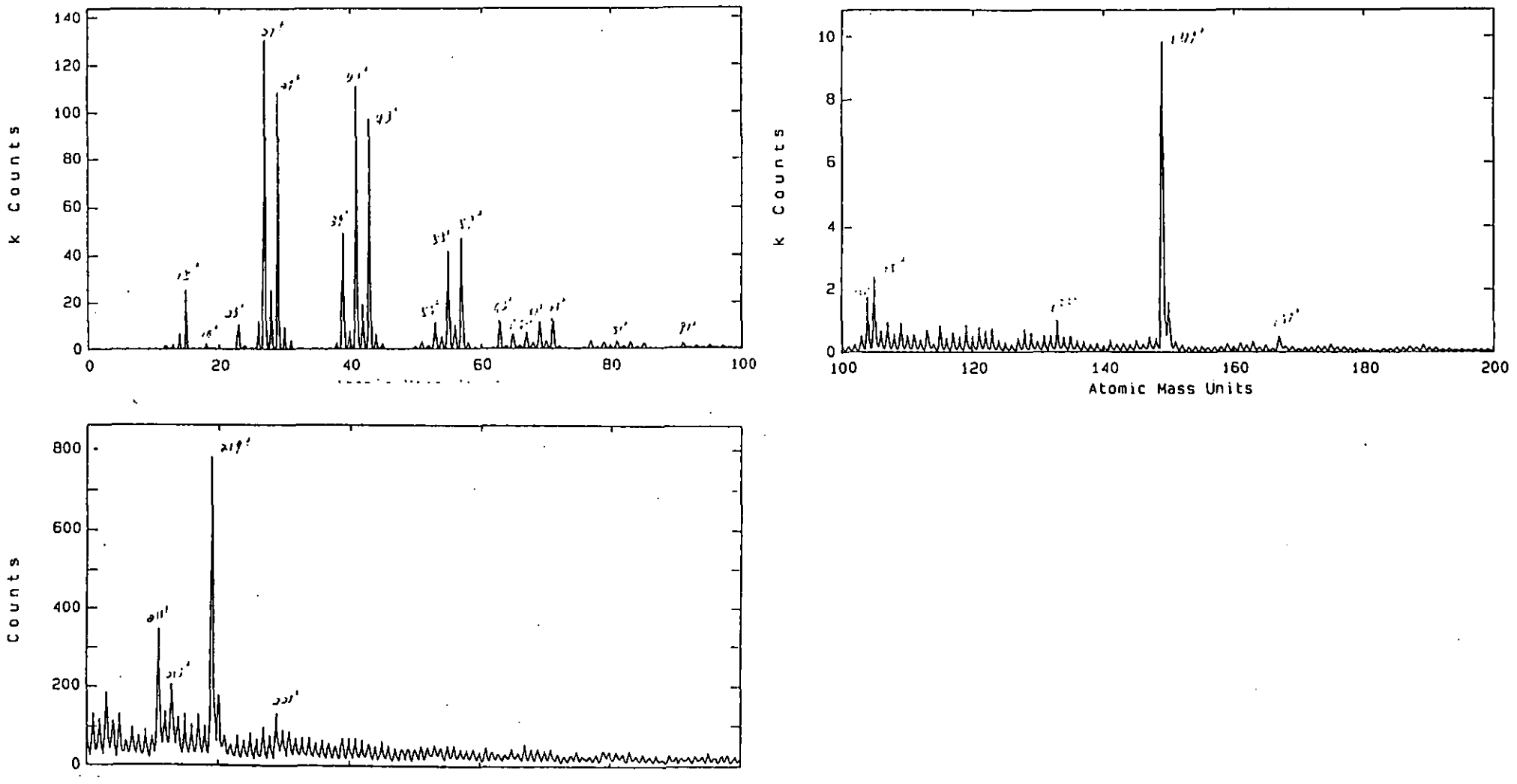

Fig. A2.3 Positive ion spectrum of ammonia plasma treated PEEK (Treatment condition: 1 min, 500 w, 0.3 torr)

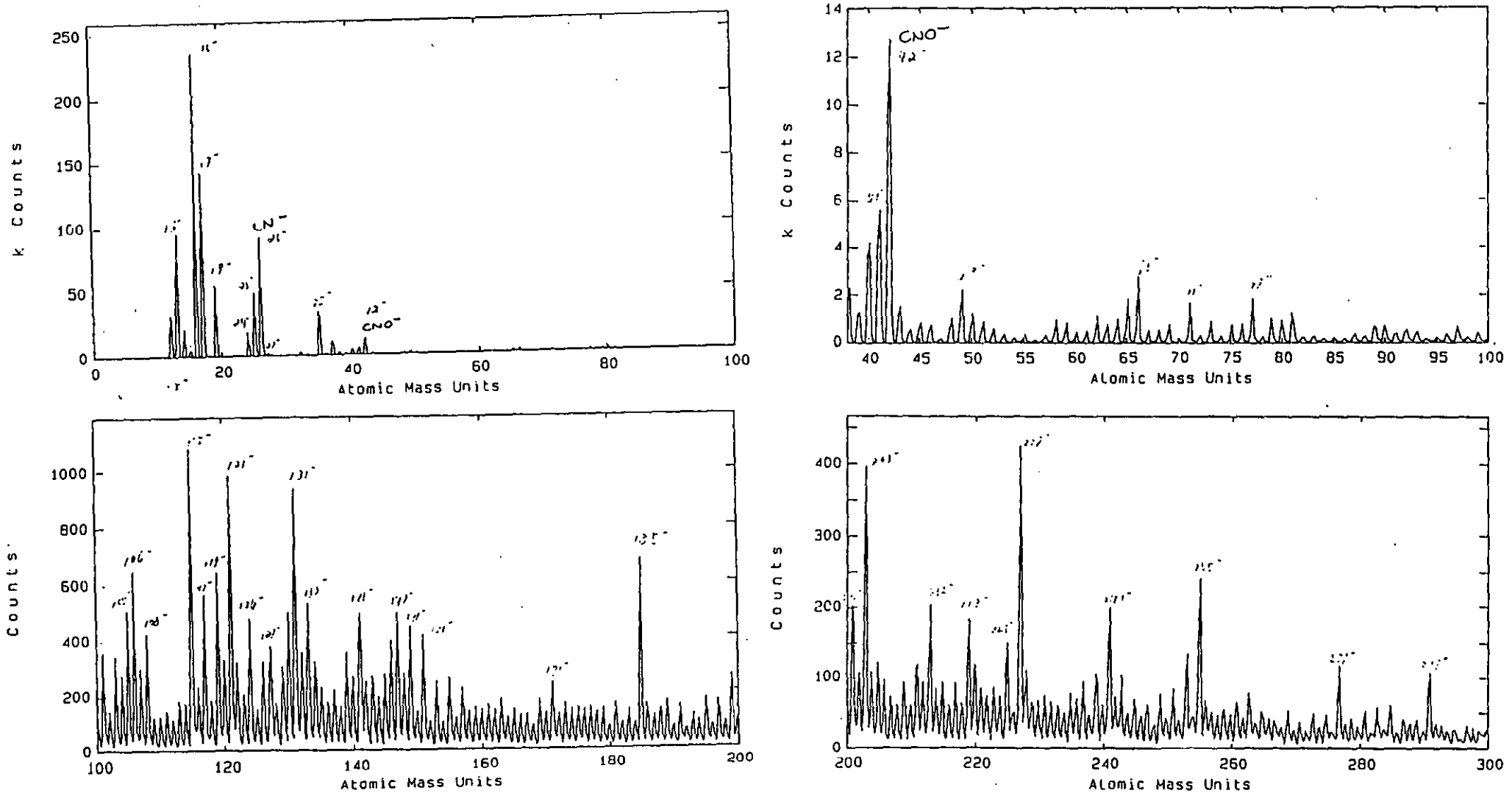

Fig. A2.4 Negative ion spectrum of ammonia plasma treated PEEK (Treatment condition: 1 min, 500 w, 0.3 torr)

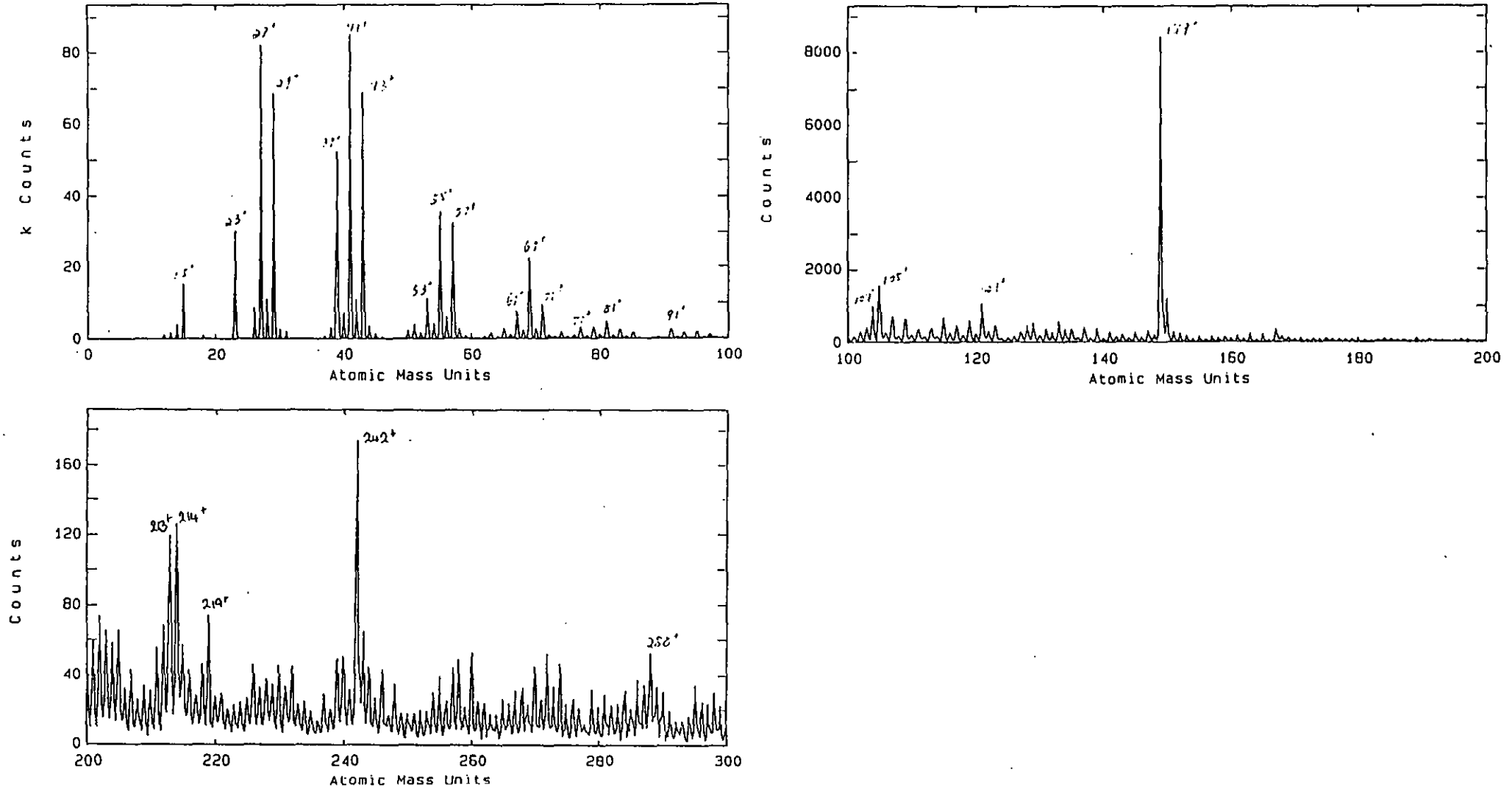

Fig. A2.5 Positive ion spectrum of oxygen plasma treated film after acetone washing (Treatment condition: 1 min, 500 w, 0.3 torr)

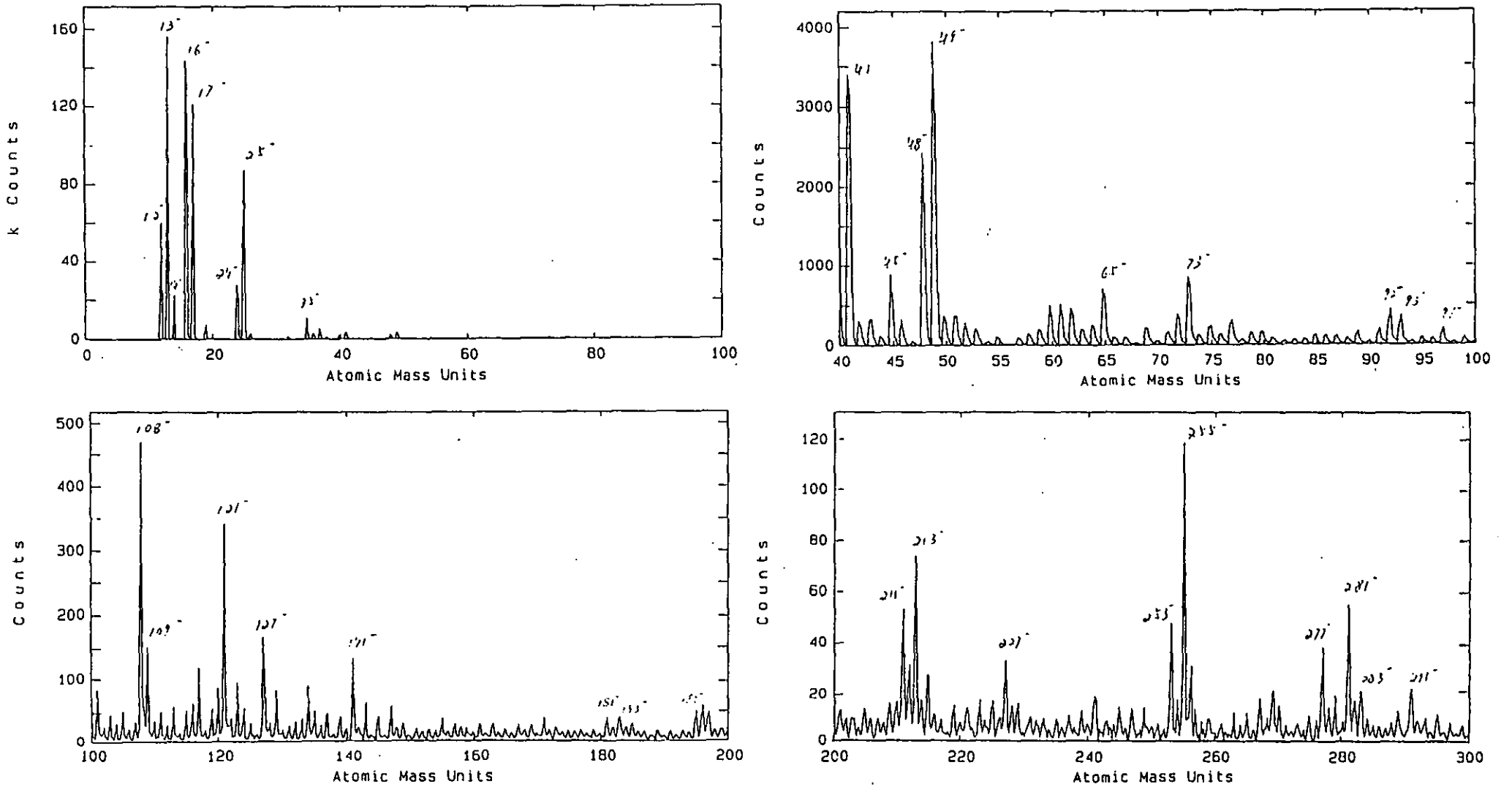

Fig. A2.6 Negative ion spectrum of oxygen plasma treated film after acetone washing (Treatment condition: 1 min, 500 w, 0.3 torr)

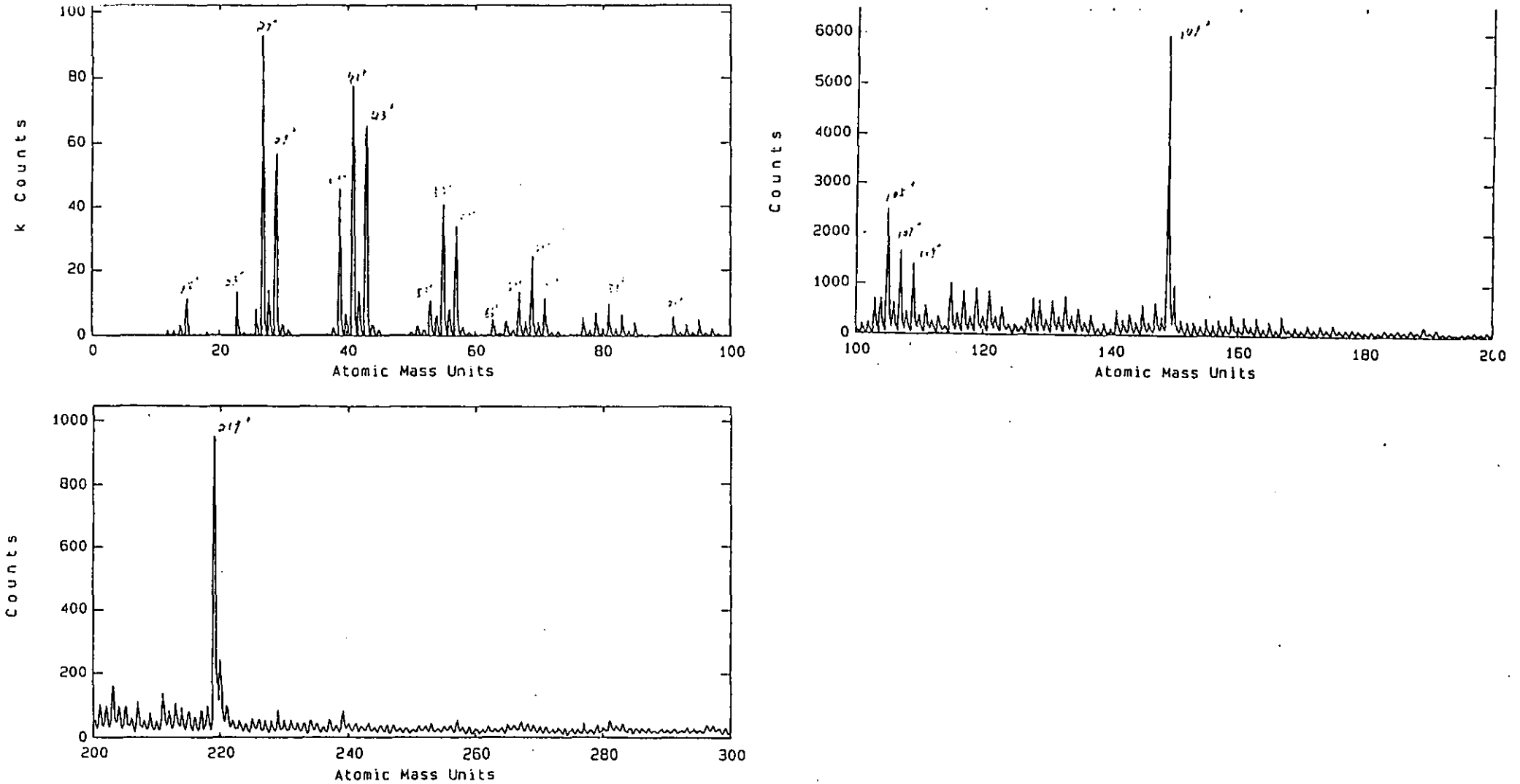

Fig. A2.7 Positive ion spectrum of ammonia plasma treated film after acetone washing (Treatment condition: 1 min, 500 w, 0.3 torr)

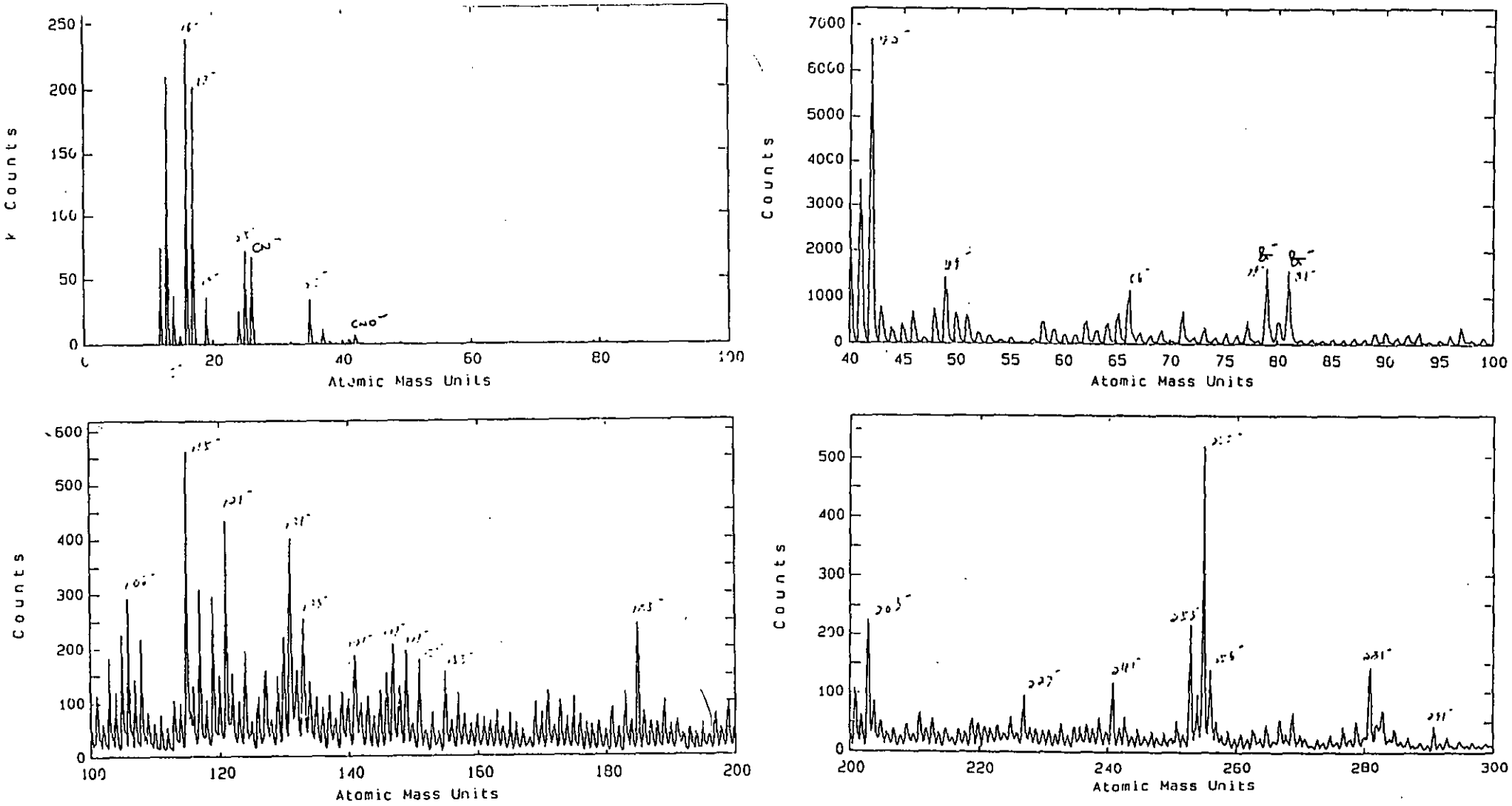

Fig. A2.8 Negative ion spectrum of ammonia plasma treated film after acetone washing (Treatment condition: 1 min, 500 w, 0.3 torr)